DECIPHERING LYSIS AND ITS REGULATION IN BACTERIOPHAGE T4

A Dissertation

by

SAMIR H. MOUSSA

Submitted to the Office of Graduate Studies of
Texas A&M University
in partial fulfillment of the requirements for the degree of

DOCTOR OF PHILOSOPHY

August 2012

Major Subject: Microbiology

Deciphering lysis and its regulation in bacteriophage T4

DECIPHERING LYSIS AND ITS REGULATION IN BACTERIOPHAGE T4

A Dissertation

by

SAMIR H. MOUSSA

Submitted to the Office of Graduate Studies of
Texas A&M University
in partial fulfillment of the requirements for the degree of

DOCTOR OF PHILOSOPHY

Approved by:

Chair of Committee, Ryland F. Young
Committee Members, Deborah Bell-Pedersen
Michael Benedik
Tatyana Igumenova
Head of Department, U.J. McMahan

August 2012

Major Subject: Microbiology

ABSTRACT

Deciphering Lysis and Its Regulation in Bacteriophage T4.

(August 2012)

Samir H. Moussa, B.S., Baylor University; M.S., Baylor University

Chair of Advisory Committee: Dr. Ryland F. Young

Like all phages, T4 requires a holin (T) to effect lysis. The lysis event depends on the temporally regulated action of T, which accumulates in the inner membrane (IM) until, at an allele-specific time, it *triggers* to form a large "hole" in the membrane. Hole formation then releases T4 lysozyme into the periplasm where it degrades the cell wall to elicit cell lysis. Unlike other phages, T4 is unique in exhibiting *real-time* regulation of lysis based on environmental conditions. Specifically, lysis can be delayed indefinitely in the lysis-inhibited state (LIN), where the normal temporal schedule for holin-triggering is over-ridden. Recently, it was shown that the imposition of LIN was correlated with the interaction of the periplasmic domains (PD) of RI and T. These studies have been extended in this dissertation using genetic, biochemical, and structural techniques to address the molecular mechanism of the RI-T LIN system.

First, the PD of RI and an RI-T complex were purified, characterized biophysically, and crystallized to yield the first atomic resolution structures of either a holin or antiholin. The RI PD is mostly alpha-helical that undergoes a conformational

change, as revealed by NMR spectroscopy studies, when bound to T. The PD of T is globular with alpha-helical, beta strand, and random coil secondary structures.

Additionally, the holin was genetically characterized by mutagenesis techniques, yielding new information on its role in both lysis and LIN. Lysis defective mutants in all three topological domains: cytoplasmic, transmembrane, and periplasmic, were isolated. Analysis of these mutants revealed that both the cytoplasmic and periplasmic domains are important in the oligomerization of T. During LIN, the RI PD binds the PD of T, blocking a holin oligomerization interface.

Finally, the signal for the imposition of lysis inhibition has been elucidated using NMR spectroscopy and other *in vitro* studies. These studies have shown that the RI PD binds DNA.

From these studies, new models for lysis and LIN have been constructed. Lysis occurs with the accumulation and oligomerization of T via cytoplasmic and periplasmic domain interactions. LIN is imposed when the ectopically localized DNA of a superinfecting phage interacts with RI, stabilizing it in a conformation competent in inhibiting T oligomerization and leading to lysis inhibition.

ACKNOWLEDGEMENTS

I would like to thank my committee members, Drs. Benedik, Bell-Pedersen, and Igumenova, for their invaluable guidance and support. I would also like to thank members of the Young lab, especially Joel, Jason, Gabby, Catrina, and Jessica, for their camaraderie, ideas, feedback and support. I would like to thank Jessica in particular for her hard work and dedication as an undergraduate student working with me for over 2 years. Special thanks go to Ms. Daisy Wilbert for her ability to get things done and for her friendship and advice.

Vladimir Kuznetsov and Dr. Sacchettini were instrumental in the crystallography work included in this dissertation. Additionally, Krystal Morales-Rivera, Mikaela Stewart, and Dr. Igumenova were instrumental in the NMR spectroscopy work. Thanks to both of these groups for their advice, knowledge, and hospitality in their labs as we worked together to answer the questions posed in this dissertation.

Thanks to my friends, especially Molly, Bryan, Joel, and Harmony, for their friendship, advice, and support. I can never thank my family enough for their support; my dad, mom, and three brothers have been invaluable in their support for me over the years. A special thanks to my fiancé and soon to be wife, Sara, for her support for me for the last four years. I really appreciate your patience with me and I know I could not have come this far without you.

Finally, I would like to thank my mentor, Dr. Ry Young. His love of science and his inquisitive mind have been a tremendous influence on me. Thank you for the many

hours spent talking in depth about science and even personal matters. While you are extraordinarily busy, you have always taken the time out of your schedule to support me and my work.

TABLE OF CONTENTS

Page

Page

Page

Page

Page

LIST OF FIGURES

Figure Page

LIST OF TABLES

CHAPTER I

INTRODUCTION

Brief history of T4 in molecular biology studies

The lysis event caused by T4 and its relatives is one of the foundational phenomena of molecular biology, studied by a roster of celebrated scientists: Max Delbrück, Alfred Hershey, Salvador Luria, Seymour Benzer, and others. Among the very first heritable characteristics assigned to any phage were the "rapid lysis", or *r*, markers of phage T2 described by Hershey (81), whose pioneering genetic maps relied largely on recombination between the *r* loci. His colleague and co-founder of the Phage Church , Max Delbrück, discovered that host cells could be lysed simply by adsorption of many T4 particles ("lysis from without") (43), a theme that, along with lysis inhibition (see below), was developed by Stent, Maaloe, Watson and others (37, 118, 167, 185, 189). The *rII* locus was the focus for Seymour Benzer's grand works that established many fundamental aspects of gene structure, recombination and mutation (17-19). George Streisinger identified and purified the T4 lysozyme, gp*e*, which now, after decades of intensive study by Brian Matthews and others, is arguably the most thoroughly characterized protein molecule (10, 170). Yet, except for the fact that the lysozyme was responsible for the degradation of the murein, and that there is another muralytic enzyme associated with the T4 base-plate assembly (8, 95, 97, 130, 178), the

---

This dissertation follows the style of the Journal of Bacteriology.

molecular basis of T4 lysis and its regulation remained obscure until very recently (136, 144-146, 179, 180). Here, the history of these studies will be summarized and updated, drawing on targeted reviews (203) and comprehensive narratives (27, 167) to fill in the gaps. The focus will be on the developing but still imprecise mechanistic understanding, setting the stage for the studies that define this thesis.

Double-stranded DNA bacteriophage lysis

The infection cycles of all dsDNA phages are programmed to terminate in host **lysis** (188, 203). Lysis, in the context of phage biology, is not the same as the eventual dissolution that all dead cells must eventually undergo. Rather, phage lysis is defined as the active destruction of the cell envelope and the complete release of progeny phage and cytoplasmic contents on a time scale that is useful for the phage (203). With its long history, T4 lysis has accumulated some specialized terminology of its own. At 37°C in broth, an *E. coli* B cell infected with a single T4 particle will, if left alone, undergo lysis at about 24 min post-infection, liberating ~100 progeny. However, T4-infected liquid cultures at visible turbidities stubbornly refuse to lyse; such cultures are, instead, **lysis-inhibited** (50, 51, 81, 83). This is because a small fraction of cells do undergo lysis at ~ 25 min and, at densities $>\sim 10^8$ cells/ml, their progeny (typically ~100 virions released per cell) adsorb so rapidly that the vast majority of the infected cells become "super-infected" prior to lysis. The adsorption of a second phage particle after 5 or more minutes of the infection cycle causes the infected cell to enter the lysis-inhibited (**LIN**) state, where the infection cycle can be almost indefinitely prolonged if super-infection events continue (179). **Lysis from without** (LO) occurs when a cell is infected with

~100 phage particles simultaneously and simply reflects the fact that gp*5*, a component of the phage tail, has a muralytic activity that plays a role in the DNA translocation machinery by effecting a local degradation of the peptidoglycan at the point of adsorption (1, 8, 96, 98). The simultaneous adsorption of so many particles, unlikely to ever occur in nature, presumably causes so much local degradation of the peptidoglycan that the cell envelope is destroyed. Although historically important and experimentally informative, it is likely safe to regard LO as a laboratory artifact which is irrelevant to a discussion of T4 phage lysis.

The physiological parameters of LIN have been addressed in numerous studies over decades; for a recent summary see Paddison *et al.* (136). The superinfecting phage that evokes the LIN state does not have to be functional; even UV-inactivated phages are LIN-capable (185). However, T4 "ghosts", in which the capsid contents have been released by osmotic shock, do not impose LIN (54, 55, 62, 182, 183). Since it is known that ghosts puncture the host membrane, this indicates that something in the capsid, either the viral DNA or an internal capsid protein (IP), is responsible for inducing LIN (136).

Programmed host lysis in dsDNA phages

Before proceeding to a review of lysis in T4, it is useful to consider an overview of the current state of the field in terms of lysis in dsDNA phages in general. Oddly, despite the early studies in T-even phages, it is phage lambda that has been the primary system for unraveling the molecular basis of phage lysis, for several reasons. First, as will be demonstrated here, phage lysis is all about timing, and the absolute best way to

obtain a population of cells synchronously undergoing the phage vegetative cycle is to use thermally-inducible lambda lysogens (145, 203). Done properly, with careful attention to physiological details like culture volume, flask volume, shaker speed and culture density, lysogens carrying a single inducible prophage will reproducibly lyse within 1-2 min of the same time after induction (193, 203, 205). There is no other way to achieve equivalently synchronous infections in liquid culture that does not require manipulations that inflict physiological stress much more severe than the brief shift to 42°C required for lysogenic induction. This useful physiology, coupled with other easily-manipulated aspects of lambda like transactivation of plasmid-borne lambda promoters and easy recombinational systems, makes the lambda platform the method of choice for studying lysis and its regulation. In fact, many other phage lysis gene systems have been studied in lambda, including that of T4, by the simple expedient of replacing the lambda lysis genes with the heterologous ones (145).

The lambda "lysis cassette" consists of four genes, encoding 5 proteins (Fig. 1): *S* encodes the **holin**, or S105, and the **antiholin**, S107; *R* encodes the **endolysin**, or λ lysozyme; and the *Rz*/*Rz1* gene pair encodes two proteins that, together, comprise the **spanin** (20, 172). The current model for lambda lysis is a three step process in which each of the components of the host envelope, cytoplasmic membrane, peptidoglycan, and outer membrane, are compromised (21). The process begins when the lysis genes are turned on, along with all the genes required for morphogenesis, at about t = 8 min in the infection cycle, when the delayed early protein Q activates pR', the late promoter (188, 203). For the next 40 minutes, the lysis proteins accumulate in three different

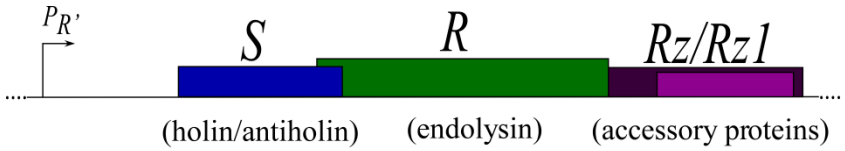

FIG 1 The lambda lysis cassette. The lambda lysis cassette is transcribed from the lambda late promoter, pR'. The S gene (blue) encodes the antiholin (107 aa) and the holin (105 aa). The endolysin gene, R (green), slightly overlaps the 3' end of the S gene. Finally, the spanin genes are encoded by Rz and Rz1 (dark and light purple, respectively). Rz1 is embedded in the Rz gene in the +1 reading frame.

subcellular compartments: the R endolysin accumulates, properly folded and with full enzymatic activity, in the cytoplasm, the holin, antiholin and Rz proteins are localized to the inner membrane with different topologies (Fig. 2), and the Rz1 protein undergoes signal peptidase II processing and sorting by the Lol system, ending as a lipoprotein attached to the inner leaflet of the outer membrane through lipoylation of its N-terminal Cys residue (21, 172).

Despite being constitutively synthesized, none of these proteins has a detectable effect on cell physiology during the latent period of the phage, which, in the case of inductions of lambda with the wild-type lysis genes, is about 50 min (188, 201). The first step of lysis occurs when, suddenly, at a programmed time, the accumulated pool of holins "triggers", causing the formation of large holes in the cytoplasmic membrane (46, 156, 193). These holes are very large (permissive for β-galactosidase; MW ~450k), non-specific, and their formation is lethal, halting all metabolic activity in the cell (187).

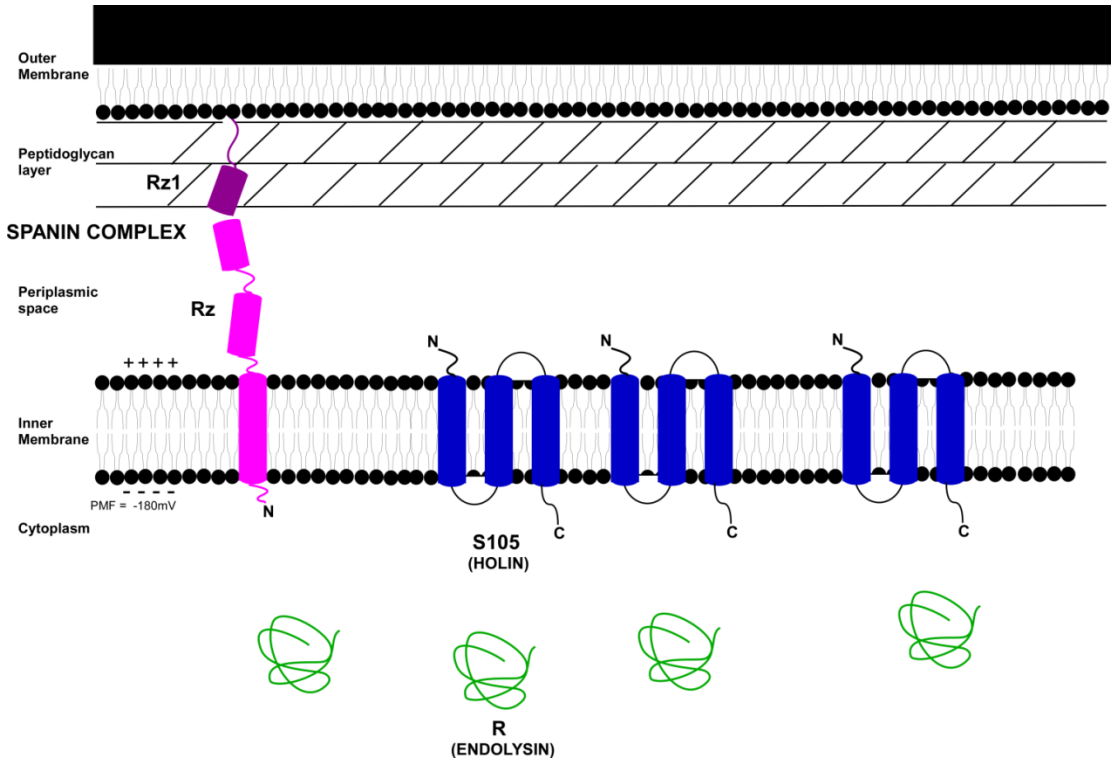

FIG 2 The lambda lysis program. The 3 physical barriers of the *E. coli* cell wall are indicated, the inner membrane, peptidoglycan layer, and the outer membrane. The holin, S (blue), is a 3 TMD protein with an N-in C-out topology that accumulates in the inner membrane. The endolysin, R (green), is a soluble cytoplasmic protein that is blocked from its substrate, the peptidoglycan layer, by the inner membrane. The spanin complex, formed by Rz and Rz1 (purple), spans the periplasmic space. Rz is an integral membrane protein with a TMD at its N-terminus while Rz1 is modified and accumulates in the inner leaflet of the outer membrane.

This membrane catastrophe allows the second step to occur; the endolysin, R, escapes from the cytoplasm and attacks the host murein, which is destroyed within seconds (76). The degradation of the peptidoglycan layer allows the third step to occur, in which the Rz-Rz1 protein complex causes disruption of the outer membrane (21). Under laboratory conditions, this step is not required for lysis, but recently acquired evidence indicates that it is an important part of the lysis program and will be discussed below (21). At the macroscopic level, lysis is observed as a very sudden drop in the turbidity of the culture, with 90% of the optical density disappearing within a few minutes (188, 203, 205). The precipitate character of this induced lysis makes this one of the few microbiological events that is evident to the naked eye, as a vigorous turbid culture in a growth flask suddenly becomes both clear and viscous.

SAR endolysins and pinholins

The canonical holin-endolysin mode of lysis is marked by the strikingly different phenotypes of knockouts in the two genes: while a mutation in either gene blocks lysis completely, a holin-defective phage has the unique property of increased virion yield (203). Hours after induction of a λS_{am} lysogen, host macromolecular metabolism continues unabated and functional virions continue to be assembled intracellularly, until the host is packed with a thousand particles or more (204). This reflects the fact that the endolysin is harmless to the cell as long as it is trapped in the cytoplasm, a trait shared by many other phage endolysins, like T4 gp*e* and T7 gp*3.5*. This ability has been exploited in the long-term and profoundly successful efforts to over-produce, purify and characterize these muralytic enzymes in detail (10, 190). However, the concept of a

universal mechanism for dsDNA phage lysis was disproven by the discovery that endolysins in some phages of Gram-positive organisms had true secretory signal sequences, despite the presence of holin genes (155). This discovery returned focus to older studies of the classic generalized transducing coliphage, P1, which retains lysis and plaque-forming ability even when the gene now thought to be its holin is deleted (89, 197). Detailed studies on the P1 endolysin, Lyz, and the endolysin of the lambdoid phage 21, R^{21}, showed that they possess an unusual N-terminal TMD, so that they are produced as type II integral membrane proteins, with their catalytic domains disposed in the periplasm (174, 196, 197). Importantly, in their original membrane-tethered form, these proteins were shown to be enzymatically inactive, which helps prevent the occurrence of premature lysis that would halt the production of virions (107, 174, 196). Unlike all other studied membrane-tethered proteins, however, Lyz^{P1} and R^{21} spontaneously escape from the membrane (107, 174, 196, 197). *In vivo*, this release occurs at a low rate as long as the cytoplasmic membrane is fully energized. However, the release of these endolysins is greatly accelerated if the membrane is disrupted or depolarized by energy poisons (107). Upon release into the periplasm, the enzymes undergo dramatic refolding, become catalytically active, and commence degradation of the murein layer (107, 174, 196). Because of their unique ability to support membrane insertion and release, these TMDs were designated SAR (signal anchor release) domains. Bioinformatic analysis reveals that SAR endolysins are, at least for phages of Gram-negative bacteria, approximately as common as the canonical cytoplasmic endolysins. For phages with SAR endolysins, the endolysin gene is essential for lysis

and plaque-formation, but the holin gene is not. Instead, the holin plays a role in the timing of lysis, as was demonstrated by studies with the holin of phage 21, S^{21} (140). Like the prototype λ holin, S^{21} accumulates in the membrane during the late gene expression period and then, at an allele-specific time, triggers hole formation (140). However, unlike the λ holin, S^{21} forms small holes that depolarize the membrane, which promotes the immediate release and consequent activation of the R^{21} SAR endolysin and immediate lysis (139, 140). As a result of this characteristic, S^{21} has been designated a **pinholin** to distinguish it from the canonical, large-hole forming holins like the λ holin (138, 140, 173).

The last step in cell disruption

Until very recently, it was thought that lysis was simply the product of the combined effects of the holin and the endolysin (201). In λ, the *S* and *R* genes are the only genes that are essential for lysis, and the only essential genes not needed for formation of functional virions (203). The immediately downstream genes, *Rz* and *Rz1*, were considered auxiliary, atypical lysis genes (203). *Rz1* is contained entirely within *Rz*, in the +1 reading frame (172). As noted above, Rz, a type II integral membrane protein, and Rz1, an outer membrane lipoprotein, interact by their C-terminal domains to form a complex that spans the periplasm (a spanin complex) (20, 21). Inactivation of either gene results in the same phenotype; in the presence of millimolar concentrations of divalent cations, thought to stabilize the lipopolysaccharide layer, infected cells progress through the first two steps of lysis, with holin-mediated hole formation and endolysin-mediated degradation of the murein, but fail to undergo lysis (21). Instead, as

seen in cryo-electron micrographs, cells become spherical double sacs, with the cytoplasmic membrane sac, permeabilized by the large holes, floating inside the intact outer-membrane sac (J. Berry, personal communication). In contrast, images of cells in which the cell wall has been degraded by a SAR endolysin and in which Rz and Rz1 are functional, show that the two membranes become disorganized and vesiculated (J. Berry, personal communication). The current model is that, once the endolysin has degraded the cell wall, the spanin complex undergoes a conformational change that brings the two membranes together (20, 21). Though an unknown mechanism, this compromises the outer membrane, possibly by local membrane fusion events, and removes the last barrier to release of the progeny virions (21). Rz-Rz1 equivalents are found in nearly all phages of Gram-negative hosts, but there is considerable variation among such genes, with at least 40 unrelated Rz families discovered thus far (172). Moreover the gene pairs, which always encode a type II integral membrane protein and an outer membrane lipoprotein, occur in three different organizations, including the fully **embedded** organization (Rz1 entirely within Rz in +1 frame), **overlapped** organization (Rz1 starts within Rz, again in +1, but extends beyond it), and **separated** organization (a separate Rz1 gene immediately distal to Rz) (172). Despite the diversity, Rz-Rz1 equivalents from different phages and different gene organizations can replace each other, irrespective of the source of holin and endolysin. However, this is only true for gene pairs, not individual Rz or Rz1 equivalents (172). Interestingly, a small minority of phages of Gram-negative hosts lack Rz-Rz1 equivalents (172). This includes the devastatingly lytic phage T1, which, because of its ability to survive desiccation and spread by

aerosolization, has probably caused more inadvertent and unwanted culture lysis in laboratories than any other phage (203). In T1, instead of an Rz-Rz1 equivalent, a natural chimera has evolved, encoded by gene *11*, which has been shown to complement the lysis defect of λ*Rz*$^{-}$*Rz1*$^{-}$ (172). Gp*11* has a "lipoprotein box", which causes it to undergo signal peptidase II processing, N-terminal lipoylation and sorting to the inner leaflet of the outer membrane, and it also has a C-terminal TMD (172). In effect, gp*11* encodes a single component spanin, although its protomeric topology is very different from the λ Rz-Rz1 spanin complex (172). It is thought that this single member spanin functions analogously to the Rz-Rz1 spanin, causing disruption of the outer membrane after endolysin-mediated removal of the cell wall (172).

Holin function and regulation

Thus far, a three-step lysis process has been described in which the second step, degradation of the murein layer by the endolysin, and the third step, disruption of the outer membrane by the spanin, follow sequentially after holin triggering. The timing of lysis thus depends on the regulation of the holin protein, and since expression of all the lysis genes is constitutive, this regulation must be at the level of protein function. The suddenness and temporal entrainment of the process was made dramatically evident by the microscopic examination of cells tethered to a glass slide by antibodies against the flagellum (76). Induction of the lambda lysis genes had no effect on the rotation speed of the tethered cells until, approximately one half-hour after induction, the cells suddenly stopped spinning, underwent a change to spherical morphology and lysed within seconds (76). These and other experiments have shown that the accumulation of the holin has no

effect on membrane integrity until the instant of triggering (193). Mutational analysis of λ S has shown that single missense changes in any of the three TMDs, which comprise most of the protein's length, as well as in the short cytoplasmic and periplasmic domains flanking the TMDs, cause unpredictable changes in lysis timing without affecting protein synthesis or stability (74, 75). This was unexpected; proteins involved in forming channels have significant fraction of the surfaces of their TMDs facing the lipid environment, where conservative hydrophobic changes in side chains typically have no effect on function (181). Similarly, malleability in the triggering time has been demonstrated for other holins, including, as described below, the T4 protein (138, 146). It has been suggested that this malleability is a fitness factor, and the ecological and evolutionary implications of this possibility will be considered below, with the focus on the T4 holin (207).

It is also clear that holin timing depends on the energized state of the membrane. For every holin tested to date, collapsing the membrane potential by chemical means causes instantaneous triggering (38, 49, 67, 92). Indeed, titration with the uncoupler dinitrophenol (DNP) was used to demonstrate that all that is required for triggering the lambda holin is a reduction of the proton motive force (pmf) by about 30%, which explains why it is impossible to collect phage-infected cells by centrifugation without causing lysis (76). Although the physical basis of the pmf-sensitivity of holins is not understood, it is clear that this makes holin triggering "all-or-nothing"; if holins are able to trigger and form a hole in one part of the cell, all the other holins in the same cell will be triggered simultaneously (188).

Antiholins

The *S* gene of λ encodes both the holin, S105, and the antiholin S107, through dual translational starts (Fig. 3A) (24, 25). Multiple lines of evidence indicate that the N-terminal TMD of S107 is blocked from entering the bilayer because of the extra positive charge at its N-terminus (Fig. 3B) (24, 29). However, collapsing the

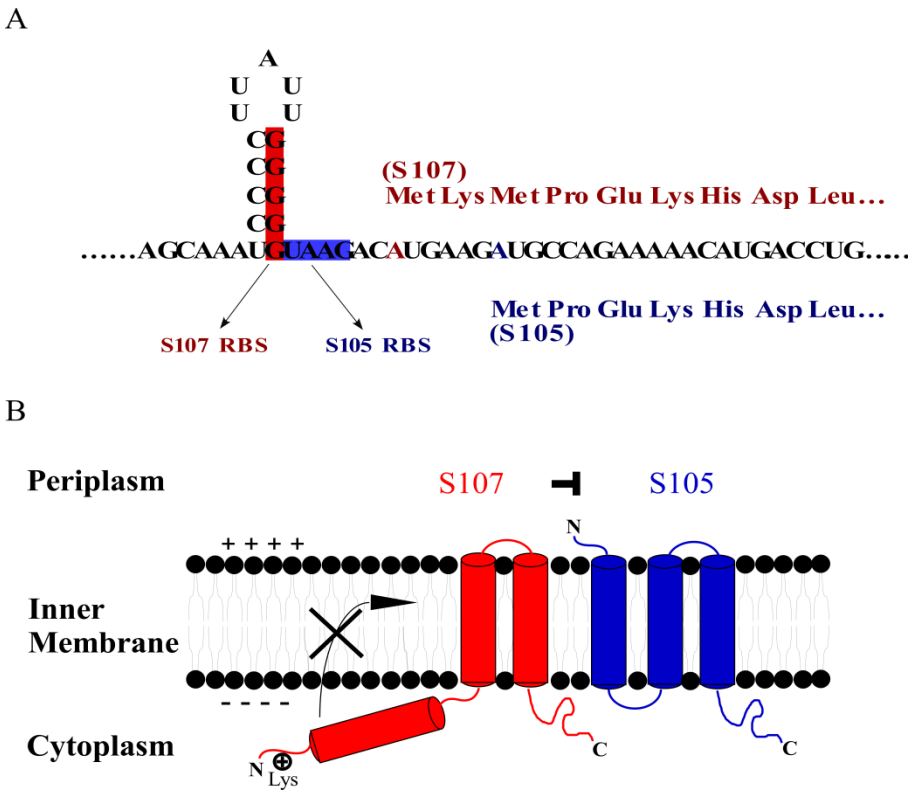

FIG 3 Dual translational start of the S gene encodes both the antiholin and holin. (A) The antiholin (S107) and holin (S105) are encoded by the S gene and differ by only 2 residues at the N-terminus. These 2 genes are served by overlapping ribosomal binding sites, yielding 2 proteins in a nearly 2:1 ratio (105:107). (B) By virtue of a positive charge at its N-terminus, the first TMD of S107 (red) cannot partition into the inner membrane. S105, however, has all 3 TMDs in the inner membrane and is functional as a holin that is inhibited when bound to the 2 TMD S107 antiholin.

membrane potential causes S107 to trigger and form holes, presumably because the N-terminal TMD is able to penetrate the membrane, and eliminate the topological differences between S105 and S107 (194). S107 forms heterodimers with S105, and it appears that these heterodimers do not contribute to lysis timing (77). Because the normal ratio of S105 to S107 is about 2:1, effectively half of the S105 that is produced accumulates in an inactive form until, at the instant of hole-formation, the de-energization of the membrane allows it, as well as the S107 protein, to be converted into the active form (77, 194). This is another level of regulation that contributes to the saltatory nature of holin function.

Two other antiholins have been characterized: the antiholin of phage 21, which is also the product of an alternative translational start in the holin gene (140, 141), and the antiholin of phage T4 (144) (see below). In the case of $S^{21}71$, the antiholin partner for the holin $S^{21}68$, the inhibitory character also depends on the extra positive charge at its N-terminus. However, at the molecular level, the inhibitory character of the antiholin comes from the inability of its TMD1 to escape from the bilayer, rather than enter it (138, 140, 141). The normal pathway towards hole-formation for the $S^{21}68$ holin is that its TMD1 exits the membrane and homodimerizes with the TMD1 of another molecule (138, 141). Hole-formation is then accomplished by TMD2 alone; $S^{21}71$ is retarded in this process. Its ability to inhibit hole-formation may derive again from the formation of inactive heterodimers with $S^{21}68$ (138, 139).

Holin structure

The first structural information for any holin was obtained for the λ holin, S105. Observed with high-resolution cryo-electron microscopy, S105 was shown to form large oligomeric rings in dodecylmaltoside (156). Whether these rings, which are estimated to contain >70 molecules of S105, are related to the structure of S-holes *in vivo*, was not clear until recently, following *in vivo* characterization of the lethal hole (see below). The rings are not formed by a defective S105 allele, A52V, which is blocked at dimer formation *in vivo*, and the S105 proteins in these rings have proteolytic susceptibility that is indistinguishable from S105 in membranes (156, 193). However, although the rings have an unprecedentedly large central hole (8.5 nm), they are not large enough to account for the unhindered release of molecules the size of β-galactosidase (156). These structures may represent a minimum energy structure for the arrangement of the protomers, S-holes, which is a hypothesis supported by the observation that assemblies with both 18-fold and 20-fold symmetries were observed (156).

Recent studies to characterize the holin-induced lesion in the inner membrane of *E. coli* have elucidated the structure of the lethal hole. Cryo-electron microscopy was used to visualize cells induced for the λ S holin alone from a low-copy plasmid (46). Cells induced for the holin appeared to have continuous perturbations in the inner membrane (46). Using cryotomography techniques, these perturbations were reconstructed, revealing the largest inner membrane channels ever observed, on the order of 300 nm in diameter (46). As opposed to the *in vitro* purified S rings, these lesions are large enough to allow for the release of the endolysin-β-galactosidase tetramer (46, 187).

In summary, any model for holin function has to account for these key features of holin function: the ability of holins to accumulate in the membrane throughout the latent period with absolutely no effect on membrane integrity, the ability to trigger to the "hole" state at virtually the same time after the beginning of the infection cycle in every cell, the aforementioned malleability of the triggering time, and of course, the ability to form such large, non-specific holes. This is particularly daunting considering the considerable diversity of holins, which, at last count, have been identified in more than 50 unrelated sequence families and three or more different membrane topologies (202).

T4 lysis genes

As a phage of a Gram-negative host, T4 has four core lysis genes: *t*, encoding the holin, *e*, encoding the endolysin, and *pseT.3* - *pseT.2* encoding the Rz and Rz1-type proteins, respectively (172, 203). Unlike most phages, these lysis genes are unlinked, scattered about as far apart as possible on the genome (124) (Fig. 4). In the following, each of these core lysis genes is described in detail.

T4 lysozyme

Gene *e* is expressed as a late protein, served by several later promoters. Its product, the well-studied T4 lysozyme, or gp*e*, has been characterized in terms of structure-function relationships probably more extensively than any other protein, primarily by the laboratory of B. Matthews (10, 122). It is far beyond the scope of this chapter to describe all of the lessons learned about protein folding from this prodigious, long-term effort. Instead, it is useful to highlight the properties that are relevant to the host lysis event. First, it accumulates in the cytoplasm during the late gene expression

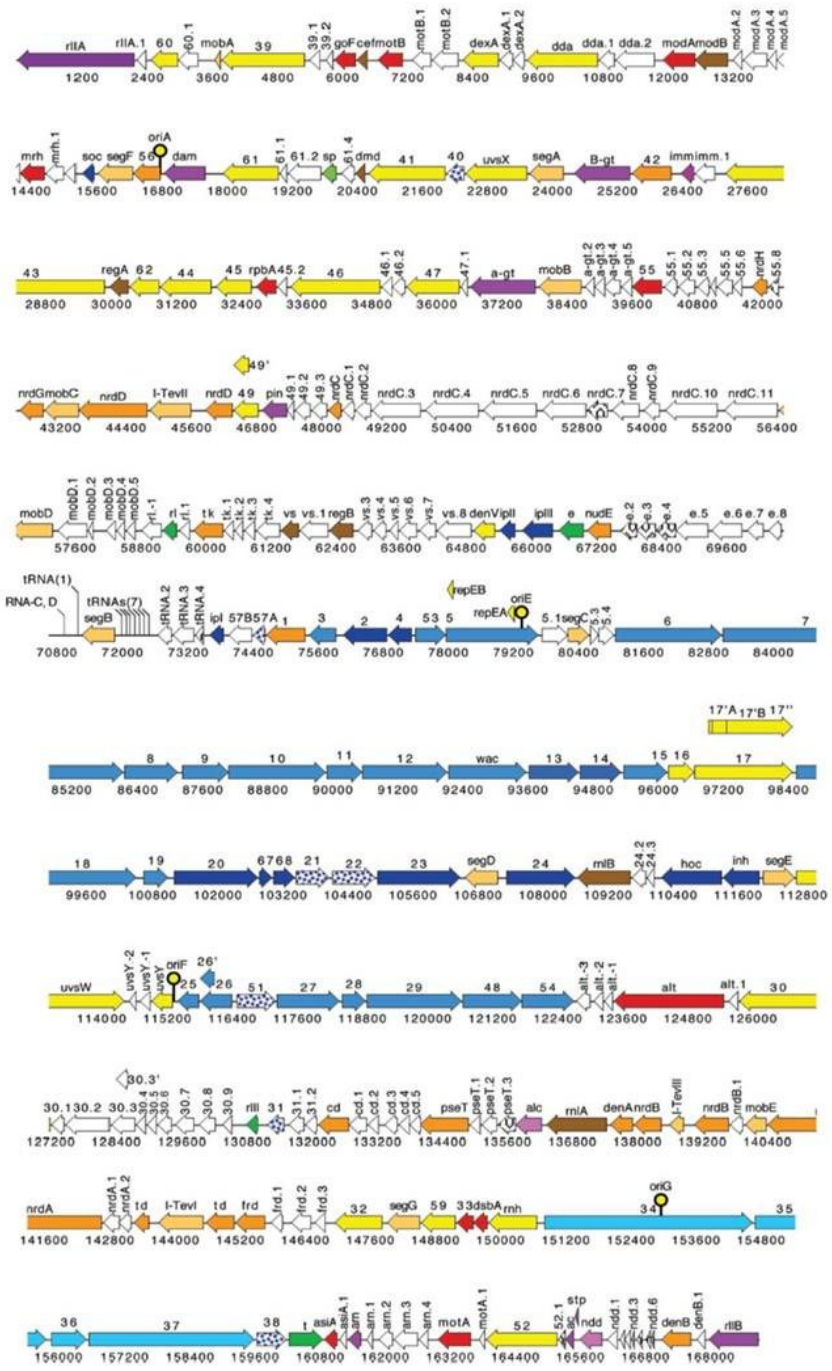

FIG 4 The genome map of bacteriophage T4. Lysis genes are colored green and are not clustered in a cassette like the bacteriophage lambda lysis genes. Note: the spanin genes, pseT.3 and pset.2, located between *alc* and *pseT* (bp 134400-155600), are colored white since their function was unknown when the original publication containing this genome map was published (124).

period as a fully folded, active protein of 163 residues (18 kDa) (203). It is roughly globular in shape, with two prominent domains, a ~7 kDa N-terminal domain (NTD) containing the catalytic residues, and ~9 kDa C-terminal domain (CTD) and connected to the NTD by a long alpha-helix (190). Enzymatically, gp*e* is a muraminidase, hydrolyzing the glycosidic bond between the C6 of N-acetylmuramic acid and C1 of N-acetylglucosamine residues in the murein (203). A triad consisting of Glu10-Asp20-Thr26 has been implicated in catalysis. Oddly, despite being arguably the most thoroughly studied enzyme in biology, the classic enzymatic constants, K_m and turnover number, are unknown, since a chemically defined murein substrate is unavailable. Indeed, the most common assays are based on lysis of bacterial cells from the outside, either using Gram-positive cells like *M. luteus* or *E. coli* cells in which the OM has been compromised, or on release of reducing units or fluorescently-labeled oligosaccharides from murein preparations, so activity measurements are defined as relative activities (10).

The smallest diameter of gp*e* is roughly 3 nm (187, 190). This size, coupled with its profoundly stable fold and lack of any secretory signal, makes it dependent on disruption of the cytoplasmic membrane for access to its substrate, the peptidoglycan. This, of course, is the role of the holin.

Finally, there has recently been dramatic progress in visualizing the structure of the T4 tail and the injection machinery, including the "puncturing device", which includes gp*5*, the "tail lysozyme" (8, 96). Within this ~60 kDa protein is a gp*e* homolog responsible for local degradation of the murein during the injection process (8, 96, 175).

In the absence of gp*e*, mutations in genes *5* and *sp* can restore plaque-forming ability, although lysis is very inefficient (59, 203). Gp*sp* is thought to inhibit the gp*5* lysozyme after injection. In the mutants, some unassembled gp*5* presumably leaks through the holin-lesion and attacks the cell wall (93, 95, 134). This shows how unreliable plaque-forming ability can be in studying lysis itself; lysis of only a fraction of the infected cells, or release of only a fraction of the accumulated phage, still leads to a plaque. Interestingly, Heineman et al. (80) used serial passaging to show that the virion-associated lysozyme of phage T7, gp*16*, can be evolved to replace gp*3.5*, the T7 endolysin. Indeed, there are phage genomes in which the virion-associated lysozyme may normally play dual roles, in both injection and lysis (80, 125).

The T4 holin, T

Genetics and protein structure

Gene *t* is located at the end of a cluster of tail fiber genes in the genome of T4 (Fig. 4); it has a consensus late promoter immediately in front and a strong predicted rho-independent terminator immediately following, between it and the *asiA* gene transcribed from the opposite strand (124). There are also predicted promoters and terminators upstream. Gp*t* has not been detected *in vivo* in T4- infected cells and whether it has any transcriptional, translational, or post-translational regulation, beyond being a late gene, is unknown (146). Gene *t* encodes a 218 residue polypeptide that accumulates in the cytoplasmic membrane when expressed from an inducible plasmid (115) or in the context of the lambda late promoter (145). As in λ *S*, nonsense mutants in T4 *t* have a lysis defect and cause the accumulation of virions in excess of the normal

burst size (91, 92). That this was not widely appreciated early on is partly due to the fact that the two amber mutants used to define *t* genetically (91, 92) are located at codons 87 and 209 and retain partial lytic function (53, 146). Expression of a plasmid clone of *t* resulted in complementation of the lysis defect of an induced λ*Sam* prophage, indicating that *t* encoded a holin protein (145). This character was thoroughly explored, along with other properties of *t*, when Ramanculov *et al.* created λ*t* chimeras in which the *S* holin gene was replaced by *t* (145). This scheme confers many experimental advantages, among which is the ability to use lysogenic induction to create a synchronous infection cycle in a culture. In this system, a nonsense codon at position 11 completely ablates holin activity in this chimeric construct (145). Other parallels with the lambda holin were established in the same system, including: the ability to substitute for the lambda holin in lysis of the host, sensitivity to premature triggering with energy poisons, and the ability to allow lytic function of non-cognate endolysins (145).

Topology

Since gp*t* is a membrane protein, analysis of its primary structure should reveal at least one TMD (Fig. 5). However, most of the sequence is highly hydrophilic and rich in charged residues, and there is only one candidate, the 21 residues from position 35 through 55, with hydrophobic character and no net charge, and even this requires that Arg50 and Asp52, despite being predicted to be on opposite sides of a TMD, are able to salt-bridge to retain overall neutrality (145, 146, 179). Gene fusion analysis confirmed this assignment, with *phoA* fusions at residue 70 and beyond exhibiting a Pho^+ phenotype; thus, with respect to the single predicted TMD, T has an N-in, C-out

topology in the membrane (146). The exact boundaries of the TMD of gp*t* have not been investigated, unlike for S105, in which the three TMDs were mapped by cysteine-scanning and accessibility studies (74). However, there is little flexibility in the TMD assignment because of the charged residues that flank the only potential TMD. The membrane topology of gp*t* is completely distinct from that of the class I and II holins, in three respects: gp*t* encodes a single TMD, and has an unusually long predicted N-terminal cytoplasmic domain (34 aa), and a large periplasmic domain (>160 aa) (203).

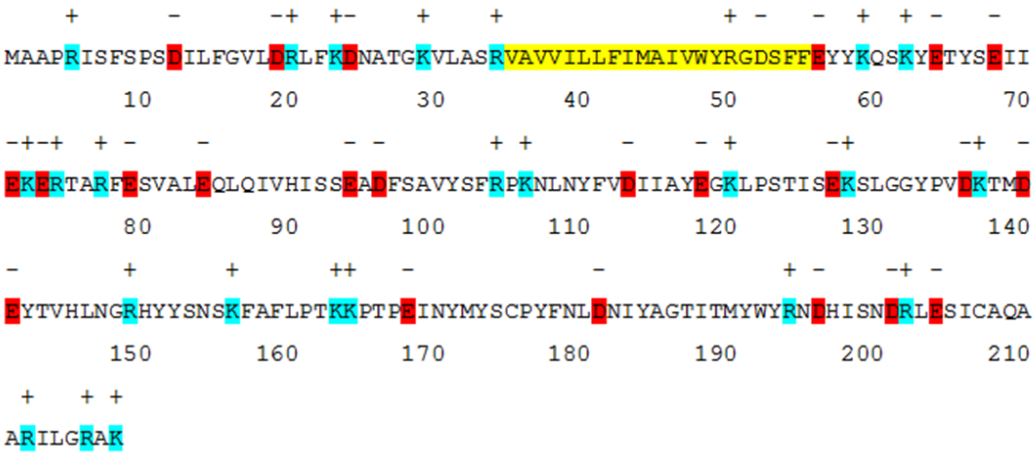

FIG 5 Sequence of the T4 holin, T. Positive charges are indicated in blue while negative charges are indicated in red. The predicted transmembrane domain is highlighted in yellow.

Mutational analysis

The gp*t* holin is also highly malleable in terms of lysis timing. In the original λ::*t* chimera, lysis occurs at 20 min after induction at which point, on average, less than 1 virion particle has been formed per cell (145). The chimera was thus not able to form plaques, facilitating selection for plaque-forming mutants. Of 116 isolated, all had missense changes in the *t* gene and exhibited delayed lysis (146). This finding highlights the exclusive role that holins have in determining the length of the infection cycle, even when operating in the context of a heterologous phage. Table 1 shows the distribution of these mutants, mutants obtained through other selections, and by directed mutagenesis. Of the mutant collection, "clock mutants" are classified as those which retain normal levels of gp*t*, as assessed by immunoblot, have a sharply-defined lysis profile in the λ context, and trigger at a time which is different from the parental triggering time. All but two of these 27 mutations map to the periplasmic domain (146). As noted by Dressman *et al.*, mutations in *t* have also been isolated in other contexts, including suppression of gene *63* defects, enhanced growth in a host marked by partially-defective *rho* termination factor, and sensitivity to hydroxyurea (53).

Deletion analysis indicates that the last ~60 residues of the periplasmic domain, if replaced with additional residues, are non-essential; greater deletions of this domain exhibit very retarded and somewhat gradual lysis (146). However, these studies were

TABLE 1 Clock mutants of T.

Amino acid change	Domain
F8S	NTD
L40F	TMD
Y57C	CTD
E73V	CTD
F78S	CTD
F78V	CTD
E79K	CTD
E84K	CTD
A95V	CTD
K106E	CTD
Y117C	CTD
P122S	CTD
S123L	CTD
S126I	CTD
L130R	CTD
T138S	CTD
T138I	CTD
H145Y	CTD
R149C	CTD
S153F	CTD
S153P	CTD
A158S	CTD
K163N	CTD
R202L	CTD
S205P	CTD
N209H	CTD
A210V	CTD

done when antibodies against gp*t* were not available, so it is not known whether the lysis defects of these deletions are due to the level of gp*t* protein or not. One mutation in the putative N-terminal cytoplasmic domain, D12C, created by site-directed mutagenesis, triggers earlier than wt (145). Thus gp*t* resembles the three other holins that have been genetically probed, in that drastically different lysis times are achievable by single missense mutations (75, 138). Gp*t* differs from the other holins discussed in that a soluble domain appears to be the primary determinant of mutational sensitivity, instead of the TMD (146). In contrast, mutations that severely debilitate gp*t*, those for which triggering and lysis are either absent or no longer sharply defined and significantly delayed, are significantly over-represented in the N-terminal domain and TMD (146). In this regard, too, gp*t* is unlike other holins, where mutations affecting timing and lytic function are dispersed throughout the sequences, which are themselves predominantly made up of TMDs (138, 193).

The drastic difference between the lambda holin, S105, and gp*t* in terms of membrane topology and amino acid sequence enabled Ramanculov *et al.* to ask the following question: if the two heterologous holin genes with different triggering times were expressed in the same cell at the same time, which "clock" would dominate (145)? The "death raft" model for S105 timing predicts that the triggering pathway for the two holins should be completely independent; since there is no effect on cell physiology or membrane energization until the instant of triggering, there is no obvious way for the two holin proteins to communicate (28). Nevertheless, when a *t* allele and an *S* allele with different triggering times were placed *in trans*, one in a lambda prophage context

and the other on a transactivating plasmid, triggering occurred earlier than with either allele alone (145). The simplest interpretation is that the two holins contributed to the same mass action pool of holin proteins; i.e., that the two holins interact somehow, either directly or indirectly. This might point to another class of model for holin timing, in which some increasing gross physical stress on the membrane determines the triggering time. In this perspective, the apparently saltatory collapse of the membrane energization observed for the induced lambda holin would be masking a deterioration in the ability of the membrane to tolerate the increasing holin-mediated stress. However, the experiments with *S* and *t in trans* were done before antibodies against the gp*t* holin were available; thus it is not possible to rule out trivial explanations involving indirect effects of the accumulation of either protein (145).

pseT.3/pseT.2: the Rz-Rz1 genes of T4

The published T4 genome possesses no *Rz*/*Rz1* equivalents (124). Because of their diversity, *Rz*/*Rz1* genes are usually identified by their proximity to other lysis genes, usually downstream from the endolysin, and by their unusual architecture, in which the *Rz1* gene is embedded within the *Rz* gene in the +1 reading frame (172). No such arrangement exists in T4, where the lysis genes are dispersed throughout the genome (124). However, a screen of all T4 reading frames for genes encoding predicted type II integral membrane proteins and lipoproteins revealed an adjacent gene pair, *pseT.3*/*pseT.2* with properties indicative of an *Rz/Rz1* equivalent (172). The upstream gene encodes PseT.3, which is 117 aa, is predicted to have a single TMD, and a periplasmic domain of 89 aa. The immediately proximal gene, PseT.2, is predicted to be

a signal peptidase II target, processed at Cys17, resulting in a mature 82 aa outer membrane lipoprotein (172). A deletion of *pseT.3*/*pseT.2* exhibited the same Mg^{++}-dependent lysis defect as characteristic of the canonical lambda *Rz* or *Rz1* mutants (172). Thus this gene pair was identified as the first separated *Rz-Rz1* equivalent, as opposed to the embedded and overlapped structures commonly found in phages of Gram-negative hosts (172). The PseT.3 (Rz-like) periplasmic domain resembles that of other Rz proteins in that it is highly hydrophilic and is predicted to be largely alpha-helical (172). One discordant note is that the nearest promoter is an early promoter, and that genes upstream (*pseT*) and downstream (*alc*) are known early genes (124) (Fig. 4). However, since the function of the PseT.3/PseT.2 spanin complex would depend on endolysin degradation of the cell wall, which does not occur until late, early expression would not be unreasonable (21). Regardless, the two proteins have not yet been detected as protein products, so direct evidence regarding the phase of expression is lacking.

Summary of the core lysis genes

The fundamentals of host lysis appear to be the same in T4 as in the canonical lambda system: the holin, gp*t*, and the Rz protein, PseT.3, accumulate in the cytoplasmic membrane, while the Rz1 protein, PseT.2, accumulates in the outer membrane and the endolysin, gp*e*, accumulates in fully active form in the cytoplasm. Presumably, PseT.3 and PseT.2 form a C-terminal to C-terminal complex spanning the periplasm and extending through the murein meshwork (21). At the programmed time, gp*t* triggers, forming holes through which gp*e* is released to attack the murein (188).

Murein degradation is followed by the actions of PseT.3/PseT.2, resulting in disruption of the outer membrane and complete lysis of the host.

Lysis regulation: the r genes

Overview

As noted above in Definitions, the *r* moniker is a misnomer; "r" stands for rapid lysis, but individual cells infected with *wt* or *r* mutant phage undergo lysis at the same time in single step infection experiments (50, 51). It is only in dense culture that the phenotype of *r* mutants is observed, in that lysis of a small fraction of infected cells leads to super-infection of the bulk culture and the imposition of lysis-inhibition, or LIN (50). Most of the attention focused on T4 lysis since the beginning of the Phage Church in the 1940s has been focused on the *r* genes. Among these, it is the *rII* locus that has been the major interest (12-17, 19, 133). A brief review of *r* biology is thus in order, to set the stage for the more recent developments; however, for detailed analysis of the *r* literature, the reader is directed to an early comprehensive review (203), and to the accounts in the two books dedicated to bacteriophage T4 (99, 120).

r loci

All *r* mutants have been isolated by screening for altered plaque morphology; *r* plaques are large and sharp-edged, compared to the small, fuzzy-edged plaques made by wild type T4 (81) (Fig. 6). The plaque morphology reflects the absence of LIN being imposed at the edges of the developing plaque, where virion and cell densities are presumably comparable to conditions of liquid cultures that are in the LIN state (203). Seven *r* genes have been identified: *rI, rIIA, rIIB, rIII, rIV, rV,* and *rVI* (58, 81, 83, 104,

106). *rV* was shown to be allelic to *t* (see below), which is not unexpected, because in the LIN system, where lysis is delayed, it is likely that this process works through the holin, the clock of the lytic process (53). Of the others, only *rI* is required for LIN in all host backgrounds, and most notably in *E. coli* K-12 (136). In fact, only *rI* and *t* are needed to re-constitute LIN in a heterologous background (144, 179). Almost all of the new information gained since the last major review (203) has been about the role of gp*rI* and its interaction with gp*t*.

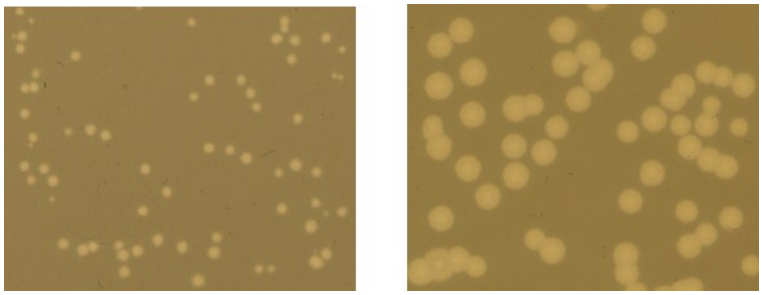

FIG 6 Plaque morphology of wild type and LIN-deficient T4. Left: Plaques of wild type T4 infections are small with fuzzy edges. Right: Plaques of LIN-deficient T4 infections result in large plaques with sharp edges.

rI: the T4 antiholin

Two major steps forward in the elucidation of the T4 lysis system and the LIN state were achieved by Paddison et al. (136) and Dressman and Drake (53), who, by mapping and sequencing both canonical and newly-isolated *rI* and *rV* alleles, identified their respective genes in the T4 genome. The *rI* reading frame encodes a short 97 residue polypeptide with a hydrophobic N-terminal domain, originally predicted to be a transmembrane domain (124) or a secretory signal sequence (136) by several different primary structure algorithms. Most of the canonical *rI* absolute-defective mutants were shown to be frameshift nulls, even as distal as codon 87 (26). In addition, there was a single missense change, R78P and a single in-frame deletion, ΔI92, serving to emphasize the importance of the C-terminus of this short polypeptide (144). The *rV* mutations mapped within the 218 codons of gene *t* (53). All were remarkably conservative (the original *ts* allele, R5K, and two unconditional alleles: I39V, and T75I) changes within the N-terminal domain of gp*t*, leading Dressman et al. to suggest that gp*rI* binds to this domain when it effects LIN (53). Moreover, all three exhibited co-dominant *r* character in mixed infections with t^+ (144).

Using the λ::*t* chimeric system described above, Ramanculov *et al.* (145) were able to reconstitute LIN by super-infecting induced λ*t* lysogens with T4 and showed that LIN depended on the allelic state of *rI* and *t* (145). Most impressively, T4 superinfection of induced lysogens in which the prophage carried lysis-proficient, LIN-defective *rV* alleles of *t* did not result in LIN (144). Moreover, LIN could only be imposed if incoming T4 phage carried a LIN-proficient *t* allele, even if the induced chimeric

prophage was t^+. This led to the idea that only newly made gp*t* can receive the LIN signal, even though pre-existing gp*t* is fully capable of supporting lysis (144). This system was also used to identify more *t* LIN mutants within a collection of delayed-lysis *t* alleles; of nine such alleles tested, all were LIN-defective and mapped to the periplasmic domain of gp*t* (146).

The ability to reconstitute LIN was further refined by substituting a plasmid carrying *rI* for the super-infecting T4 phage, thus eliminating the difficulties associated with T4-mediated host gene shut-off (144). Remarkably, expression of LIN-proficient *rI* alleles in trans to the induced λ::*t* chimera resulted in a full LIN state, susceptible to instantaneous collapse by energy poisons and sensitive to the allelic state of both *rI* and *t* (144). Thus not only are *t* and *rI* the only genes required to establish LIN in T4 infections but also the same two genes are capable of imposing LIN on the lambda infection cycle. The control experiment, with *rI in trans* to the parental lambda with its cognate holin gene, showed no LIN (144). Moreover, using a relatively poor antibody raised against an OmpAΦT fusion protein, Ramanculov *et al.* found that, during the extended LIN infection cycle, gp*t* continued to accumulate and formed SDS-resistant oligomers in the cytoplasmic membrane (144). In addition, using cross-linking, direct evidence was obtained for the formation of gp*t*-gp*rI* complexes. By several criteria, including that gp*rI* binds to gp*t*, blocks its hole-formation function specifically, and does so in a manner that requires continued membrane energization, gp*rI* satisfies the definition of the T4 antiholin (144).

Mechanistic aspects of the holin-antiholin interaction

Tran *et al.* further exploited the chimeric λ::*t* system to probe the molecular basis of the gp*t*-gp*rI* interaction (179). By dissecting gp*rI* into a hydrophobic N-terminal domain (gprI^{NTD}) and hydrophilic C-terminal domain (gprI^{CTD}) and making hybrids between these domains and the complementary domains of the canonical periplasmic protein, PhoA (alkaline phosphatase), it was shown that periplasmic expression of the latter in the presence of LIN-competent gp*t* was necessary and sufficient to establish LIN (179). A similar topological dissection was done with *t*, generating a chimera with the PhoA signal sequence fused to the gpt^{CTD} (179). It was shown that over-expression of this chimera abolished LIN in T4 infections and conferred *r* morphology on wild-type (wt) T4 plaques, suggesting that the secreted gpt^{CTD} could titrate out the available gp*rI* in infected cells (179). Interestingly, the presence of gp*rI* seemed to interfere with the signal sequence cleavage of the $phoA^{ss}$-gprI^{CTD} chimera, suggesting that the gp*rI* interaction occurs with the nascent holin (179).

A major technical block in these studies has been the difficulty in detecting gp*rI*. Although gp*rI* could be detected by immunoblot in whole cell samples, it proved to be too unstable to monitor in subcellular fractionation (180). However, fusing green fluorescence protein (GFP) to the N terminus of RI resulted in a more stable chimera that could be shown to form complexes with gpt^{CTD} (179). The binding was unaffected by the *rV* mutation, T75I, suggesting that it is the response of gp*t* that is compromised in this mutant. With the *rI* missense mutant, R78P, no protein could be detected despite the GFP-mediated stabilization, which suggests that the Pro substitution is not tolerated in

the gp*rI* structure (179). Thus the model that emerged was that gp*rI* binds to gp*t* by interactions between the CTDs of the two proteins.

A remaining issue, whether gp*rI* possessed a secretory signal sequence, and thus would be processed by leader peptidase, or whether it was a type II integral membrane protein, was also addressed by the gene fusion approach (180). Surprisingly, neither model was correct; instead, the N-terminal segment of gp*rI* was found to be a SAR domain, so that gp*rI* is initially exported to the periplasm tethered to the cytoplasmic

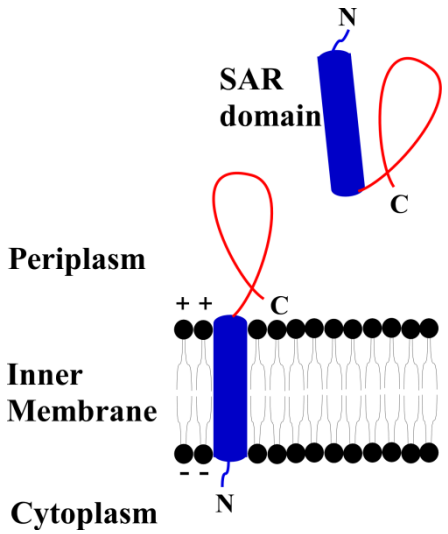

FIG 7 The N-terminal domain of RI is a SAR domain. The signal-anchor-release (SAR) domain of RI, indicated in blue, can spontaneously escape the inner membrane, resulting in a soluble RI in the periplasmic space. The periplasmic domain of RI is indicated in RI.

membrane and then is released to the soluble phase, without proteolytic processing (180) (Fig. 7). Moreover, subverting the SAR character by progressively substituting Leu residues for less hydrophobic amino acids progressively reduces the ability of gp*rI* to inhibit gp*t*-mediated lysis, indicating that the release into the cytoplasm is critical for gp*rI* function (180). In addition, the SAR domain confers significant proteolytic instability on gp*rI* ($t_{1/2}$ ~2 min); replacing it with the cleavable signal sequence from PhoA and blocking membrane release by Leu-substitution both greatly increases its stability, although only the former increases its function *in vivo* (180). A prominent periplasmic protease DegP was implicated in gp*rI* degradation, which is retarded significantly in a *degP* background (180). However, this stabilization is not reflected in lengthening of the functional half-life of gp*rI*, suggesting that functional inactivation takes place before proteolytic degradation (180).

A molecular model for LIN

Considering the paucity of molecular data, any model for LIN must be considered highly speculative. Nevertheless, a simplest-interpretation, or Occam's Razor model can be constructed from the consideration of the results summarized above and from suggestions previously elaborated (53, 136, 179, 180). In the simplest scenario, gp*rI* is produced constitutively from early in infection, initially localized to the membrane in an inactive form, then releasing to the periplasm where it can either (a) bind to the periplasmic domain of newly-made gp*t*, creating a complex that can block hole-formation or (b) become inactivated and then proteolytically degraded (180). The requirement for new gp*t* in the *rI*-mediated establishment of LIN suggests that the effect

of the antiholin is in preventing the holin from getting into a lysis-competent state (144). In view of parallels with the lambda holin and some direct observations of *t* (144), the simplest notion for this putative lysis-competent state would be a homo-oligomeric complex of gp*t*. The fact that the t_{T75I} allele is dominant to t^+ (53) but does not seem to be defective in the gp*rI*-gp*t* interaction suggests that the antiholin may cause a conformational change in the holin that blocks productive homo-oligomerization (and that gpt_{T75I} resists that change).

In this model, gp*rI* in its initial, membrane-tethered form is stable but unable to bind to the holin (180). When it is released from the membrane, it becomes competent for holin-binding but also highly unstable, both functionally and proteolytically (180). Since it is already established for P1 Lyz that a SAR protein undergoes refolding after release from the membrane (196), it is not unreasonable to suggest that this instability represents refolding of newly released gp*rI* into an inactive, proteolytically sensitive form, perhaps because of the sudden and proximate availability of the SAR domain. The simplest notion is that the LIN signal increases the functional stability of gp*rI* and thus increases the formation of gp*rI*-gp*t* complexes (180). In this model, the lability of the LIN state, which requires continuous infection for its maintenance, could reflect an equilibrium state of gp*t*-gp*rI* complex formation; if gp*rI* dissociates, it would be subject to the same potential rapid inactivation unless the LIN signal is maintained (Fig. 8).

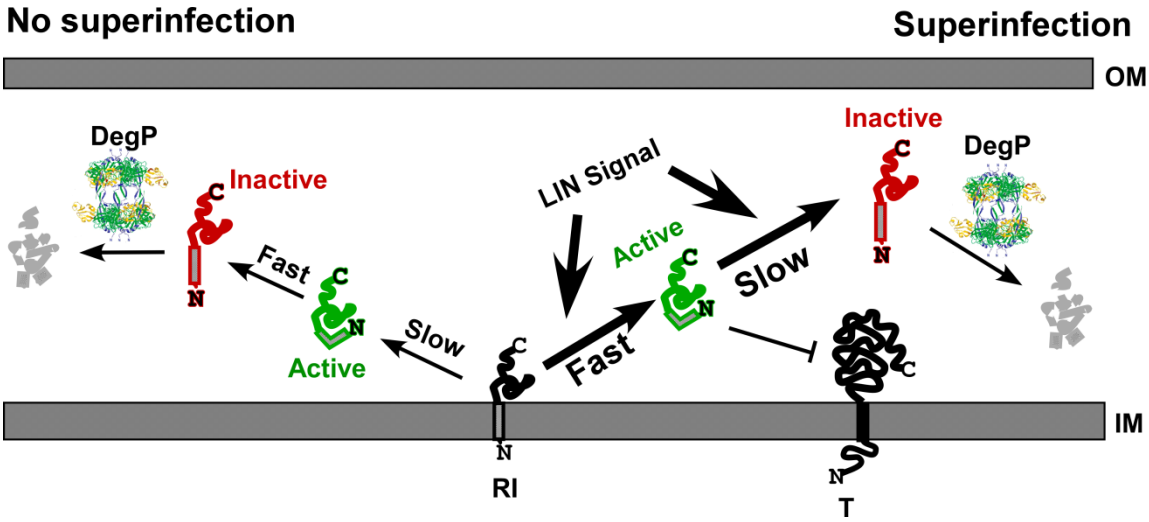

FIG 8 Model for lysis inhibition. RI, tethered to the inner membrane (IM), is spontaneously released and quickly functionally and proteolytically inactivated when no superinfection/LIN signal exists. The membrane-tethered form of RI is not competent for inhibiting the holin. When superinfection occurs and a LIN signal exists in the periplasmic space, the released RI is active and competent for LIN (180).

The LIN signal

How can super-infecting phage particles, but not ghosts, effect stabilization of gp*rI*? The simplest possibility is that something in the intact capsid, but not in ghosts, is involved: the DNA or the internal proteins (136). This in turn suggests that it is ectopic localization of the capsid contents, either the massive DNA molecule or the >1000 copies of the internal protein species, that is the signal for LIN (136). Since all T-even phages can induce LIN in T4-infected cells, and since most of the internal proteins are highly variable within the T-even family, the DNA may be the best candidate (136). If a single T4 chromosome is mislocated to the periplasm, which has ~10% of the volume of the cytoplasm, the concentration of DNA, in terms of nucleotides, would be ~3.5 mM, or

~1000 μg/ml. It is apparent that this high concentration can have dramatic effects on many aspects of the periplasm, including its proteolytic character.

Ectopic localization of the super-infecting DNA may be the most attractive candidate for the LIN signal, but the mechanism is unclear. Two genes, *imm* and *sp*, have been under scrutiny for this phenomenon (134). The Imm protein is absolutely required for super-infection exclusion and seems to provide some protection against ghost killing (36). It is an 83 residue protein that accumulates in the cytoplasmic membrane from early in infection (117, 124). Most significantly, Lu and Henning presented elegant and compelling micrographs showing that superinfecting T4 DNA, pre-labeled with a fluorescent DNA stain, enters cells infected by T4*imm* but not T4wt (114). However, T4*imm* mutants have been reported to be fully LIN+ (36). *sp*, originally identified as a locus for mutations that suppress lysozyme defects (59, 60), is absolutely required for protection from ghosts. Moreover, at least at 37°C, *sp* mutants make *r* plaques and are LIN-incompetent in liquid infections (36). Genomic analysis has established that *sp* is allelic to *rIV*, identified along with *rV* (= *t*) by Krylov and colleagues as a locus for temperature-sensitive *r* plaque morphology mutations (105, 106). It is predicted to be a 97 aa type II integral membrane protein, identical in size and similar in membrane orientation to gp*rI*. However, no direct experiments to test whether *sp* is also required for the injection of superinfecting DNA have been reported, or even experiments testing whether *sp* is required for LIN on all *E. coli* strains, as is the case for *rI* and *rV* (*t*) but not the other identified *r* genes (136).

The other r genes

Benzer's rII genes

To this point, the Occam's razor model for T4 lysis and LIN specifies essential roles for four genes: *t* (*rV*), encoding the holin, *rI*, encoding the gp*t*-specific antiholin, *e*, encoding the endolysin, and *pseT.3* and *pseT.2,* encoding the spanin genes. Additionally, there are potential roles for *sp* (*rIV*) and/or *imm* in transducing the LIN signal, i.e., the presence of super-infecting T-even phage. There remain four other loci which have been reported to have *r* plaque phenotypes: *rIIA*, *rIIB*, *rIII*, and *rVI*. The most widely studied of these are of course, *rIIA* and *rIIB*. Upon infection by T4*rII* on *E. coli* B lawns, r-type plaques appear; however, T4*rII* mutants do not exhibit any plaques on *E. coli* K-12(λ) (13, 52, 82). The *rII* locus is actually composed of 2 genes (*rIIa* and *rIIb)* as was elegantly shown by Seymour Benzer (17, 18). The gene product of *rIIa* is composed of 725 amino acids while the gene product of *rIIb* is composed of 312 amino acids. Additionally, both of these gene products are highly charged with both containing nearly 27% charged amino acids (both positive and negative) (Fig. 9). Neither visual inspection nor computational prediction of either of these sequences reveals membrane spanning domains, but previous data have shown that both of these proteins are associated with the inner membrane (61, 86, 192).

rIIa and rIIb requirement in infection of *E. coli* K-12 (λ)

Nearly 65 years after their discovery and extensive genetic analysis, the molecular mechanism of *rIIa* and *rIIb* function has yet to be characterized, other than

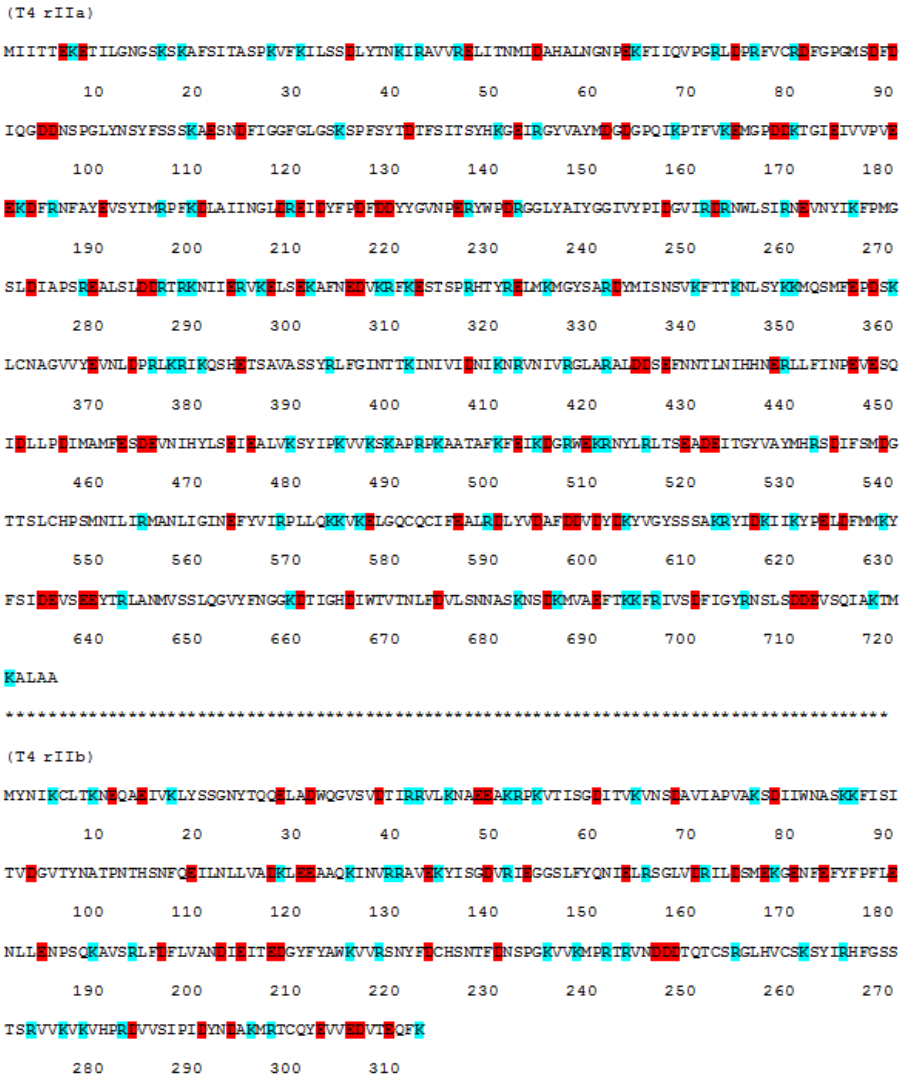

FIG 9 RIIA and RIIB sequences of phage T4. Positively charged residues are highlighted blue while negatively charged residues are highlighted red.

their essentiality by T4 to avoid exclusion by *E. coli* K-12(λ). *rII* mutants cannot grow on λ lysogens; the infection is instead aborted nearly 10 minutes post infection, yielding no viable phage and no plaques on bacterial lawns (66). In the first 10 minutes, the infection proceeds like a wild type T4 infection, with T4 DNA synthesis proteins being expressed as well as other normally expressed early gene products being translated. However, after 10 minutes, DNA and protein synthesis abruptly stops and cell respiration ceases. This abortive action can be bypassed with the inclusion of divalent cations (Mg^{2+}) and the exclusion of monovalent ions (Na^{+}) in the growth medium (66).

Lambda mutants deleted for a small region of the genome, however, are defective in the exclusion of T4*rII* (85, 94). This region contains the lambda repressor (*cI*) transcribed from the repressor maintenance promoter (P_{RM}), but the *rII* exclusion (rex) factor is distinct from *cI* (78, 85). Rex is composed of 2 genes, *rexA* and *rexB* (109). RexA is a protein with 279 amino acids and based on sequence analysis accumulates in the cytoplasm. RexB, on the other hand, partitions into the cytoplasmic membrane, based on sequence analysis of its 144 amino acid content. Additionally, it is predicted that RexB contains four membrane spanning domains (142). Both genes appear to be transcribed evenly during lysogeny and presumably yield equivalent quantities of the gene products. During lytic growth however, RexB transcription is greater than RexA due to the action of an additional promoter, P_{lit} upstream of *rexB* (109, 123) (Fig. 10).

Both RexA and RexB are required for the exclusion of T4*rII* as well as other phages. Other lysogenic phages that exclude phage infections also have *rexA* and *rexB*-

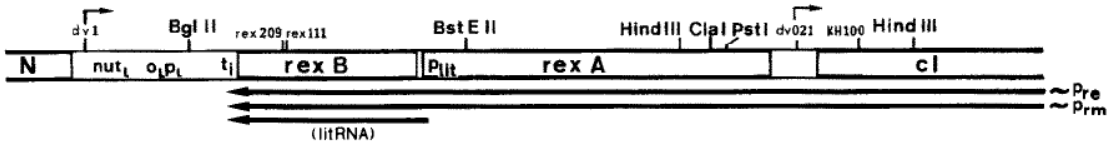

FIG 10 λ region containing cI. λ region containing cI. RexA and rexB with promoters labeled. Transcripts from both promoters are below coding region (109).

like genes in their genome with the same type of transcriptional regulation as lambda. These genes are always linked; they are either both present in the genome in phages proficient in exclusion, or they are absent in those that cannot exclude phage infections (123). These observations led to the conclusion that the two gene products interact with each other to function in the exclusion of phage infection. Overexpression of both of these genes from a plasmid system (with equal ratio of protein made) not only excludes T4*rII* phage infection but also wild type T4, showing that there is a quantitative relationship between the rex and rII genes (158). Additionally, overexpression of RexA alone from a plasmid system in a lambda lysogen ([RexA] >> [RexB]) leads to an abortive infection phenotype without phage superinfection (166). This leads to the conclusion that the *rII* gene products interact with RexA and/or RexB to inhibit their function on a cellular target.

Parma and coworkers in 1992 focused their work on RexB. First, they showed that RexB is an integral membrane protein with 4 transmembrane domains using various PhoA fusions. Additionally, they showed that RexB is targeted to the inner membrane of the bacterial cell (142). Finally, plasmids carrying *rexB-phoA* were transformed into

E. coli cells lysogenic for lambda. Surprisingly, overexpression of RexB in these lysogens did not exclude the infection of a *rII* deletion mutant nor of T4 wild type (as expected). The *rexB* in these plasmids was sequenced to ensure that it was wild type. While T4 *rII* gene products are not expected to cause overexpression of RexB upon infection, the P_{lit} promoter of lambda that expresses RexB exclusively gives us a clue as to how RexB concentrations could exceed those of RexA. This promoter is used by lambda to ensure that, once induced, lambda does not exclude itself.

A potential mechanism by which the *rex* and *rII* genes interact was also proposed by Parma and coworkers. They believe that RexB is an ion channel protein that causes the cell to leak to death. RexA is triggered to act once T4 infects and signals RexB to open this channel. More than one RexA is needed to activate RexB due to the known ratio of RexA/RexB needed to cause exclusion. The rII gene products serve to block leakage by RexB or to inhibit RexA from signaling RexB, allowing T4 phage propagation (142, 159).

The signal for the activation of this 2-component regulatory system by phage infection may be a DNA-protein complex arising during replication and recombination of phage DNA (165). An indirect observation of this is that phage infections by T4*rII* of lambda lysogens proceed like wild type infections for about 10 minutes. Once DNA replication and recombination ramp up (around 10 min past infection), the infection is quickly halted. A direct piece of evidence that such a DNA-protein complex signals the activation of RexA/RexB comes from the observation that UV irradiation of cells lysogenic for lambda (expressing RexA/B) in the dark triggers a loss of membrane

potential (similar to the exclusion of a T4*rII* infection) (111, 165). In the dark, the photolyase forms a complex with pyrimidine dimers (hence a DNA-protein complex) that resembles a DNA-protein complex during replication/recombination (111, 165).

The most recent work done on the effects of RexA and RexB on T4*rII* infection comes from Sidney Hayes' lab. These papers represent the bulk of work done on this system in the past 20 years. Slavcev and Hayes' work represents a paradigm shift in the thinking of what occurs during a T4*rII* infection of K-12(λ). While most work up to 2002 supports the theory that RexA and RexB impart an altruistic death mechanism to prevent the spread of T4 in a bacterial culture, Slavcev and Hayes contend that RexA and RexB actions do not cause death of the infected cell; instead, the cell is shunted into stationary phase (161). Lambda lysogens (Rex^+), lysogens with defects in either Rex gene (Rex^-), or non-lysogens were infected with T4*rII* in liquid culture (MOI=10) and then spread plated to observe bacterial colony formation. As expected, Rex^- lysogens and non-lysogens resulted in no colonies on the plate (cells lysed) after 24 hours. Rex^+ lysogens also resulted in no colonies after 24 hours; however, further incubation of the plates at 37˚C resulted in small colonies (161). The number of colonies appearing after nearly 48 hours of incubation represented approximately 40% of the colonies that appeared on plates containing uninfected cells. Their findings suggest that *rex* confers a symbiotic relationship with the host, preventing a secondary infection by providing the T4*rII* infection an inhospitable environment. This action can lead to death in a part of the infected population, but overall, Rex action is protective rather than suicidal. This conclusion is in direct contradiction to prior findings.

Further work on the imposition of stationary phase was conducted in 2003 by Slavcev and Hayes (162). Microscopic investigation of lambda lysogen cells (Rex^+) infected by T4*rII* revealed that cells contracted, formed aggregates, and shed flagella (Fig. 11). Additionally, lambda lysogenic cells defective in RpoS, the sigma factor responsible for stationary phase gene expression in *E. coli*, revealed a much lower survival of cells when infected by T4*rII* compared to cells with wild type RpoS, further revealing that the shift to stationary phase is needed for long term survival of Rex^+ cells infected by T4*rII*.

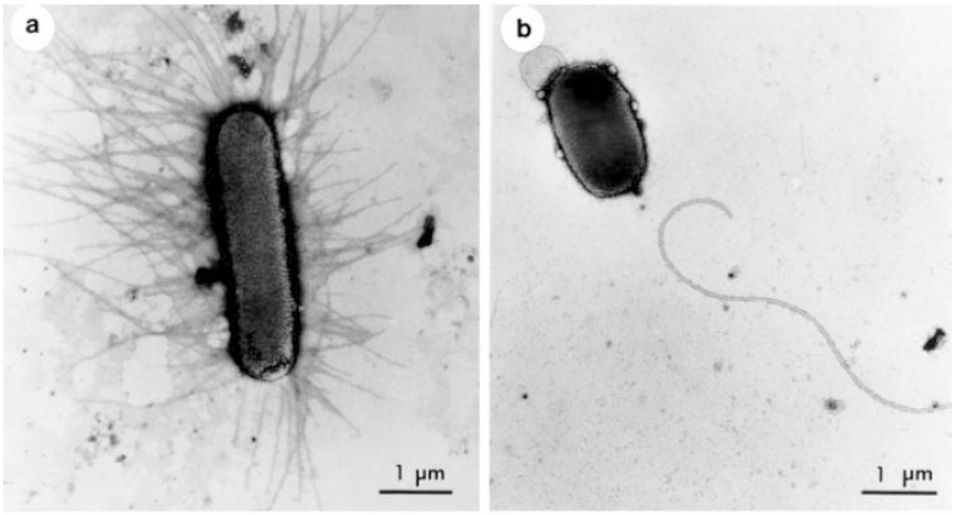

FIG 11 Infection of lambda lysogens with T4*rII* causes severe morphological defects. (A) Uninfected lambda lysogenic *E. coli* (Rex+); (B) Lambda lysogen (Rex+) infected with T4*rII* (162).

A final report by Slavcev and Hayes in 2004 studied the effect of shifting the RexA: RexB stoichiometry in infections of T4*rII*. Stoichiometry of RexA:RexB was mentioned previously in studies from Snyder, Parma, and Shinedling (142, 158, 166). These three studies showed that shifts in RexA:RexB stoichiometry imparted different phenotypes. Overexpression of RexA in the presence of lysogen-level RexB leads to the exclusion phenotype, even without T4*rII* infection (166). Overexpression of RexB in the presence of lysogen-level RexA leads to the suppression of exclusion (142). Finally, overexpression of RexA and RexB at equal levels leads to exclusion of both T4 and T4*rII* (158). Slavcev's work showed that overexpression of RexA in a Rex^+ background during T4*rII* infection nullifies Rex exclusion (160). This is in direct contradiction to Snyder's work showing that the overexpression of RexA alone, even in the absence of T4*rII* infection, exhibited the exclusion phenotype.

rIIa and rIIb requirement in infection of *E. coli* B

While T4*rII* infections are aborted on *E. coli* K-12(λ), infection of *E. coli* B by *rII* mutants leads to the formation of *r* type plaques (large with sharp edges). Growth of *rII* mutants in B is much less studied than the mutant phenotypes in lambda lysogens. However, Paddison and coworkers showed that rII^- infection leads to gradual lysis of *E. coli* B nearly 5 min earlier than wild type T4 and rI^- when infected at a low MOI (136).

The *E. coli* B strain does not have a λ lysogen (no RexA/B), but much like K-12, it does have several defective prophage remnants. Of particular interest, as it relates to *T4rII*, is a hybrid P2 prophage that is present in the B strain. When the Bc strain, a B strain that has been cured of the P2 hybrid prophage (33), was accidentally infected by

T4*rII*, no rapid lysis phenotype appeared; instead, plaques were WT (small with turbid edges) (153). This observation was seen exclusively for *rII* mutants of T2, T4, and T6. Other *r* (*rI, rIII,* etc.) mutants behaved as expected, showing *r* type plaques on both B and Bc. The wild type phenotype of *rII* mutants on the Bc strain does not occur due to reversion since phage from these plaques, when plated on the B strain containing the prophage, show the *r* type plaques (153). Wild type P2 lysogens in strain K infected by T4*rII* do exhibit wild type plaques however, so the *r* feature is not necessarily due to an interaction with P2. Also, strain BB, which is immune to infection from the P2 hybrid prophage, and so contains at least a part of the P2 hybrid prophage, still shows wild type plaques when it is infected by T4*rII* (153).

Studies unrelated to *rII* infection of *E. coli* B may also give some insight into the mechanism of lysis employed. Genome sequences of lambda K-12 and B as well as studies related to P2 phage mutants may clarify some part of this process. Studies of the *ogr* gene of phage P2 have shown that the defective P2 hybrid phage found in *E. coli* B contains many of the P2 late genes, including *ogr,* the late gene effector (163). Ogr is expressed constitutively in *E. coli* due to the similarity of its promoter region to that of *E. coli* genes. K-12 also has the *ogr* gene, as seen by complementation studies, but it seems to lack much of the rest of the P2 genome. The B strain, however, appears to have the entire late gene region of P2 and might even have the complete genome. The immunity region has been changed however, which is the reason that P2 phage can infect this strain. The *ogr* gene, an immunity gene, or a late gene might be involved the appearance of *r* type plaques during T4*rII* infection of *E. coli* B.

rIII

Like *rI* and *rII*, the first *rIII* mutants were isolated by Hershey following the appearance of *r* plaques (81). However, the origin of a heavily-used mutant of *rIII, r67*, like the function of *rIII* during lysis inhibition, remains unclear. The first mention of the *r67* mutant was made by Edgar in 1962, but it appears to have been isolated by Doermann sometime in the mid-late 1950s (58, 147). The *r67* allele forms *r* plaques on *E. coli* B but appears to form r^+ plaques on other tested strains, including K-12 and K-12(λ) (151). This mutant was widely used for mapping purposes and was shown not to map with *rI* or *rII* mutants, so it was designated *rIII* (58). The position of *rIII* relative to other identified T4 genes was in dispute for decades (70, 127, 149, 169) but was finally identified as ORF 30.10 by sequencing (147, 148). Based on promoters near *rIII*, it is predicted to be transcribed by early, middle, and late promoters and so would be present throughout the morphogenesis period of the phage (124).

The *rIII* gene product is composed of 82 residues with a predicted molecular weight of 9.3 kDa and a pI of 8.06. Based on inspection of the primary structure, RIII is predicted to be a soluble, cytoplasmic protein (Fig. 12). Few experiments have been performed to understand the role of *rIII* during LIN. Ramanculov showed that, for cells induced for the holin, T, from a lysogen, infection with T4*rIII* shows a moderate LIN phenotype, unlike isogenic cells infected with wild type T4 showing *bona fide* LIN (145). It was proposed that the role of RIII was to interact with the cytoplasmic domain of T, stabilizing LIN that was enacted by RI in the periplasm. A more recent study by Golec confirmed Ramanculov's proposal by showing that not only does overexpression

of *rIII* complement the LIN defect of T4*rIII*, but it also stabilizes LIN for a much longer time period (72).

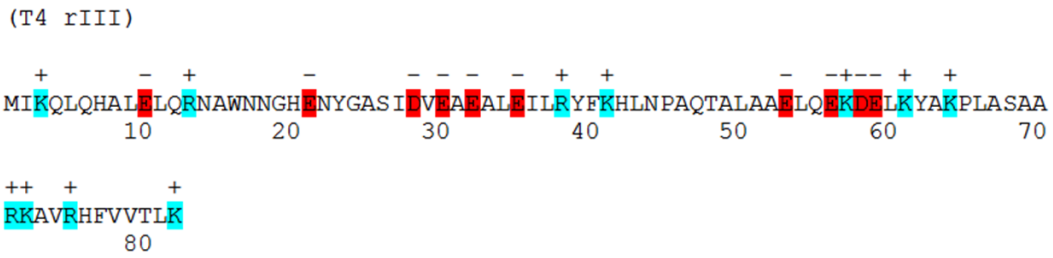

FIG 12 RIII sequence of phage T4. Positively charged residues are highlighted blue while negatively charged residues are highlighted red.

rVI

The *rVI* mutants are by far the least well-characterized and studied of the *r* mutants. The first *rVI* mutants were described in 1975 for their ability to suppress mutations in *rV* (the holin, T) (88). These mutants mapped between genes 39 and 56, an area that consists of more than 10 kbp and contains nearly 24 ORFs (88, 124). A recent study by Burch *et al.* sequenced this area of interest in *r* mutants in their library which were not located in *rI – rV* (26). No mutants have been found in the area mapped by Iankovskii (88), so the *rVI* mutant locations remain unclear.

Roadmap for this dissertation

Four major studies are described in this dissertation.

Chapters II and III: A biochemical and biophysical/structural characterization of the periplasmic domains of the T4 holin (T), antiholin (RI), and the T-RI complex was carried out. Genetic, biophysical and structural information about T and RI, as well as a

complex of both, is important for understanding the biophysical aspects of lysis inhibition (LIN) as well as holin-dependent lysis. Specifically, the interaction of the periplasmic domains of T and RI gave insight into the mechanism of LIN.

Chapter IV: A saturating mutational analysis of the T-hole formation pathway was undertaken. Missense mutants defective in T-hole formation were isolated, with the goal of characterizing the steps of the hole-formation pathway. The mutant library has also leveraged the structural information obtained in the first aim towards an understanding of T function and RI-mediated inhibition.

Chapter V: The signal for LIN was characterized. LIN is induced in a T4-infected cell as a result of super-infection by another T-even phage particle. Because empty T4 "ghosts" do not induce LIN, the LIN signal is thought to be either T-even DNA or an internal capsid protein. A combination of genetic, biophysical, and *in vitro* experiments were used to determine the signal.

Chapter VI: A collaborative study is described showing that the mitochondrial outer membrane protein, Bax, activated during the apoptotic pathway of eukaryotic cells, is functionally related to holins.

CHAPTER II

PROTEIN DETERMINANTS OF BACTERIOPHAGE T4 LYSIS INHIBITION*

Introduction

For most bacteriophages, the host lysis event depends on the temporally regulated action of holin, an extremely diverse class of small phage-encoded membrane proteins (202, 205). The holin proteins accumulate harmlessly in the inner membrane (IM) throughout the morphogenesis period of the infection cycle. Suddenly, the holin forms lethal membrane lesions, or holes, that results in a cessation of respiration and termination of macromolecular synthesis (76). This lethal event, called holin triggering, occurs at a time specified by the allelic state of the holin gene. The timing of triggering is thought to reflect the instant when the holin reaches a critical concentration within the membrane, leading to massive oligomerization and then lethal hole formation (193). Hole formation can also be prematurely triggered by artificial depolarization of the membrane. The mechanistic and structural linkages between oligomerization and triggering are not yet known. For many phages, including the well-studied lambda and T4, the holes formed are sufficiently large to allow non-specific escape of the phage endolysin, a small cytoplasmic protein with muralytic activity, across the bilayer, resulting in the rapid destruction of the peptidoglycan (46, 187). Holins are genetically malleable, in that conservative mutations throughout the primary structure, and

---

* Reprinted with permission from "Protein determinants of phage T4 lysis inhibition" by Moussa, S.H., V. Kuznetsov, T.A. Tran, J.C. Sacchettini, and R. Young, 2012. Protein Science, 21, 571-582. Copyright 2012 by John Wiley & Sons, Inc.

especially in the transmembrane domains (TMDs), can have drastic effects on the triggering time (207). Since the triggering time defines the length of the infection cycle and indirectly the average burst size of the infection, it has been proposed that the apparent universality of holin-controlled lysis reflects the requirement for phages to be able to rapidly evolve to shorter or longer infection cycles as the environment changes (188, 207).

Real-time regulation of lysis timing, however, has been observed only with phage T4 and its close relatives. Specifically, lysis can be delayed indefinitely in the lysis-inhibited state (LIN) depending on the supply of free virus particles in the vicinity of the infected cell (50, 81). LIN has been the focus of numerous studies since its discovery in the 1940s (50), leading researchers to many fundamental advances, including the definition of a gene (17, 18), the nature of the genetic code (39), and the basics of recombination (52, 82, 83). At the cellular level, LIN is imposed when a T4-infected cell is superinfected at 5 min or later after the original infection. The basic physiology of this event has been established in detail. The superinfection begins normally, with irreversible adsorption to the host surface leading to massive conformational changes in the virion and penetration of the outer membrane by the central tail tube. However, the cytoplasmic membrane is not punctured, and the contents of the virion capsid, including the 170 kb DNA molecule and more than 1000 protein molecules, are instead ectopically ejected into the host periplasm. Somehow, this abortive injection leads to activation of a small (11.1 kDa) phage protein, RI, which then inhibits T (25.2 kDa), the T4 holin, blocking it from triggering and thus prolonging the

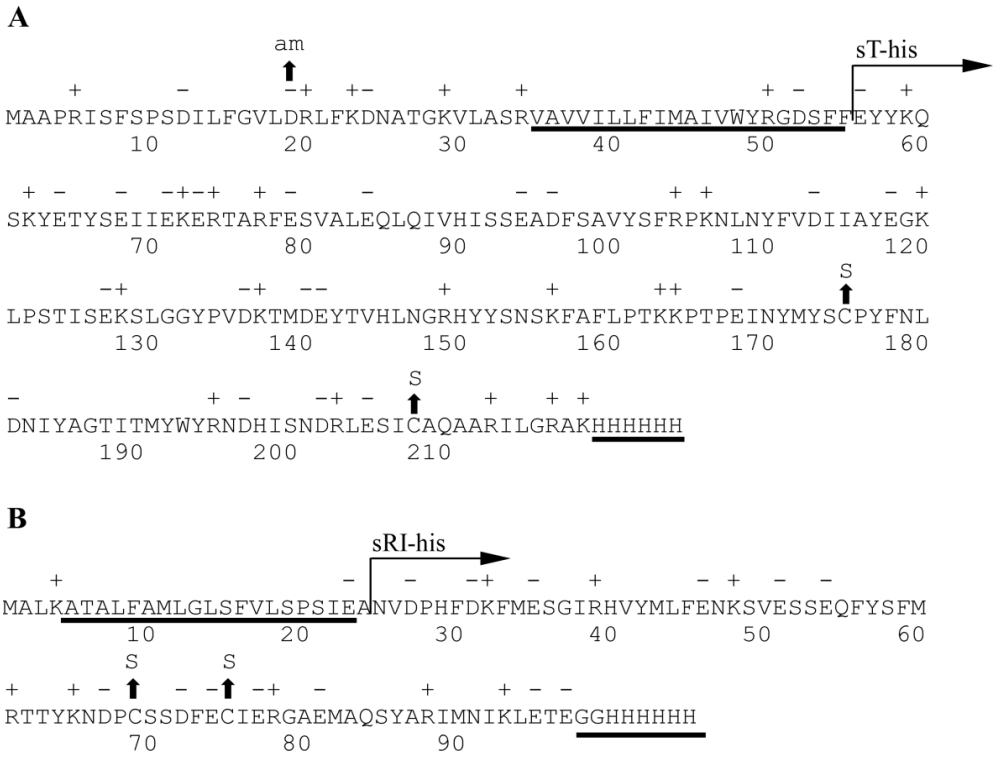

FIG 13 The primary structure of T4 T and RI. (A) T4 T. The predicted transmembrane domain and location of the C-terminal oligohistidine tag are underlined. The region of T cloned into pET11a and purified is labeled with 'sT-his' (see "Materials and Methods"). Locations of the amber and cysteine-to-serine substitution mutants are indicated by arrows. (B) T4 RI. The SAR domain and C-terminal oligohistidine tag are underlined. The region of RI cloned into pET11a and purified is labeled with 'sRI-his' (see "Materials and Methods"). Location of cysteine-to-serine substitution mutants are indicated by arrows.

infection cycle. If superinfections continue to occur at <10 min intervals, RI-mediated inhibition of T persists indefinitely, so that virions can accumulate intracellularly to levels ten-fold or more higher than the normal burst size (179).

Both T and RI are synthesized as type II integral membrane proteins, with an N-terminal transmembrane domain (TMD) tethering 19.2 kDa (163 aa; Fig. 13A) and 8.8

kDa (75 aa; Fig. 13B) periplasmic domains to the bilayer, respectively. The presence of a significant periplasmic domain makes T unique among holins, which in general consist of two or more transmembrane domains linked by short loops (202). In addition, the TMD of RI escapes spontaneously from the membrane and is thus designated a SAR domain, for "signal-anchor-release" (180). In vivo, the SAR domain confers extreme functional and proteolytic instability ($t_{½}$ ~ 2 min) on the periplasmic form of RI (180). We have proposed a model in which the abortive superinfection, specifically the ectopic injection of the capsid contents in the periplasm, stabilizes RI and allows it to bind to the periplasmic domain of T (179), which in turn blocks oligomerization of T and thus prevents triggering. Replacement of the SAR domain with a cleavable signal sequence results in the accumulation of the periplasmic domain of RI, designated as sRI (Fig. 13B) (179). In this situation, sRI binds to the soluble domain of T (sT; Fig. 13A) and blocks lysis. Moreover, secretion of sT to the periplasm can spare full-length T from RI inhibition (179).

The proteolytic instability of RI and the lethality of T have been major impediments to studying the mechanism of T-hole formation and RI-mediated LIN at the biochemical or structural level. Here we report the results of efforts to purify and characterize the soluble periplasmic domains, sRI and sT. The results are discussed in terms of a model for the RI-T interaction and its role in LIN.

Materials and methods

Bacterial growth and induction

The phages, bacterial strains, and plasmids used in this study are listed in Table 2. Bacterial cultures were grown in standard LB media supplemented with ampicillin (100 μg mL$^-$) and/or chloramphenicol (10 µg mL$^-$) when appropriate.

TABLE 2 Phages, Strains and Plasmids

Phages	**Description**	**Source**
T4 wt	Bacteriophage T4D	Lab Stock
T4Δ*rI*	Deletion of *rI* from nt 59204 to nt 59496 in bacteriophage T4D genome	(19)
λ*kan*Δ(*SR*)	λb$_{515}$ b$_{519}$ *att*::Tn*903 cI*$_{857}$ *nin*5 Δ(*SR)*	(17)
Strains	**Description**	**Source**
CQ21 *recA srl::Tn10*	*E. coli* K-12 *ara leu lacI* ^{q1} *purE gal his argG rpsL xul mtl ilv*	
CQ21 λ*kan*Δ(SR) *recA srl::*Tn*10*	CQ21 lysogen carrying λ*kan*Δ(*SR*) prophage	(17)
BL21(DE3)	*E. coli* B *ompT r$_B^-$ m$_B^-$ (P$_{lac}$UV5::*T7 *gene1*) *slyD::Kan* fhuA::Tn*10*	Lab Stock
MC1000	*E. coli* K-12 *Δ(araA-leu)7697[araD139]$_{B/r}$Δ(codB-lacI)3galK16galE15*(GalS) *λ$^-$e14-relA1rpsL150*(strR) *spoT1mcrB1*	(23)
Origami(DE3)	*E. coli* MC1000 *ΔlacX74 ΔphoA Pvu*II *phoR araD139 ahpC galE galK rpsL*F'[*lac$^+$ lacI^q pro*] (DE3) *gor522*::Tn*10 trxB::Kan*	(23)
SHuffle T7 (SHuffle(DE3))	*E. coli* K-12 *fhuA2 lacZ::T7 gene1 [lon] ompT ahpC gal λatt::pNEB3-r1-cDsbC ΔtrxB sulA11 R(mcr-73::miniTn10)2 [dcm] R(zgb-210::Tn10) endA1 Δgor Δ(mcrC-mrr)114::IS10*	New England Biolabs
B834	*E. coli* B *ompT r$_B^-$ m$_B^-$ met$^-$*	Lab Stock

TABLE 2 continued

Plasmids	Description	Source
pER-t	Carrying lysis cassette of λ except *S* is replaced by T4 *t* gene	(145)
pSM-t	pER-t with in-frame deletion of *Rz/Rz1* in the lysis cassette of λ	This study
pSM-t C175S	pSM-t carrying C175S mutation in *t*	This study
pSM-t C207S	pSM-t carrying C207S mutation in *t*	This study
pZA-RI	pZA32Δ*luc*::*rI*	(179)
pZA-ssPhoAΦsRI	Codons 1-24 in pZA-RI replaced by codons 1-26 of *phoA,* encoding signal sequence	(179)
pZA-ssPhoAΦsRI C69S	pZA-ssPhoAΦsRI carrying C69S mutation in ssPhoAΦsRI	This study
pZA-ssPhoAΦsRI C75S	pZA-ssPhoAΦsRI carrying C75S mutation in ssPhoAΦsRI	This study
pZA-ssPhoAΦsRI C69,75S	pZA-ssPhoAΦsRI carrying C69S and C75S mutations in ssPhoAΦsRI	This study
pET11a-sRI^{his}	pBR322 origin, T7 promoter, carrying DNA fragment with Met codon, then codons 25-97 of *rI*, followed by codons for sequence GGHHHHHH	(179)
pET11a-T^{his}	pBR322 origin, T7 promoter, carrying T4 *t*, followed by codons for sequence HHHHHH	(179)
pET11a-sT^{his}	pET11a-T^{his} with deletion in codons 2-55 of *t*	This study

Cultures were grown from overnight starter cultures of a single colony from a fresh plate. Starter cultures were diluted 300:1 and grown with aeration at 30˚C for lysogenic strains and 37˚C for cultures of BL21(DE3), Origami(DE3), and SHuffle(DE3) utilized for over-expression of proteins. The over-expression strains carrying the indicated plasmids were induced for expression by the addition of 1mM final concentration of isopropyl β-D-thiogalactosidase (IPTG) at an A_{550} of 0.6, at 37˚C or 16˚C when appropriate.

Monitoring lysis function

To assess lysis function under physiologically relevant conditions, a plasmid complementation system used with a thermo-inducible lambda lysogen (λ*kan*Δ(*SR*)) and a medium-copy plasmid carrying the *t* holin gene and the lambda R endolysin gene under the control of the lambda late promoter (179). In this system, the induction of the prophage provides *RzRz1* function and transactivates the plasmid promoter, ensuring that the necessary lysis proteins (holin, endolysin and Rz-Rz1) are provided with physiologically relevant timing and expression level. Lysogens were thermally induced at A_{550} ~0.3 by aeration at 42˚C for 15 min, followed by continuous growth at 37˚C.

DNA manipulations and plasmid construction

Isolation of plasmid DNA, DNA amplification by polymerase chain reaction (PCR), DNA transformation, and DNA sequencing were performed as previously described (179, 180). Oligonucleotides (primers) were obtained from Integrated DNA Technologies (Coralville, IA) and were used without further purification or modification. Restriction and DNA-modifying enzymes were purchased from New England Biolabs (Ipswich, MA); all reactions using these enzymes were performed according to the manufacturer's instructions. Site-directed mutagenesis was performed using the QuikChange kit from Stratagene (La Jolla, CA) as described previously (179, 180). Primer sequences are listed in Table 3. Inverse PCR was carried out through a modified version of QuikChange site-directed mutagenesis as previously described (20). The DNA sequence of all constructs was verified by automated fluorescence sequencing

performed at the Laboratory for Plant Genome Technology at the Texas Agricultural Experiment Station and by Eton Bioscience Inc. (San Diego, CA).

TABLE 3 Sequences of oligonucleotides used in this study

Primer	**Sequence**
pERtdelRzRz1For	AGTTGCCCATATCGATGGGC
pERtdelRzRz1Rev	TCATACATCAATCTCTCTGAC
T4TC175SFor	CTACATGTACAGTTCTCCATATTTTAATTTGG
T4TC175SRev	CCAAATTAAAATATGGAGAACTGTACATGTAG
T4TC207For	CGCCTTGAATCAATATCTGCTCAGGCGGCCAG
T4TD19amFor	CTTGAATTCTATTTGGTGTTCTATAGCGCTTGTTCA AAGATAAC
T4TD19amRev	GTTATCTTTGAACAAGCGCTATAGAACACCAAAT AGAATTCAAG
T4TC207SRev	CTGGCCGCCTGAGCAGATATTGATTCAAGGCG
T4RIC69SFor	CCTATAAAAATGACCCGTCTTCTTCTGATTTTGAA TGTATAG
T4RIC69SRev	CTATACATTCAAAATCAGAAGAAGACGGGTCATT TTTATAGG
T4RIC75SFor	CTTCTGATTTTGAATCTATAGAGCGAGGCGCG
T4RIC75SRev	CGCGCCTCGCTCTATAGATTCAAAATCAGAAG
T56-218For	GAGTACTATAAGCAATCAAAG
T56-218Rev	CATATGTATATCTCCTTC

All plasmids used and generated in the course of this study are listed in Table 2. The plasmid pSM-t, used for the expression of T in the lysogenic background, was constructed by Inverse PCR using plasmid pER-t as the template and primers pERtdelRzRz1For/Rev to delete the Rz/Rz1 genes. Cysteine to serine substitutions at positions 175 and 207 of the *t* gene in pSM-t were constructed by site-directed mutagenesis using the primer pairs T4TC175SFor/Rev and T4TC207SFor/Rev, respectively. Cysteine to serine substitutions at positions 69 and 75 in RI were achieved by site-directed mutagenesis of the template pZA-ssPhoAΦsRI using primer pairs

T4RIC69SFor/Rev and T4RIC75SFor/Rev. The plasmid pET11a-sT^{his}, used for over-expression of sT was constructed by deletion of codons 2-55 of *t* in the plasmid pET11a-T^{his} using inverse PCR and primers T56-218For/Rev.

Assessment of protein solubility

Induced 25 mL cultures at either 37˚C or 16˚C (80 and 640 min inductions, respectively) were collected by centrifugation at 5000 x *g* for 15 minutes in a Sorvall Superspeed RC2-B centrifuge and resuspended in 3 mL of buffer (20 mM sodium phosphate, 0.1M NaCl, pH 8.0) supplemented with Protease Inhibitor Cocktail (Sigma, St. Louis), and 100 μg mL^{-1} final concentrations of DNase and RNase (Sigma, St. Louis). Cells were disrupted by passage through a French pressure cell (Spectronic Instruments, Rochester, NY) at 16,000 lb/in^2. 250 μL of pressate was set aside on ice and corresponded to the total protein sample (T) while another 250 μL was centrifuged at 15,000 x *g* in a tabletop microcentrifuge at 4˚C for 20 min. The supernatant was set aside and corresponded to the soluble protein fraction (S) while the pellet fraction was resuspended with an equivalent volume of buffer (250 μL) and corresponded to the insoluble or pellet protein fraction (P). Protein from each sample was precipitated with trichloroacetic acid (TCA, Sigma, St. Louis) and washed with acetone as previously described.(20) Pelleted protein was air dried and resuspended in reducing protein sample buffer (0.5 mg mL^{-1} bromophenol blue in 0.25 M Tris, pH 6.8, and 100 mM β-mercaptoethanol) so that 30 μL contained 0.3 O.D. units of culture.

Protein purification

Proteins containing oligohistidine tags were isolated through immobilized metal affinity chromatography (IMAC), as previously described (20). Six 2 L cultures of SHuffle(DE3) carrying the plasmid pET11a-sRI^{his} or pET11a-sT^{his} were grown at 37˚C to an A_{550} of ~0.5, cooled on ice to 16˚C, and induced overnight (12-16 hrs.) with 1 mM IPTG, final. Cells were harvested by centrifugation in a Beckman JA-10 rotor at 8,000 rpm for 15 min at 4˚C. Cell pellets were resuspended in 120 mL of 20 mM sodium phosphate, 0.1 M NaCl pH 8.0 (purification buffer) supplemented with Protease Inhibitor Cocktail (Sigma, St. Louis), and 100 μg mL^{-1} final concentrations of DNase and RNase. Cells were disrupted in a French pressure cell, as previously described (20), and passed over Talon metal affinity resin (Clontech, Mountain View, CA) and eluted with purification buffer supplemented with 0.5 M imidazole. For purification of the sT-sRI complex, sT was eluted from the Talon metal affinity resin into a 500 μL bed volume containing 4 mg mL^{-1} of purified sRI. Elution fractions of each bed volume for purification of sRI and the sT-sRI complex were assessed for purity by SDS-PAGE and Coomassie blue staining before further analysis.

Quantitation of T and RI in T4 wild type and LIN-deficient infections

Wild type T4 (T4D) and LIN-defective T4 (T4Δ*rI*) bacteriophages were used to infect *E. coli* B834 cells in order to quantify the amount of T and RI produced during a T4 infection. Cultures of B834 were grown to an A_{550} = 0.3 (1.1x10^8 cells mL^{-1}) and were infected with either T4D or T4Δ*rI* at a multiplicity of infection of 10. Ten milliliter samples were collected after 60 or 30 min for T4D and T4Δ*rI* infections,

respectively, and total protein precipitated with TCA and resuspended in reducing sample buffer, as described above. The protein standards used were collected from gel filtration experiments in which sT and sRI were purified (see 'Results' below). Standards were prepared by dilution, with sT standards of 7, 3.5, 1.75, and 0.875 pmol while the sRI standards were 30, 15, 7.5, and 3.75 pmol. All samples were run on SDS-PAGE gels, Western blotted, and analyzed using the software ImageJ (NIH).

SDS PAGE and Western blotting

SDS-PAGE, Western blotting, and immunodetection were performed as previously described (74). sRI and sT in over-expression experiments were detected using a mouse monoclonal antibody against the oligohistidine epitope tag at a dilution of 1:3000 (GE Healthcare, UK). sT and full length T in the T quantification experiments was detected using a rabbit polyclonal antibody against the periplasmic domain of T at a dilution of 1:1000. The anti-mouse and anti-rabbit IgG horseradish peroxidase-conjugated secondary antibodies, which were supplied with the chemiluminescence kit, were used at a 1:5000 dilution. Blots were developed with the West Femto SuperSignal chemiluminescence kit (Thermo Scientific, Rockford, IL). Chemiluminescence signal was detected using a Bio-Rad Chemidoc XRS.

Gel filtration

Gel filtration chromatography was carried out using either an analytical or prep grade Superdex 75 column calibrated with the Low Molecular Weight Gel Filtration Calibration kit on an AKTA FPLC (GE Healthcare, UK). Columns were equilibrated with 20 column volumes of purification buffer before sample injection. Once sample

was injected, gel filtration was performed at 0.4 mL min^{-1} (for analytical grade) or 1 mL min^{-1} (for prep grade) until one column volume of buffer had eluted.

Circular dichroism spectroscopy

CD spectra were obtained using an Aviv model 62DS spectropolarimeter (Lakewood, NJ). The sRI and sT-sRI complex protein were purified in 20 mM sodium phosphate and 0.1 M NaCl pH 8 buffer and concentrated using an Ultra-4 3K MWCO concentrator (Amicon) to 1 μM. Protein concentrations of sRI and sT-sRI were determined by A_{280} using calculated extinction coefficients (135). Three milliliter samples were loaded into 1 cm quartz cuvettes and equilibrated to 25˚C for 3 min before being scanned. Scans from 250-195 nm with a 1 nm step size and 30 s averaging time were applied to all samples. All CD spectra were fitted by K2D2 (143) using data from 200-240 nm that were converted to differential absorption units (Δε) (73).

Analytical ultracentrifugation

Sedimentation velocity experiments were performed on 3 sRI samples (0.3, 1, and 1.6 mg/mL) and 3 sT-sRI complex samples (0.15, 0.4, and 0.6 mg/mL) in purification buffer. Samples and buffer (380 and 400 μL, respectively) were loaded into cells assembled with 12-mm double sector Epon charcoal-filled centerpieces and sapphire windows. Samples were run in a Beckman Model XL-A analytical ultracentrifuge at 50,000 rpm (for sRI) and 37,500 rpm (for sT-sRI complex) at 25˚C in an An-60Ti rotor for 8 and 5 hours, respectively. Scans were performed at 280 nm, with ~3 min elapsed between each scan. Data were analyzed and sedimentation coefficients for each sample determined using the programs SVEDBERG version 6.39 and UltraScan

II version 9.9, using a genetic algorithm and Monte Carlo analysis, as previously described (44, 177). Sedimentation equilibrium experiments were performed on sRI samples (0.3, 1, and 1.6 mg/mL) in purification buffer. Samples and buffer (110 and 120 μL, respectively) were loaded into cells assembled with a 6 channel Epon charcoal-filled centerpiece and sapphire windows. Samples were run in a Beckman Model XL-A analytical centrifuge at 24,000, 28,800, 33,600, 38,400, 43,200, and 48,000 for 13, 14, 13.5, 13.5, 12, and 11 hours, respectively at 25˚C. Two scans were performed at 280 nm at the end of each equilibration time. Data for each sample were analyzed with UltraScan II version 9.9, as previously described (44, 45).

Assessment of sulfhydryls by Ellman's reagent

The state of the sulfhydryls in purified sRI and sT-sRI complex was assessed with Ellman's reagent, also known as 5,5'-dithio-bis(2-nitrobenzoic acid) (DTNB, Sigma, St. Louis, MO), as previously described (47). Briefly, solutions of reduced glutathione, cystine, and purified sRI (40, 20, and 10 μM) for sRI analysis or sT-sRI complex (20, 10, and 5 μM) for complex analysis were prepared in a volume of 90 μL in purification buffer. Ten μL of 10mM DTNB, dissolved in ethanol, was added to each reaction, samples mixed, and incubated in the dark at room temperature for 30 min. Samples were assayed for the presence of the anionic by-product 2-nitro-5-thiobenzoate at 412 nm on a UV/Vis spectrophotometer (Hitachi, Tokyo) (47).

Results

Cysteines are required for T lytic and RI LIN function

The choice of strategies for over-production and purification of the T4 holin and antiholin was affected by the presence of two Cys residues in both RI and T. If the Cys residues could be replaced by conservative substitutions like Ser, the potential for oxidative damage during purification would be minimized. However, sequence alignment of the holins (T) and antiholins (RI) of T4-like phages revealed that in both proteins the Cys residues were conserved both in terms of number (always two), spacing (30-31 intervening residues for T proteins; 3-5 intervening residues for RI proteins), and position in the sequence (C-terminal 20% of both proteins) (Fig. 14 & Fig. 15). This suggested that, like many periplasmic proteins, both RI and T are likely stabilized by intramolecular disulfide bonds. To test whether these residues were essential for the lytic function of T, single and double Ser substitutions were made, generating Cys175Ser, Cys207Ser, and Cys175/207Ser. Induction of the wild type construct

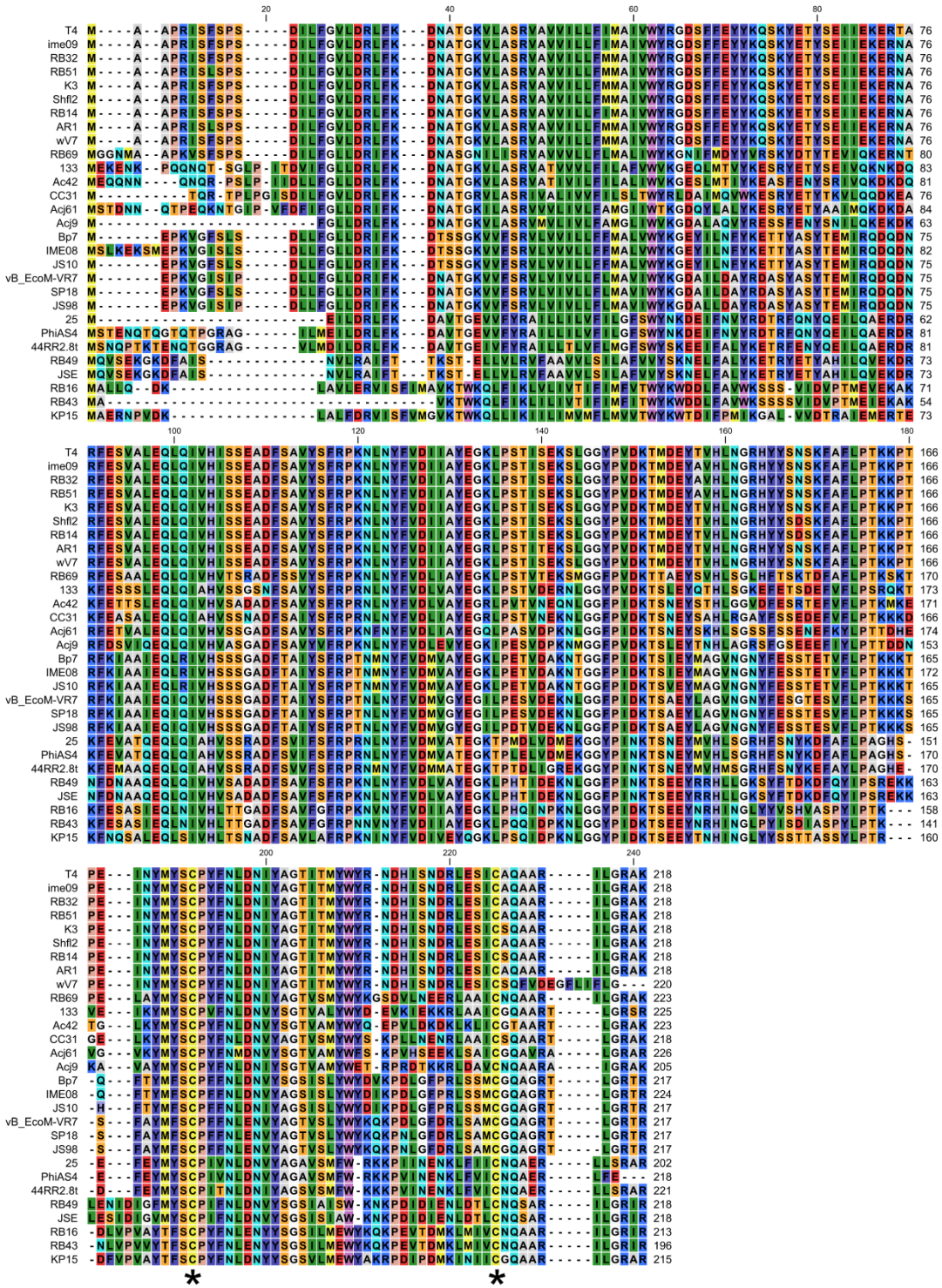

FIG 14 Alignment of T4-like holin (T) sequences. Phage identity is listed on the left and corresponds to GenBank entries. Each conserved cysteine residue is indicated with an asterisk.

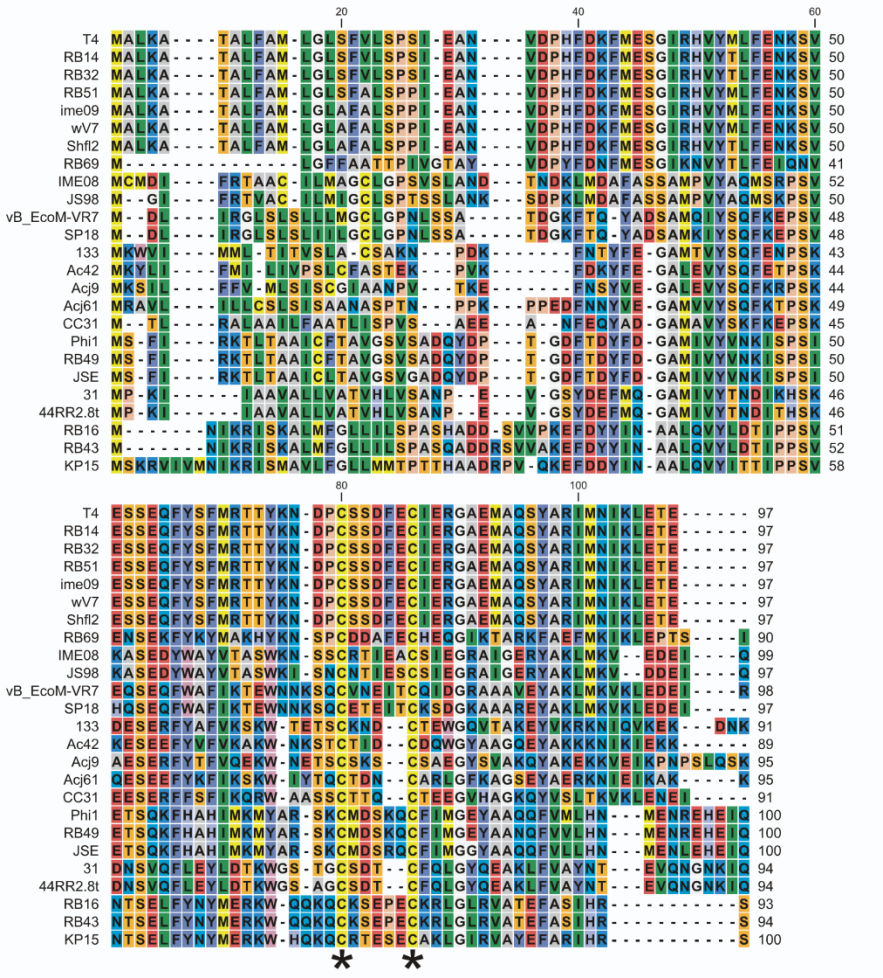

FIG 15 Alignment of T4-like antiholin (RI) sequences. Phage identity is listed on the left and corresponds to GenBank entries. Each cysteine residue is indicated with an asterisk.

resulted in the characteristic, sharply defined lysis at 20 min (Fig. 16A). In contrast, each of the cysteine substitution alleles exhibited an identical absolute lysis defect. Similarly, to test whether the two Cys residues in RI are essential for LIN, the Cys69Ser, Cys75Ser, and Cys69/75Ser single and double substitutions were constructed. Synchronous induction of *t* and the parental *rI* resulted in *bona fide* lysis inhibition (Fig.

16B). Addition of 1% chloroform at 60 minutes after induction resulted in immediate clearing of the T and RI induced culture, indicating that the lack of lysis was not due to the lack of expression of the endolysin, co-expressed on the plasmid, but rather due to a holin defect. In contrast, all 3 substitution alleles failed to support LIN, with lysis occurring at 20 min, as it does in inductions of t alone. Thus the conserved pairs of Cys residues in the periplasmic domains of both the holin T and antiholin RI are essential for lytic and LIN functions, respectively. Even-numbered complements of Cys residues in periplasmic proteins are almost always associated with disulfide bonds important for stable folding (56), so these results indicated that a useful over-production and purification strategy must retain the capacity to form and maintain disulfide bonds in both T and RI.

Soluble sRI accumulates in a host cytoplasm optimized for disulfide bond formation

Attempts to obtain native, full length RI by overexpression were unsuccessful, and in fact no native RI could even be detected by immunoblot (not shown). The SAR domain directs RI to the *sec* translocon, which itself severely constrains the maximum output from over-expression systems (186), and also confers extreme proteolytic instability on periplasmic RI (180). In view of the fact that the periplasmic domain, sRI, is fully functional *in vivo* when directed to the periplasm by a normal, cleavable signal sequence, a strategy focusing on sRI was pursued. Using the T7-based hyper-expression vector, pET11a (171), we constructed a plasmid encoding sRI with a C-terminal hexahistidine tag.

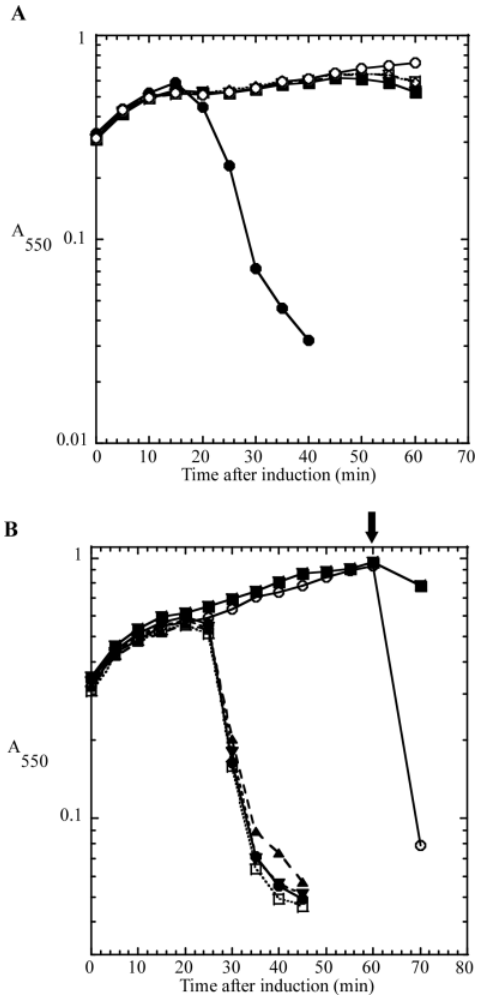

FIG 16 Lysis and lysis inhibition defect in cysteine to serine substitutions. (A) Cysteine-to-serine substitutions in T show a severe lysis defect. CQ21 λ*kan*Δ(SR) cells carrying the indicated plasmids were grown to A_{550} ~ 0.3 and induced by a shift to 42˚C. Symbols: ●, pSM-t; ■, pSM-t C175S; ◊, pSM-t C207S; □, pSM-t C175,207S; ○, pSM-t D19am. (B) Cysteine-to-serine substitutions in RI show a LIN-defective phenotype, similar to inductions of T alone. CQ21 λ*kan*Δ(SR) cells carrying the indicated plasmids were grown to A_{550} ~ 0.3 and induced by a shift to 42˚C and addition of IPTG. Symbols: ●, pSM-t only; ■, pZA-ssPhoAΦsRI only; ○, pSM-t and pZA-ssPhoAΦsRI; ▲, pSM-t and pZA-ssPhoAΦsRI C69S; ▼, pSM-t and pZA-ssPhoAΦsRI C75S; □, pSM-t and pZA-ssPhoAΦsRI C69,75S. Arrow indicates addition of $CHCl_3$.

Cultures of BL21(DE3) carrying this construct and induced at 37˚C accumulated detectable levels of the 9.7 kDa sRI-his product (Fig. 17A). However, none of the protein proved to be soluble. In view of the essential character of the cysteine residues, it was suspected that the sRI protein was misfolding and aggregating in the host cytoplasm. Nevertheless, there was no improvement when using Origami(DE3)™ cells, in which the cytoplasm is more conducive to disulfide bond formation as a result of *gor* and *trxB* mutations (22). In contrast, nearly 25% of total sRI was soluble when SHuffle® T7 (SHuffle(DE3)) cells were used. SHuffle(DE3) cells are similar to Origami(DE3) cells except for the ectopic, cytoplasmic presence of the disulfide bond isomerase, DsbC (110). Finally, nearly 75% of the sRI protein was found in the soluble fraction when cells were incubated at 16˚C overnight, following induction. sRI was purified by immobilized metal affinity chromatography (IMAC) at 4˚C and yielded 4 mg L^{-1}.

sRI is a predominantly helical monomer in solution

In an effort to determine whether the purified sRI was properly folded, the secondary structure of the periplasmic domain of RI was assessed by circular dichroism (CD) spectroscopy. Analysis of the spectrum using the deconvolution program K2D2 (143) indicated that sRI was ~78% alpha-helical, slightly higher than the 65% predicted by the secondary sequence prediction program JPred3 (34), and strongly indicating that,

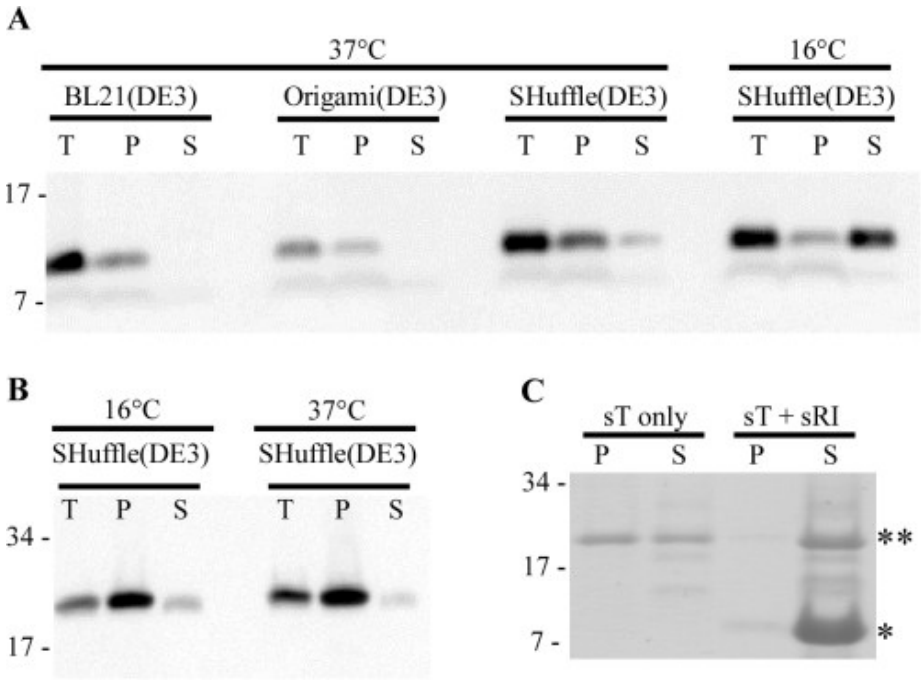

FIG 17 Protein solubility in various over-expression backgrounds and temperatures. Determination of protein solubility of sRI (A) and sT (B) in various over-expression backgrounds and temperatures. T: total sample, P: insoluble fraction, and S: soluble fraction. Molecular mass standards used are indicated on left. (A) Western blot of sRI samples over-expressed at 37˚C in BL21(DE3), Origami(DE3), and both 37˚C and 16˚C in the SHuffle(DE3) backgrounds. (B) Western blots of sT samples over-expressed at 16˚C and 37˚C in the SHuffle(DE3) background. (C) Coomassie-stained gel of samples in which sT was eluted with or without the presence of sRI. Migration of sRI, * and sT, ** are indicated.

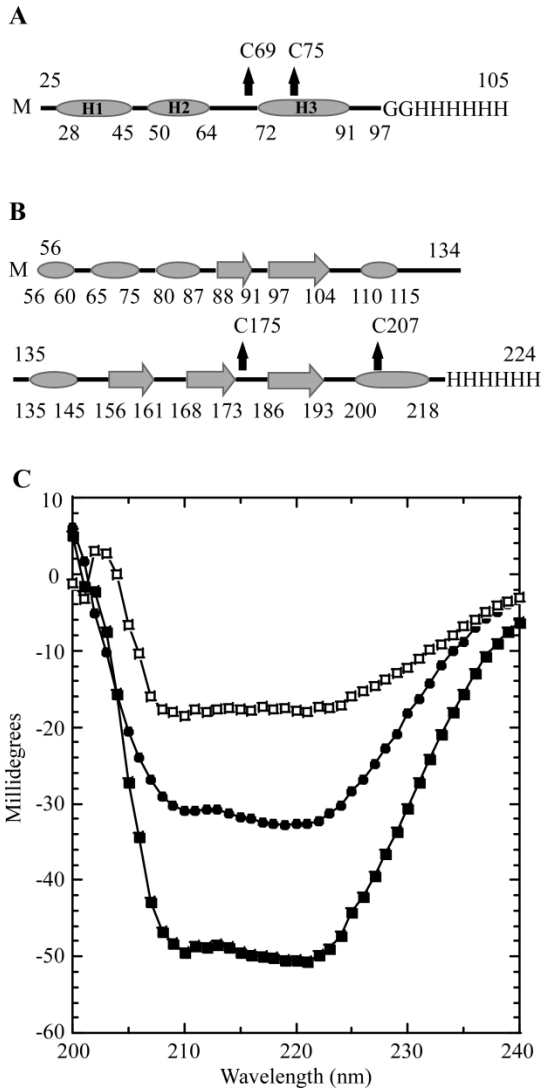

FIG 18 Secondary structure prediction and CD spectroscopy. (A) Secondary structure prediction of sRI by JPred. α-helices are indicated by ovals and unstructured elements indicated by lines. The location of the two cysteine residues are indicated by arrows and the C-terminal oligohistidine tag is labeled. sRI is predicted to contain 65% alpha-helical content with no other structured elements predicted. (B) Secondary structure prediction of sT by JPred. α-helices are indicated by ovals, β-sheets are indicated by large arrows, and unstructured elements are indicated by lines. The location of the two cysteine residues is indicated by arrows and the C-terminal oligohistidine tag is labeled. sT is predicted to contain 30.5% alpha-helical character, and 19% beta-sheet with no other structured elements predicted. (C) Circular dichroism spectra of sRI (●) and sT-sRI complex (■) at a final concentration of 1 μ*M* each. The difference spectrum (of sRI and the sT-sRI complex) is indicated (□).

despite its small size and its ectopic expression, the purified sRI protein was quantitatively folded (Fig. 18A,C). The oligomeric status of the purified sRI was assessed by gel filtration chromatography, where it eluted in a major peak corresponding to 10 kDa, consistent with monomeric status, and a minor peak at 20 kDa (Fig. 19A). This conclusion was buttressed by sedimentation velocity and equilibrium experiments performed on the purified sRI. Sedimentation velocity analysis of 3 samples at varying concentrations revealed a coefficient of 1.4S and a frictional ratio (f/f_0) of 1.3, consistent with a globular monomer of 9.7 kDa (Fig. 19B,C) (35). Additionally, a sedimentation equilibrium analysis experiment revealed a protein of 9.2 kDa in solution, within 5% of the 9.7 kDa calculated from the sRI primary structure (Fig. 19D). Taken together, these results indicate that sRI exists as a globular monomer of primarily helical character in solution.

sT oligomerizes at high concentrations and requires sRI to remain soluble

Previous experiments showed that the periplasmic domain of T, sT, is fully capable of interacting with RI (179). Accordingly, a pET11a construct encoding sT with a C-terminal oligohistidine tag was used for over-expression. Because sT also contains two essential cysteine residues, over-expression was carried out in the SHuffle(DE3) background with inductions at 37˚C and 16˚C. Inductions at 16˚C slightly increased the amount of soluble protein as compared to 37˚C (Fig. 17B). The inductions at 16˚C yielded ~1.5 mg of soluble sT per liter. However, unlike sRI, elution of sT from the IMAC resin resulted in immediate precipitation of more than 60% of the protein, presumably reflecting the tendency of holin proteins to oligomerize. Since experiments

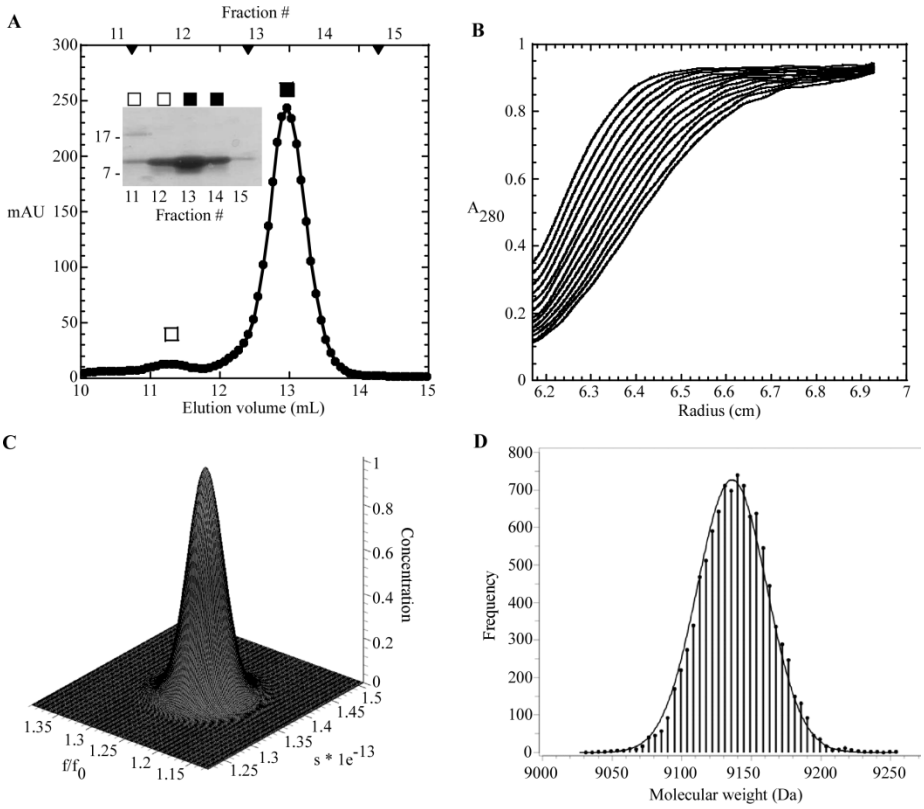

FIG 19 S-75 gel filtration and analytical ultracentrifugation of sRI. (A) Elution profile of sRI with major monomer peak (■) and minor dimer peak (□) indicated. S-75 standards are indicated by arrow heads, from left to right: 29, 13.7, and 6.5 kDa. Inset: Coomassie-stained gel of samples collected from each gel filtration fraction. (B) Sedimentation velocity of sRI (at various concentrations, see "Materials and Methods"). The positions of the moving boundaries shown are at ~6 min intervals by spectrophotometric scanning at 280 nm. (C) Genetic algorithm/Monte Carlo analysis of the sRI sedimentation velocity data with frictional ratio and sedimentation coefficient shown. The concentration axis shows that no other species exist in the samples analyzed in the sedimentation velocity experiment. (D) Measurement of the molecular mass of sRI by fitting of sedimentation equilibrium data performed at varying sRI concentrations (see "Materials and Methods"). The frequency distribution describes the statistical confidence level for each molecular weight calculation.(45)

carried out *in vivo* had shown that sRI binds to T and inhibits hole formation, we reasoned that sT eluted into excess sRI might form stable complexes blocked from

aggregation (179). This was indeed the case, since very little aggregation (<5%) was detected after elution of sT into a molar excess of sRI (Fig. 17C).

The sT-sRI complex is a heterodimer in solution that contains both helical and beta sheet character

Gel filtration analysis of the sT-sRI mixture was performed to gauge the molecular mass of the formed complex (Fig. 20A,B). An apparent sT-sRI complex eluted in a major peak corresponding to 45.6 kDa, calculated using previously analyzed standards (Fig. 20A). This mass was not consistent with the 29.7 kDa mass predicted for a heterodimer of sT-his (20 kDa) and sRI-his (9.7 kDa). N-terminal analysis by Edman degradation sequencing of the complex revealed that sT and sRI were present in a 1:1 ratio (data not shown). At this ratio, the predicted mass of the complex would be either 29.7 kDa for the heterodimer or 59.4 kDa for the sT_2-sRI_2 heterotetramer. To resolve this apparent discrepancy, sedimentation velocity experiments were performed, revealing the complex to have a sedimentation coefficient of 4.1S, consistent with the 29.7 kDa heterodimer state (Fig. 20C). CD spectroscopy was performed to assess the secondary structure found in the complex. Using K2D2, the complex exhibited 48.5% α-helical character along with 10% β-strand, with nearly 40% unstructured elements (Fig. 18C). A difference spectrum of the sT-sRI complex and sRI only CD spectra was performed to understand the secondary structure character of sT alone, assuming that secondary structures of sT and sRI are not changed significantly upon binding. Based on this analysis, sT is slightly more than 23.7% α-helical, 26.2% β-strand, and

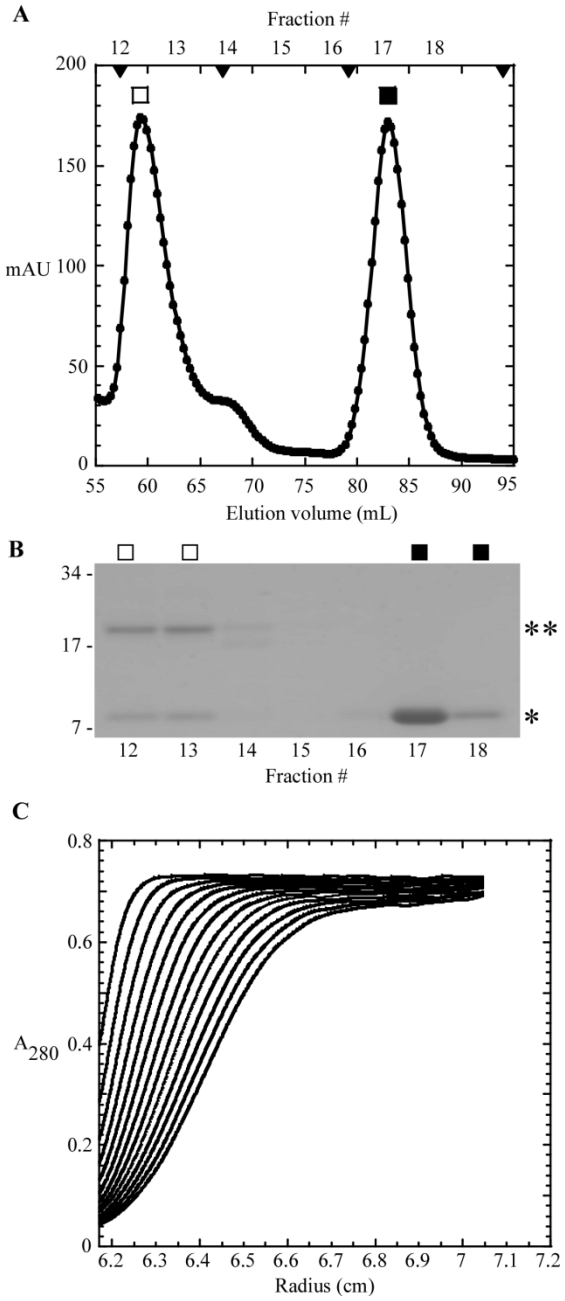

FIG 20 S-75 gel filtration and analytical ultracentrifugation of the sT-sRI complex. (A) Elution profile of sT-sRI complex (□) and sRI (■). S-75 standards are indicated by arrow heads, from left to right: 44, 29, 13.7, and 6.5 kDa. (B) Coomassie-stained gel of samples collected from each gel filtration fraction in FIG 20A. * : sRI and **: sT. (C) Sedimentation velocity of sT-sRI complex (at various concentrations, see "Materials and Methods").

nearly 50% unstructured, similar to what is predicted by JPred3 (30% α-helical, 20% β-strand, and 50% unstructured) (Fig. 18B,C).

The RI and T cysteines form a disulfide bond necessary for function

The state of the RI and T thiols in the purified sRI and sT-sRI complex protein was assessed with Ellman's reagent (5,5'-dithio-bis-(2-nitrobenzoic acid). The purified sRI and sT-sRI complex exhibited no reactive thiols (Table 4 and Table 5). These results indicate that formation of the disulfide bond between Cys69 and Cys75 of sRI and Cys175 and Cys207 of sT is essential for the proper function of sRI and sT. Taken together with the results from Fig. 16A and Fig. 16B, disulfide formation is essential for T and RI function.

TABLE 4 Assessment of sulfhydryls in sRI by Ellman's reagent

Sample	A_{412}
40 μM glutathione	0.39
20 μM glutathione	0.21
10 μM glutathione	0.08
40 μM cystine	0.01
20 μM cystine	0.01
10 μM cystine	0
40 μM sRI	0.02
20 μM sRI	0.02
10 μM sRI	0

TABLE 5 Assessment of free sulfhydryls in sT-sRI complex by Ellman's reagent

Sample	A_{412}
20 μM glutathione	0.22
10 μM glutathione	0.11
5 μM glutathione	0.05
20 μM cystine	0.03
10 μM cystine	0.02
5 μM cystine	0
20 μM sT-sRI complex	0.04
10 μM sT-sRI complex	0.03
5 μM sT-sRI complex	0.03

Quantitation of T and RI during T4 infections

Useful models for holin and antiholin function during the phage infection cycle require knowledge of the stoichiometry of these proteins *in vivo*. The availability of purified periplasmic domains of RI and T made it possible to address this issue, using quantitative Western blotting. In both cases, antibodies previously raised against RI and T could be used for detection of the periplasmic domains. Using purified sT as a standard, quantitative blotting was performed on samples taken from wild-type T4 infections of mid-log (~1.1 x 10^8 cells/ml; input MOI=10) (Fig. 21). Care was taken to sample the cultures directly into ice-cold TCA for rapid and quantitative denaturation of all cell proteins, so that the immunoblots would reflect an instantaneous snap-shot of the T and RI content. Under these infection conditions, LIN is imposed, so samples could

be taken from cells at 60 min after infection, revealing, reproducibly, that ~8,000 molecules of T had accumulated at this point. A T4*rI* infection under the same conditions results in lysis at ~30 min; accordingly the level of T in these samples was found to be ~4,000 molecules, reproducibly. Since holin triggering stops macromolecular synthesis, this quantity represents the critical concentration for T. These numbers are roughly comparable to the levels of the lambda S and phage 21 S[68], the only other holin proteins whose quantities have been determined during a phage infection.

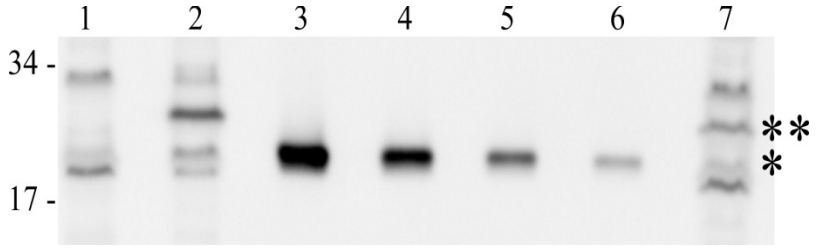

FIG 21 Quantitation of T in a wild type and LIN-defective phage infection. Quantitative Western blot of samples that were collected. Molecular mass standards are indicated at the left. Lane 1, B834 cells only; 2, wild-type T4 infection at 60 min; 3-6, sT standards, from left to right: 30, 15, 7.5, and 3.75 pmol; 7, T4*rI* infection at 30 min. *: sT and **: T, full length.

RI could not be detected in the samples from T4 wild type infections at t=60 min. Using the sensitivity of the anti-RI antibody, we determined that there could be no more than 10,000 molecules of RI in the average LIN-inhibited cell.

Discussion

Previous work from our laboratory has shown that, *in vivo*, the soluble domains of T and RI interact in the periplasm and that this interaction is essential for the inhibition of lysis (146, 179). Here we have presented results from an effort to purify and characterize these periplasmic domains, sRI and sT, as the initial steps in determining a mechanistic basis for this inhibition. Ultimately, structural information will be required, but the findings presented here have a number of useful implications.

Essential Cys residues and cytoplasmic over-expression in the SHuffle® host

The pair of Cys residues in the C-terminal region of the soluble domains of both RI and T were found to be essential for biological function. Since, in the sRI-sT complex described in this work, there are no free thiols detectable, the two Cys residues in each protein are likely to be involved in a disulfide bond. Since there is no precedent for intermolecular disulfides in native periplasmic proteins, presumably both disulfides are intramolecular linkages important for the stable fold of the protein. Whether or not either or both disulfides are involved in T or RI function or just required for the stable fold cannot be determined from our data. Nevertheless, the requirement for the disulfides in T should make the host *dsb* system essential for T4, although it is not for the host itself. To our knowledge, this has not been tested, despite the extensive genetics of the T4 system, including screens for host mutants that block T4 vegetative growth. It will be interesting to test this idea by constructing *E. coli* B mutants with various *dsb* mutations and then assessing plating efficiency and the kinetics of viral reproduction on isogenic hosts. If the *dsb* dependency is sufficiently strict, it may be possible to exploit

it by looking for intragenic suppressors within *t*, to explore the structure-function relationship of the holin periplasmic domain.

Interestingly, cytoplasmic production of soluble sRI and sT was much better in the SHuffle® host compared to the parental BL21(DE3) or the Origami™ host. Both Origami and SHuffle strains are *E. coli* B derivatives carrying mutations in *gor*, *trxB* and *aphC* that, together, allow disulfide bond formation in the cytoplasm (22, 110). The substantive genotypic difference between Origami and SHuffle strains is supposed to be the presence of an engineered *dsbC* gene encoding a DsbC disulfide bond isomerase lacking its signal sequence, thus causing DsbC activity to be redirected to the cytoplasm. sRI and sT have only a pair of Cys residues each and are thus unlikely substrates for a disulfide bond isomerase. However, there are reports that DsbC can participate in other as yet uncharacterized ways in disulfide bond formation, perhaps by acting as a chaperone (30, 41, 184).

sRI is monomeric, globular and highly alpha-helical

Analysis of purified sRI by gel filtration chromatography and sedimentation equilibrium both indicate that sRI exists as a monomer in solution. In addition, CD spectroscopy indicates that sRI is nearly completely in alpha-helical conformation, even more so than suggested by predictions based on secondary structure propensity analysis of the polypeptide sequence. Moreover, sedimentation velocity analysis indicates that sRI has an axial ratio of a rather compact globular shape, suggesting that the extensive alpha-helices must be bundled in some way, rather than existing in an extended conformation. Indeed, the position of the disulfide bond that we have inferred from the

results discussed above suggests that sRI has a hairpin structure, with the two predicted alpha-helical domains H2 and H3 linked by a Cys69-Cys75 disulfide bond (Fig. 18A).

The periplasmic domain of the T holin has a propensity for oligomerization that is blocked by complexing with sRI

The periplasmic domain of the T4 holin, sT, can be produced in soluble form in the host cytoplasm. However, upon elution from an IMAC matrix, sT oligomerizes into insoluble aggregates. These insoluble aggregates can be rescued by elution from the IMAC matrix into buffer containing purified sRI. Gel filtration and ultracentrifugation experiments confirmed that a complex of sT and sRI is indeed formed. This complex is formed at a 1:1 ratio and is completely soluble as shown in Fig. 17C. These results unambiguously confirm the direct role of the periplasmic domain of T for both oligomerization, a necessary step in holin-mediated hole formation, as well as regulation by RI during LIN by the inhibition of oligomerization. This system is the first well-studied example of holin regulation by a protein that shares no sequence homology. The bacteriophage lambda holin, S105, is negatively regulated by S107, another product of the *S* gene protein with a translation start 2 codons upstream (24). Likewise, the holin of lambdoid phage 21 is also regulated by a second protein produced from an upstream translational start (141). In both of these cases, the antiholin has a polypeptide sequence nearly identical to that of the holin and thus complex formation with the holin is essentially homomeric.

The T holins have been specialized for real-time regulation by environmental cues

Unlike other holins characterized by experiment or identified by bioinformatics, which have at least 2 transmembrane segments, the holins of T4-like phages have only a single predicted TMD. Moreover, the holins of T4-like phages are the only holins which have a substantial soluble domain, in contrast to other predicted holins which consist almost entirely of TMDs connected by short loops and a short but highly hydrophilic C-terminal tail. The T4-like holins appear to have been adapted so that a signal for superinfection can be recognized and transduced to a lysis inhibition output in the periplasmic space before the inner membrane can be compromised. Presumably this gives the phage an advantage in preserving membrane integrity and host energetics for the purpose of continued macromolecular synthesis and virion production. Extrapolating from our results with the purified periplasmic domains, it seems likely that in superinfected cells, activated RI acts as an antiholin by complexing stoichiometrically with T and thus blocking T homo-oligomerization. However, in the aqueous context of the periplasm, which is rich in proteolytic activity, soluble RI is highly unstable. This confers an important transitory character to lysis inhibition, so that when superinfections cease, indicating that the extra-cellular environment is no longer over-stocked with virions, the LIN signal dissipates, allowing lysis to occur.

Despite the regulatory advantages of having a globular soluble domain controlling the formation of homo-oligomeric holes, the presence of a bulky 19.2 kDa periplasmic component tethered to the single TMD puts constraints on models for the formation and structure of the T-hole. The quantification of T done here using the

purified sT as a protein standard indicates that at the normal lysis time of an infected cell (t ~ 30 min) there are ~4,000 holin molecules (Fig. 21). Assuming that the T-hole is lined by the single transmembrane domain, this indicates a maximum of ~4 μm in hole perimeter could be supported by T, consistent with the micron scale holes observed for the lambda holin S105, which has three TMDs (46). However, there are two conceptual issues that distinguish T-hole formation and structure from that of the S105-hole. First, our results suggest that the oligomerization of the T holin is driven, at least in part, by the oligomerization of the sT domain, while transmembrane domain interactions drive the oligomerization of S105 (24). Moreover, although both the lambda antiholin, S107, and the T4 antiholin, RI, function by specifically inhibiting oligomerization of the respective holin, in the latter case the entire interaction is within the soluble phase, by the formation of the sT-sRI complex. The simplest interpretation is that the sT domain dominates in the lysis timing function of the holin, in that oligomerization of the sT domain results in creating a high local two-dimensional concentration of the hole-forming component, the single TMD. This perspective could explain why a very conservative missense change in the transmembrane domain, I39V (179), confers RI-insensitivity on T, presumably by increasing the intrinsic self-affinity of the TMD, even though it is unlikely to affect RI-T complex formation. In any case, the 19.2 kDa periplasmic domain of T will likely have a diameter several-fold greater than the ~1 nm of hole perimeter occupied by the TMD. Unless the sT domain undergoes a dramatic conformational reorganization during hole-formation, any model of the hole structure would thus require a flexible linker between the membrane and soluble domains. In

addition, accommodating the sT domain along the perimeter of the hole wall will likely require multiple homomeric but heterotypic interaction surfaces for sT, any one of which if blocked by RI occupancy could disrupt hole formation. Structural analysis potentiated by our ability to generate purified sRI and sT-sRI in crystallographically-useful quantities should further delineate these issues.

CHAPTER III

THE STRUCTURAL BASIS OF LYSIS INHIBITION

Introduction

If T4-infected cells are superinfected by secondary T4 virions, the infection cycle is extended indefinitely in a state called lysis inhibition (LIN) (50, 81). Rather than lysing at the normal time of 25 min and liberating approximately 100 progeny virions, infected cells in the LIN state can accumulate $>10^3$ particles intracellularly during hours of unabated growth (203). LIN gives T4 plaques a distinct morphology, small and fuzzy-edged (81). Hershey and others identified phage genes required for LIN by the simple expedient of looking for mutants that gave large, sharp-edged plaques (81). These "r" (for rapid lysis) mutants were mapped to seven loci (83). Beginning in the 1940s, experiments with the *r* genes were foundational in the development of modern molecular biology (17, 18, 39, 82). Moreover, the LIN phenomenon is the only documented example of an environmental cue exerting real-time control of a viral infection cycle (203). Despite this rich history and appealing physiology, the molecular basis for the LIN phenomenon remained obscure for the rest of the century, until Ramanculov *et al.* showed that the product of the *rI* gene (RI) was the antiholin for the T4 holin, T, encoded by gene *t* (144).

In general, holins are the master timing elements of phage infection cycles, accumulating harmlessly in the cytoplasmic membrane until suddenly oligomerizing to form lethal membrane lesions, or holes, that terminate energy metabolism and initiate the process of lysis (203). This event, termed "triggering" is associated with a dramatic

change in the distribution of holin proteins from a highly mobile form dispersed throughout the bilayer to a few large protein aggregates, presumably the site of the holes (193). Antiholins that act to retard the timing of lysis have been identified for a number of phages. In the two cases that have been studied, the lysis-control gene has dual translational starts, with the downstream start producing the lethal holin (137, 194). In these cases, the antiholin is identical to the holin except for additional N-terminal residues that alter the membrane topology of the first TMD. It is thus not surprising that these products confer negative-dominant character to impede holin oligomerization. The mode by which RI inhibits T in T4 infections must be completely different, since the RI and T proteins are unrelated proteins encoded by distinct, unlinked early and late genes, respectively. Moreover, the lysis timing effected by the dual start holin/antiholin systems is set by the ratio of the two products, while in T4, RI-inhibition requires environmental information, in the form of a super-infecting 250 MDa virion (136). Subsequent genetic and biochemical analysis has revealed intriguing features of the two proteins. Both RI and T are synthesized as proteins integral to the cytoplasmic membrane (Fig. 22), each with a single transmembrane domain (TMD) and a periplasmic C-terminal domain (146, 180). However, the TMD of RI is a SAR domain that allows it to spontaneously exit the bilayer, whereas T accumulates stably in the membrane (180). SAR domains have been found at the N-terminus of other lysis proteins, including endolysins and holins (107, 141, 196, 197). In each case, the exit of the SAR domain from the bilayer serves to relieve inhibition of lytic function (107, 141, 174, 196, 197). The opposite is the case for T4, where the release of RI from the bilayer

is necessary for T inhibition (180). The SAR domain also confers an extreme lability on the periplasmic form of RI, which has a half-life of nearly 2 min.

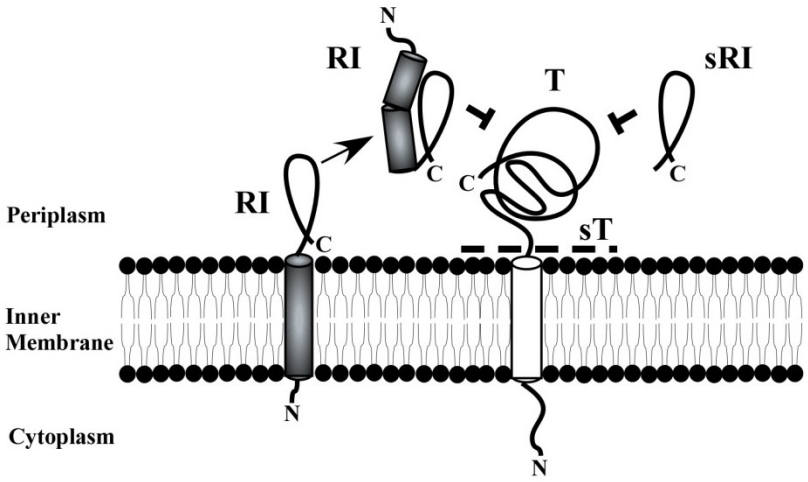

FIG 22 T and RI are localized to the inner membrane. RI has a SAR domain that is spontaneously released as a soluble protein in the periplasm. T is an integral membrane protein that can be inhibited by the soluble RI via periplasmic domain interactions or by the periplasmic domain of RI alone (sRI). The periplasmic domain of T (sT) is indicated above the dashed line.

Genetic and biochemical studies have shown that a complex involving the periplasmic domains of the two proteins, designated as sRI and sT (Fig. 22), is necessary and sufficient to block T-hole formation (179). Additionally, the periplasmic domains of RI and T have been purified and biophysically characterized (128). Here we report the crystal structures of sRI and of the sRI-sT complex and interpret these results in terms of a new model, at the atomic level, for this ancient signaling paradigm.

Materials and Methods

Bacterial growth and induction

Bacterial cultures were grown in either standard LB media or M9 minimal glucose media (for selenomethionine substitution) supplemented with ampicillin (100 μg mL^{-1}) as previously described (128). Briefly, cultures of SHuffle(DE3) or B834(DE3), transformed with either pET11a sRI-his or pET11a sT-his were grown with aeration at 37°C until reaching an A_{550} of ~0.5 (see Chapter II for description of strains and plasmids used in this study). The SHuffle(DE3) cultures were cooled to 16°C and induced for expression by the addition of 1 mM final concentration of isopropyl β-D-thiogalactosidase (IPTG) for 12-16 hours. The B834(DE3) cultures were harvested by centrifugation in a Beckman JA-10 rotor at 8000 rpm for 15 min at 4°C and resuspended in an equal volume of M9 minimal glucose, supplemented with all amino acids except methionine, which was substituted for with selenomethionine, and ampicillin. Cultures were grown at 16°C for 30 min then induced with IPTG as described above.

Protein expression and purification

Cultures of SHuffle(DE3) or B834(DE3) transformed with either pET11a sRI-his or pET11a sT-his that were induced overnight (see above) were harvested by centrifugation in a Beckman JA-10 rotor at 8000 rpm for 15 min at 4°C, resuspended in purification buffer (20 mM sodium phosphate pH 8.0, 0.1M NaCl) supplemented with Protease Inhibitor Cocktail (Sigma, St. Louis) and 100 μg mL^{-1} final concentrations of DNase and RNase, and finally disrupted in a French pressure cell and passed over Talon metal affinity resin (Clontech, Mountain View, CA) as previously described (128). Both

sRI and sT were eluted with purification buffer supplemented with 0.5 M imidazole; however, sT was eluted into a tube containing 500 µL containing 4 mg mL^{-1} of previously purified sRI, as previously described (128). Elution fractions of the purification of sRI and sT-sRI complex were assessed for purity by SDS-PAGE and Coomassie blue staining before further analysis. Protein was further purified by gel filtration chromatography using a prep grade Superdex 75 column then concentrated to 12 mg mL^{-1} or 8 mg mL^{-1} for sRI and the sT-sRI complex, respectively using an Amicon centrifugal filter unit (Millipore).

Crystallization of sRI native and Se-Met protein

Sitting drop crystallization of sRI was initially performed using a Crystal Phoenix robot in 96-well format plates. Over 900 conditions for sRI were screened using ratios of 1:1 and 2:1 for native protein and buffer condition, respectively. Two conditions, of similar conditions, yielded crystals, both from a crystallization screen called "Adventure Dive" designed by Inna Krieger, a research scientist in the Sacchettini group at Texas A&M. One of these 2 conditions was further optimized with crystals forming within a week in 100 mM Na citrate (pH 4.5), 1M Na acetate, 0.5% Anapoe X114 using the hanging drop method. The Se-Met substituted protein crystallized in the same condition as well with no further optimization required.

Crystallization of sT-sRI complex native and Se-Met protein

The native sT-sRI complex was also crystallized using the sitting drop method, initially, with crystals forming in a condition containing 3.2M NaCl and 0.1M sodium acetate trihydrate, pH 4.6 found in the "Salt RX" screen from Hampton Research.

Unlike sRI in which both native and Se-Met protein crystallized in the same condition, crystallization trials of Se-Met substituted sT-sRI complex failed in the "Salt RX" screen used previously. The Se-Met sT-sRI complex was rescreened using the hanging drop method, yielding crystals in a condition in the "Index" screen from Hampton Research. This screen is composed of 1 M ammonium sulfate, 0.1 M Bis-Tris, pH 5.5, and 1% PEG 3350.

Data collection and structure determination

Before data collection was performed, the crystals of sRI and sT-sRI complex were cryoprotected using either the reservoir solution supplemented with 24% (w/v) ethylene glycol for sRI or with 30% ethylene glycol added directly to the sitting drop containing the sT-sRI crystals.

Data for both crystals were collected at the 19-ID and 23-ID beamlines at the Advanced Photon Source located at Argonne National Laboratory by Vladimir Kuznetsov and other members from the Sacchettini group. Both structures were determined by the single wavelength anomalous dispersion (SAD) method using data from the Se-Met substituted protein crystals collected by V. Kuznetsov. Structure determination and further refinement were performed by V. Kuznetsov and other members of the Sacchettini group. Briefly, the sRI structure was determined by first locating the selenomethionine molecules using the SHELXD and Sharp software. Automated building of the structure was performed using the PHENIX suite of program while manual building was performed with COOT. Further refinement experiments were performed using PHENIX. The sT-sRI complex structure was solved by the

PHENIX software with manual manipulations performed using the COOT software. Final refinement was performed with PHENIX.

Results

Crystal structure of the periplasmic domain of RI

To understand the proteins involved in phage T4 lysis inhibition at the atomic level, we first purified the periplasmic domain of RI (sRI, residues 25-97 with a C-terminal hexahistidine tag) to homogeneity and crystallized it. The purification of full length RI was not feasible due to its instability and lability in the periplasmic space (180). Elongated square bipyramidal crystals (Fig. 23) diffracted to 2.2 Å on the 19-ID and 23-ID beamlines at the Advanced Photon Source (APS) located at Argonne National Laboratory. A structure of a protein similar to sRI has yet to be solved, so phase information was obtained using selenomethionine substituted protein crystallized in similar conditions to the native protein. Analysis of the native and selenomethionine-substituted protein by MALDI-TOF confirmed that all six Met residues were substituted for with Se-Met (Fig. 24).

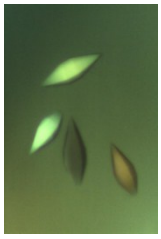

FIG 23 Photograph of typical sRI protein crystals.

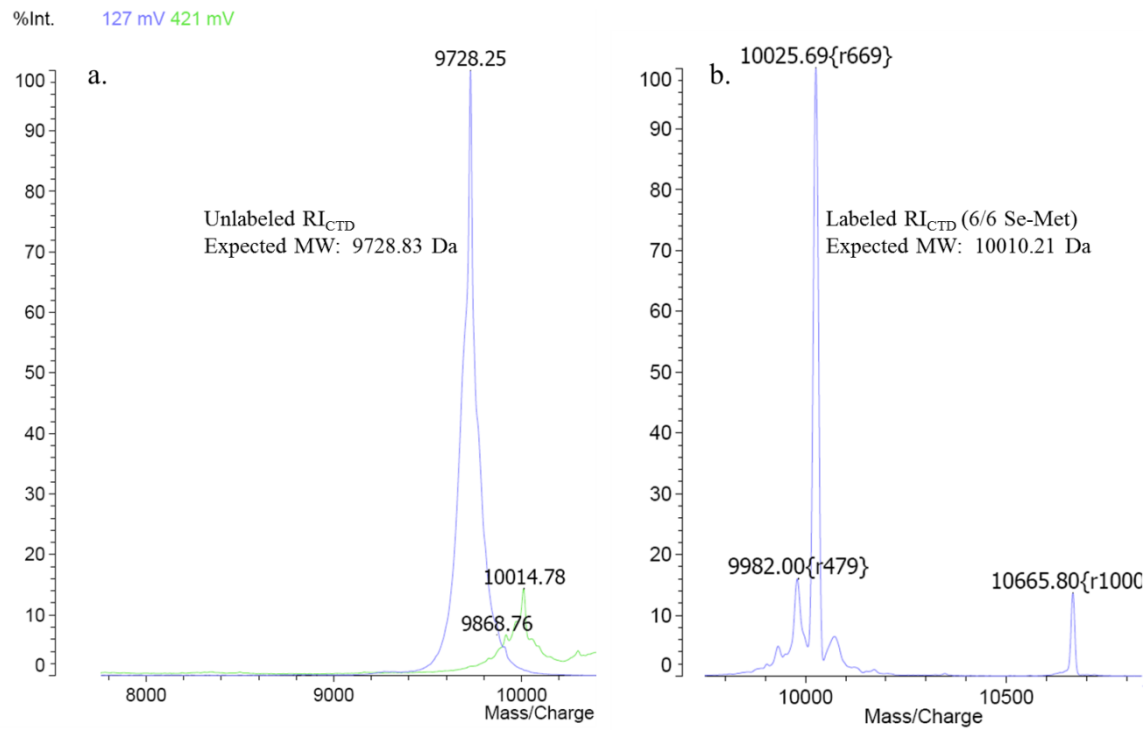

FIG 24 MALDI-TOF analysis of purified native and Se-Met sRI protein. A. Analysis of the native sRI reveals that the major peak is consistent with expected MW. B. The Se-Met protein peak is consistent with all six Se-Met residues being incorporated into the protein, however, there is a ~300 Da difference.

TABLE 6 Crystal data and refinement statistics for sRI

Data Collection Statistics	
wavelength (Å)	0.97929
data set	Peak
resolution (Å)	40.66 – 2.21
completeness % (last shell)	97.92 (95.1)
I/σ(I) (last shell)	
no. of unique reflections	
R_{sym} (%)	
Refinement statistics	
unit cell dimensions	a=b=49.975 Å, c=118.677 Å
space group	P 62 2 2 (180)
no. of protomers per assymetric unit (Z)	1
no. of reflections in the working set	4758
completeness (%)	97.9
R_{factor} (%) / R_{free} (%)	22.4 / 25.9
no. of protein residues	68
no. of solvent molecules	27
average B factor for protein (Å)	69
rmsd for bond length (Å)	0.008
rmsd for bond angles (deg)	0.988

The resulting electron density maps, solved by using the single wavelength anomalous dispersion method (SAD), were of high quality and the structure was built and refined (statistics are shown in Table 6).

One molecule of sRI was found in the asymmetric unit (Fig. 25). 93% of the residues are present, excluding Met1 and the hexahistidine tag preceded by two Gly residues. No density for the C-terminal 5 residues (Lys93-Glu97) exists, presumably due to the flexibility of the sRI tail. From the structure, the sRI molecule consists of three alpha-helical domains; helices 1 and 2 are separated by a single residue (Phe45) which forms a 15° kink, while helices 2 and helix 3 are connected by a turn domain.

The latter helices and the turn are stabilized by a single disulfide bond between Cys69 and Cys75, essential for RI function (128).

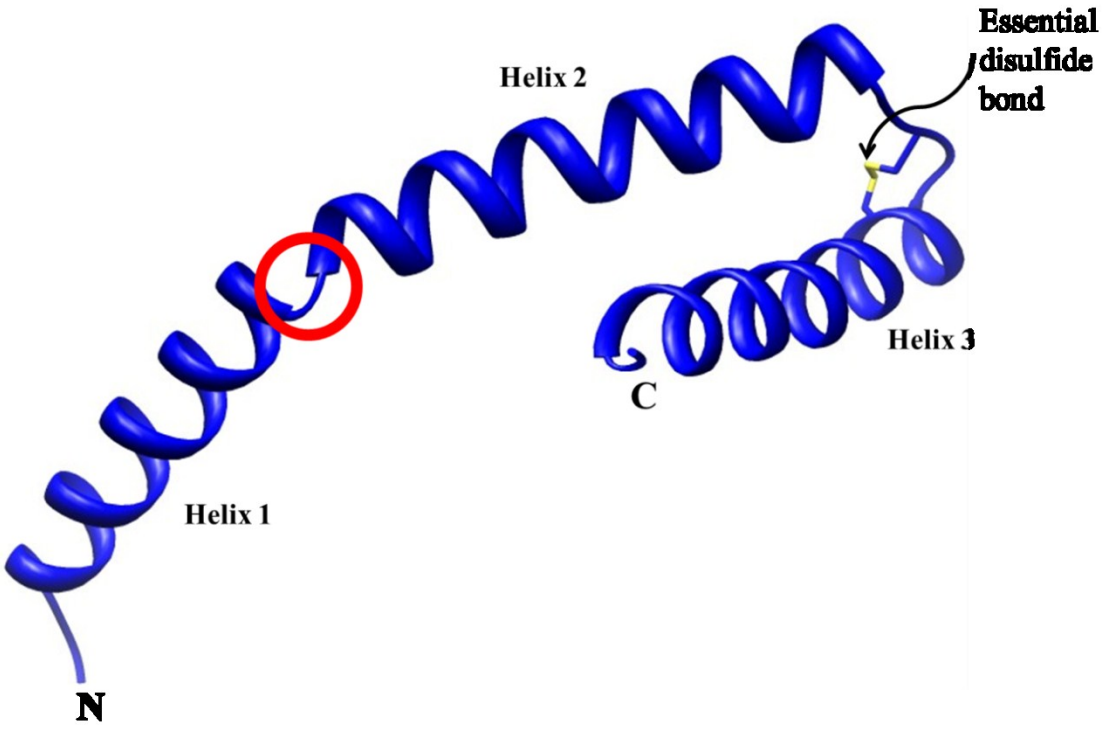

FIG 25 Structure of the periplasmic domain of RI. The red circle indicates the location of the 15° kink at Phe45, separating helices 1 & 2. The essential disulfide bond between Cys69 and Cys 75 is indicated and links the loop between helices 2 & 3 to helix 3.

While only one molecule exists in the asymmetric unit, a dimer of sRI is visible. The dimer appears to be two molecules of sRI in a head to tail fashion so that helix 1 of the first molecule interacts with helices 2 and 3 of the second molecule, and vice versa (Fig. 26). Whether this structure is physiologically relevant is unknown; however, analytical ultracentrifugation experiments previously performed to characterize the periplasmic domain of RI show that sRI is monomeric and nearly globular (128). This dimeric structure might be a result of the concentrations required for obtaining protein crystals and might represent the lowest energy state in the buffer conditions that the crystals were grown in.

Crystal structure of the complex of RI and T periplasmic domains

As shown by Tran *et al*, the interaction of the periplasmic domain of RI and T is necessary and sufficient for the induction of lysis inhibition (179). Purification of full length T, while not labile like RI, is lethal to cells by virtue of being a holin, causing large inner membrane lesions and mass culture lysis within 20 minutes of induction (128, 145). So, the purification of the periplasmic domain of T (sT, with a C-terminal hexahistidine tag) was undertaken. Unlike sRI, concentration of sT during purification lead to the precipitation of more than 50% of the protein (128). Removal of the precipitate and further concentration of the supernatant lead to additional precipitation,

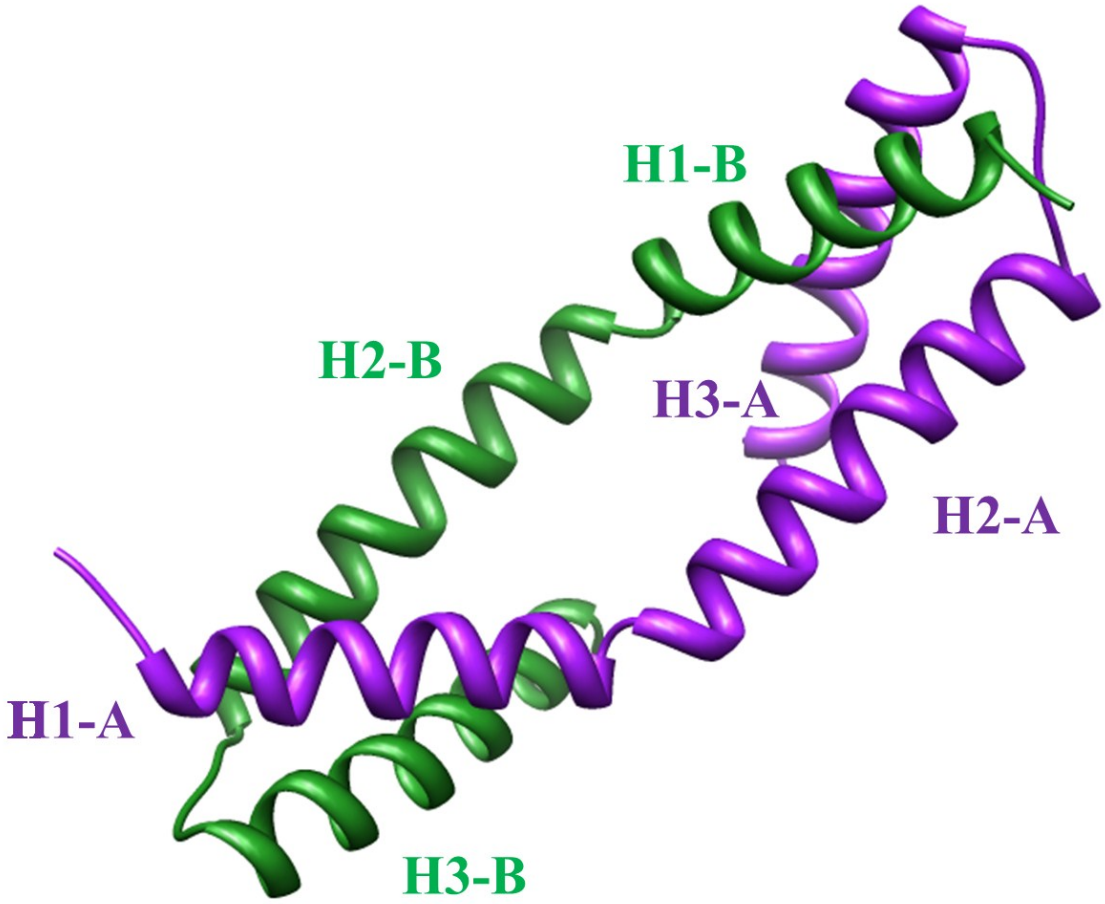

FIG 26 Structure of the RI periplasmic domain dimer form. The two sRI molecules (A and B) are arranged in a head to tail fashion. Helix 1 of molecule B (green) interacts with helices 2 and 3 of molecule A (purple), and vice versa.

probably reflecting the fact that T oligomerization leads to its ultimate function of inner membrane lesion formation. This observation, therefore, lead to the understanding that unlike other holins that oligomerize via their transmembrane domains, T utilizes its periplasmic domain as well. The inclusion of previously purified sRI, in molar excess, during the purification of sT rescued it, forming a sRI-sT complex (128).

The complex was purified to homogeneity and crystallized, yielding cubic crystals that diffracted to 2.3 Å on the 23-ID beamline at APS. Like sRI, proteins similar to sT have not had their structures solved, so phase information was again obtained by the SAD method using selenomethionine substituted RI and T protein. Unlike sRI, the selenomethionine substituted sT-sRI complex did not crystallize in the same buffer conditions as the native protein, so re-screening was required. The resulting electron density maps were of high quality and the structure was built and refined (statistics are shown in Table 7).

The sRI-sT was crystallized, with a single heterodimer in the asymmetric unit (Fig. 27). The sT molecule is globular, with a single helix at the N-terminus, leading into 5 anti-parallel beta sheets and several loops and turns. The sT structure terminates with an alpha helix which is parallel to the N-terminal helix. A disulfide bond is formed between Cys175 and Cys207, linking the C-terminal helix and the 4th beta sheet and presumably stabilizing the structure of sT. Substitution of either or both Cys residues with Ser leads to the abolishment of lysis *in vivo*. RI is bound to the opposite face of the N-terminal and C-terminal helices; however, its structure is different from that of the sRI monomer.

TABLE 7 Crystal data and refinement statistics for sRI-sT complex

Data Collection Statistics	
wavelength (Å)	0.97947
data set	Peak
resolution (Å)	40.39 – 2.50
completeness % (last shell)	99.64 (98.5)
I/σ(I) (last shell)	
no. of unique reflections	11577
R_{sym} (%)	
Refinement statistics	
unit cell dimensions	a=b=120.134 Å, c=85.159 Å
space group	P 65 2 2
no. of protomers per assymetric unit (Z)	1
no. of reflections in the working set	
completeness (%)	
R_{factor} (%) / R_{free} (%)	19.7 / 23.7
no. of protein residues	213
no. of solvent molecules	62
average B factor for protein (Å)	43.7
rmsd for bond length (Å)	0.009
rmsd for bond angles (deg)	1.04

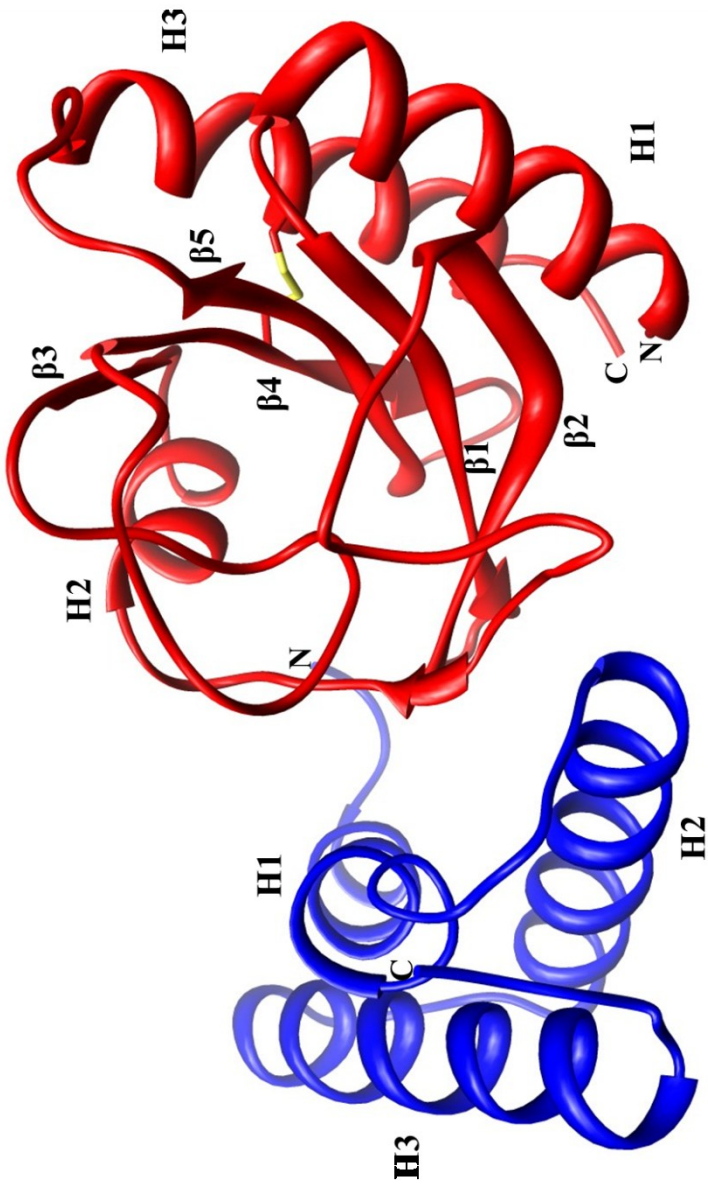

FIG 27 Structure of the complex of RI-T periplasmic domains. The periplasmic domain of T (red) binds directly with the periplasmic domain of RI (blue). The secondary structure elements are labeled for each domain.

RI undergoes a drastic conformational change when bound to T

A comparison of the sRI monomer and the complex sRI reveals a significant shift in the spatial location of helix 1 occurring around the kink separating helices 1 and 2 (Fig. 28). This shift unwinds portions of the 2 helices, creating a turn region from Val41 – Ser49 and brings helix 1 in close proximity to helices 2 and 3. The turn between helices 2 and 3 remains unchanged, presumably due to the formed disulfide bond, resulting in minimal changes to these 2 helices. The location of helix 1 in the complex is reminiscent to its location in the sRI dimer structure, in that helix 1 of the first molecule is interacting with helices 2 and 3 of the other, in a domain-swap manner. Whether only one or both of these structures are relevant in the function of RI will be addressed in a later chapter of this dissertation (Chapter V). Finally, additional residues are present in the complex sRI, with Lys93 – Glu95 now present; however, the terminal 2 residues and hexahistidine tag remain absent from the density map.

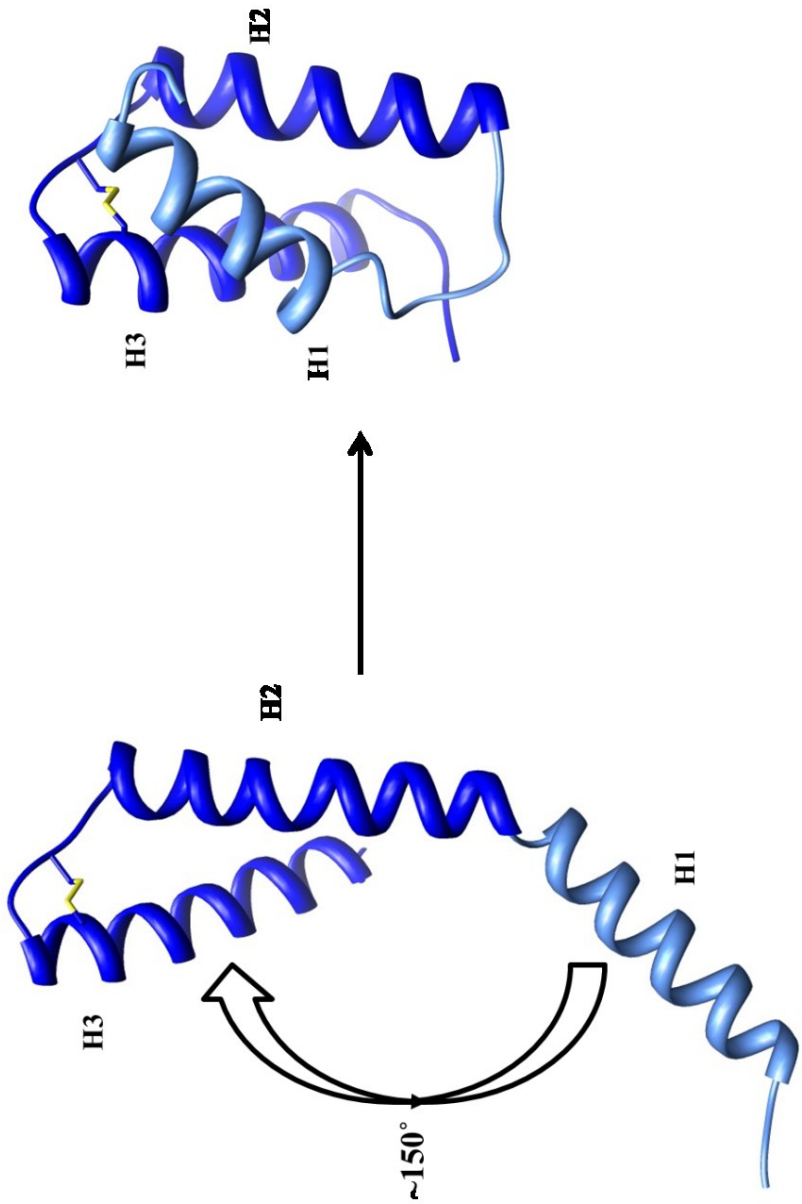

FIG 28 The change in conformation of sRI. The sRI monomer is an extended structure with H1 separated by kink from H2. The bound form of sRI is more compact with H1 making a nearly 150° swap towards H2 & H3. The spatial position of H2 & H3 remains the same between both structures, possible due to the stability of the essential disulfide bond. The movement by H1 unwinds both H1 and H2 helices, creating a large loop.

Structure of sT is similar to GAF domains

While there are no structures in the protein data bank with similar sequences to sRI or sT, a search of the sT structure against others in the PDB revealed several similar structures. The majority of these belong to proteins containing "GAF domains", so named due to their presence in c**G**MP-specific phosphodiesterases, **A**denylyl cyclases and **F**hlA (7, 84). These proteins are involved in signal transduction, binding small messenger molecules such as cGMP and cAMP (84). These domains are found in all domains of life, mostly found in bacteria but also present in archaea and eukaryotes, with more than 16,000 GAF-domains in over 14,000 different proteins.

A detailed inspection of the sT structure and that of one of the most closely related structure of a GAF-domain containing protein, RpBphP3 (PDB: 2OOL), a bacteriophytochrome from *Rhodopseudomonis palustris*, reveals dramatic similarities (199). While this protein includes several other domains, the presence of the N-terminal helix, 5 stranded anti-parallel beta sheet, and C-terminal helix in the same configuration as that of sT is striking (Fig. 29). Whether the similar structural folds between sT and those of GAF domains infers that sT might be competent in binding a small messenger molecule, such as cGMP or cAMP, has yet to be tested.

FIG 29 Overlay of sT and a GAF domain. Red: The sT domain, Brown: Crystal structure of the GAF domain of the the chromophore-binding protein RpBphP3 from *R. palustris* (PDB ID: 2OOL).

Discussion

After nearly 60 years of study, the major determinants for the imposition of lysis inhibition were determined in 2001 (144). Expression of the first *r* gene discovered in the 1940s, *rI*, in cells expressing the T4 holin, T, led to *bona fide* lysis inhibition. Additional genetic work from the Young lab led to the conclusion that periplasmic domain interactions between RI and T impose lysis inhibition (180). Here, the periplasmic domains have been purified and their structures determined by X-ray crystallography, in a collaborative effort with the Sacchettini group at Texas A&M, to understand the proteins and their interaction on the atomic scale.

The periplasmic domain of RI

The periplasmic domain of RI (sRI) was previously purified and characterized genetically, biochemically, and biophysically. The sRI domain is 72 residues and was determined to be mostly alpha-helical by CD spectroscopy (128). Analytical ultracentrifugation (AUC) work also showed that the domain is monomeric and nearly globular. Many of these observations have been confirmed by the crystal structure of the sRI domain. The structure is mostly alpha-helical, composed of three alpha helices connected by short loop stretches. Additionally, the conserved disulfide bond (Cys69-Cys75), determined by genetic studies as essential for the function of RI (128), links the loop between helices 2 and 3, to helix 3, presumably stabilizing the structure. However, the structure is extended, rather than globular as determined by AUC. Also, dimeric assembly of the sRI protein is visible in the crystal lattice, with proteins arranged in a head to tail conformation, in contrast to the previously performed biophysical

experiments (gel filtration chromatography and AUC) which determined that the purified sRI is monomeric in solution. Whether the dimeric assembly in the crystal lattice is due to crystallographic contacts that occur in the highly concentrated nature of protein crystals will be developed in a later section in this chapter and in Chapter V.

The periplasmic domain of T and complex formation

The purification and crystallization of the periplasmic domain of T (sT) was hindered by precipitation once the protein was concentrated to ~1 mg mL^{-1}. This precipitation is reminiscent of the action of holins, which is to form high-order oligomers once a certain concentration of the protein is achieved. However, the oligomerization of other studied holins, λ S and phage 21 S^{68}, is achieved through transmembrane domain interactions rather than soluble (periplasmic) domain interactions (137, 139, 194). Precipitation of sT could only be rescued when the purified protein was incubated with sRI, its inhibitor. A complex of the two proteins could be concentrated to crystallography-relevant concentrations and was crystallized and structure solved. The complex crystallized as a heterodimer of the two proteins. The sT protein is composed of both alpha helical and beta sheet secondary structure, consistent with CD spectroscopy previously performed (128). Like sRI, the sT domain also has a single conserved disulfide bond (Cys175-Cys207) which links a beta strand in the antiparallel beta sheet to the C-terminal alpha helix. Like the disulfide bond in sRI, this sT disulfide bond presumably stabilizes the globular structure of sT. When searched against other crystal structures deposited in the protein data bank, sT strongly aligns with crystal structure of proteins containing GAF domains. GAF domains are predominantly

found in proteins involved in signal transduction. These domains bind small molecules, such as cGMP. Analysis of the sT domain however, revealed that the small molecule pocket present in the GAF domains is not present in sT, at least not when sRI is bound. Whether sT not bound by RI is competent in binding a small molecule is yet to be established.

Conformational change in sRI between the apo and bound structures

An unexpected observation in the sT-sRI complex structure is the conformation of sRI. While sRI is extended in the apo (unbound) form, it is globular when bound to sT. The conformation of this bound form is consistent with the AUC determined for the purified sRI. A comparison of the two sRI structures reveals that while helices two and three remain in the same conformation, presumably stabilized by the essential disulfide bond, the first helix makes a dramatic shift. The first helix is in the same conformation as found in the dimeric assembly of sRI in that the first helix of one molecule is interacting with helices two and three of the other. Two possibilities exist that could explain this conformational change: 1) the extended monomer/dimer structure of sRI is due in part to the high concentrations used to crystallize it and also in part to the buffer conditions used, and 2) the sRI structure is dynamic in the region between helix one and two and the two structures represent one of the two conformations with the buffer conditions use to crystallize the apo structure favoring the extended conformation. The latter possibility will be tested in depth in a later chapter (Chapter V).

A model for T4 lysis and lysis inhibition

Using the two crystal structures described in this chapter, sRI and the sT-sRI complex, a preliminary model for lysis and lysis inhibition can be developed. Based on the precipitation of sT, it appears that the periplasmic domain is important in oligomerization of T, leading to hole formation. This is in stark contrast the oligomerization characteristics of other studied holins. The inclusion of the antiholin, RI, to rescue the precipitation of sT leads us to the conclusion that their interface is especially important for the oligomerization tendency of sT. The binding of sRI probably terminates a chain of holin-holin interactions. This would lead to the inhibition of lysis, as seen when RI is present in cells also expressing T. Since RI is made from early in infection, it is still unclear how it is activated or stabilized and is competent for interacting with the holin and inhibiting lysis only when a superinfection is present. Whether the apparent structural change in sRI between the two structures contributes to the activation/stabilization of RI during superinfection will be characterized in depth in Chapter V.

CHAPTER IV

GENETIC DISSECTION OF T4 LYSIS

Introduction

It is not widely appreciated that the *t* gene of phage T4 casts a long shadow in the history in modern molecular genetics. It was one of six loci identified to give rise to *r* mutants, among the first subjects for genetic analysis in phage biology (50, 81, 136). "r" stands for "rapid lysis", a phenotype associated with large, sharply-edged plaques, easily distinguished from the small, fuzzy-edged plaques of the wt phage (81). We now know that the *r* phenotype reflects a defect in establishing or maintaining the state of lysis inhibition, or LIN (136). LIN is imposed when a T4-infected cell is super-infected by another T4 virion. Essentially, when this happens the normal schedule for lysis, dictated in T4 as in all dsDNA phages by the phage-encoded holin protein, is abrogated. The infection cycle is allowed to continue, resulting in the intracellular accumulation of more progeny virions (50).

The molecular roles of two *r* loci, *rI* and *rV*, have been established (144). *rV* is allelic to *t*, encoding the T4 holin (T), and *rI* encodes the antiholin, which somehow transduces the information of the super-infection event to the capacity for inhibiting T function (53, 144). As part of our long-term effort to understand how holins effect the tight temporal regulation of host lysis, we have focused on T as a paradigm, because it not only exhibits all of the characteristic features of canonical holins but is also subject to LIN, the only established example where environmental information is used to affect lysis timing (145).

We have previously subjected *t* to genetic analysis by using it to replace the holin gene *S*, in the lambda lysis cassette (146). In the lambda context (and thus in the absence of the antiholin), *t* causes lysis to occur too early in the infection cycle, with the result that plaque formation is defective due to the lack of production of progeny virions. Plaque-forming suppressor alleles were thus easily obtained (146). Primary structure analysis indicates that the *t* gene product, T, has three structural domains: a short N-terminal cytoplasmic domain of 34 residues, a single TMD, and a 163 residue periplasmic domain (Fig. 30A,B). Most of the lysis-delay mutants mapped to the periplasmic domain (146).

Despite this long tradition of genetic analysis of *t*, including our own efforts in identifying timing mutants, there has been a complete lack of lysis-defective missense alleles (146). This has impeded both physiological and biochemical analysis of T. By comparison, many lysis-defective missense alleles have been identified for two other canonical holins, lambda S and S^{21} (75, 137, 138). The analysis of these mutants, both *in vivo* and *in vitro*, has allowed the formulation of detailed molecular pathways for holin function (137). These models have received considerable support from biochemical, cell biological and ultra-structural studies. In both cases, the holin accumulates in the cytoplasmic membrane as mobile homodimers until, at an allele-specific time, suddenly aggregating to form highly oligomeric, lethal membrane lesions,

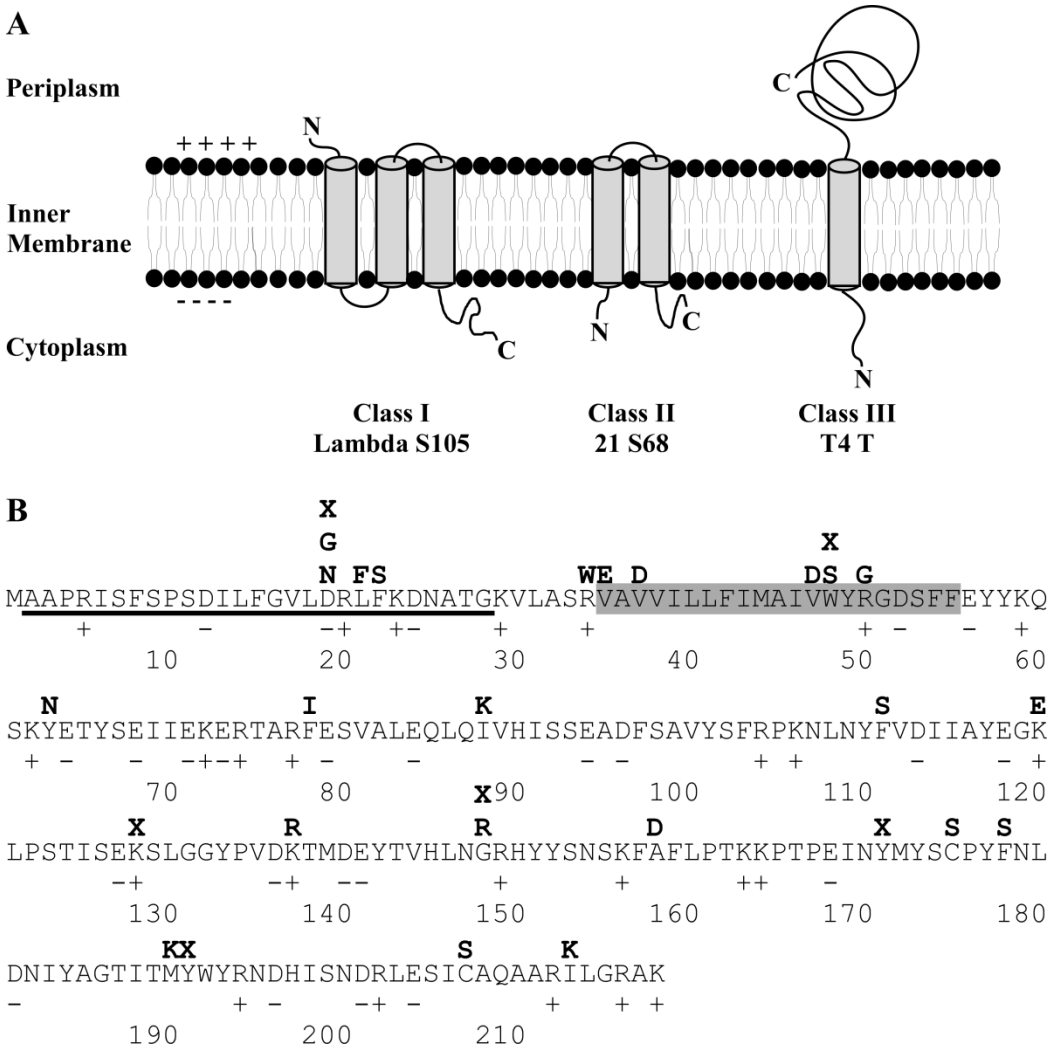

FIG 30 Lysis-defective missense mutations are obtained in all 3 topological domains of the T4 holin. (A) Topologies of the 3 classes of holin with examples of each indicated. (B) Primary structure of the T4 holin, T, with lysis-defective missense alleles indicated. The N-terminal domain is underlined and the TMD is highlighted in grey.

or holes (75, 137). S and S^{21} are prototypes of the two topology classes, I and II, into which all holins identified to date, including dozens of unrelated protein families, can be

parsed, except for T and its homologs (202) (Fig. 30A). The latter comprise a unique class (III), and are the only holins with significant soluble domains (146) (Fig. 30A).

These considerations suggest that similar mechanistic insight for class III holins might derive from analysis of a collection of *t* lysis-defective alleles. Here we report efforts to generate and characterize such a collection. The results are discussed in terms of a model for T function and its regulation by RI.

Materials and Methods

Bacterial strains, plasmids, bacteriophages and culture growth

The bacterial strains, bacteriophages, and plasmids used in this study are described in Table 8. Bacterial cultures were grown in standard LB medium supplemented with ampicillin (100 μg mL^{-1}), kanamycin (40 μg mL^{-1}), and chloramphenicol (10 μg mL^{-1}) when appropriate. Growth and lysis of cultures were monitored by A_{550} as described previously (128). When indicated, isopropyl β-D-thiogalactopyranoside (IPTG), KCN, or $CHCl_3$ was added to give final concentrations of 1 mM, 10 mM, or 1%, respectively. For the dominance/recessiveness tests, CQ21 cells lysogenized with a derivative of λ with the *S* holin substituted for the parental *t* gene (145) were transformed with pZA-ssPhoAΦsT* plasmids and induced at A_{550} of 0.3 by shift to 42°C and addition of IPTG (1 mM). Experiments testing whether the mutant periplasmic domains were competent in binding RI were performed by infecting CQ21 cells transformed with pZA-ssPhoAΦsT* with wild type T4 at an $A_{550} \sim 0.2$.

TABLE 8 Phages, strains, and plasmids used in this study.

Phages	**Description**	**Source**
T4 wt	Bacteriophage T4D	Lab Stock
λΔ(*SR*)	Δ(*stf-tfa*)::*cat c*I857 Δ(*SR*)	Lab Stock
Strains	**Description**	**Source**
MC4100ΔtonA	*E. coli* K-12 F *araD139* Δ(*argF-lac*)*U169 rpsL15 relA1 flbB3501 deo pstF25 rbsR tonA-*	Lab Stock
MC4100 λ*cam*Δ(*SR*)	MC4100ΔtonA lysogenized with λΔ(*SR*)	Lab Stock
CQ21 *recA srl::Tn10*	*E. coli* K-12 *ara leu lacI* ^{q1} *purE gal his argG rpsL xul mtl ilv*	Lab Stock
CQ21 λ*kan*Δ(SR) *recA srl::*Tn*10*	CQ21 lysogen carrying λ*kan*Δ(*SR*) prophage	Lab Stock
SHuffle T7 (SHuffle(DE3))	*E. coli* K-12 *fhuA2 lacZ::T7 gene1 [lon] ompT ahpC gal λatt::pNEB3-r1-cDsbC ΔtrxB sulA11 R(mcr-73::miniTn10)2 [dcm] R(zgb-210::Tn10) endA1 Δgor Δ(mcrC-mrr)114::IS10*	New England Biolabs
Plasmids	**Description**	**Source**
pER-t	Carrying lysis cassette of λ except *S* is replaced by T4 *t* gene	(145)
pER-t$^{\Delta 2\text{-}28}$	pER-t with residues 2-28 deleted in *t*	This study
pSM-t	pER-t with in-frame deletion of *Rz/Rz1* in the lysis cassette of λ	(128)
pSM-t*	pSM-t carrying lysis-defective mutations of *t*	This study
pZA-T	pZA32Δ*luc*::*t*	(179)
pZA-ssPhoAΦsT	Codons 1-55 in pZA-T replaced by codons 1-26 of *phoA,* encoding signal sequence	(179)
pZA-ssPhoAΦsT*	pZA-ssPhoAΦsT carrying lysis-defective mutations of *t* found in the periplasmic domain	This study
pET11a-sT^{his}	pET11a-T^{his} with deletion in codons 2-55 of *t*	(128)
pET11a-sT^{his} I88K	pET11a-T^{his} carrying I88K mutation	This study

Error-prone PCR mutagenesis and selection for lysis defective alleles of t

Error-prone PCR mutagenesis was performed using the GeneMorph II Random Mutagenesis kit and was used with no modification from the manufacturer's instructions, except for optimization of PCR cycle number and temperature conditions to maximize the number of alleles with single nucleotide changes. Oligonucleotides for PCR mutagenesis were obtained from Integrated DNA Technologies (Coralville, IA) and were used without further purification. Mutagenized PCR fragments of *t* were double-digested using NcoI and BglII from New England Biolabs and ligated into the parental plasmid, pSM-t with T4 ligase (NEB). This plasmid carries the lambda lysis cassette except λ *S* was substituted with T4 *t* and the *Rz/Rz1* have been deleted. Both *t* and *R*, the lambda endolysin, are under control of the pR' promoter. *E. coli* XL1 blue cells were transformed with these mutagenized plasmids (pSM-t*), each transformant plate slurried (~500 colonies/plate), and plasmids purified using the Qiagen spin miniprep kit. *E. coli* MC4100 cells carrying a thermo-inducible lambda lysogen [λcamΔ(*SR*)], defective in lysis, were transformed with the pSM-t* plasmids candidate *t* defective plasmids. In this system, the induction of the prophage provides *Rz/Rz1* function and transactivates the plasmid promoter, ensuring that the necessary lysis proteins (holin, endolysin, and Rz-Rz1) are provided with physiologically relevant timing and expression levels. An initial enrichment for lysis-defective alleles was performed by slurrying a freshly transformed plate with ~500 transformant colonies with LB, dilution, and inoculation into 100 mL LB with appropriate antibiotics to a starting A550 ~0.05. Cultures in LB broth supplemented with ampicillin were grown at 30°C to A_{550} of 0.3, plasmids induced by

heat shift for 60 min, and non-lysed cells were collected by filtration. Plasmids of the collected cells were prepared using the Qiagen spin miniprep kit and used to transform MC4100 λcamΔ(*SR*) cells. Single colonies were picked, grown to $A_{550} \sim 0.3$ in 5 mL of LB supplemented with ampicillin at 30°C, induced by aerating at 42°C for 15 min, then grown for 45 more minutes at 37°C. These cultures were assessed for lysis activity by monitoring culture growth throughout the induction period. $CHCl_3$ was added to each culture at the end of each experiment to ensure that the lack of lysis was due to a defective holin, rather than a defective plasmid not expressing the wild type *R* endolysin gene. Plasmids of defective *t* alleles were sequenced by Eton Biosciences (San Diego, CA) to determine mutation responsible for the defective gene.

TCA precipitation, subcellular fractionation, SDS-PAGE, and Western blotting

To quantify the amount of protein produced from pSM-t*, 10 mL of a culture induced for 15 min were collected and 1.1 mL of 100% cold TCA was added (10% final), as described previously (128). Precipitates were collected by centrifugation at 7,000 rpm in a clinical centrifuge, washed in 5 mL of cold acetone, and pellets dried. The pellets were resuspended in sample loading buffer containing 5% β-mercaptoethanol. Subcellular fractionation of cells, to determine whether the *t* allele was present in the membrane fractionation was performed as previously described (107). Briefly, 25 mL of induced cultures were collected by centrifugation at 4000 x *g* in a Sorvall Superspeed RC2-B centrifuge and resuspended in 2 mL of purification buffer (0.1 M sodium phosphate pH 8.0, 0.1 M NaCl) supplemented with Protease Inhibitor Cocktail (Sigma, St. Louis), and 100 μg mL^{-1} final concentrations of DNase and RNase.

Cells were disrupted in a French pressure cell at 16,000 lb/in^2 and the membrane and soluble fractions were separated by centrifugation at 100,000 x *g* in a Beckman TLA100.3 rotor for 60 min. Equivalent amounts of each fraction were examined by SDS-PAGE and Western blotting. SDS-PAGE and Western blotting were performed as previously described (128).

Blue-native PAGE

Blue-native PAGE was performed as previously described (137) with minor modifications. Cultures expressing wild type T or its lysis defective alleles were harvested at wild type T lysis time (15 min after induction) and disrupted by French pressure. Membrane fractions were collected by ultracentrifugation in a 50.2 TI rotor. Membranes were resuspended with 1 mL extraction buffer (50 mM NaCl, 50 mM imidazole, 1 mM EDTA, 10% (v/v) glycerol, and 1% n-dodecyl-β-D-maltopyranoside) and extracted overnight at 4°C. Insoluble material was removed by ultracentrifugation at 100,000 x *g* in a TLA100.3 rotor for 60 min and 20 µL of supernatant was mixed with 1 µL 5% (w/v) Coomassie Brilliant Blue G-250 (Bethesda Research Laboratories, MD). Samples were loaded on a 4-16% NativePAGE gel (Invitrogen), with electrophoresis and Western blotting performed as described previously (137).

Gel filtration

Gel filtration chromatography was carried out using an analytical grade Superdex 200 column, calibrated with standards purchased from Bio-Rad, on an AKTA FPLC. Column was equilibrated with 20 column volumes of purification buffer with 1% DDM

before sample injection. Once sample was injected, gel filtration was performed at 0.4 mL min^{-1} until one column volume of buffer had eluted. Fractions were collected and analyzed by SDS-PAGE and Western blotting as described previously (128). Results

Results

Missense mutations conferring defective lysis are isolated in all 3 topological domains of the T holin

To obtain a pool of lysis-defective *t* mutants, the *t* gene was subjected to error-prone PCR mutagenesis. This pool of mutant DNAs was used to construct a library of medium copy plasmids with the *t* gene cloned under the control of the λ late promoter, pR'. The library was first enriched for lysis defective alleles and then screened for failure to complement the lysis defect of a holin-defective lambda prophage (Fig. 31). Using this screen, 45 lysis-defective alleles were identified (Fig. 30B and Fig. 32). Among the lysis defective alleles, 10 had two or more missense changes, and 20 had single missense alleles. The mutant hunt did not approach saturation for single missense changes, as judged by the fact that 20 nonsense alleles were obtained out of 78 that could be expected from random single base changes in the *t* reading frame. Nevertheless, missense mutations in all three topological domains of T were isolated, and are considered below in each context.

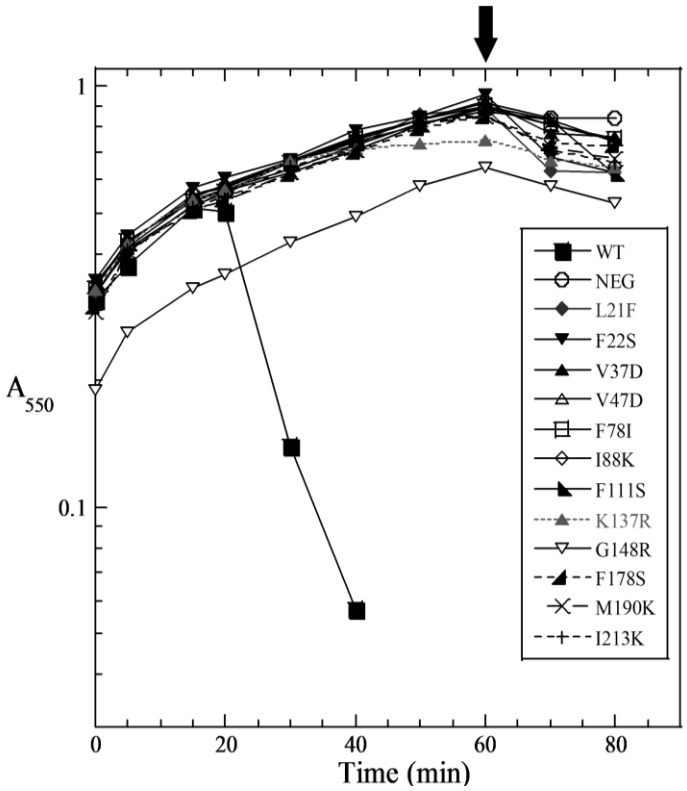

FIG 31 Lysis defect of *t* missense mutants. Cells carrying the indicated *t* alleles in the context of the pSM-t plasmid were thermally induced in logarithmic growth at t=0. The arrow at 60 min indicates the addition of 10 mM KCN (final).

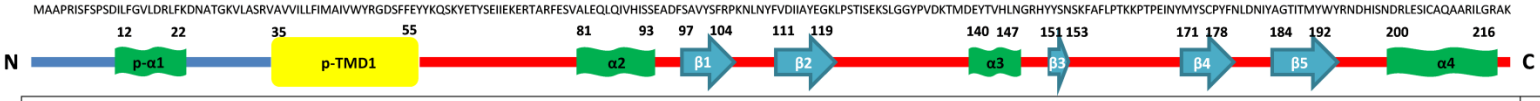

D12N W48R	2
I43K L203H	2
E56D R216G	2
K62E S174Y	2
E84G A208T	2
L121W K137E	2
P134S M172I	2
I188K A208D	2
A3T Y58C S155P	3
L18P V37L P105R	3
L21S F103I L108I	3
K23I K62T E141K	3
A32T S33P M190K	3
E73G E118G S174N	3
V81D E118V I188K	3
L83M F159C F178L	3
Y171F T189S H197R	3
E56G E84G D136N M139T	4
R5X D19E	2 - X
I43L C175X	2 - X
Y49F W192X	2 - X
F54Y Y173X	2 - X
Y63X S80Y	2 - X
Y117X F157L	2 - X
Y49X D96Y D196V	3 - X
K62X V112D C207Y	3 - X
Q87L E118X S129X	3 - X
D12S M44V Q85X S153T	4 - X
Y117X P134H E168X T189I	4 - X
I43V E118D G148E E204X R216W	5 - X

FIG 32 Other mutants that deem the T4 holin non-functional. The primary and secondary structures are indicated. Various missense and nonsense mutations of T are indicated at their approximate location below.

The N-terminal cytoplasmic domain (residues 1 – 34; T^{NTD})

Among the experimentally confirmed holins, all but T have a very short cytoplasmic domain, usually only a few residues. Extensive mutational analysis of lambda *S* and phage 21 S^{21} has shown that these small cytoplasmic peptide sequences control the topology of the first TMD, and thus the lytic function of the holin, through the presence or absence of charged residues. In both cases, mutations that increase the positive charge in the short cytoplasmic domain change the membrane topology and cause a loss of lytic function. T has a predicted 31 aa cytoplasmic domain, easily the largest of any identified holin (188). Previously, the only two *t* missense changes conferring an absolute lysis defect, D19N and D19G, were also in the N-terminal cytoplasmic domain and also caused an increase in net positive charge of the domain (146). However, selection using the PCR-mutagenized pool yielded two more lysis-defective mutants, L21F and F22S, in the cytoplasmic domain, with neither affecting an alteration in the predicted charge. This brought the total to four independent lysis-defective mutants with missense changes clustered within a four residue stretch of the cytoplasmic domain. Secondary structure analysis using JPred indicated that this sequence is predicted to form an amphipathic alpha helix (Fig. 33); moreover, this predicted secondary structure is conserved in *t* genes from other phages even when sequence similarity in the cytoplasmic domain is absent. Taken together, these results suggest that the amphipathic helix is required for T hole formation. Given this perspective, we predicted that a deletion of the N-terminal domain would be lysis-defective. Fig. 34 shows that induction of a $t^{\Delta(2\text{-}28)}$ deletion construct delayed the

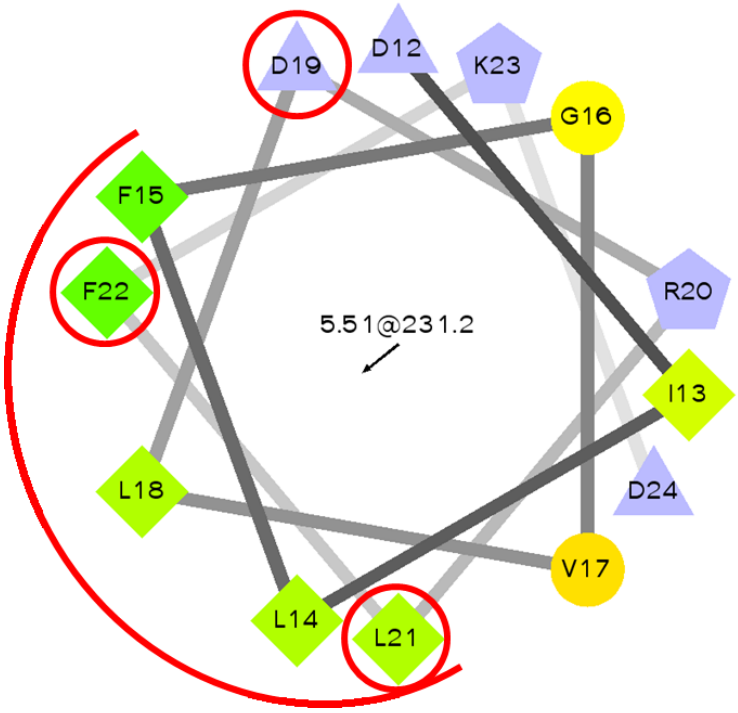

FIG 33 The N-terminal domain of T contains a predicted amphipathic helix. A helical wheel projection of the predicted amphipathic helix from residues 12-24, with hydrophobic residues indicated by green diamonds, charged residues in blue, and weakly hydrophobic residues in yellow. The hydrophobic face of the helix is indicated with a red arc. Defective alleles of T in amphipathic helix residues are indicated by red circles.

sharply-defined lysis characteristic of T and other holins. The optical density of the culture was observed to begin slowly dropping at ~80 min. Addition of cyanide to depolarize the membrane causes instant triggering of experimentally-confirmed holins, and thus can be used as an indicator of holin function. Cyanide does trigger the deletion mutant with a gradual decline in optical density, suggesting that it is indeed functional in lysis but delayed in lysis timing. The third mutant in this domain is considered below.

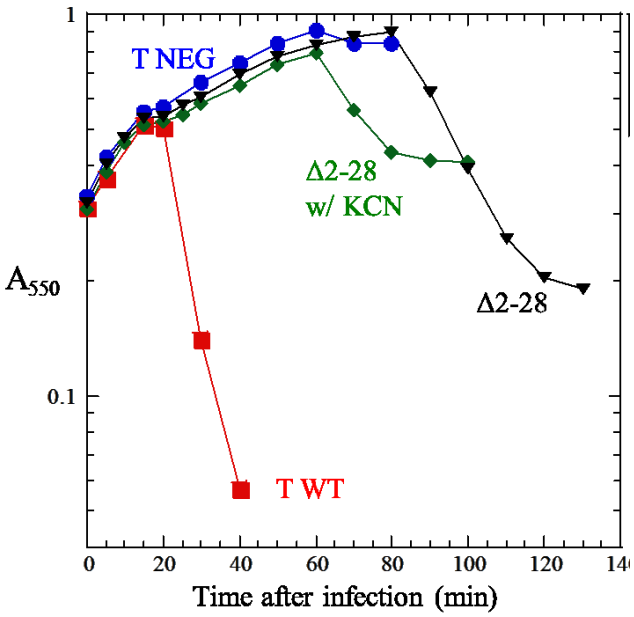

FIG 34 Lysis defect in T N-terminal deletion. Growth curves of cultures expressing the indicated *t* allele. Induction of T deleted for residues 2-28 in the N-terminus results in growth to 80 min where the O.D. begins to slightly decrease. Addition of 10 mM KCN does trigger lysis of the N-terminal truncation mutant.

The TMD (residues 35 – 55; T^{TMD})

T is unambiguously an integral membrane protein. Nevertheless, most algorithms designed to predict TMDs fail to identify a TMD in the T primary structure, because the longest stretch of hydrophobic sequence uninterrupted with charged residues is only 15 aa (Val36 to Try49), too short for a TMD to span the bilayer. However, in a helix, R50 and D52 could form a 1 – 3 salt bridge, as is seen in three positions in the TMDs of lambda S (75). Incorporating this salt-bridge would allow the TMD to extend to a more reasonable length of 20 residues, through Phe55 (Fig. 30B). The mutants in this region support the notion that the TMD spans this region. V37E, V39D, and V47D would each directly introduce a charged residue and shorten or destroy the predicted TMD, whereas R50G would have the same effect indirectly, by eliminating the required salt bridge. W48S would also drastically reduce the hydrophobic character of the TMD. In this light, the absolute lysis defect of R34W is intriguing and suggests that the positioning of the TMD with respect to the soluble cytoplasmic and periplasmic domains is critical. The most striking aspect of this collection of mutants is the absence of lysis-defectives with conservative changes not predicted to alter the hydrophobic character or positioning of the TMD. In all three other holin systems where lysis-defective missense alleles have been obtained, multiple alleles have been isolated with conservative changes within the TMD segments. This suggests that the TMD of the T holin is relatively less important in terms of the pathway to lethal hole formation, presumably because the soluble domains carry the critical determinants.

The periplasmic domain (residues 56 to 216; T^{CTD})

The periplasmic domain of T has been subjected to extensive analysis as an independent domain. It is the binding target of the T4 antiholin, RI. Hetero-dimeric complexes between the periplasmic domains of RI and T have been purified and characterized. In the absence of RI, T^{CTD} rapidly oligomerizes. Thirteen lysis-defective missense changes were found in this domain. However, unlike the lysis-defective mutants in T^{NTD}, the T^{CTD} mutations do not cluster but are instead spread evenly across the entire domain (Fig. 30B). Most of the changes are dramatic alterations, representing charge changes (I88K, G148R, A158D, M190K, and I213K) or charge reversal (K120E). However, two conservative changes were also obtained: F78I and K137R. The most distal nonsense mutation obtained was in position 191, indicating that the extreme C-terminus of the protein is required for T function. The I213K mutation is notable in that the mutation adds yet another positive charge to an already highly basic C-terminal peptide sequence. In both S and S^{21}, the extreme C-terminal domain is also rich in basic residues. Although charge-change mutations can alter lysis timing, the domain is non-essential in both cases, indicating that the C-terminal domain plays an essential functional role in this prototype class III holin.

Lysis-defective T proteins accumulate in the membrane

To determine whether the missense changes that confer an absolute lysis defect affect accumulation of the protein, whole cell extracts taken at 15 min after induction were examined by immunoblot with a T-specific antibody. Every allele tested exhibited normal T accumulation, with only a few showing slight reductions in T levels and others

showing increased accumulation (Fig. 35A). Additionally, when cells from the induced cultures were collected, lysed and fractionated to assay the soluble and

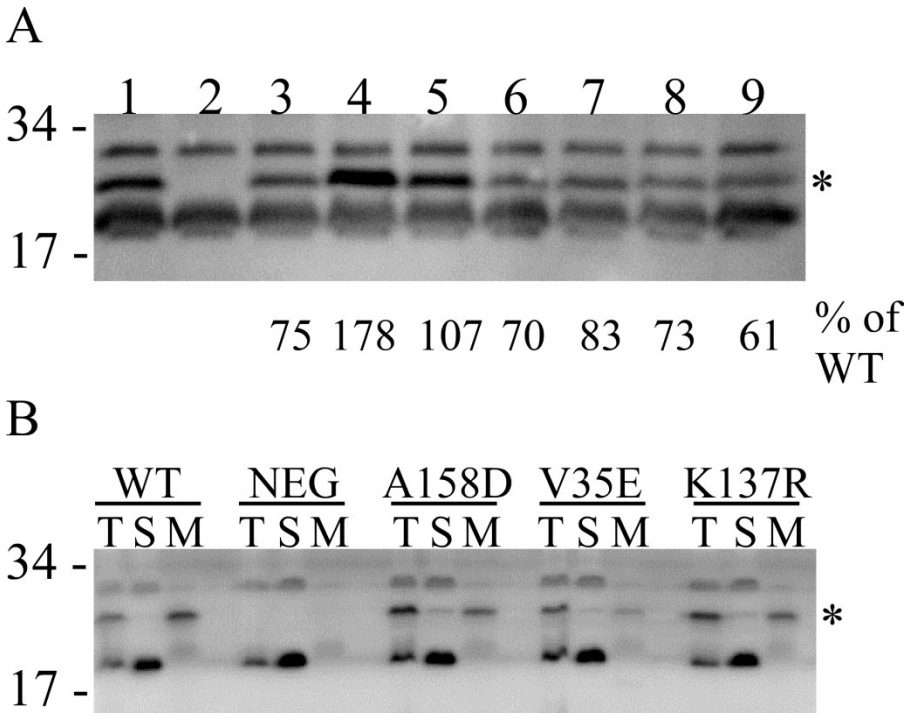

FIG 35 Non-functional mutants of T accumulate to near wild type T levels and are targeted to the membrane. (A) Assessment of protein accumulation at 15 min after induction of various non-functional alleles of *t.* Lanes 1-9: wild type, D12X (negative control), F22S, Y63N, A158D, V35E, K137R, G148R, and V37D, respectively. Percent accumulation of mutants compared to wild type is indicated. (B) Membrane fractionations of the indicated alleles of *t.* * indicates migration of T. T: total protein, S: soluble fraction, M: membrane fraction.

membrane-bound levels of T, all of the lysis-defective mutants exhibited proper localization to the membrane. Studies with the other holin proteins have shown that similar variations of the level of holin accumulation affect lysis timing but not the ability to effect lethal hole formation (29). Thus these *t* alleles are qualitatively dysfunctional, with the missense changes affecting holin-holin interactions and blocking the hole formation pathway, as demonstrated for the class I and II holins previously (75, 137) (Fig. 35B).

Lysis-defective mutants are in conserved residues

Residues important for the function and structure of a protein are usually conserved in their homologues. We aligned 30 T homologues to determine whether the lysis-defective missense mutations corresponded to conserved residues. The result shows that, while the T holins are well conserved in general, the residues in which mutants were isolated are conserved to an even higher degree (Fig. 36). In particular, residues D19, F22, and F178 are more than 80% conserved and residues I88 and K148 are 100% conserved among the sequences analyzed.

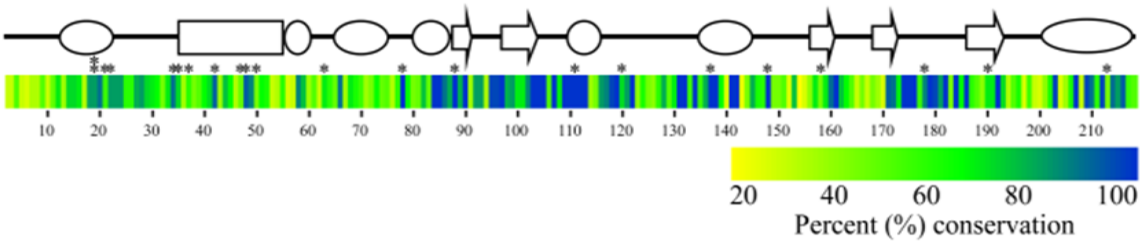

FIG 36 Mutants in T are in conserved residues. The secondary structure elements of T are indicated with a heat map of the percent conservation of each residue based on an alignment of all T4-like phage holin. Asterisks indicate location of non-functional mutants of the T4 holin.

TABLE 9 Dominance/Recessiveness of the non-functional missense mutants of T.

Lysis-defective alleles of *t*	Dominant/Recessive
D19N	Recessive
D19G	Recessive
L21F	Recessive
F22S	Recessive
R34W	Recessive
V35E	Dominant
V37D	Dominant
F42S	Recessive
V47D	Recessive
W48S	Recessive
R50G	Recessive
Y63N	Recessive
F78I	Dominant
I88K	Dominant
F111S	Recessive
K120E	Recessive
K137R	Dominant
G148R	Dominant
A158D	Dominant
F178S	Dominant
M190K	Recessive
I213K	Dominant

Dominance/recessiveness of mutants in a background expressing wild type T

The lysis defective T holins were also tested for dominance-recessiveness by inducing in the presence of prophage-borne wild type T induced from a λ*t* hybrid prophage. Under these conditions, 9 of the 22 alleles exhibited at least some dominant character, in that lysis was delayed as compared to induction of wild type T from both a plasmid and prophage (Table 9). The rest exhibited recessive character, lysing at the same time as wt.

Mutants are defective in oligomerization

In order to characterize the oligomerization propensity of the wild type and defective alleles of *t*, crosslinking experiments with dithiobis [succinmydyl propionate], glutaraldehyde, formaldehyde, and benzophenone-4-maleimide were carried out, similar to previous studies characterizing holin mutants (75, 139, 206). However, these methods failed to show crosslinking results in wild type T, so were abandoned. Instead, wild type and lysis defective T proteins were extracted with 1% n-dodecyl-β-D-maltopyranoside (DDM) from the inner membrane and characterized by blue-native PAGE and gel filtration. Blue-native PAGE analysis of cells induced for wild type T revealed a discrete band at approximately 650 kDa, corresponding to ~27 T molecules (Fig. 37). This observation was buttressed by the gel filtration of micelles containing wild type T which eluted at nearly 900 kDa. Lysis-defective alleles of T were also extracted and did not show the same oligomerization propensity as wild type based on both blue-native PAGE and gel filtration (Fig. 38A,B).

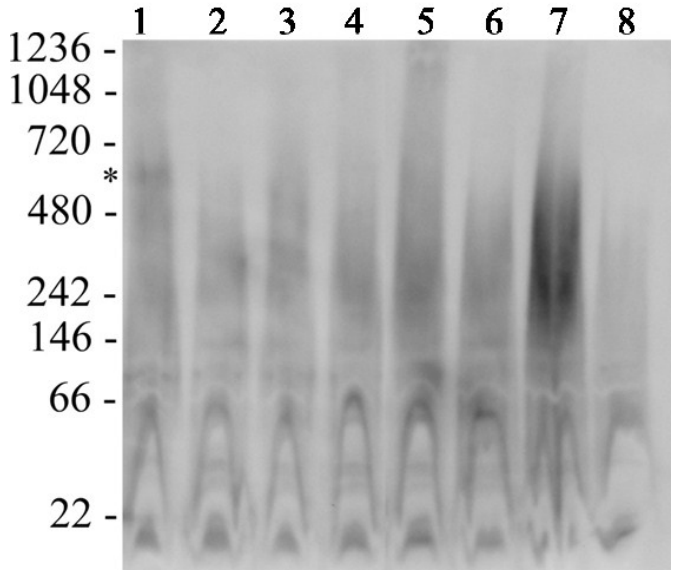

FIG 37 Blue Native PAGE analysis of various non-functional alleles of T indicates they are non-functional in oligomerization. Lanes 1-8: wild type, D12X, L21F, F22S, F78I, I88K, F111S, and G148R, respectively. * indicates migration of wild type T.

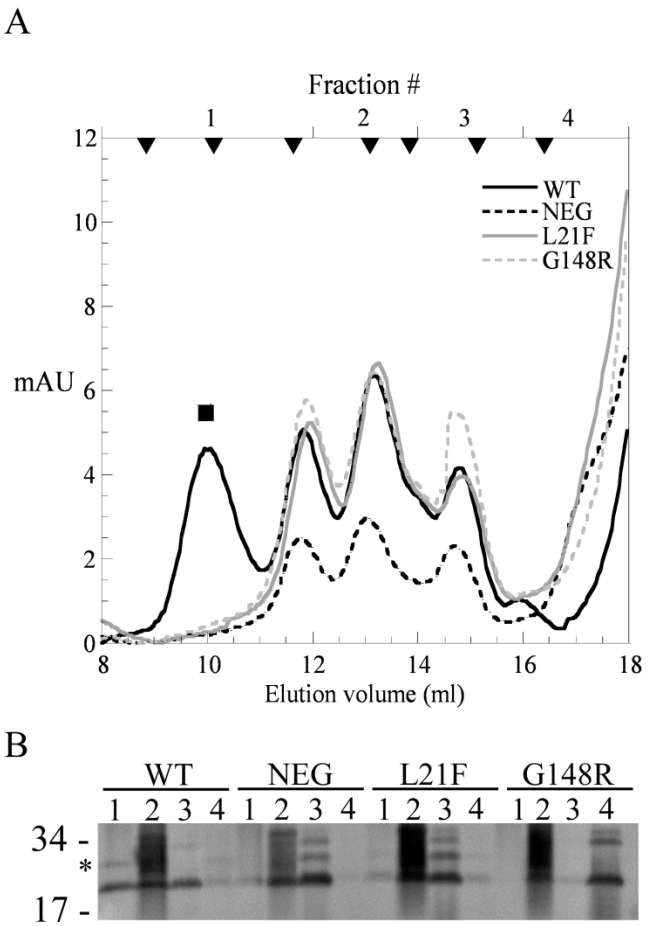

FIG 38 Gel filtration of non-functional alleles indicates that they are defective in oligomerization. (A) Gel filtration profiles of extracted *t* alleles. (B) Western blot of fractions from the gel filtration experiment in (A).

Periplasmic domain of T is soluble with non-functional mutations

Previously, we showed that the purification of the periplasmic domain of T was hindered by precipitation at high concentrations (128). The protein could be rescued from precipitation by incubation with the periplasmic domain of the antiholin, RI. We tested whether non-functional mutants of T were also destined to precipitation or if the mutations were somehow defective in oligomerization and hence precipitation. The periplasmic domain of T with the I88K mutation was overexpressed, as previously described, and purified with an affinity column. Unlike the wild type periplasmic domain, the I88K mutant remained completely soluble (Fig. 39A). Gel filtration of the purified soluble protein supported this observation with the protein eluting in a single peak consistent with monomeric status (Fig. 39B).

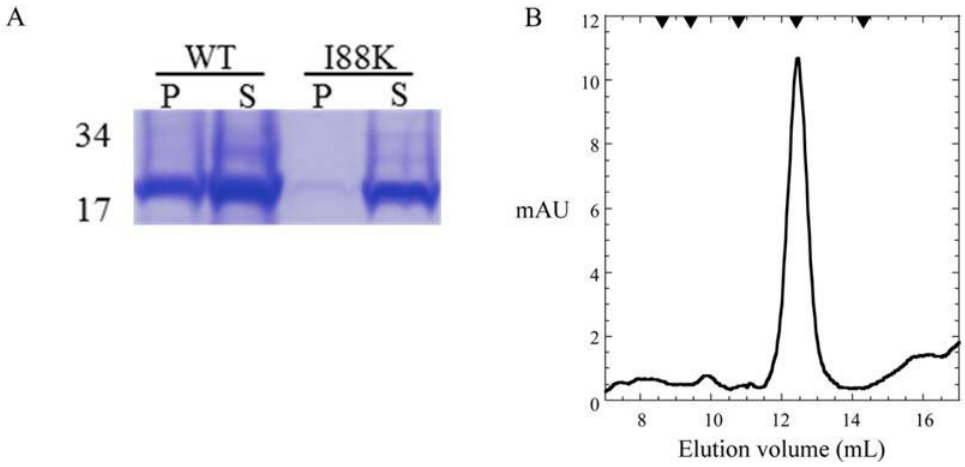

FIG 39 The periplasmic domain of T is soluble in non-functional alleles. (A) Purification of the periplasmic domain of T results in nearly 50% of protein remaining soluble while nearly 100% of the I88K periplasmic domain remains soluble. (B) Gel filtration of the I88K periplasmic domain indicates that the protein elutes in a single fraction consistent with monomeric status. P: pellet, S: soluble

Lysis-defective alleles of T are also defective in binding the antiholin, RI

When lysis inhibition (LIN) is imposed, the lysis function of T is overridden by the binding of RI to the periplasmic domain of T (128, 144, 179). In view of the

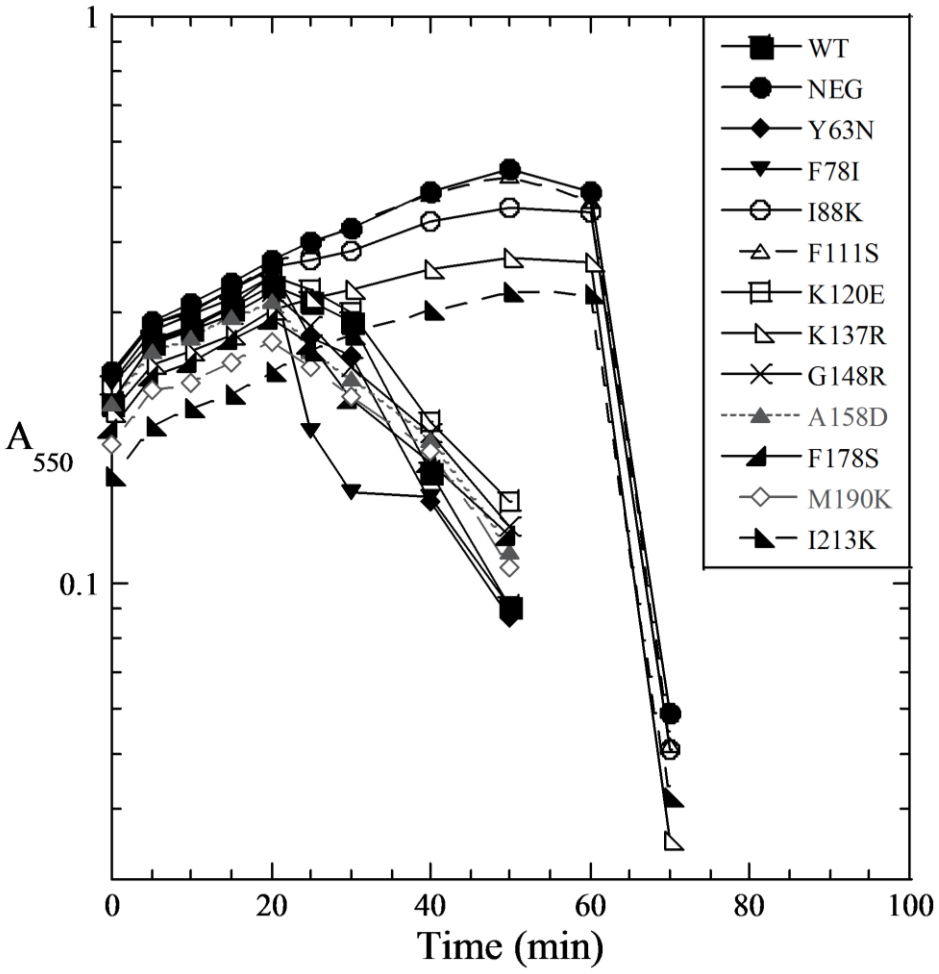

FIG 40 Four lysis defective alleles of *t* abrogate interactions with RI. *E. coli* CQ21 cells transformed with pZA-ssPhoAΦsT* with the indicated mutations and plasmid were induced with IPTG and infected with wild type T4 at time = 0. Lysis indicates that the sT domain can bind RI, titrating it away from full length T encoded by the wild type phage while no lysis indicates that the mutated periplasmic domain of T is not competent in RI binding.

isolation of a significant number of non-functional missense mutations in the periplasmic domain of T in this study, we wondered if any were also defective in the binding of RI as well. To test this possibility, cells transformed with a plasmid encoding a chimeric protein of the PhoA signal sequence fused with the periplasmic domain of T were infected with wild type T4. Previously, Tran *et al*. showed that the expression of this chimera during a wild type T4 infection nullified LIN due to the titration of RI by the soluble periplasmic domain of T (179). We used this system, with the periplasmic domain mutants encoded on the PhoA-T chimera to determine if these mutant alleles were capable of titrating RI and preventing LIN. While 7 of the 11 mutants exhibited lysis at ~20 min, indicating that these proteins are able to bind T and prevent the onset of LIN, four failed, leading to lysis inhibition of the cultures. The mutations in residues I88, F111, K137, and I213 fail to bind RI and are likely to be residues important for the T-RI interaction (Fig. 40).

Discussion

Holins, in their role of controlling the length of the phage infection cycle, are arguably among the oldest and simplest of biological timing systems. Holins are very diverse, but despite the sequence diversity, the vast majority of holins identified to date are largely defined by linked TMDs, with either class I (3 TMDs; N-in, C-out) or class II (2 TMDs; N-in, C-in) topologies (202). Most of the progress in investigating holin function has been made with two prototypes, λ S for class I and phage 21 S^{68} for class II (74, 75, 137, 138). In each case molecular analysis was initially based on an extensive collection of lysis-defective mutants, obtained by selecting for loss of lethal function. In

contrast to class I and class II, the holins of class III belong to a single sequence family, the homologs of T4 T, found in two virulent phage types, the T4-like myophages and the T5-like siphophages. The class III holins are unique not only in size but also in topology, composed of a single TMD.

Here we have reported the selection and characterization of a collection of lysis-defective missense alleles of T4 *t*. Besides providing essential control materials for biochemical, biophysical and cell biological analysis of T holin function, aspects of the distribution, location and character of these lysis-defective mutations are informative, especially in terms of a comparison to the findings of our previous extensive mutational studies on two prototype holins, the class I lambda S and the class II S^{68}.

Distribution of lysis-defective mutations in t

By selecting for loss of lethality, missense mutations abolishing lethal T function, without compromising accumulation or membrane localization, were obtained in all three topological domains: the N-terminal cytoplasmic domain, the TMD, and the C-terminal periplasmic domain. In contrast, all such mutations isolated in the S and S^{68} systems were located in the TMDs or connecting loops (74, 75, 138). In S and S^{68}, the cytoplasmic and periplasmic oligopeptide sequences at the N and C termini have been shown to be regulatory domains, non-essential for hole-formation (138, 194). Why is T different? We suggest two constraints may be operative. First, T, like lambda S, is a canonical, "large-hole forming" holin. With canonical holins, it has been established that the product of triggering must be a very large lesion in the membrane, to allow fully-folded, soluble endolysin to escape non-specifically from the cytoplasm and attack

the cell wall (187). More recently, the ultra-structural basis of this non-specific release was established, at least for lambda S, by cryo-EM and tomographic studies (46). These studies showed the final holes to be of varying size and on the scale of hundreds of nanometers in diameter, which would require thousands of S molecules to form. In contrast, S^{68} forms heptameric complexes with internal channels of ~2 nm, which serve only to kill the cell and depolarize the membrane; S^{68} has been designated as a "pinholin" to distinguish it from the canonical, large-hole forming holins (139). What differentiates a canonical, large-hole forming holin like S from a pinholin like S21? One difference is that S has three TMDs, all of which are required for hole formation (194). In contrast S^{68}, at the time of hole formation, has only a single TMD, because, as part of the timing mechanism, the N-terminal TMD must be removed from the bilayer (137). Thus it may be that a single TMD simply cannot form pores of micron-scale as observed for the lambda holin. From this perspective, the participation of the soluble N and C terminal domains in T hole formation may simply reflect the need for more interaction domains to seed the high order oligomerization needed for large hole formation.

Another rationale for the participation of N and C-terminal soluble domains in the lethal function of T may lie in the necessity for transducing the environmental signals for real time control of T. To date, T is the only holin known to respond to environmental signals, in that, *in vivo*, superinfection by a T-even phage leads to inhibition of the lethal function of T; i.e., to a blockage of triggering and the LIN state (128). *In vivo*, this requires, in addition to T, two T4 proteins: the periplasmic protein RI and the cytoplasmic protein RIII. The LIN state is reversible, in that it spontaneously

collapses (allowing lysis to proceed) if the environmental signal (i.e., superinfection) is not renewed at intervals not exceeding 10 min (179). This allows the T4-infected cell to proceed with normal lysis once the environment is no longer rich in virions and thus presumably depleted in hosts. By having soluble domains controlling oligomerization, a soluble antiholin, subject to aqueous-phase ligand binding and to proteolytic degradation, can be used to transduce the LIN signal. In contrast, other holins have integral membrane proteins as antiholins, none of which have been shown to respond to environmental signals other than the generalized loss of the pmf (137). By extension, this reasoning also suggests that RIII, a 82 aa protein predicted to be a cytoplasmic protein by virtue of its hydrophilic character and lack of a secretion signal, interacts with T_{NTD} to facilitate LIN.

Homotypic and heterotypic interactions in T_{CTD}

The T_{CTD}, spanning residues 56 to 216, is the location of 11 missense changes that abrogate T lethality without affecting accumulation or localization of the holin. Four of these alleles, in addition to losing lytic function, also lose the ability to bind the RI antiholin *in vivo* (Fig. 40): I88K, F111S, K137R, and I213K. Moreover, to date two of these have been tested in the context of the purified, independent His-tagged T_{CTD} and both have been shown to remain soluble after elution from an IMAC, in contrast to the WT T_{CTD}, which quantitatively oligomerizes to the point of insolubility upon elution (Fig. 39) (128). We suggest that these residues define an interface that is important for both homotypic T interactions leading to oligomerization and a heterotypic interaction with RI. The implication is that RI acts by occluding one of the oligomerization

interfaces used by T in the pathway to lethal hole formation, rather than by some allosteric effect on T conformation. Three of these changes are in highly conserved residues (Fig. 36). The allele K137R is of interest because of its extremely conservative nature. Among these positions, only I213 is not strongly conserved. However, even here a basic residue is not found in any T homolog.

CHAPTER V

NMR STUDIES OF THE PERIPLASMIC DOMAIN OF RI

Introduction

Unlike all other phages, T4 and the other T-even phages (T2 and T6) exhibit *real-time* regulation of lysis using environmental conditions (136, 203). Specifically, lysis can be delayed indefinitely in the lysis-inhibited state (LIN) depending on the supply of host cells in the vicinity of the infected cell (50, 81). LIN has been the focus of numerous studies since its discovery in the 1940s, leading researchers to fundamental discoveries in molecular biology (17, 18, 39, 52, 82, 83).

After nearly 60 years, the protein determinants of LIN have been discovered (144). To inhibit lysis, one must inhibit the holin, the master regulator of lysis (188). In the case of bacteriophage T4, the holin is T, a 218 residue protein with a single transmembrane domain that accumulates in the inner membrane (145). At an allele-specific time, the holin molecules oligomerize to form a large hole in the inner membrane, leading to host lysis (203). Ramanculov *et al.* showed that *rI*, one of the first *r* genes to be discovered whose mutants showed LIN defects (81), is a T-specific inhibitor (144). Expression of *rI* alone in the presence of T leads to lysis inhibition, similar to that seen during wild type T4 infections. Further work by Tran *et al.* revealed that the mechanism of inhibition is by RI-T periplasmic domain interactions (179). Additionally, RI is a labile protein, inactivated and then degraded by DegP, the periplasmic protease, when a superinfection is absent (180).

The RI periplasmic domain has been purified and characterized genetically, biochemically, and biophysically (128, 180). The RI periplasmic domain contains a single disulfide bond that is essential for its function and is completely conserved in all T4-like RIs. Based on the atomic structure of RI, it is an extended protein with three α-helices; helices two and three are linked by a disulfide bond (see Chapter III). The structure of RI when bound to the periplasmic domain of T, however, is in a different conformation. Instead of the extended conformation observed when crystallized alone,

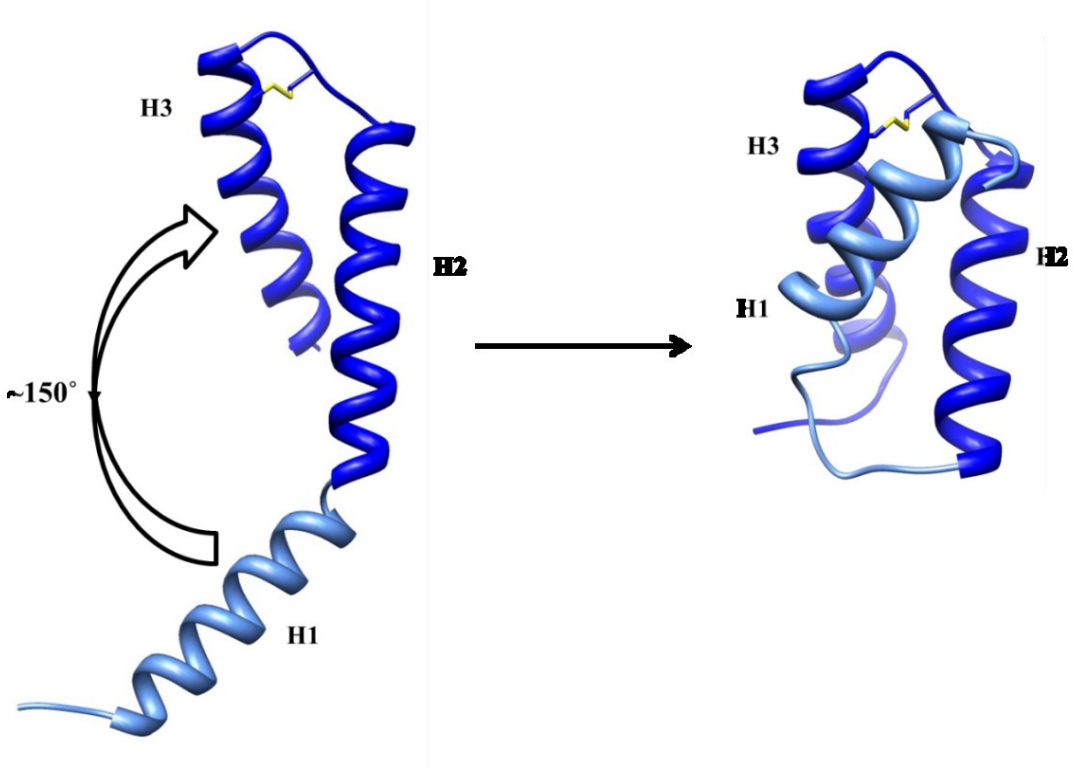

FIG 41 Conformational change of the periplasmic domain of RI. The sRI monomer is an extended structure with H1 separated by kink from H2. The bound form of sRI is more compact with H1 making a nearly 150° swap towards H2 & H3. The spatial position of H2 & H3 remains the same between both structures, possible due to the stability of the essential disulfide bond. The movement by H1 unwinds both H1 and H2 helices, creating a large loop.

the first helix of RI makes a dramatic shift, moving into close proximity to helices two and three and becoming more globular when bound to T (Fig. 41). The relevance of these two structures will be discussed in this chapter.

In addition to T and RI, a lysis inhibition signal is required to effect LIN (136, 180). The head contents of a superinfecting T-even phage are shunted into the periplasmic space by action of the *imm* and *sp* gene products made within the first 3 minutes of the initial infection (116) (Fig. 42). Discoveries which contributed to

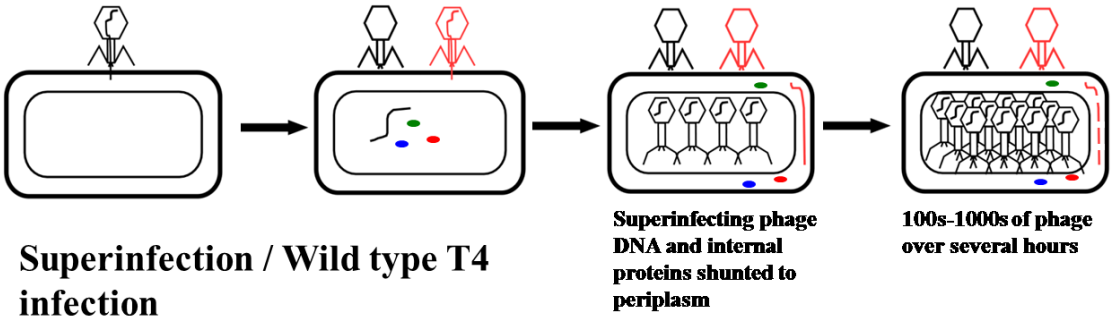

FIG 42 Wild type T4 infection cycle. Unlike other bacteriophage infection, wild type T4 infections exhibit a unique phenomenon called lysis inhibition. Lysis inhibition is imposed when T-even phages superinfect an already infected cell. The superinfecting head contents, including its dsDNA genome and internal proteins are shunted into the periplasmic space. The superinfecting phage somehow signals the inhibition of the lysis program begun by the initial phage infection, leading to the hyper-accumulation of phage.

understanding the lysis inhibition signal come from superinfections with phage ghosts. Phage ghosts are phages that have been osmotically shocked to release their capsid contents. This includes the 170 kbp genome, which contains no cytosines, rather cytosines are modified by hydroxymethylation and glycosylation (Fig. 43), and ~1000 internal head protein molecules. These ghosts cannot impose LIN (152). Ghosts are competent in binding to the host as well as injection by the penetration of the tail tube, however ghosts do not contain nucleic acids or internal head proteins and thus do not

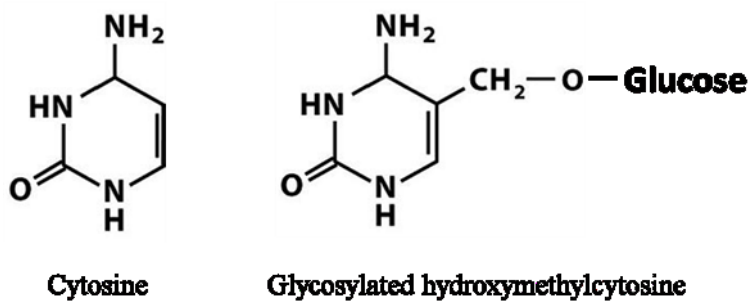

FIG 43 Structure comparison of cytosine and glycosylated hydroxymethylcytosine. The T4 genome contains glycosylated hydroxymethylcytosine rather than cytosine, in part, to evade the host restriction systems.

impose LIN (152). Additionally, superinfections with phage that use a different DNA injection method, such as phage T7, are also incapable of effecting LIN (152). Taken together, these observations have led to the conclusion that the ectopically injected DNA and/or internal head proteins signal the imposition of LIN, probably through an interaction with RI (136, 180).

This chapter will describe work on characterizing the dynamics of the periplasmic domain of RI and investigating whether the two conformations of that domain are physiologically relevant. Additionally, the signal for LIN will be investigated. Both of these topics will be studied using nuclear magnetic resonance (NMR) spectroscopy techniques.

Materials and Methods

Overexpression and purification of sRI

The RI periplasmic domain construct (residues 25-97), sRI, was cloned into the overexpression vector, pET11a, with a C-terminal hexahistidine tag for purification purposes, as previously described (128) (Table 10). SHuffle(DE3) cells, optimized for the overexpression of proteins containing disulfide bonds in the cytoplasm, were transformed with the pET11a sRI-his construct for purification purposes. The sRI-his protein was overexpressed and labeled with ^{15}N and/or ^{13}C (Cambridge Isotope Laboratories, Inc., Andover, MA), as previously described (119). SHuffle(DE3) pET11a sRI-his cultures in LB broth were grown to an $A_{550} \sim 0.5$ at 37°C. Cells were collected by centrifugation in a Sorvall H-6000A rotor at 4000 rpm and cells were resuspended in ¼ original volume of pre-cooled M9 minimal medium containing ^{15}N-labeled ammonium chloride (1 g L^{-1}) and supplemented with either natural abundance or ^{13}C labeled glucose (2 g L^{-1}), depending on the experiment performed. After a 1 hour recovery period at 16°C, cultures were induced by addition of 1 mM (final) isopropyl-β-D-thiogalactoside (IPTG) overnight at 16°C.

TABLE 10 Phages, strains, and plasmids used in this study

Phages	**Description**	**Source**
T4 wild type	Bacteriophage T4D	Lab Stock
T4Δ*rI*	Deletion of *rI* from nt 59204 to nt 59496 in bacteriophage T4D genome	(180)
T4 UM-DNA1	*amE51 nd28 (denA) denB point pseT del3*	L. Snyder
T4 UM-DNA2	*amE51 denA denB point rli-13 alc2*	L. Snyder
T4 UM DNA3	*amE51, denA, denB point, pseT1, alc8*	L. Snyder
Strains	**Description**	**Source**
SHuffle T7 (SHuffle(DE3))	*E. coli K12 fhuA2 lacZ::T7 gene1 [lon] ompT ahpC gal λatt::pNEB3-r1-cDsbC ΔtrxB sulA11 R(mcr-73::miniTn10)2 [dcm] R(zgb-210::Tn10) endA1 Δgor Δ(mcrC-mrr)114::IS10*	New England Biolabs
B834	*E. coli* B *ompT* r_B^- m_B^- *met*$^-$	Lab Stock
Plasmids	**Description**	**Source**
pET11a-sRI^{his}	*rI* carrying a deletion from residues 2-25 and a hexahistidine tag at the C-terminus for purification	(128)

After overexpression, cells were again collected by centrifugation, as described above, and resuspended in purification buffer (10 mM HEPES and 100 mM KCl, pH 7) supplemented with Protease Inhibitor Cocktail (Sigma, St. Louis), and 100 μg mL^{-1} final concentrations of DNase and RNase. Cells were disrupted in a French pressure cell, as previously described (20), passed over Talon metal affinity resin (Clontech, Mountain View, CA) and eluted with purification buffer supplemented with 0.5 M imidazole. Elution fractions were assessed for purity by SDS-PAGE and Coomassie blue staining. Fractions containing protein were further purified by gel filtration chromatography on a prep grade Superdex 75 column equilibrated with 20 column volumes of purification

buffer before sample injection. Purified protein was concentrated to appropriate concentrations, based on experiment performed, using an Ultra-4 3K MWCO concentrator (Amicon).

Site-specific resonance assignment of sRI

All NMR experiments were carried out at 25°C on Varian Inova spectrometers operating at ^{1}H Larmor frequencies of 500 MHz and 600 MHz. Sequence-specific assignments of $^{1}H_{N}$, $^{13}C\alpha$, $^{13}C\beta$, and ^{15}N resonances for sRI were obtained by HNCACB, CBCA(CO)NH (129), and C(CO)NH (126) experiments using ^{15}N and ^{13}C enriched sRI in 8% $^{2}H_{2}O$ (v/v). NMR data were processed with nmrPipe (42) and assigned with Sparky (71).

Relaxation experiments

The relaxation rate constants R_1 and R_2, longitudinal and transverse, respectively, as well as the [^{1}H]-NH nuclear Overhauser effect (NOE) were measured for all spectrally resolved N-H groups of the protein backbone, as judged by Heteronuclear single quantum coherence (HSQC) experiments (63). Measurements were carried out on the ^{1}H-^{15}N labeled periplasmic domain of RI (220 μM) at 25°C on a Varian Inova spectrometer operating at a ^{1}H Larmor frequency of 500 MHz. The data were collected with 7 relaxation time delays (3 of which were duplicates) ranging from 50 ms to 1 s (R_1) and from 8 to 140 ms (R_2). R_1 and R_2 values were determined by fitting the time dependence of peak intensities to an exponential function using the Curve-fit software available from Dr. Arthur Palmer's laboratory at Columbia University (http://www.palmer.hs.columbia.edu/software/curvefit.html). The NOE data were

acquired in an interleaved manner with a 3 s saturation period and 5 s recycle delay, as previously described (168).

Liquid and plate assays for determination of lysis inhibition of T4 and T4 mutants

Wild type T4 (T4D), a LIN-defective T4 (T4Δ*rI*), and three T4 mutants defective in modification of cytosines (T4 UM-DNA 1, 2, & 3), were tested for their ability to impose lysis inhibition. Cultures of *E. coli* B834 were grown to an A_{550} = 0.2 (1 x 10^8 cells mL^{-1}) in LB at 37°C and were infected with the various T4 phages (mentioned above and described in Table 10) at a multiplicity of infection (MOI) of 10. The optical density of the cultures was monitored throughout the experiment. At 110 minutes post infection, 1% chloroform (v/v) was added to all cultures. Addition of chloroform to cells containing endolysin (indicating that the phage replication cycle is normal) causes immediate clearing of the culture.

The plaque morphologies of the above phages were also investigated using standard plating assays. Various dilutions of phage stocks were performed and 200 µL of *E. coli* B834 was added to each, in addition to 3 mL of molten soft agar. The solutions were then poured onto prepared LB agar plates and incubated at 37°C overnight. Plaque morphologies of the WT and mutants were recorded the next day.

In vitro electrophoretic mobility shift assay (EMSA) of sRI and DNA

EMSAs were performed to determine whether the periplasmic domain of RI is capable of binding dsDNA. EMSA samples included 4 µl 5x binding buffer (50 mM Tris-HCl pH 7.5, 250 mM KCl, and 25% glycerol), 2 µL BSA (3 µg mL^{-1}), 1-5 µL sRI (11.8 µM), and 1-2 µL of 20 bp or 30 bp dsDNA (11.8 µM) of randomly generated

sequence. The sequences of the duplex dsDNA fragments used in this study are as follows: 30 bp duplex (5'CTAATCGAGTACCTGATCACGACTTACTTA3') and (5'TAAGTAAGTCGTGATCAGGTACTCGATTAG3') and the 20 bp duplex (5'GTTATTGTGGTGCTATGTTT3') and (5'AAACATAGCACCACAATAAC3'). Samples were incubated at room temperature or 37°C for 1 hour and then loaded onto pre-run 5% acrylamide (0.5 x TBE) gels. Gels were visualized with 3x gel red dye (Biotium, Hayward, CA).

NMR-monitored binding of dsDNA to sRI

The 30 bp dsDNA used in binding studies was obtained from Integrated DNA Technologies (Coralville, IA), resuspended in H_2O and extensively dialyzed against H_2O to remove impurities. DNA solutions in water were lyophilized and resuspended in purification buffer. The concentration of ^{15}N-enriched sRI in 8% D_2O was maintained at 100 μM, while the concentration of the dsDNA was adjusted to 50, 100, 200, 400, and 500 μM in a set of NMR samples. Binding of 30 bp dsDNA to sRI was monitored using ^{15}N-^{1}H HSQC and chemical shifts of each residue were calculated using the equation:

$$\Delta = \sqrt{(\Delta\delta_N * 0.152)^2 + (\Delta\delta_H)^2}$$

where $\Delta\delta_N$ and $\Delta\delta_H$ are the residue-specific chemical shift changes between a sample containing protein and DNA and one containing no DNA, respectively, and 0.152 is the scaling factor (157).

Results

Assignment of the sRI backbone residues

The decision to characterize the periplasmic domain of sRI using NMR spectroscopy techniques was made based on the two structures of sRI solved in collaboration with the Sacchettini laboratory and Texas A&M. While the apo sRI structure is in an extended conformation, the protein adopts a globular conformation when bound to the periplasmic domain of the T4 holin, T (Fig. 41). It was unknown whether the protein was dynamic or if the structures, especially that of the apo structure, represent low energy state conformations in the buffer conditions used to crystallize the protein.

To study sRI using NMR spectroscopy, assignment of the protein backbone was undertaken. The assignment of all ^{15}N-^{1}H HSQC backbone peaks was accomplished using a 500 μM sample of ^{15}N ^{13}C-labeled sRI. The protein peaks were well-resolved and all peaks were assigned (Fig. 44). Peaks were present for all non-proline residues except Met1, Asn26, and the terminal four histidines of the hexahistidine tag (H102-H105). A peak for Asp72 does not appear in the HSQC experiment but can be assigned using the three assignment experiments performed, HNCACB, CBCACONH, and C(CO)NH.

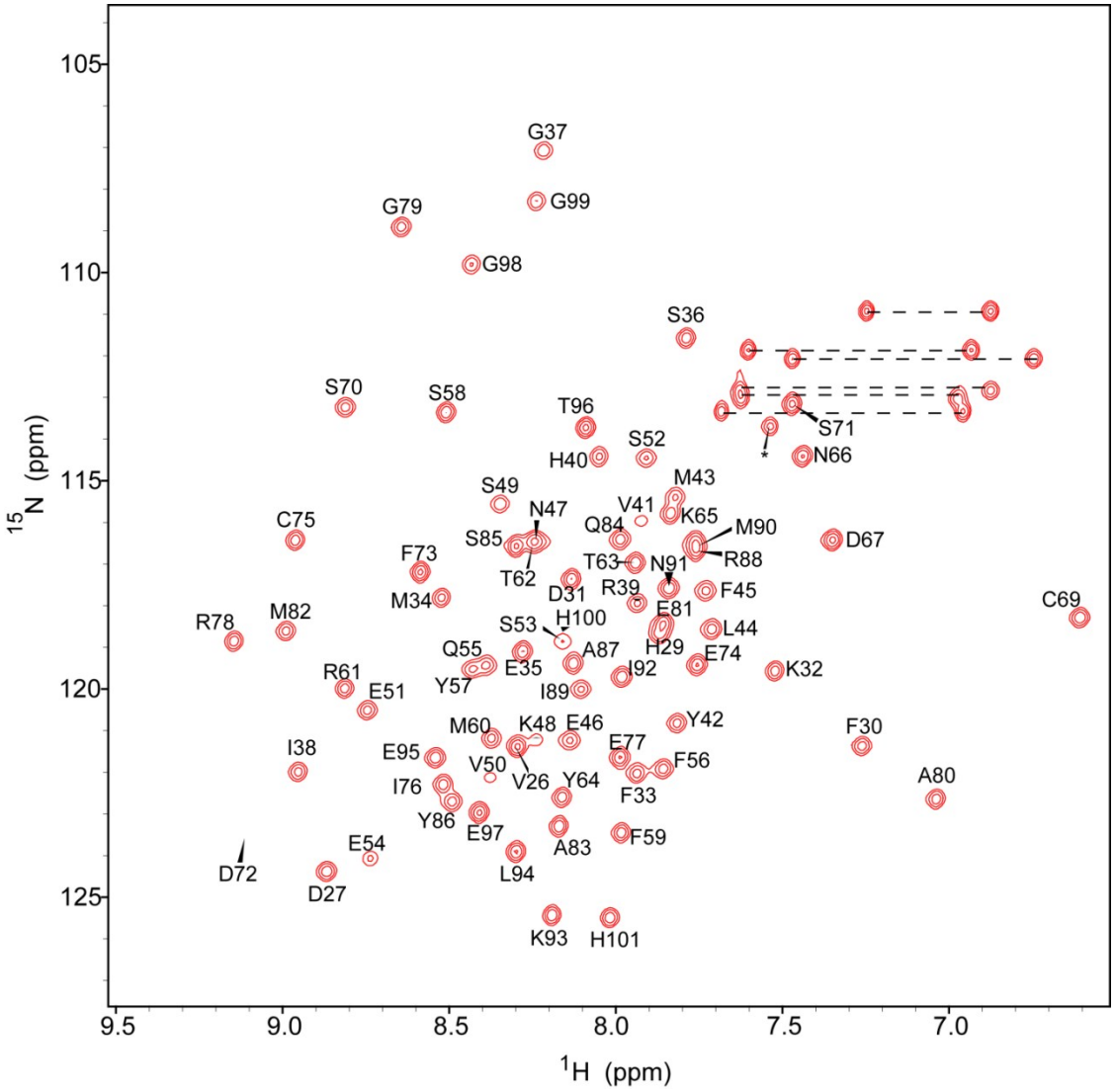

FIG 44 Assignment of the backbone peaks of the periplasmic domain of RI. The assigned peaks are labeled with each residue of sRI. The D72 peak is not present in the HSQC experiment; however, it is assigned using other experiments. Side chain peaks are depicted by asterisks or are connected with dashed lines.

Dynamics of sRI

To determine whether the RI periplasmic domain is dynamic in solution, and to reconcile the two conformations of the protein (apo and bound), experiments measuring protein dynamics were performed. The relaxation rates R_1, R_2, and the NOE were determined for spectrally resolved ^{15}N-^{1}H residues. These experiments were performed on ^{15}N-labeled sRI (220 μM) with the parameters described in the Materials and Methods section. Analysis of these three experiments revealed that residues of sRI are dynamic in both the picosecond (ps) – nanosecond (ns) and microsecond (μs) – millisecond (ms) timescales (Fig. 45). While it is unclear which residues are dynamic in the R_1 dataset (ps – ns timescale) due to low signal:noise and high error rates, the NOE data clearly show that residues Glu46, Lys48, and Ser49 are dynamic in the ps – ns timescale. Additionally, the majority of residues between Gly37 and Glu54 are dynamic in the μs – ms timescale, as seen with the increase in R_2 rates (Fig. 45). All dynamic residues, in both the ps – ns and μs – ms timescales, are those involved in the conformational change between the apo and bound sRI crystal structures, located in the region between the C-terminal end of the first helix and N-terminal end of the second helix (Fig. 46).

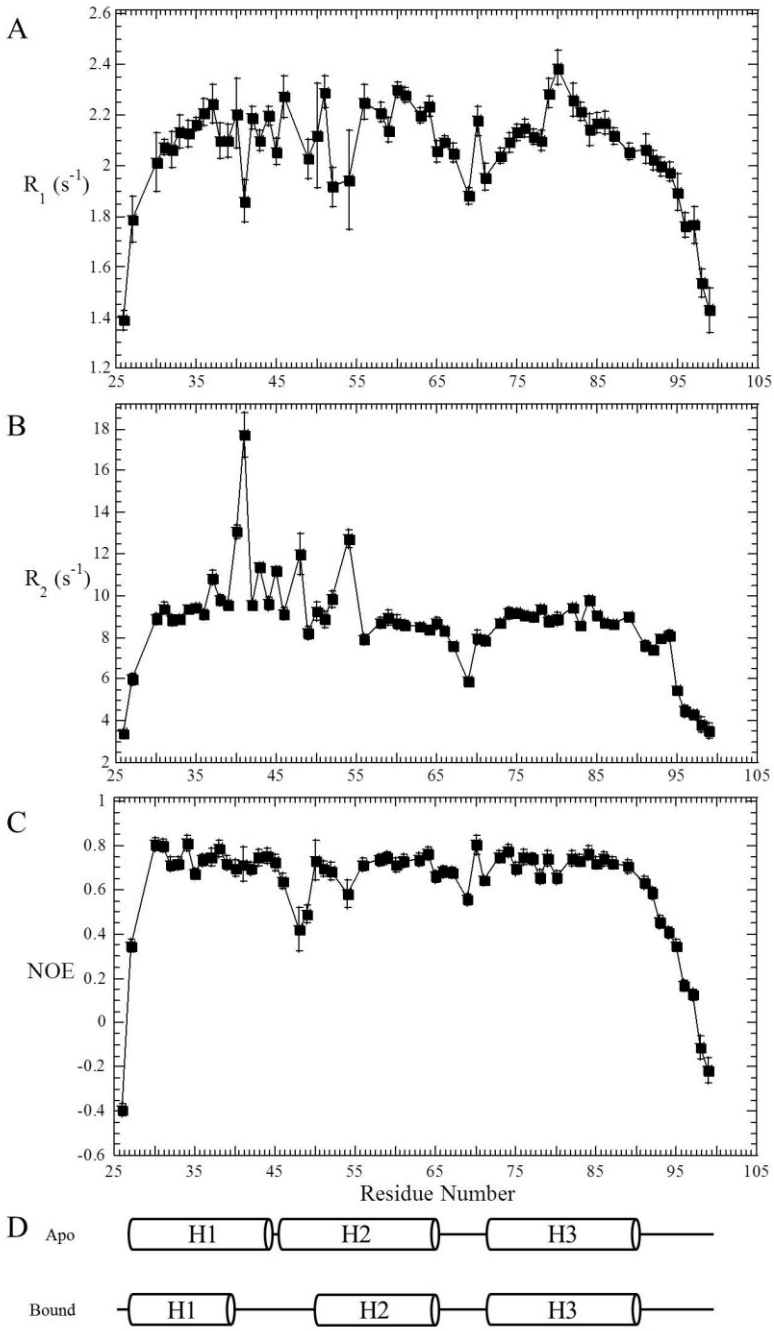

FIG 45 R1, R2, and NOE experiments to determine whether sRI is dynamic in solution. (A) The dynamics at the ps – ns timescale of spectrally resolved sRI residues cannot be determined by the R_1 rates due to high error rates. (B) Elevated R_2 rates, specifically between residues 37 and 54 indicate that sRI is dynamic on the µs – ms timescale in this region. (C) Depressed NOE rates indicate that residues 46, 48, and 49 are dynamic on the ps – ns timescale. (D) Secondary structure depiction of the apo and bound sRI structures.

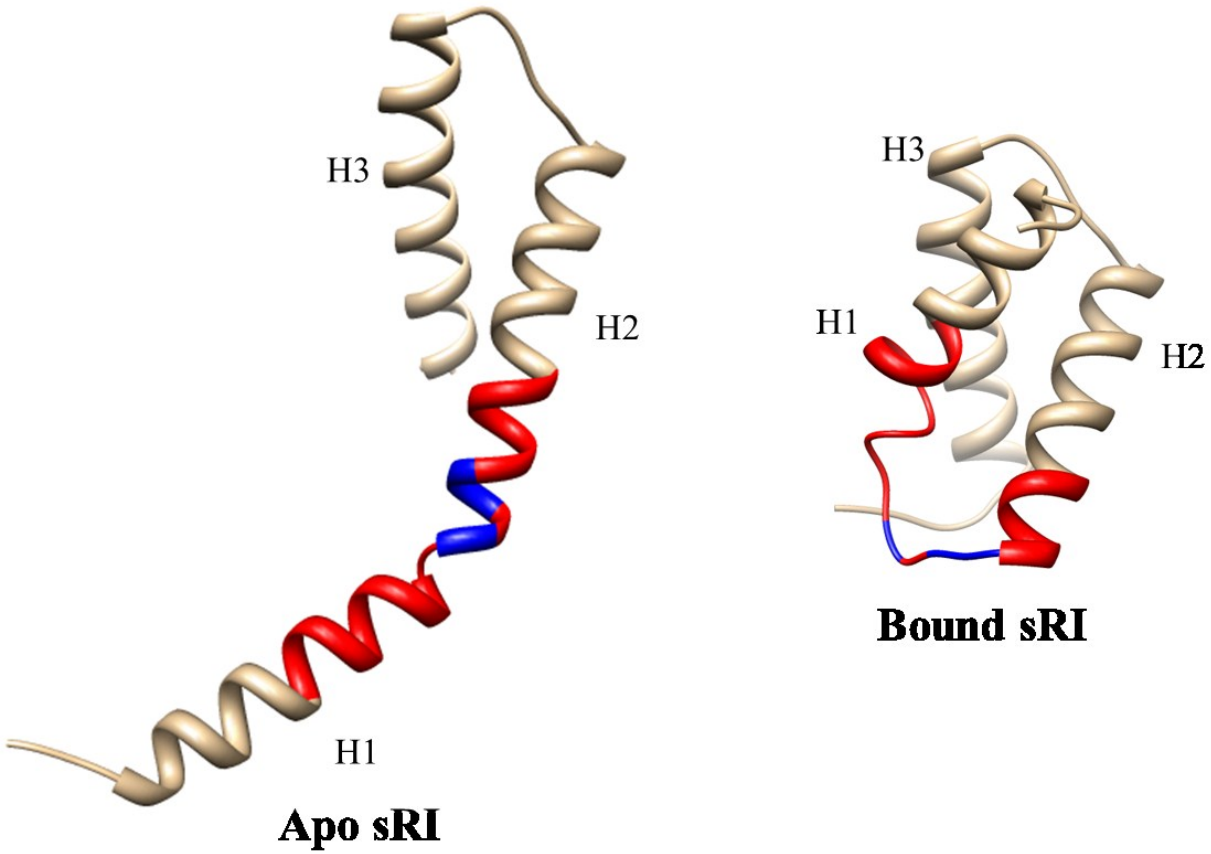

FIG 46 The periplasmic domain of RI contains residues that are dynamic. Left: Structure of the apo sRI structure with dynamic regions between helices 1 and 2 highlighted. Right: Structure of the T-bound sRI with the same residues highlighted as in the apo sRI structure. Red: residues dynamic in the μs – ms timescale, blue: residues dynamic in both the μs – ms and ps – ns timescales.

Internal head proteins likely have no effect on lysis inhibition

The lysis inhibition signal, presumably stabilizing RI or stabilizing the interaction between RI and the T4 holin, T, is localized in the phage capsid of a superinfecting T-even bacteriophage (136, 152). In general, the capsids of T-even

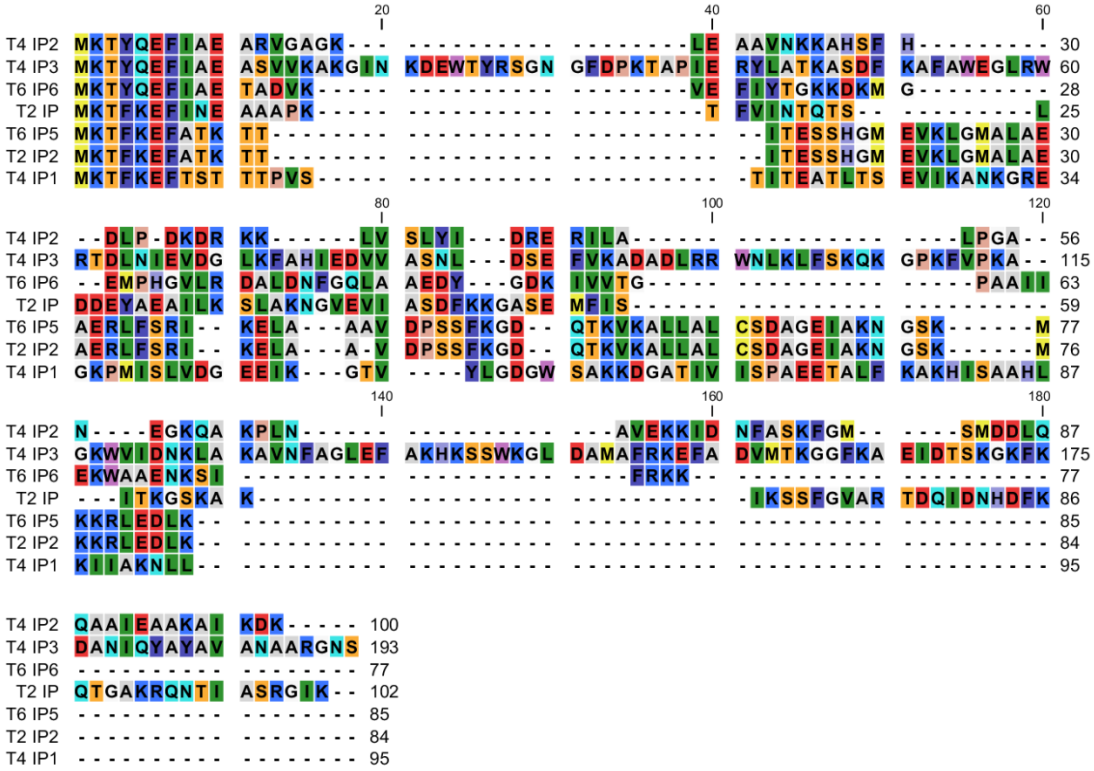

FIG 47 Alignment of the bacteriophage T2, T4, and T6 internal proteins. Sequences of the T-even bacteriophage internal proteins are aligned to determine potential conserved residues that might serve as a signal for lysis inhibition.

phages contain the genome of the phage as well as internal proteins (IPs) required for the inhibition of host restriction systems (136, 180). An alignment of the internal proteins from T2, T4, and T6 was performed to determine whether any common sequence elements exist (Fig. 47). While the first seven residues of the different IPs are very well conserved, no other elements of conservation exist amongst the seven sequences. Without significant conservation of the internal proteins, it is unlikely that they are involved in signaling lysis inhibition. As a result, further investigation of the role of the IPs in signaling lysis inhibition was not pursued.

T4 phages with non-HMC containing DNA still impose lysis inhibition

Since lysis inhibition can be imposed by any of the T-even phages, a very common element must be involved in signaling LIN. All functional bacteriophages, of course, contain nucleic acids in their capsids. In the case of the T-even phages, the nucleic acid is modified, in that glycosylated hydroxymethylated cytosines (HMC) replace cytosines, mostly to evade restriction systems. Whether the HMC DNA of the T-even phages signals lysis inhibition was tested by superinfection experiments using T4 mutants defective in the modification of cytosines. *E. coli* B834 cells were infected with wild type T4, a LIN-defective T4, and three different T4 mutants defective in cytosine modification at a MOI of 10, which should be sufficient to induce lysis inhibition. Cultures infected with the LIN-defective phage lysed at ~ 25 min, consistent with previous observations (Fig. 48). The cultures infected with the wild type or the DNA-modification mutants were stably lysis inhibited for nearly 2 hours. The immediate

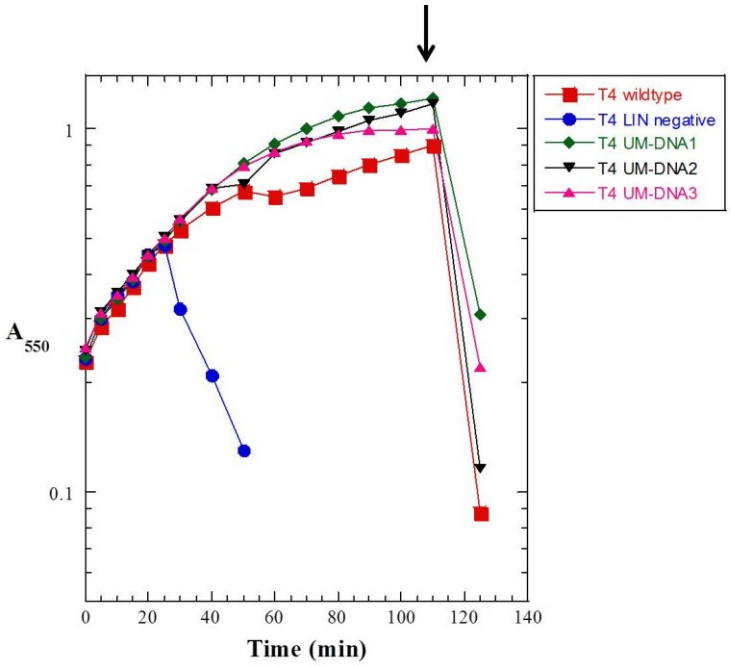

FIG 48 Infections with T4 mutants defective in DNA modification are lysis inhibited. *E. coli* cultures were infected with the indicated T4 phage at an $A_{550} = 0.2$. The LIN-defective phage lysed the culture at ~ 25 min (blue) while all other phages imposed lysis inhibition of their respective cultures. Arrow indicates addition of 1% chloroform (final). UM: unmodified.

clearing of the culture after the addition of chloroform confirmed that these cultures were indeed lysis inhibited.

These observations were buttressed with plating assays to observe the plaque formations of all phage tested. The LIN-defective phages produced large plaques with sharp edges while the wild type and the DNA-modification mutant plaques were small with turbid edges, consistent with plaques of lysis inhibited cells (Fig. 49).

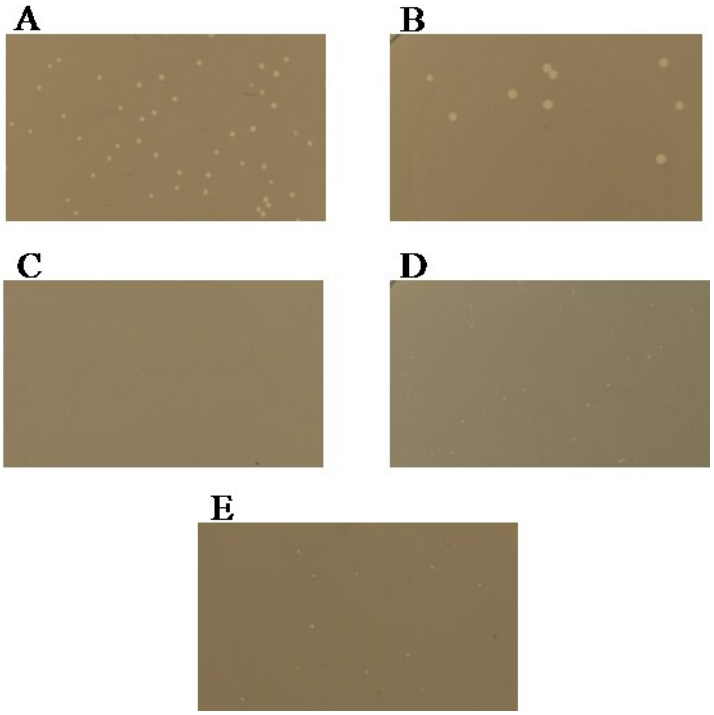

FIG 49 Plaque assays of T4 mutants defective in DNA modification. (A) Wild type T4, (B) LIN-defective T4 (T4Δ*rI*), (C) T4 UM-DNA1, (D) T4 UM-DNA2, and (E) T4 UM-DNA3 were plated on *E. coli* B834 cells. The wild type T4 and UM DNA mutants plaques are small with turbid edges, indicative of LIN, while the T4Δ*rI* plaques are large with sharp edges, indicated of a LIN defect.

sRI binds DNA and is likely the lysis inhibition signal

Since the absence of HMC DNA modification has no effect on lysis inhibition, electrophoretic mobility shift assays (EMSA) were used to investigate the dsDNA binding properties of the purified periplasmic domain of sRI, pointing to DNA as the LIN signal. This approach was supported by the prediction of DNA-binding elements in the RI periplasmic domain by the DNA-binding protein program DP-Bind (87) (Fig. 50). Two dsDNA fragments of random sequence were generated, in lengths of 20 bp and 30 bp. These fragments were incubated with varying concentrations of purified sRI protein and bands were visualized. While no shift appears in the presence of the 20 bp

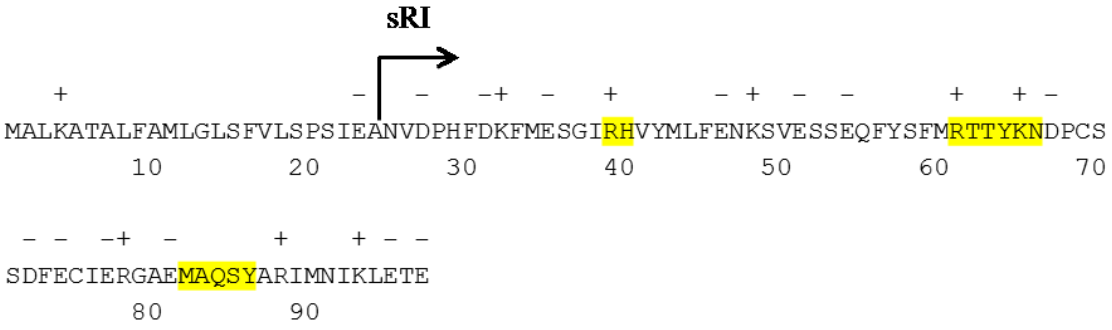

FIG 50 Prediction of DNA binding residues in RI. The primary structure of RI with the periplasmic domain of RI (sRI) indicated. Residues predicted to bind DNA, using the program DP-bind (87), are highlighted in yellow.

dsDNA (data not shown), it was evident that the purified sRI protein was competent in binding the 30 bp dsDNA (Fig. 51, lanes 5-6 and 7-8). This binding, however, is very weak, with only a small percentage of the dsDNA shifting in response to the increasing amount of sRI.

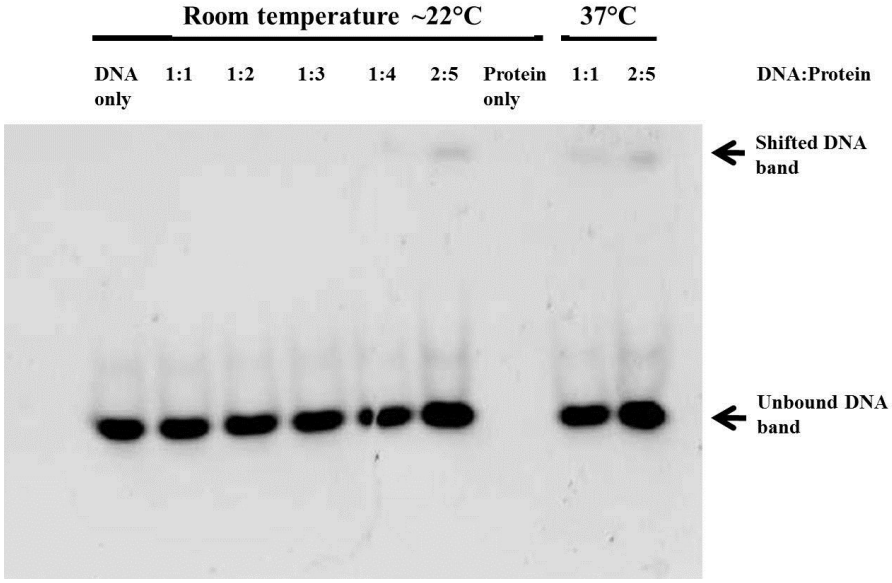

FIG 51 *In vitro* EMSA of purified sRI and 30 bp dsDNA. A 30 bp dsDNA fragment was incubated with increasing concentrations of purified sRI. Lane 1: DNA only control, lanes 2-6: Increasing concentrations of sRI with a constant concentration of DNA incubated at room temperature (See Materials and Methods). Lane 7: protein only control. Lanes 8-9: DNA and protein at the indicated ratios incubated at 37°C. The positions of the free/unbound DNA bands as well as those of the shifted DNA are indicated with arrows.

NMR-monitored sRI binding of DNA

The weak affinity of sRI to DNA prompted the investigation of DNA-binding by a more sensitive technique, NMR spectroscopy. This analysis was only possible due to the well-resolved nature of the sRI residue cross-peaks and because the assignment of these peaks was performed to completion. HSQC experiments were performed for samples containing protein only (100 μM of ^{15}N-labeled sRI) and samples with increasing concentrations of the 30 bp dsDNA fragment previously used (50-500 μM). Analysis of these experiments revealed that the chemical shifts of several cross-peaks changed with increasing amounts of DNA (Fig. 52).

Most of the cross-peaks perturbed by the addition of DNA correspond to positively charged residues in sRI. This confirms the observation that this interaction is nonspecific in nature, relying on electrostatic forces for the binding of DNA. The residue whose cross-peak was perturbed the most was His40, located at the C-terminal end of the first helix, at the junction of the loop between helices one and two which is highly dynamic in sRI (see above). Additionally, with the increasing concentration of DNA, a cross-peak appeared for Asp72, which without DNA does not appear in HSQC experiments. Overall, 15 residues of the 73 residues assigned were perturbed by the addition of DNA with several likely interacting with DNA.

The chemical shift perturbations were visualized in both the apo and T-bound structures of sRI to determine which residues might directly interact with the DNA at the surface of the protein (Fig. 53).

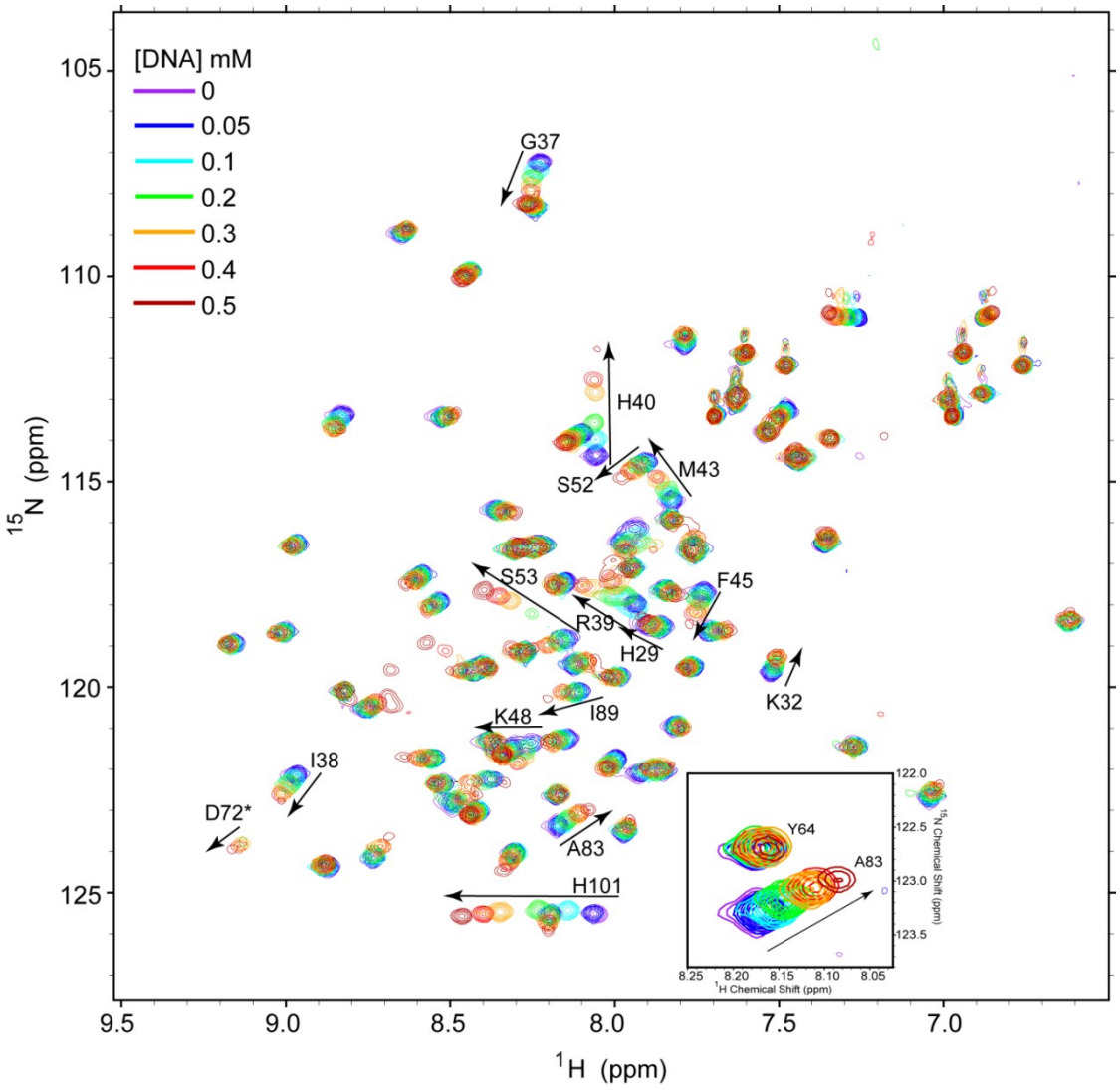

FIG 52 HSQC of sRI titrated with various amounts of dsDNA. Seven HSQC experiments are overlaid to visualize chemical shifts of sRI residue cross peaks in response to increasing amounts of dsDNA. Cross peak shifts are indicated by arrows in the direction of the shift and are labeled with the residue identity.

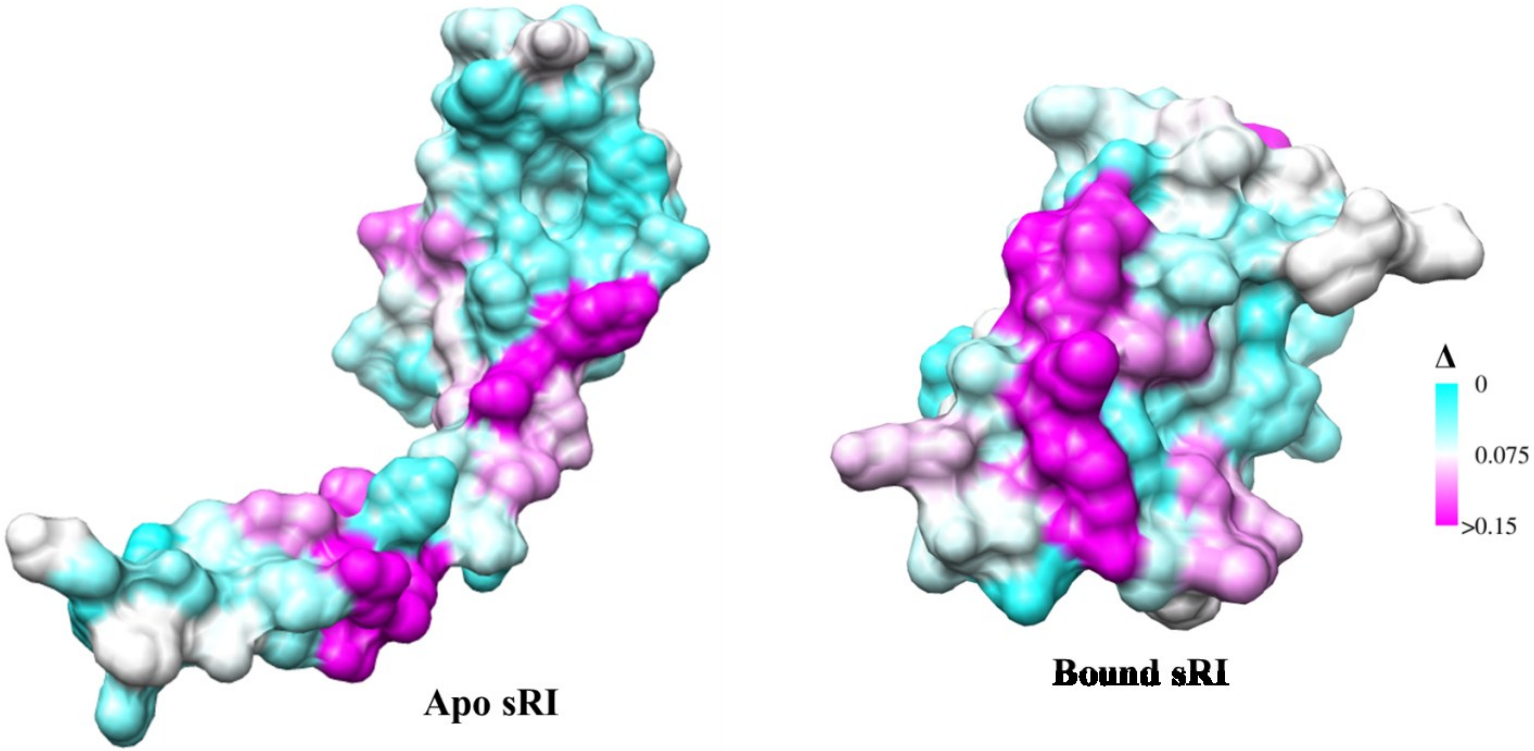

FIG 53 Chemical shifts due to increasing amounts of dsDNA visualized on the apo and T-bound sRI structures. Calculated cross peak shifts between the sRI only and sRI incubated with 500 μM dsDNA are visualized on the 2 solved crystal structures of sRI. Residues in pink are those whose cross peaks shifted the most.

Discussion

The objectives of this chapter were: 1) to determine whether the RI periplasmic domain is dynamic, as seen by the conformational change between the apo and T-bound structures of sRI, and 2) to elucidate the lysis inhibition signal that acts through RI to delay lysis when superinfections occur. Both objectives were studied, in large part, using various NMR spectroscopy techniques due to the ability to study residue-specific dynamics in solution and due to its sensitivity in determining ligand binding.

The periplasmic domain of sRI is dynamic in solution

Before studying the dynamic in solution of sRI, the NMR spectrum had to be assigned to completion. The NMR spectrum of sRI was well-resolved, indicating that the protein was relatively stable in solution and that little or no aggregation occurred at the highest concentrations used (500 μM). All backbone peaks in the HSQC spectrum were assigned; these peaks corresponded to nearly 95% of the protein. Peaks for the initial methionine residue, Asp72, and histidines 102 – 106 in the hexahistidine tagged used for purification of sRI were not visible in the spectrum, probably due to their extreme dynamic nature in solution. Asp72 was assigned, however, and a peak did appear in later experiments in which a ligand was titrated into the sRI solution (see below).

The relaxation parameters R_1, R_2, and the nuclear Overhauser effect (NOE) were used to study the dynamics of sRI in solution. All three experiments indicated that sRI is dynamic in the loop region between helices one and two. This is the same region in which a conformation change exists between the apo and T-bound structures of sRI

solved previously by X-ray crystallography. These experiments indicated that the residues in this loop region are dynamic on both the sub-nanosecond (ps – ns) and the microsecond – millisecond timescales. These data are indicative that sRI is indeed dynamic in nature; however, whether the extended conformation of the apo form of RI is physiologically relevant cannot be concluded using these data.

DNA binds sRI and is likely the LIN signal

Previous work indicated that the contents of a T-even bacteriophage signal the inhibition of lysis. This occurs due to the actions of the *imm* and *sp* gene products which are made early in infection. Imm and Sp exert immunity to superinfections, inhibiting bacteriophage DNA from entering the cytoplasmic space; instead, head contents are shunted into the periplasmic space. This is a phenomenon that is unique to myophage superinfections as superinfections with the other types of tailed-bacteriophages, siphophages (λ) and podophages (T7) do not cause the imposition of LIN. This is due to the different DNA ejection mechanisms used by the three types of tailed bacteriophages.

By aligning the various internal head proteins found in the T-even phages (T2, T4, and T6), we were able to exclude their role in LIN based on the lack of conservation. Additionally, we were able to test the role of the modified DNA (HMC DNA) present in the T-even phage capsid. Various mutants of T4 defective in modification of the DNA were still competent in LIN, so modification of the DNA is not the signal. Analysis of the RI sequence yielded several target sequences that were competent in DNA binding. *In vitro* electrophoretic mobility shift assays indicated that sRI indeed binds DNA. In particular, a 30 bp randomly generated dsDNA fragment was competent in binding sRI

while a 20 bp fragment was not. This binding was weak and so NMR spectroscopy was used to monitor DNA binding to sRI.

Titration of various concentrations of the 30 bp dsDNA to a fixed concentration of protein led to chemical shift perturbations in the HSQC spectrum of sRI. These perturbations are in mostly positively-charged residues, indicative that the binding is electrostatic in nature, and explains why random sequences are competent in binding. Several residues, such as Arg39 and His40, in the dynamic region of sRI, as determined by relaxation experiments, are involved in DNA binding. All chemical shift perturbations were visualized on the structures of sRI to understand where the DNA interaction on the protein occurs.

Model for the imposition of lysis inhibition

It is possible that the dynamics of sRI and its ability to bind DNA are related. The current model is that the release of RI into the periplasmic domain yields a dynamic molecule, which *may* transition through the two different conformations crystallized previously, the apo and T-bound structures. If no DNA is present in the periplasmic space, due to the lack of superinfection, RI is quickly inactivated and degraded. If DNA is present, RI binds the DNA, partly in the dynamic region, stabilizing it in the globular form that is competent in binding T. In essence, the binding of DNA to the periplasmic domain stabilizes the structure in the globular form to evade degradation and promote T inhibition.

CHAPTER VI

ACTIVE BAX AND BAK ARE FUNCTIONAL HOLINS*

Introduction

In response to most apoptotic stimuli, the cell undergoes mitochondrial outer membrane permeabilization (MOMP), releasing cytochrome c and other mitochondrial proteins into the cytosol to initiate the caspase cascade (40, 90, 132). As a central event during apoptosis, MOMP is primarily controlled by the Bcl-2 family proteins, which include the anti-apoptotic (e.g., Bcl-2, Bcl-xL), the multi-domain pro-apoptotic (e.g., Bax and Bak), and the pro-apoptotic BH3-only (e.g., Bik, Bim, Puma) proteins. While the anti-apoptotic proteins are believed to inhibit MOMP by suppressing the function of pro-apoptotic Bcl-2 family proteins, the BH3-only proteins positively regulate MOMP either by neutralizing the anti-apoptotic proteins or by directly triggering Bax/Bak activation (32, 64, 101, 113, 195). Genetic analysis of mice doubly deficient for Bax and Bak established the essential role of these two proteins in mitochondria-dependent apoptosis (191). During apoptosis, both Bax and Bak become activated and form homo-oligomers in the outer membrane of mitochondria (OMM) (6, 102, 131). These homo-oligomers are believed to cause pore formation on the OMM and function as effectors for MOMP, as they have been demonstrated to permeabilize liposomes and outer

---

* Reprinted with permission from "Active Bax and Bak are functional holins" by Pang, X., S.H. Moussa, N.M. Targy, J.L. Bose, N.M. George, C. Gries, H. Lopez, L. Zhang, K.W. Bayles, R. Young, and X. Luo, 2011. Genes and Development, 25, 2278-90.

membrane vesicles *in vitro* (108, 113). However, the physical make-up (lipidic or proteinaceous), molecular composition, shape, and size of the putative pores remain unclear (5, 176).

As single-cell organisms, bacteria share many similarities with mitochondria, including their sizes, membranes, genomes, and ribosomes, etc., and have been widely considered the origin of mitochondria during an endosymbiotic evolution process (57). Of importance, like MOMP, the bacterial plasma membrane becomes permeabilized and allows the release of functional proteins during bacteriophage-mediated lysis (11, 188). In canonical phage lysis, the holin, a small membrane protein, is one of two phage-encoded effectors essential for host lysis (3, 188). The other effector, endolysin, is a soluble cell wall-degrading enzyme (23). During the latent period of bacteriophage infection, the holin accumulates in the cytoplasmic membrane until under a genetically programmed schedule, forms homo-oligomers, and produces membrane holes large enough for the nonspecific passage of endolysin (11, 150, 188). Once across the cell membrane, the endolysin degrades the cell wall, causing an explosive disruption of the cell due to osmotic forces (76). The similarities between the strategies used in MOMP during mammalian apoptosis and holin-mediated bacterial cell death has been noted earlier (11). In this study, we explore the functional link between active Bax/Bak and the holin, characterize the Bax/Bak-mediated lesions in the bacterial membrane, and investigate the involvement of Bax helices in the control of the membrane pores.

Materials and Methods

Reagents and Antibodies

The following chemicals were used in this study. These include Ampicillin (Fisher Scientific, NJ), Kanamycin (Fisher Scientific, NJ), isopropyl β-D-thiogalactopyranoside (IPTG) (Acros Organics, NJ), Maltose (Fisher Scientific, NJ), BMH (Pierce Biotechnology, IL). The antibodies used are anti-Flag antibody (Sigma, MO), α-Myc antibody (Santa Cruz, Inc., CA). α-Bcl-xL antibody (Cell signaling Technology, Inc., MA).

Bacterial strains and culture growth

Bacterial strains used in this study include: BL21(DE3)pLysS (Novagen), MC4100[λΔ(*SR*)] (76, 164), MC4100Δ*tonA* (207). For convenience, MC4100[λΔ(*SR*)] cells was referred to as Δ(*SR*) cells in this study. Bacterial cultures were grown in LB medium supplemented with 50 μg/ml kanamycin or 100 μg/ml ampicillin as appropriate. Lysis curves were obtained by measuring A_{550} after IPTG or thermal induction. Since the plasmids containing cDNA of Bax were easily mutated after overgrowth of the host (9), all the cultures used for the lysis study avoided the stationary state. Briefly, cells from a single colony were inoculated into a 5 ml culture, and grown until A_{550} reached around 1.0, and kept at 4^{o}C overnight. The culture was diluted into a 25 ml volume of medium to achieve a starting $A_{550} \sim 0.04$. BL21(DE3)pLysS cells carrying pET24b+-derived plasmids were grown at 37^{o}C, and induced by IPTG (0.3 mM) at $A_{550} \sim 0.3$. For lysis curves of Δ(*SR*) cells carrying pS105-derived plasmids, cultures were grown at

30°C until A_{550} ~ 0.3 thermally induced by aeration at 42°C for 15 min, and aerated at 37°C thereafter.

Plasmid construction

The parental plasmids used in this study are pET24b(+) (Novagen) , pS105 (164) or pS105/R-LacZ, which was called pS105mycRϕlacZ in an earlier study (187). The pS105 plasmid is a medium-copy-number vector with the entire λ SRRzRz1 lysis cassette placed downstream of S gene's native pR' promoter. This plasmid and its derivatives are carried in a lysogenic host, Δ(*SR*) cells, and expression of genes in the lysis cassette is induced by thermal induction from the prophage, which supplies the late gene activator Q to transactivate the pR' promoter on the plasmid. The pS105/R-LacZ plasmid is identical to pS105, except that the *R* gene was replaced by the cDNA encoding a c-Myc-tagged R fused to the *LacZ* reading frame (187). Newly constructed plasmids were created by site-directed mutagenesis using the QuikChange kit from Stratagene (La Jolla, Calif.) or ligation, and were verified by DNA sequencing. Detailed description of these constructs is provided in the Extended Experimental Procedures.

Bacterial extracts for SDS-PAGE and western blot

Unless otherwise indicated, the cells in 1 ml of culture were collected by centrifugation following thermal induction by centrifugation at 22,000g for 10 min at 4°C 1 hour after induction by IPTG or by thermal shift. The cell pellets were lysed in EBC buffer (0.5% NP-40, 120 mM Tris-HCl, pH 7.5, 120 mM NaCl, 1 mM EDTA) for 1 hr. at 4°C with gentle rotation. The extracts were cleared by centrifugation at 22,000 ×g for 20 min. The supernatant was mixed with 4× SDS sample buffer and subjected to

SDS-PAGE. EBC lysates were directly mixed with 4× SDS protein sample buffer and subjected to SDS-PAGE without removing the pellet.

Time lapse microscopy

Cultures of Δ(*SR*) cells transformed with pS-F-miniBax or pS-F-miniBaxH3A were grown to A_{550} ~ 0.3 at 30˚C, induced at 42˚C for 15 min, and then grown at 37˚C, as described above, except for the pS-F-miniBax cultures which were induced for only 5 min at 42˚C. 10 µL aliquots of the culture were collected ~ 5 min before the onset of lysis (as judged from lysis curves) and placed on pre-heated microscope slides (37˚C). Cells were visualized at 400X magnification by phase contrast illumination on a Zeiss Axio Observer inverted microscope and recorded at 4 frames per second until the end of the experiment. Videos were processed using the AxioVision software from Zeiss.

R-LacZ release assay

Cultures of Δ(*SR*) cells carrying the indicated plasmids were thermally induced as described before. Sample from 1 ml culture each was collected at the indicated time points and precipitated by centrifugation at 22,000g for 10 min at 4^{o}C. The pellet was then lysed in 1 ml EBC buffer for 1 hr. with gently rotation at 4^{o}C. Equal volumes of the supernatant and lysate of the pellet were mixed with 4× SDS sample buffer and subjected to SDS PAGE. R-LacZ was detected by an α-c-myc antibody.

Plaque-forming assay

Recombinant phages were isolated from lysates of thermally induced Δ(*SR*) cells carrying pS105-derived plasmids as described earlier (207). Briefly, the lysates were

collected at 75 min by centrifugation at 22,000g for 10 min at 4°C. The supernatant was diluted in 300 μl SM buffer (100 mM NaCl, 10 mM $MgSO_4$, 50 mM, pH 7.5 Tris-Cl) plus gelatin (0.01% w/v) and mixed with another 300 μl of a culture of MC4100Δ*tonA* (A_{550} ~ 0.6, freshly grown in LB supplemented with 10 mM $MgSO_4$ and 0.2% maltose). As a negative control, SM buffer plus gelatin without lysate was also mixed with MC4100Δ*tonA* cells. After 25 min at RT, the mixtures were added to 10 ml LB-agar (LB with 0.5% agar and 10 mM $MgSO_4$) on a 10 cm plate and incubated at 37°C for 12 to 16 hr.

Generation of lysogens by recombinant λ phage and induction

Individual plaque of recombinant λ phage was picked by pipette and washed out into the tube by 500 μl SM buffer. Bacteriophage particles were allowed to diffuse into the SM buffer from the agar by gentle shaking at room temperature for 2 to 3 hrs. 100 μl of the bacteriophage suspension was diluted in SM buffer with gelatin and subjected to plaque forming assay. The whole plate of bacteriophage plaques were eluted with 5 ml of SM buffer. Phages, which were purified by replating, and picked again for 3 times, were then used to lysogenize MC4100Δ*tonA* cells. Lysogens were selected by plating infected cells on plain LB plates at 30°C, screened by PCR for the presence of prophage. Lysogens carrying indicated plasmids were also grown and thermally induced as described earlier for Δ(*SR*) cells. A_{550} of each culture was measured at a 15 minute interval.

BMH cross-linking

Expression from the plasmids pS-F-miniBax/R⁻, pS-F-miniBaxΔH2/R⁻, and pS-F-miniBaxL63P/R⁻ was induced in Δ(*SR*) cells at A_{550} ~ 0.3. At 45 min, cultures from 50 ml were passed through EmulsiFlex-C5 twice at the pressure of 16,000 psi. The membranes were collected by ultracentrifugation at 100,000g for 60 min at 4°C, and resuspended in 250 μl PBS. For the cross-linking reaction, the protein amount used of each reaction was adjusted by normalizing cell amount, assessed as total A_{550} units collected. Typically, a final reaction mixture of 50 μl with or without BMH (0.2 mM) was incubated at room temperature with gentle shaking for 1 hr. The reaction was stopped by the addition of DTT (50 mM) and incubation at room temperature for another 15 min. The membranes were collected again by ultracentrifugation as described above, and solubilized by EBC buffer for 1 hr. at 4 °C with gentle rotation. The insoluble material was removed by centrifugation at 22,000 g for 20 min at 4°C. The soluble fraction was mixed with 4× SDS sample buffer, and subjected to SDS-PAGE and analyzed by western blotting with an anti-Flag antibody.

Results

An active mutant of Bax (miniBax) displayed holin-like behavior, causing rapid bacterial lysis

In our earlier study, a truncation mutant of Bax containing helices 2 through 5 and helix 9 was found to be constitutively active in inducing apoptosis in Bax/Bak double knockout cells (DKO) (68). We named this mutant “miniBax” (Fig. 54A) due to

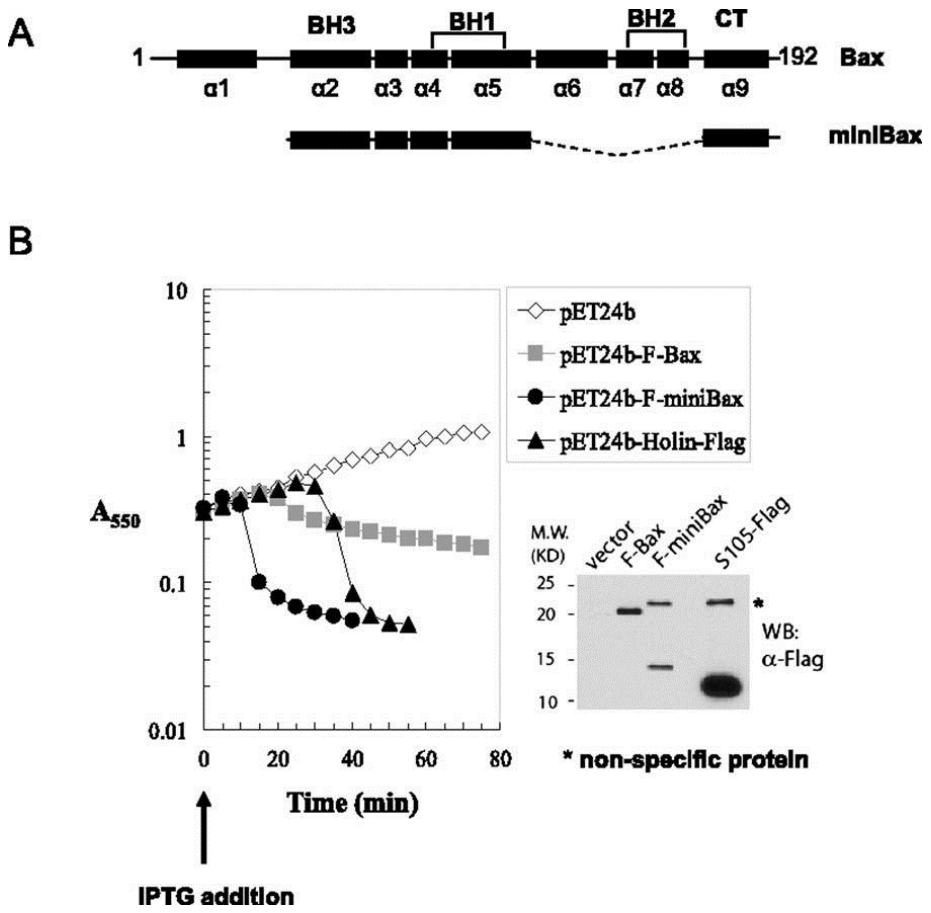

FIG 54 An active Bax mutant displays a holin-like bacterial lysis activity. (A) Diagram of Bax and miniBax. (B) Behavior of miniBax, Bax, and S105 in the pET system. BL21(DE3)pLysS *E. coli* transformed with the pET24b vector or pET24b constructs expressing F-miniBax, F-Bax, or S105-Flag were grown to A550 ~0.3. Following the addition of IPTG (0.3 mM), A550 was measured at 5-min intervals. After 1 h, the cultures were harvested and subjected to SDS-PAGE, followed by Western blot with an α-Flag antibody.

its much reduced size and the retained apoptotic activity in the DKO cells as compared to full-length Bax (68). Due to numerous failed attempts to construct a plasmid intended for expressing miniBax in bacterial extracts, we suspected that an unintended expression

of miniBax might have an adverse effect on the growth of the competent *E. coli* cells used in the ligation procedures, consistent with a toxic effect of Bax on bacteria reported earlier (9). We therefore cloned the N-terminally Flag-tagged *miniBax* gene or a similarly tagged full-length *Bax* gene into a pET vector, in which the expression of the target protein in *E. coli* is under the tight control of an IPTG-inducible promoter. As shown in Fig. 54B, with the empty vector as a negative control, the IPTG-induced expression of Bax initially caused a reduced growth rate, followed by a gradual decrease in A_{550} during the seventy-five minute time-course experiment, indicative of a partial bacteriolytic activity. In contrast, the expression of miniBax caused a dramatic drop in optical density ~ 10 minutes after IPTG induction (Fig. 54B). Strikingly, the culture became clear and viscous, highly reminiscent of bacterial lysis caused by phage infection. However, an involvement of contaminating bacteriophages in this "culture clearing" phenomenon is unlikely due to the dependence on IPTG-induced miniBax expression (Fig. 54B). In this system, it appears that miniBax is serving as a holin to release the T7 endolysin produced during the BL21(DE3) pLysS induction. In fact, expression of a C-terminally Flag-tagged S105, the phage λ holin, in the same context also caused a precipitous drop in A_{550}, albeit at a later time (~ 30 min) (Fig. 54B).

Functional replacement of holin S105 by miniBax during bacterial lysis

To explore the functional link between miniBax and holin S105, we resorted to an inducible system in which the coupled expression of a holin and an endolysin (*R*) gene causes bacterial lysis. This system is comprised of the plasmid pS105 or its derivatives and the Δ(*SR*) *E. coli* cells. The pS105 plasmid (Fig. 55A) contains the well-characterized λ lysis cassette, consisting of the lysis genes *S105, R* (endolysin)*, Rz* and *Rz1*, downstream from its native λ late promoter, pR' (29, 164). The Δ(*SR*) cells harbor a thermally inducible λ prophage, which is lysis defective due to deletions of both *S* (*S105*) and *R* genes. When carried in the Δ(*SR*) cells, pS105 directs the expression of the lysis cassette genes upon thermal induction of the prophage, which supplies the late gene activator Q and transactivates the pR' promoter on the plasmid. As expected, when this gene activator Q and transactivates the pR' promoter on the plasmid. As expected, when this system is induced with pS105 or a version in which the S105 gene has been altered to encode a Flag-tagged product (pS105-Flag), abrupt lysis is observed at 30 and 35 min after induction, respectively (Fig. 55B), whereas no lysis is observed for pSam7, which is identical to pS105 except for a nonsense mutation in the *S105* gene.

FIG 55 MiniBax functionally replaces bacteriophage holin (S105), causing endolysin- dependent lysis of Δ(SR) cells. (A) Diagram for the construction of the pS105-based isogenic plasmid replacing S105 with F-miniBax. The DNA segment encoding the first 92 amino acids of S105 in the S105/R lysis cassette within the plasmid pS105 was replaced by the reading frame of F-miniBax. (B) Lysis of Δ(SR) cells by the miniBax/R cassette. The plasmid pSam7 is identical to pS105 except for an Amber mutation in the S105 gene that abolished S105 expression. Upon reaching A550 ~0.3, the Δ(SR) cells carrying the indicated plasmids were induced by thermal induction for 15 min at 42°C, followed by aeration at 37°C. A550 was measured for each culture at 5-min intervals. The cultures were harvested as described in the Materials and Methods and subjected to SDS-PAGE and Western blot with an α-Flag antibody. (C) Diagram of the lysis cassettes of S105 and F-miniBax with or without functional endolysin (R). (D) Lysis phenotypes of the lysis cassettes listed in C in Δ(SR) cells. Expression of the indicated proteins was detected by Western blot with an α-Flag antibody. (E) Diagram of truncation mutants of miniBax. These miniBax mutants were cloned into the pS105 plasmid by the same strategy as shown in A. (F) Lysis induced by miniBax and its truncation mutants in Δ(SR) cells was measured the same way as in B. The expression of these mutants was detected by Western blot with an α-Flag antibody. (G) Δ(SR) cells carrying either pS-F-miniBax or pS-F-miniBaxH3A were monitored by time-lapse microscopy. Still images of the cells undergoing lysis at different time points are shown.

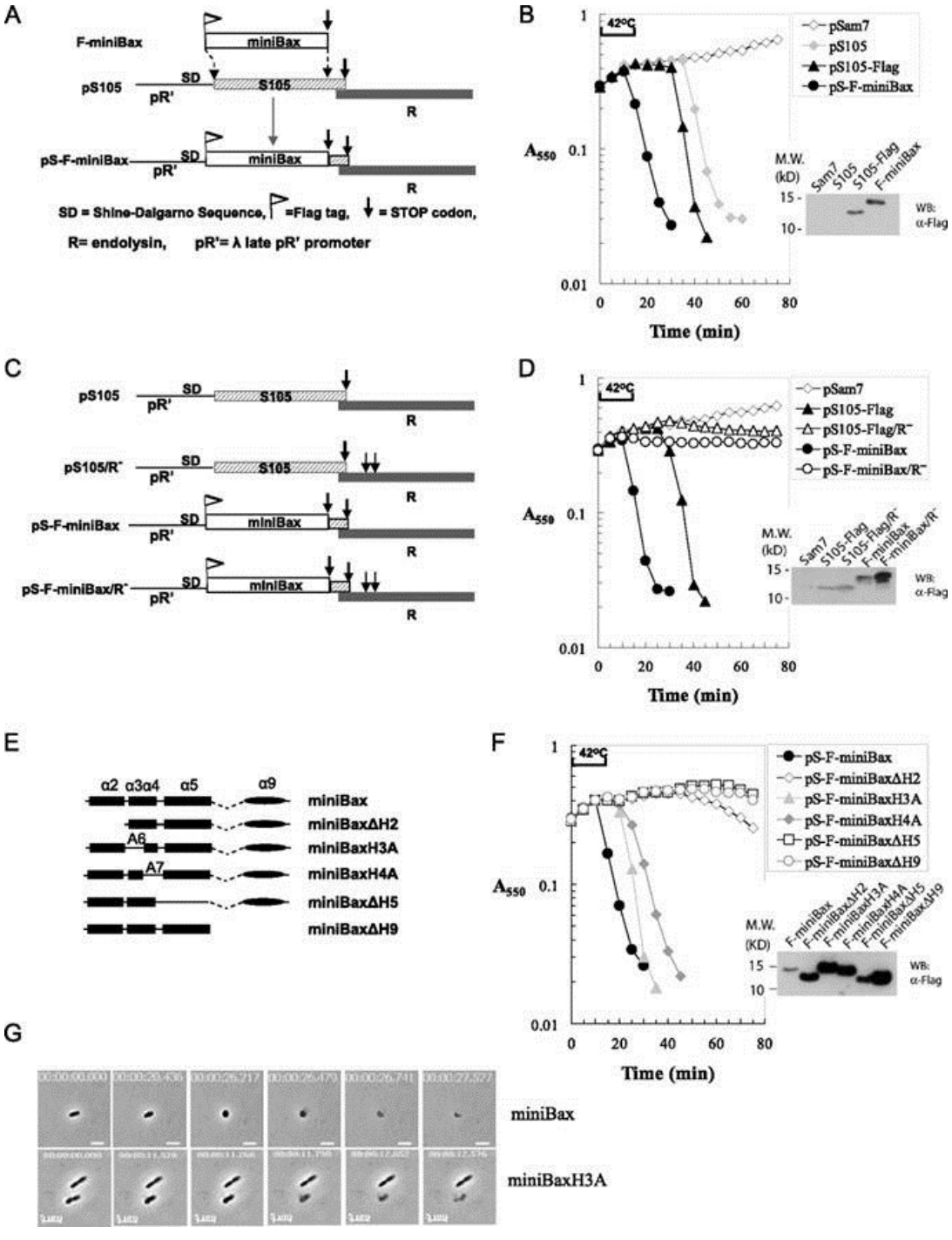
A
F-miniBax
miniBax
pS105
SD
S105
pR'
R
pS-F-miniBax
SD = Shine-Dalgarno Sequence, =Flag tag, = STOP codon,
R= endolysin, pR'= λ late pR' promoter
B
42ºC
pSam7
pS105
pS105-Flag
pS-F-miniBax
A550
Time (min)
M.W. (kD)
Sam7
S105
S105-Flag
F-miniBax
WB: α-Flag
C
pS105/R-
pS-F-miniBax/R-
D
pS105-Flag/R-
pS-F-miniBax/R-
E
α2 α3α4 α5 α9
A6
A7
miniBax
miniBaxΔH2
miniBaxH3A
miniBaxH4A
miniBaxΔH5
miniBaxΔH9
F
pS-F-miniBaxΔH2
pS-F-miniBaxH3A
pS-F-miniBaxH4A
pS-F-miniBaxΔH5
pS-F-miniBaxΔH9
G

By placing the *miniBax* gene in the same genetic background as *S105*, the behaviors of these two proteins in bacteria can be directly compared. We therefore generated an isogenic construct based on pS105, replacing *S105* with the reading frame of *Flag-miniBax* (Fig. 55A). Upon thermal induction, this construct showed an abrupt culture-wide lysis, starting at around 10 min during thermal induction (Fig. 55B). To test the requirement of the endolysin for the observed lysis, we introduced stop codons in the *R* gene in both pS105-Flag and pS-F-miniBax (Fig. 55C). As shown in Fig. 55D, the null mutations of *R* in both plasmids completely abolished the lysis, indicating that lysis activities of both S105 and miniBax are strictly dependent upon the release of the cytoplasmic endolysin, R. Furthermore, in the absence of endolysin, both S105 and miniBax caused an abrupt cessation of cell growth, indicative of the triggered formation of lethal membrane lesions (Fig. 55D). Thus, miniBax complements S105 activity.

To further test the specificity of the lysis activity of miniBax, we constructed pS105-based isogenic constructs expressing miniBax mutants that lack each of the five helices (Fig. 55E). Alleles lacking helices 2 (BH3), 5, or 9 exhibited no lysis activity (Fig. 55F). In contrast, mutants in which helices 3 or 4 were replaced by oligo-Ala sequences (miniBaxH3A and miniBaxH4A, respectively) showed lysis kinetics comparable to that of S105, albeit delayed as compared to that of miniBax (Fig. 55F). Time lapse microscopy was also used to monitor the bacterial lysis by miniBax and miniBaxH3A. In both cases, the lysis event required only a few seconds after onset of morphological change, as observed previously with S105 (Fig. 55G) (76). These results demonstrate that miniBax can functionally replace S105 in mediating a triggered

bacterial lysis, and that helices 2, 5, and 9 are absolutely required for this activity. Furthermore, these lysis phenotypes correlate well with the apoptotic activity of these proteins in *Bax*$^{-/-}$/*Bak*$^{-/-}$ DKO cells (68). It is worth noting that miniBaxH4A showed robust bacterial lysis, although somewhat delayed as compared to miniBax and miniBaxH3A (Fig. 55F), whereas it displayed a reduced apoptosis phenotype in the DKO cells (68). This partial exception may be due to the differential level of expression of this mutant in the two systems.

Next, we examined the membrane localization of miniBax and its truncation mutants by cell fractionation. As shown in Fig. 56, the majority of miniBax, miniBaxH3A, and especially miniBaxΔH2 are in the membrane fraction, but with a small fraction in the cytosol. While miniBaxH4A displays a decreased level of membrane localization, deletion of helix 5 or 9 shows a predominantly cytosolic localization, suggesting that helix 4, 5, and 9 contribute to the targeting of miniBax in the context of the bacterial cell.

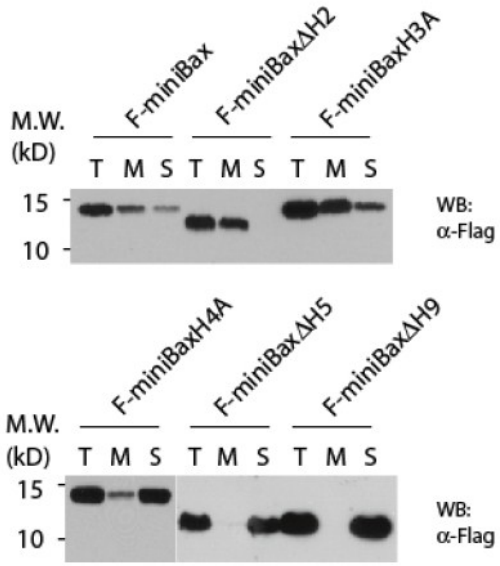

FIG 56 Subcellular localization of miniBax and its truncation mutants. Δ(*SR*) cells carrying miniBax and its truncation mutants in the pS105 vector were grown and thermally induced, as previously described. Cell fractionation was carried out as described in Materials and Methods, and examined by Western blot with an α-Flag antibody. T: Total protein. M: membrane fraction. S: supernatant.

Bacterial lysis activity of miniBax is dependent on homo-oligomerization

Homo-oligomerization has been shown to be critical for the apoptotic activity of Bax/Bak (6, 48, 68) and for S105 (75). In addition, the BH3 domain (helix 2) has been shown to be critical for homo-oligomerization of Bax/Bak (48, 68). We therefore examined the role of the BH3 domain in the bacterial lysis activity of miniBax. As shown in Fig. 57A, unlike miniBax, the mutants that contain either a L63P or L63E missense mutation in the BH3 domain were lysis-defective, despite unperturbed

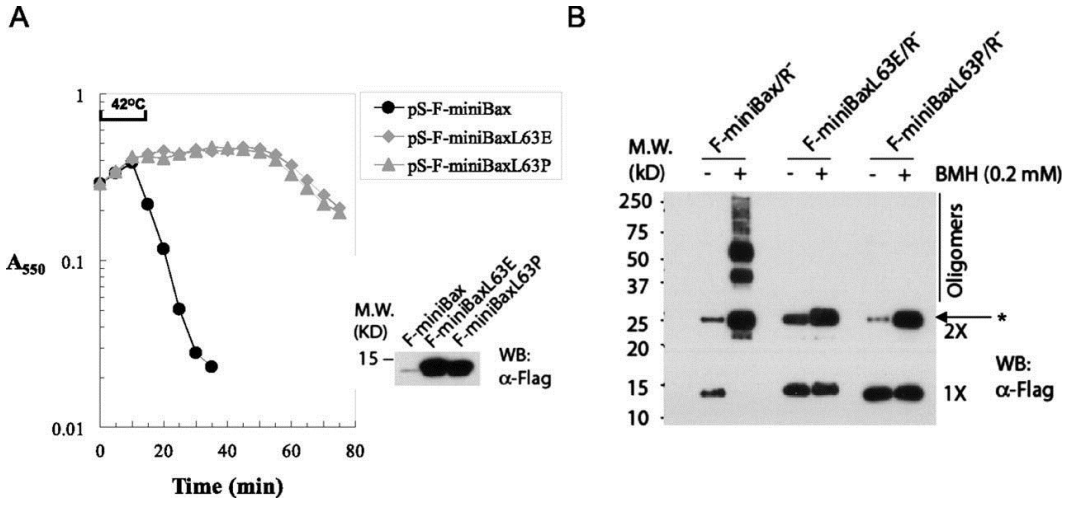

FIG 57 Dependence of the bacterial lysis activity of miniBax on homo-oligomerization. (A) Lysis phenotypes of miniBax and its two BH3 mutants, miniBaxL63E and miniBaxL63P, in Δ(SR) cells. The expression of these proteins was detected by Western blot. (B) Homo-oligomerization of miniBax and its mutants. BMH cross-linking was carried out as described in the Materials and Methods, followed by SDS-PAGE and Western blot analysis with an α-Flag antibody. The asterisk (*) stands for nonspecific protein.

membrane targeting (Fig. 58). The homo-oligomerization of these proteins was examined by BMH (bis-maleimidohexane)-mediated crosslinking. To avoid the potential non-specific effects on homo-oligomerization by bacterial lysis, the BMH assay was carried out in an R^- background. Both BH3 mutants lost the triggering phenotype (Fig. 58A) and were detected predominantly in the membrane fractions (Fig. 58B). Not surprisingly, miniBax displayed a robust homo-oligomerization, whereas little or no homo-oligomerization was detected for the two BH3 mutants (Fig. 57B). These results indicate that homo-oligomerization is essential for the bacterial lysis

activity of miniBax, similar to its role in full-length Bax-mediated mitochondrial damage and apoptosis.

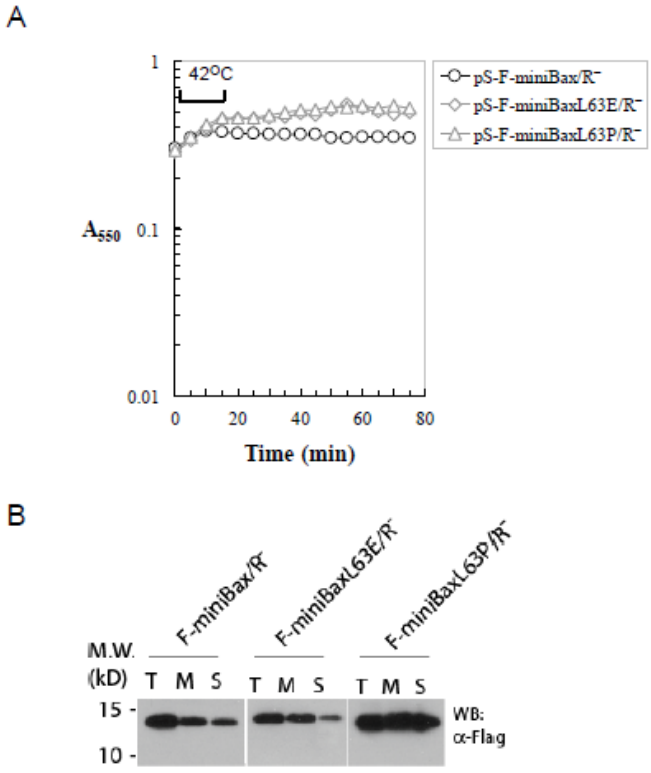

FIG 58 Subcellular localization of miniBax and its BH3 mutants. A. Lysis curves of Δ(*SR*) cells carrying the indicated plasmids were performed as described in 'Materials and Methods'. B. At 45 min after induction, samples were collected for cell fractionation. T: total protein, M: membrane fraction, S: supernatant.

Active mutants of Bax and Bak, but not any other Bcl-2 family member, are competent for bacterial lysis

In view of the sequence and structural homology among the Bcl-2 family members, we generated isogenic constructs based on pS105, replacing *S105* gene with

the reading frame of each Bcl-2 family protein (Fig. 59A), and tested them for bacterial lysis activity in the Δ(*SR*) cells. Of the 10 BH3-only proteins, including truncated Bid (tBid), the active form of Bid, none showed lysis activity (Fig. 59B,C). We next tested the Bax/Bak proteins, which are considered to act as gateway proteins for mitochondria-dependent apoptosis (191). Due to the close sequence and structural homology between Bax and Bak, we also generated the corresponding "miniBak", which contains helices 2, 3, 4, and 5 of Bak fused to the helix 9 of Bcl-xL, a well characterized mitochondrial targeting sequence (100) (Fig. 59E). In addition, a Bak mutant that lacks only helix 1 (BakΔH1), which showed constitutive apoptotic activity in Bax/Bak DKO cells, was generated in the pS105 replacement system. While full-length Bax displayed a much delayed lysis phenotype as compared to that of miniBax, full-length Bak failed to show any lysis activity. In contrast, miniBak, especially BakΔH1, showed a potent lysis activity (Fig. 59D). Lastly, when the anti-apoptotic Bcl-2 proteins were tested, none showed any lysis activity (Fig. 59F,G). However, since Bcl-xL and Bax share similar 9 α-helix structures, we asked if an arrangement of the Bcl-xL helices similar to that of miniBax would result in an "active" Bcl-xL mutant. We therefore generated "miniBcl-xL", which contains helices 2, 3, 4, 5, and 9 of Bcl-xL in the chimeric lysis cassette (Fig. 59G). Despite a higher level of expression than that of miniBax, miniBcl-xL did not cause lysis in Δ(*SR*) cells (Fig. 59F,G). Together, these results strongly suggest that, among the Bcl-2 family members, the holin-like bacterial lysis activity is specific for the active Bax/Bak proteins.

FIG 59 Lysis of Δ(SR) cells by active mutants of Bax or Bak, but not by any other Bcl-2 family protein. (A) Diagram for the replacement of the first 92 amino acids of S105 by Bcl-2 family proteins in the S105/R lysis cassette in pS105. (B) Lysis curves for the BH3-only proteins were measured as previously indicated. (C) Expression of the indicated BH3-only proteins in Δ(SR) cells. Protein samples from cells expressing F-Bid, F-BimEL, F-Bmf, and F-Bik were diluted 1:10. Protein samples from F-Bnip3 and F-Noxa were diluted 1:5. The asterisk (*) stands for nonspecific protein. (D) Lysis phenotypes of the Bax/Bak and their mutants in Δ(SR) cells. (E) Expression of Bax/Bak and their mutants. Due to low expression, the protein sample from F-BakΔH1-expressing cells was concentrated fourfold. The asterisk (*) stands for nonspecific protein. Diagrams of miniBax, miniBak, and BakΔH1 are shown at the bottom. (F) Lysis phenotypes of anti-apoptotic Bcl-2 family proteins. (G) Expression of the indicated anti-apoptotic Bcl-2 family proteins. Protein samples from cells expressing these proteins were diluted 1:20 as compared with F-miniBax. A diagram of a truncation mutant of Bcl-xL, “miniBcl-xL,” is shown at the bottom.

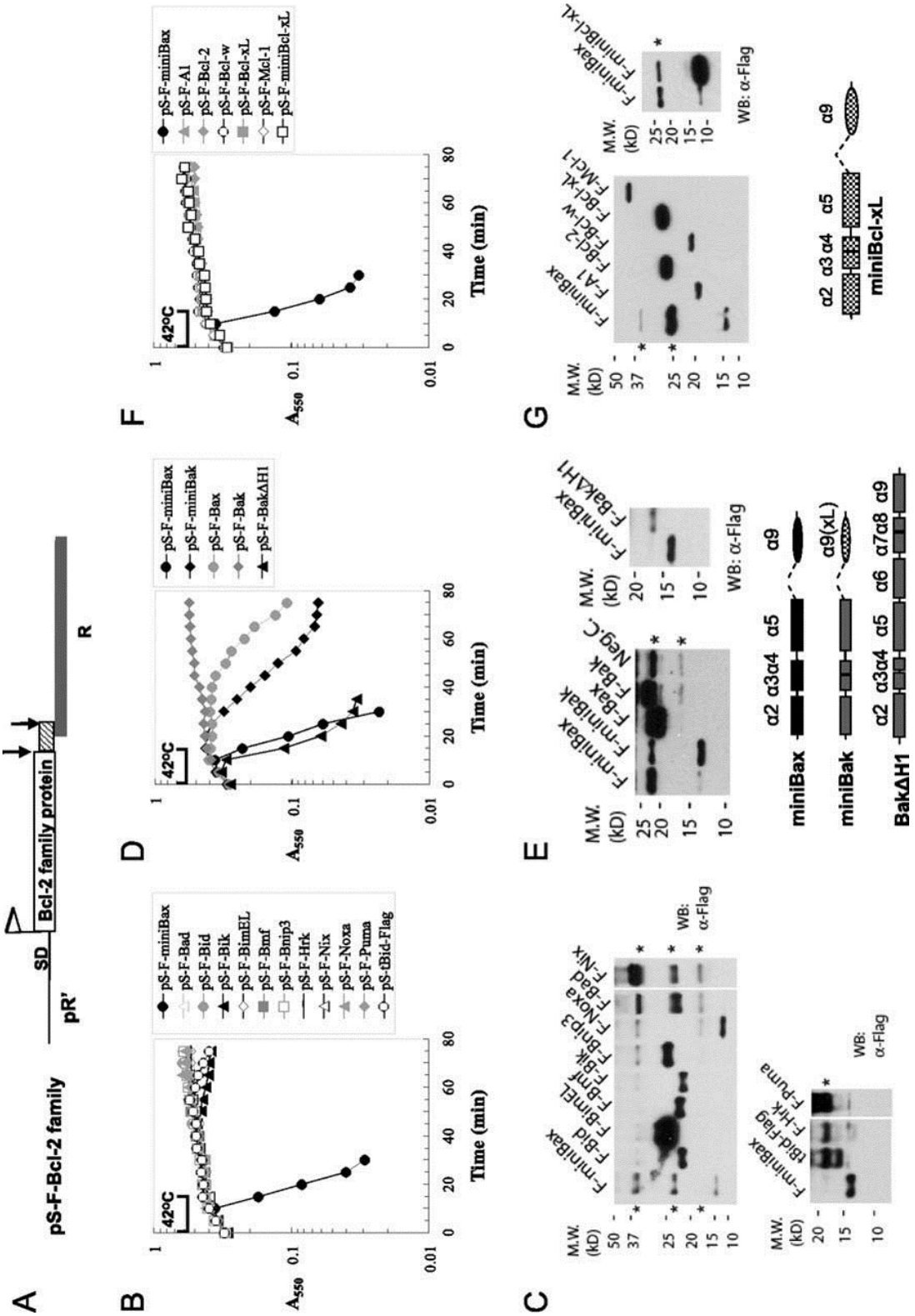
A
pS-F-Bcl-2 family
SD
Bcl-2 family protein
pR'
R
B
42°C
pS-F-miniBax
pS-F-Bad
pS-F-Bid
pS-F-Bik
pS-F-BimEL
pS-F-Bmf
pS-F-Bnip3
pS-F-Hrk
pS-F-Nix
pS-F-Noxa
pS-F-Puma
pS-tBid-Flag
A550
Time (min)
C
M.W. (kD)
WB: α-Flag
D
pS-F-miniBax
pS-F-miniBak
pS-F-Bax
pS-F-Bak
pS-F-BakΔH1
E
F-miniBax
F-miniBak
F-Bax
F-Bak
Neg.C.
F-BakΔH1
α2 α3α4 α5 α9
miniBax
α9(xL)
miniBak
α2 α3α4 α5 α6 α7α8 α9
BakΔH1
F
pS-F-miniBax
pS-F-A1
pS-F-Bcl-2
pS-F-Bcl-w
pS-F-Bcl-xL
pS-F-Mcl-1
pS-F-miniBcl-xL
G
F-miniBax
F-A1
F-Bcl-2
F-Bcl-w
F-Bcl-xL
F-Mcl-1
F-miniBcl-xL
α2 α3 α4 α5 α9
miniBcl-xL

Generation of chimeric phages by replacing S105 with mutants of Bax/Bak in the lambda genome

A more stringent test for the functional homology between miniBax and S105 would be to examine the generation of recombinant phages that contain miniBax in the place of S105 in the λ genome. A convenient way to assess this is to quantify the production of plaque forming units (PFUs) from the inductions described above, relying on homologous recombination in the induced cells to generate chimeric phages (207). To our surprise, while Δ(*SR*) cells harboring the pS105 cassette produced large numbers of plaques, cells harboring the pS-F-miniBax plasmid failed to produce any plaques, despite complete lysis following thermal induction (Fig. 60B,C). Considering the observation that miniBax causes lysis consistently earlier than S105 (Fig. 55), we reasoned that the early lysis induced by miniBax may not allow enough time for the packaging of the chimeric phage particles. To test this possibility, it is necessary to generate mutants of Bax or Bak that exhibit delayed onset of lysis, preferably similar to the lysis timing of S105. Three mutants in our collection, miniBaxH3A, BaxΔH6

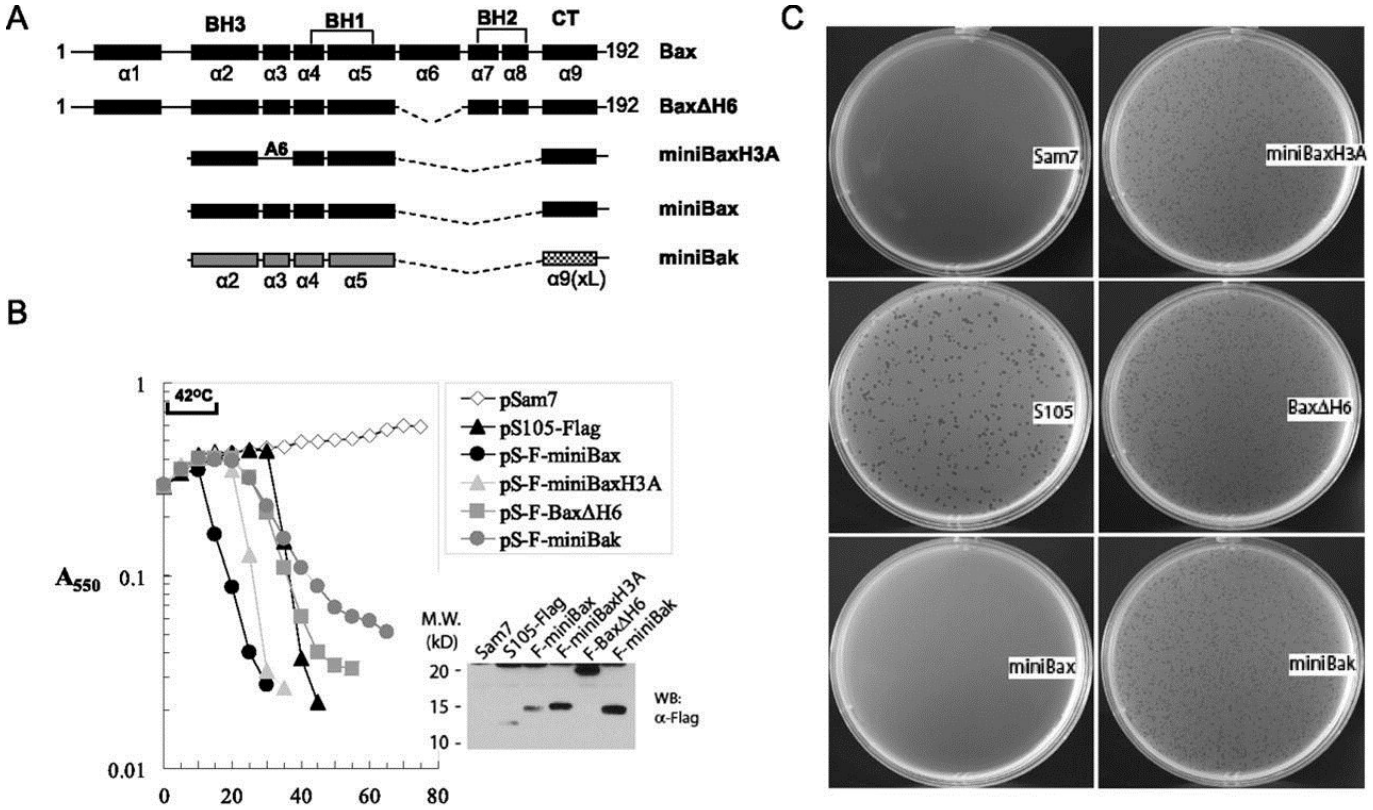

FIG 60 Replacement of the holin gene by functional Bax/Bak mutants generates viable chimeric λ phages. (A) Diagrams of Bax and Bak mutants. These mutants were cloned into the pS105 plasmid to replace S105. (B) Lysis phenotypes of the indicated Bax/Bak mutants. Expression of the indicated Bax and Bak mutants in Δ(SR) cells was detected by Western blot with an α-Flag antibody. (C) Plaque formation by Bax/Bak mutants. At 75 min, the cultures were centrifuged at 22,000g for 10 min, and the supernatant was assayed for plaque formation using the MC4100ΔtonA as indicator cells as described in the Materials and Methods.

(68, 69), and miniBak (Fig. 60A) were compared to miniBax in the lysis assay. Following thermal induction, these alleles exhibited retarded onset of lysis as compared to miniBax (Fig. 60B). Strikingly, with all three alleles, the ability to support the generation of plaque-forming recombinants was similar to that of S105 (Fig. 60C and Table 11).

TABLE 11 Plaque formation by Bax and Bak mutants

Plasmid name	PFU/ml
pS105-Flag	5.8×10^5
pS-F-miniBax	0
pS-F-miniBaxH3A	3.5×10^5
pS-F-BaxΔH6	3.4×10^5
pS-F-miniBak	3.2×10^5

Furthermore, these chimeric phages were able to generate lysogens expressing the relevant proteins (Fig. 61A,B). For unclear reasons, however, the plaques from these alleles were consistently smaller than those from S105 in size (Fig. 60C). Together, these results indicate that Bax/Bak mutants with lysis times comparable to S105 can replace the latter *in vivo* for the generation of viable phages.

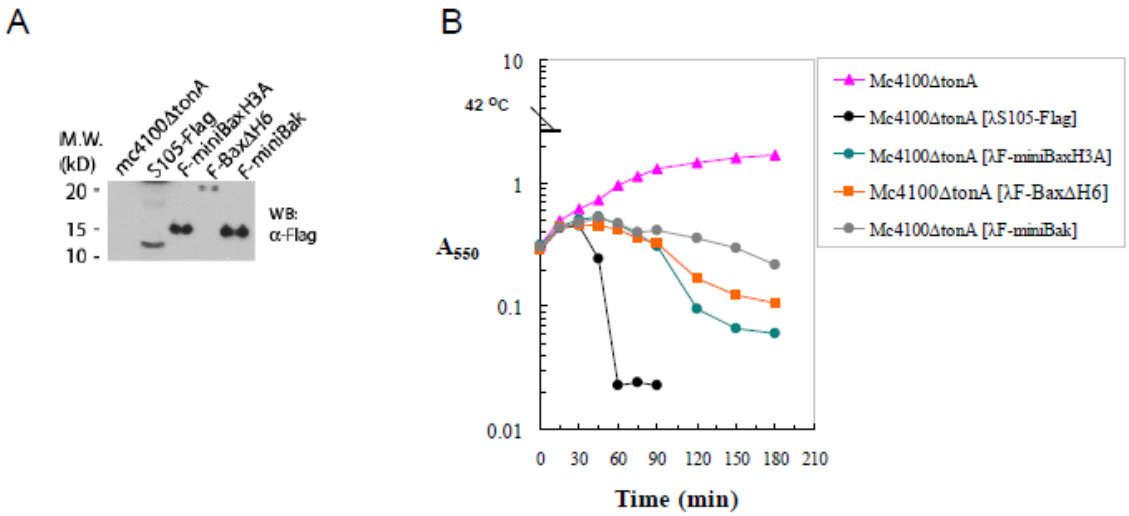

FIG 61 Expression of S105 or Bax/Bak mutants from lysogens. A. The expression of S105 or Bax/Bak mutants by Western blot with α-Flag at 75 min. B. Lysis curves of MC4100Δ*tonA* cells or MC4100Δ*tonA* lysogens carrying λS105-Flag, λF-miniBaxH3A, λF-BaxΔH6, or λF-miniBak prophages were carried out, with optical density measured at 15 min intervals.

Sizing the holes produced by active Bax mutants

Our results indicate that active Bax, like S105, can form membrane lesions that allow the release of a functional endolysin, see above. We next set out to address the size of these lesions. The earliest estimates of the S105 lesion size were obtained by characterizing the lytic function of recombinant phages in which the *R* endolysin gene (158 aa.) was fused in-frame to the full length *lacZ* gene (1,024 aa.) (187). The chimeric R-LacZ product was shown to have normal β-galactosidase activity and formed a stable tetramer of over 500 kDa (121, 187). Despite the gross increase in the size of the endolysin, S105 retained the ability to allow the release of R-LacZ into the periplasm, as judged by the full plaque-forming ability and lytic function of the recombinant phage (187). The analogous F-miniBax/R-LacZ cassette was constructed based on

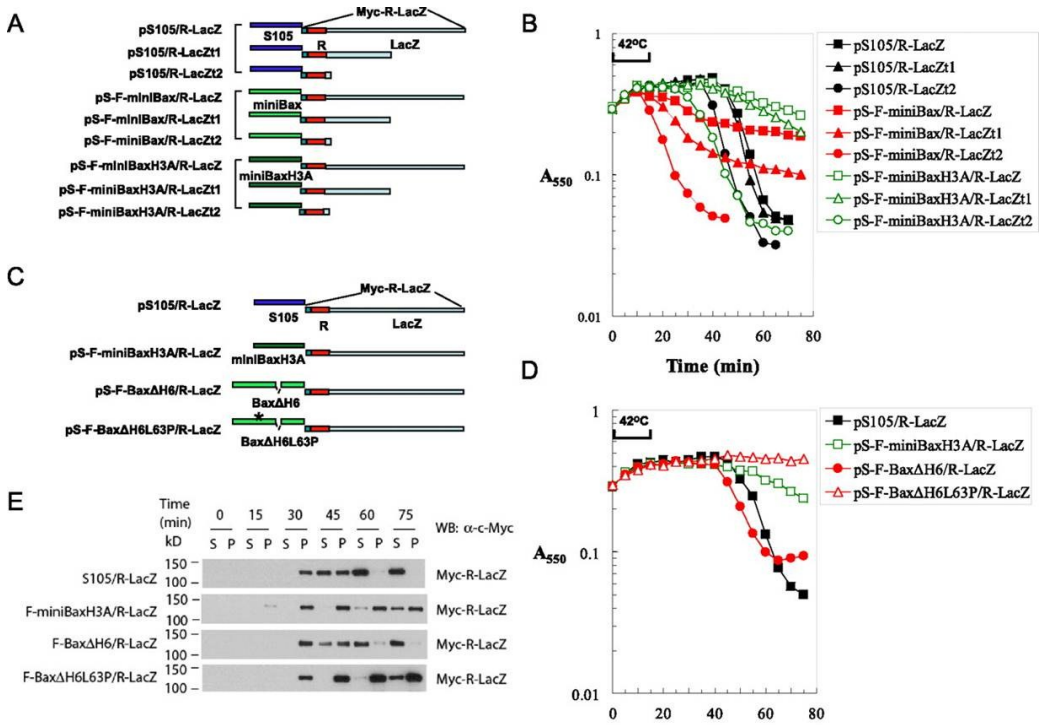

FIG 62 Sizing the membrane holes induced by active Bax mutants through the R-LacZ fusion proteins. (A) Diagram of the various lysis cassettes with LacZ or its truncation mutants fused to the reading frame of R. The R-LacZ fusion protein has a Myc tag on the N terminus. R-LacZt1 is the fusion between R and the first 497 amino acids of LacZ. R-LacZt2 is the fusion between R and the first 8 amino acids of LacZ. (B) Lysis curves of the different lysis cassettes listed in A in Δ(SR) cells. (C) Diagram of the lysis cassettes expressing Bax mutants in conjunction with R-LacZ. (D) Lysis curves of the indicated Bax mutants with R-LacZ cassettes in Δ(SR) cells. (E) Δ(SR) cells carrying the indicated plasmids were thermally induced. At the indicated time points, 1-mL samples of the culture were collected and pelleted by centrifugation at 22,000g at 4°C. The supernatant (S) and the pellet (P), which was resuspended in 1 mL of EBC buffer, were loaded onto SDS-PAGE followed by Western blot analysis with an α-Myc antibody.

pS105 R-LacZ and tested in Δ(*SR*) cells for lytic activity (Fig. 62A). Unlike S105/R-LacZ, lysis by F-miniBax/R-LacZ or F-miniBaxH3A/R-LacZ is markedly impaired (Fig. 62B). Since all three constructs showed comparable levels of R-LacZ expression (Fig. 63A-C), these results suggest that most of the holes induced by miniBax or miniBaxH3A were not large enough to allow the passage of the 500 kDa R-LacZ complex (Fig. 62B).

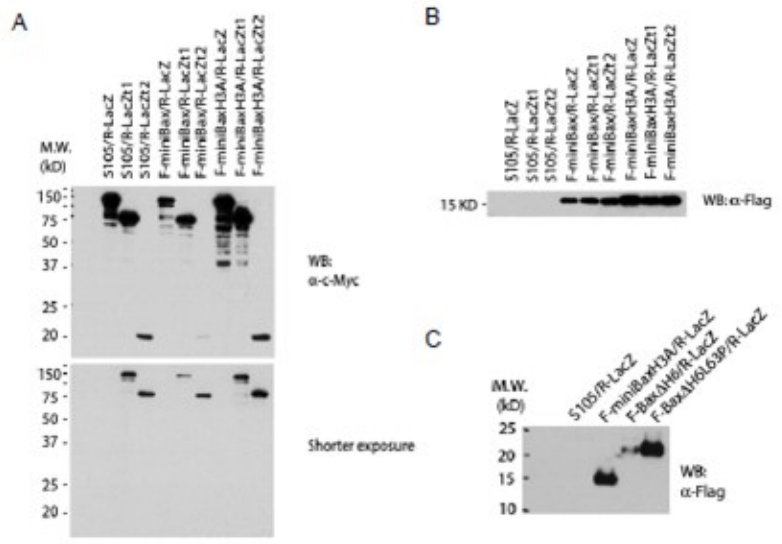

FIG 63 Expression of relevant proteins in the R-LacZ background. (A) At 15 min, cultures carrying the indicated plasmids were examined for the expression of R-LacZ and its truncation mutants by Western blot with an α-c-Myc antibody. (B) Expression of miniBax and miniBaxH3A at 15 min in FIG 62B by Western blot with α-Flag antibody. C. Expression of Bax mutants at 30 min in FIG 62D.

The above mentioned possibility would predict that the lysis defect of miniBax/R-LacZ or miniBaxH3A/R-LacZ may be overcome by reducing the size of R-LacZ. We therefore constructed F-miniBax/R-LacZt1 and F-miniBax/R-LacZt2

cassettes, which express R-LacZ fusion proteins with 497 aa. and 8 aa., respectively, from the N-terminus of β-galactosidase following the reading frame of R (Fig. 62A). Indeed, while miniBax/R-LacZt1 shows a weak but somewhat improved lysis as compared to that of miniBax/R-LacZ, miniBax/R-LacZt2 regains full lytic activity (Fig. 62B). These results indicate that the induced miniBax hole is not much in excess of the size required for the passage of the monomeric R endolysin (16 kDa) and non-permissive even for an R endolysin with an ~50 kDa addition (R-LacZt1). Similar results were obtained with miniBaxH3A in conjunction with different R-LacZ derivatives (Fig. 62B). These results strongly suggest that the majority of the membrane holes generated by miniBax and miniBaxH3A are significantly smaller than those generated by S105.

In theory, an alternative strategy to rescue the lysis defect of miniBax/R-LacZ or miniBaxH3A/R-LacZ is to increase the size of the hole. Considering the extensive deletion of helices from Bax that resulted in miniBax, we wanted to test the possibility that Bax mutants with fewer deletions might support the formation of larger holes. We therefore replaced S105 in pS105/R-LacZ with another active Bax mutant, BaxΔH6 (Fig. 60A), which contains three additional helices as compared to miniBax (Fig. 62C). Unlike miniBaxH3A, BaxΔH6 was proficient in lysis under the *R-LacZ* background, whereas its BH3 mutant, BaxΔH6L63P, failed to cause lysis in the same setting (Fig. 62D). This is in contrast with the observation under the *R* background, in which miniBaxH3A showed an even earlier lysis than BaxΔH6 (Fig. 60B). In addition, we also monitored the release of the soluble R-LacZ fusion protein into the culture media during

induced lysis. As shown in Fig. 62E, similar to S105, BaxΔH6 was able to cause the release of R-LacZ following thermal induction. In contrast, miniBaxH3A and BaxΔH6L63P were both unable to efficiently release R-LacZ following thermal induction. Consistently, under the *R-LacZ* background, the lysis defect was also observed for another miniBax derived mutant, miniBax$Y^{115A}F^{116A}$, but not for full-length Bax (Fig. 64). Taken together, these results suggest that the minimum homo-oligomerization domain (helices 2-5 in miniBax or miniBaxH3A (68) predominantly produces membrane holes with sizes only comparable to the endolysin (R), whereas additional helices (helices 1, 7, and 8 in BaxΔH6) facilitate the formation of much bigger

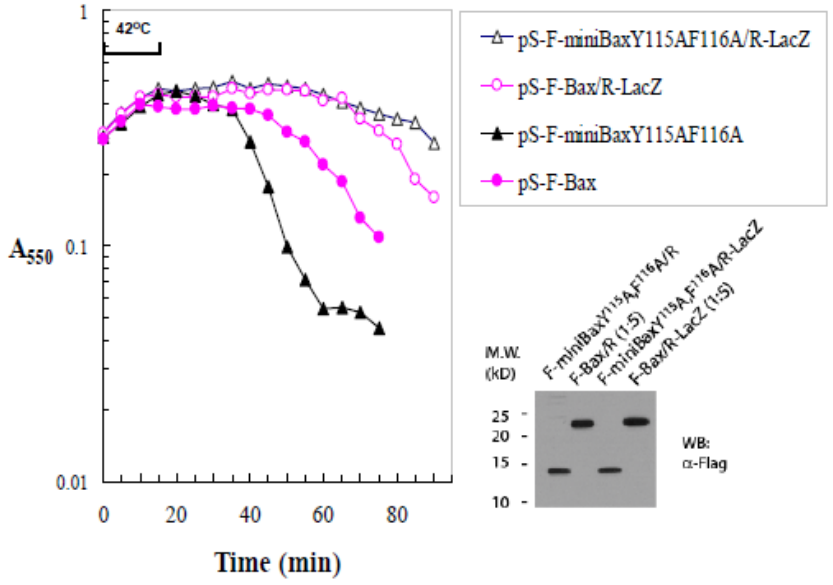

FIG 64 Differential lysis activity of full-length Bax and a miniBax mutant under R and R-LacZ background. Lysis curves of Δ(*SR*) cells carrying the indicated plasmids and expression of Bax and miniBax Y^{115A},F^{116A} collected at 30 min and examined by Western blot with an α-Flag antibody.

holes, which allow the release of proteins as large as the 500 kDa LacZ tetramer (R-LacZ).Regulation of the lysis activity of Bax parallels the control of MOMP

As the apoptotic activity of Bax is regulated by other Bcl-2 family proteins, we set out to test if the bacterial lysis activity of Bax is similarly regulated. The phages carrying Bax or its derivatives allowed for the generation of lysogens with prophages directing the expression of the corresponding proteins, albeit at a lower level. Expression plasmids can then be introduced into these lysogens for the co-expression of Bax or its derivatives with other proteins. This lysogen-based co-expression system was first used to test the effect of Bcl-xL on the lysis activity of active Bax mutants. MiniBaxH3A lysogens were generated through the corresponding recombinant phages (Fig. 60C). Subsequently, a plasmid expressing Bcl-xL was introduced into these cells, in which both miniBaxH3A and Bcl-xL were expressed following thermal induction. As shown in Fig. 65A, expression of Bcl-xL inhibited the lysis activity of miniBaxH3A. In contrast, the expression of GFP or a mutant Bcl-xL, Bcl-xLmt8, which was shown to be defective in anti-apoptotic function (31), had little effect. Similarly, Bcl-xL showed a strong inhibitory effect on the lysis mediated by BaxΔH6 (Fig. 65B).

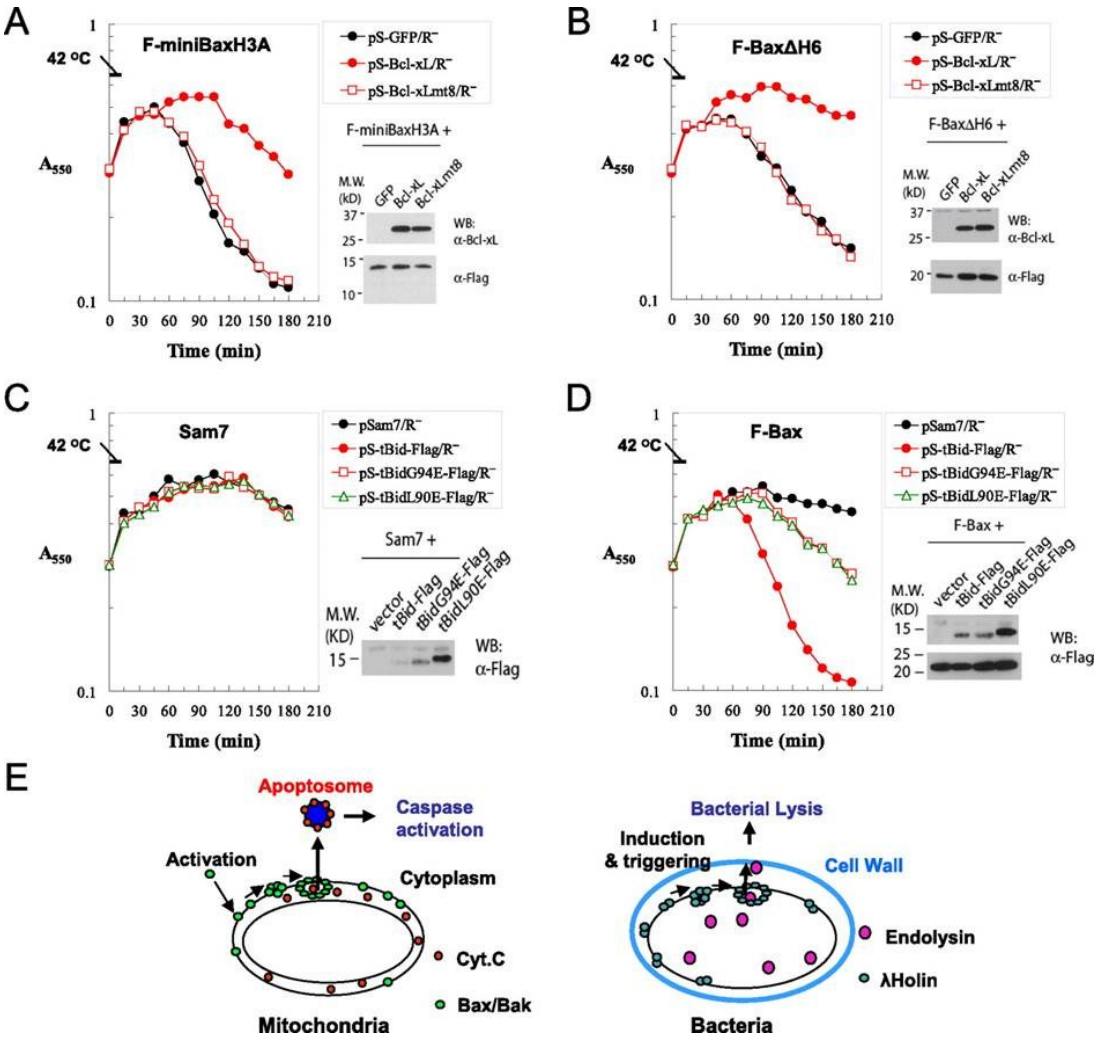

FIG 65 Regulation of Bax-mediated bacterial lysis by Bcl-xL and tBid. (A) Suppression of miniBaxH3A-mediated bacterial lysis by Bcl-xL. Lysis curves of F-miniBaxH3A lysogens carrying the indicated plasmids were measured at a 15-min interval. The expression of Bcl-xL and Bcl-xLmt8 at 15 min was detected using an α-Bcl-xL antibody, and the expression of miniBaxH3A was detected using an α-Flag antibody. (B) Suppression of BaxΔH6-mediated bacterial lysis by Bcl-xL. (C) Lysis phenotypes of sam7 lysogen carrying the indicated plasmids. The expression of tBid, its mutants, and Bax at 60 min was detected by Western blot with an α-Flag antibody. (D) Lysis phenotypes of F-Bax lysogen carrying indicated plasmids. (E) A diagram depicting the functional homology between MOMP and hole formation in bacterial membrane.

The inhibitory effect of Bcl-xL on lysis is likely through an inhibition on the homo-oligomerization of the effectors. Indeed, using the BMH crosslinking assay, we found that the homo-oligomerization of miniBaxH3A was strongly inhibited by Bcl-xL, but not by GFP or Bcl-xLmt8 (Fig. 66). These results suggest that the anti-apoptotic Bcl-2 family proteins inhibit the activities of Bax/Bak in bacteria.

Next, to test the potential regulation of the lysis activity of Bax by the BH3-only proteins, we introduced an expression plasmid for tBid or its BH3 domain mutants into cells that contain a prophage expressing either a nonsense mutant of holin S105 (Sam7 lysogen) or the wild-type Bax (Bax lysogen). As expected, in the absence of Bax (the Sam7 lysogen), GFP, tBid, or its BH3 mutants tBidL90E and tBidG94E, showed no lysis activity (Fig. 65D). When introduced into the Bax expressing cells, tBid greatly stimulated the lysis activity of Bax, whereas GFP, or tBidL90E, or tBidG94E showed little stimulatory activity, suggesting that tBid stimulates the Bax-mediated lysis through a BH3-dependent mechanism (Fig. 65E). Together, these results suggest that the lysis activity of Bax is regulated through similar mechanisms as it is during MOMP.

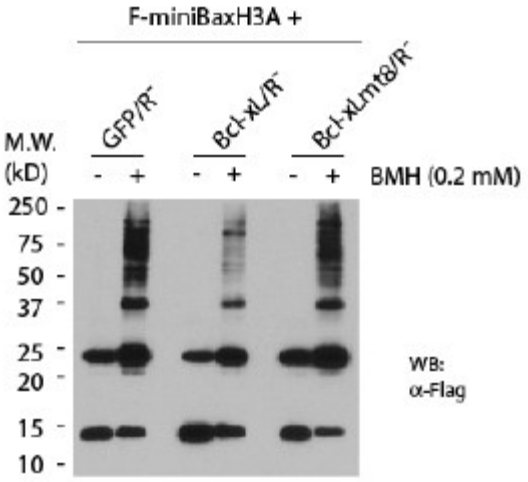

FIG 66 Suppression of homo-oligomerization of miniBaxH3A by Bcl-xL. At 60 min, cultures of F-miniBaxH3A lysogens carrying the indicated plasmids were collected and subjected to to BMH crosslinking assay as described in 'Materials and Methods' followed by SDS PAGE and Western blot analysis with an α-Flag antibody.

Discussion

Here we have presented evidence that constitutively active Bax/Bak proteins competent for mitochondrial damage are capable of serving as holins in phage-mediated bacterial cell lysis. These results suggest a mechanistic link between MOMP and hole formation in the bacterial membrane, and provide new perspectives on the size control of the Bax/Bak-induced pore.

A close correlation between the apoptotic activity of Bax/Bak in the DKO cells and their bacterial lysis activity in bacteria

Activated Bax and Bak function as essential effectors in MOMP and apoptosis by causing damage on the mitochondrial outer membrane (176, 191, 200). In this study,

we demonstrate that the expression of active mutants of Bax/Bak potently causes membrane lesions and the lysis of bacteria. Of the entire collection of Bcl-2 family members, only active mutants of Bax/Bak possess this novel activity. In addition, miniBax and miniBak displayed significantly more potent lysis activities as compared to their respective full-length proteins (Fig. 59), consistent with an activation of Bax or Bak through structural changes (68). Furthermore, the apoptotic activity of Bax in *Bax*$^{-/-}$/ *Bak*$^{-/-}$ DKO cells and the bacterial lysis activity seem to be mediated essentially by the same structural elements (Fig. 55) (68). Of note, similar to the regulation of the apoptotic activity of Bax in the mammalian cells, the bacterial lysis activities of active Bax mutants were found to be inhibited by Bcl-xL, and on the other hand, the lysis activity of Bax is stimulated by tBid in a BH3-dependent manner (Fig. 65). These results strongly suggest that the apoptosis activity or the MOMP inducing activity of Bax/Bak are functionally equivalent to the bacterial lysis activity. Thus, we speculate that the bacterial system may be suitable for studying the regulation of Bax and Bak by Bcl-2 or even non-Bcl-2 family proteins.

Active Bax and Bak as functional holins, mechanistically linking MOMP and bacterial lysis

The holins constitute a large functional group of small membrane proteins with diverse amino acid sequences (188). To date, 105 known or putative holins within more than 30 unrelated ortholog groups have been identified in bacteriophages. Most holins are less than 150 aa. in length, with two or three alpha helical and hydrophobic transmembrane (TM) domains followed by a short C-terminal cytoplasmic domain

enriched in basic residues. Importantly, holins share the ability to permeabilize the bacterial cell membrane. Several salient features are shared by Bax/Bak, especially active Bax/Bak, i.e. miniBax/Bak, and typical holins. These include: 1) MiniBax contains at least two bona fide hydrophobic TM domains, helix 5 and helix 9, both of which have been shown to insert into the OMM (4, 65), and a short stretch of basic residues at the C-terminus (Fig. 67); 2) Both miniBax/Bak and the canonical holin, S105, are primarily composed of alpha helices (74, 164); 3) Bax/Bak and S105 both exist as monomer/dimers before triggering to a pore-forming state but require the formation of large homo-oligomers in the membrane for function; 4) Both active Bax/Bak and S105 inflict irreparable damages to the membrane in a lethal process; 5) Both form large oligomeric membrane pores that allow the escape of fully folded functional proteins, which are effectors for downstream lethal events; 6) Both proteins were shown to permeabilize liposomes in a reconstituted *in vitro* system (108, 154, 164); 7) Both are inhibited by closely related endogenous proteins, Bcl-xL and anti-holin, respectively (150, 188). It is worth noting, however, that Bax/Bak showed at least one difference from a typical holin. The holins are sensitive to the energization state of the bacterial membrane, in that treatment with energy poisons or uncouplers can trigger holin-mediated hole formation prematurely (188), whereas active Bax/Bak did not exhibit such a feature (data not shown). The sensitivity to the membrane potential is thought to be critical for the precise control of lysis timing in holins (188). This appears to be absent in Bax/Bak, which may partially account for the smaller plaque size of the chimeric λBax/Bak derivatives (Fig. 60). Nonetheless, the common features and the

functional replacement of holin by active Bax/Bak in triggered bacterial lysis and phage production strongly indicate that active Bax/Bak are functional holins. Of note, when expressed in mammalian cells, S105 has been reported to cause a caspase-independent and non-apoptotic cell death in eukaryotic cells (2). It will be interesting to test if S105 can functionally replace Bax/Bak in the mitochondrial pathway of apoptosis when it is properly targeted to the mitochondria.

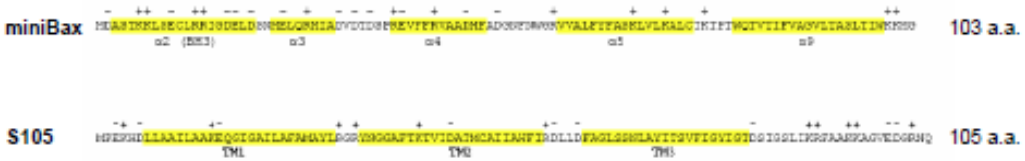

FIG 67 Amino acid sequences of miniBax and λ holin S105.

In the mitochondria-dependent pathway of apoptosis, activated Bax/Bak causes the formation of non-specific OMM lesions of sufficient size to allow the non-specific egress of fully folded native proteins, such as cytochrome c and SMAC, to initiate the caspase cascade. Similarly, holins initiate the lysis pathway by formation of "holes", non-specific lesions, in the cytoplasmic membrane, allowing fully folded, active muralytic enzymes to escape and attack the peptidoglycan cell wall (Fig. 65F). The functional replacement of the effector for bacterial lysis (holin) by the effector (active Bax/Bak) for MOMP suggests a mechanistic link between these two operationally similar processes.

The size control and composition of the pore

Although the observation of cytochrome c release from mitochondria during apoptosis has been reported more than a decade ago (103, 112, 198), efforts to define the physical nature of the OMM pore have not been fruitful (68). The characterization of bacterial membrane lesions caused by holins, however, has been more advanced. It has been demonstrated that S105 allows the escape of a tetrameric R-LacZ chimeric protein with a molecular weight of ~ 500 kDa (187). Using the same endolysin-LacZ chimera strategy, the miniBax derivatives were found to exhibit relatively slow and incomplete lysis, suggesting that either the pores were relatively small and restricted the egress of the chimeric endolysin, or that the pore sizes are heterogeneous, with only a subset of sufficient size. However, a full-length Bax lacking only the helix 6 (BaxΔH6) was proficient at lysis with R-LacZ (Fig. 62). This suggests that the domains deleted in our miniBax construct, although not essential for holin-like function in bacteria or OMM permeabilization in mitochondria, serve a modulating role in controlling the size of the hole. In support of this notion, full-length Bax was previously found to be much more efficient at making high-order oligomers in the OMM than the miniBax constructs (68). The simplest idea is that these modulating domains influence the degree of homo-oligomerization that occurs before concerted hole-formation. Alternatively, these helices may affect the architecture and shape of the hole. Of importance, the novel notion that helices in Bax play a role in modulating the size of the pore provides strong support for the hypothesis that the membrane pores are proteinaceous in nature and are composed of Bax/Bak homo-oligomers (68).

Using electron microscopy and recombinant proteins purified in non-ionic detergent, Savva *et al.* (156) found that functional S105 formed multimeric ring structures, which likely reflect a minimum-energy arrangement in the membrane. In addition, recent cryo-electron microscopy and tomography studies revealed that the lesions caused by holin S105 of phage lambda could be visualized as interruptions in the bilayer spanning very large areas of the cytoplasmic membrane, averaging >350 nm in diameter (46). Assuming these lesions correspond to the holes, this latter observation fully accounted for the ability of holins to allow the rapid, non-specific escape of proteins not only of endolysins, of which the lambda R endolysin, a soluble, 15 kDa monomeric protein is typical, but also of much larger proteins, including the ~500 kDa R-LacZ chimeras (46). However, the lesions that are formed by the Bax proteins in the bacterial cytoplasmic membrane do not appear to be of the near micron-scale holes like those formed by the S105 holin, since they could not be observed using cryo-electron microscopy at a 50 nm resolution (data not shown). Higher resolution cryo-electron microscopy and tomography studies should help uncover the physical nature of active Bax/Bak and the membrane lesions.

Overall, results presented in this study establish a functional homology between active Bax/Bak and bacteriophage holin. Considering the similarities and evolutionary relationships between bacteria and mitochondria, our results also suggest that the phage/bacteria system is potentially a powerful model system to study the mechanisms and regulation of MOMP.

CHAPTER VII

CONCLUSIONS AND FUTURE DIRECTIONS

Despite the fact that lysis inhibition in bacteriophage T4 is one of the foundational phenomena of molecular biology, leading to the understanding of recombination, the genetic code, and many other pioneering work solved since the 1940's, the molecular mechanism of its imposition has only recently been addressed. Work by Ramanculov established that (1) T is the holin of bacteriophage T4; (2) lysis timing mutants of T can be selected for using the λ::*t* genetic system; (3) that RI is a specific inhibitor of T, and (4) T and RI are the major determinants in the imposition of LIN (144-146).

Follow-up work by Tran extended Ramanculov's studies, leading to the understanding that (1) RI is transiently an inner membrane protein, released spontaneously via its SAR domain; (2) periplasmic domain interactions between RI and T are necessary and sufficient for the imposition of LIN; (3) RI is a labile protein with a half-life of ~2 min due to inactivation and degradation by the periplasmic protease, DegP, and (4) the holin, T, has a single transmembrane domain and is the prototype of class III holins (79, 179, 180).

The work described in this dissertation has followed on from the studies of Ramanculov and Tran and made a number of advances. First, the work in this dissertation has provided evidence for the following conclusions: (1) the RI periplasmic domain is monomeric in solution and composed of mostly alpha-helical secondary structure character; (2) the periplasmic domain of T oligomerizes but the oligomerization

can be prevented by forming a complex with the periplasmic domain of RI, supporting the conclusion that the periplasmic domain of T has a large role in oligomerization of the holin leading to hole-formation; (3) the RI-T periplasmic domains form a heterodimer with RI binding to a homo-oligomerization surface of T; (4) lysis-defective mutants are found throughout the T protein so all three topological domains of T are important in the lysis pathway; (5) the periplasmic domain of RI is dynamic in the region between helices one and two, and (6) RI is a DNA binding protein, leading to the conclusion that dsDNA in the periplasmic space is likely the lysis inhibition signal. Some of these conclusions warrant further discussion.

T-mediated lysis and its inhibition

The T4 holin is unique in size and topology when compared to the other studied holins from bacteriophage λ and 21, in that T has a single transmembrane domain, rather than multiple, and large N-terminal and C-terminal (periplasmic) domains, rather than just a few residues. Using genetic and biophysical techniques, it has been shown that the periplasmic domain is a major determinant in the oligomerization of the holin. As such, it is not unexpected that this domain would be the target for inhibition by RI. Additionally, mutants in the periplasmic domain are mostly localized to the surface of sT, as judged by the sT-sRI structure solved. By performing an alignment of nearly 30 T4-like holins and mapping that conservation on the sT structure, it appears that there are four "patches" of conservation at the surface of sT, including one that is the T-RI interface (Fig. 68). Taken together with the mutagenesis data, these four patches are likely holin-holin interfaces, needed for the oligomerization

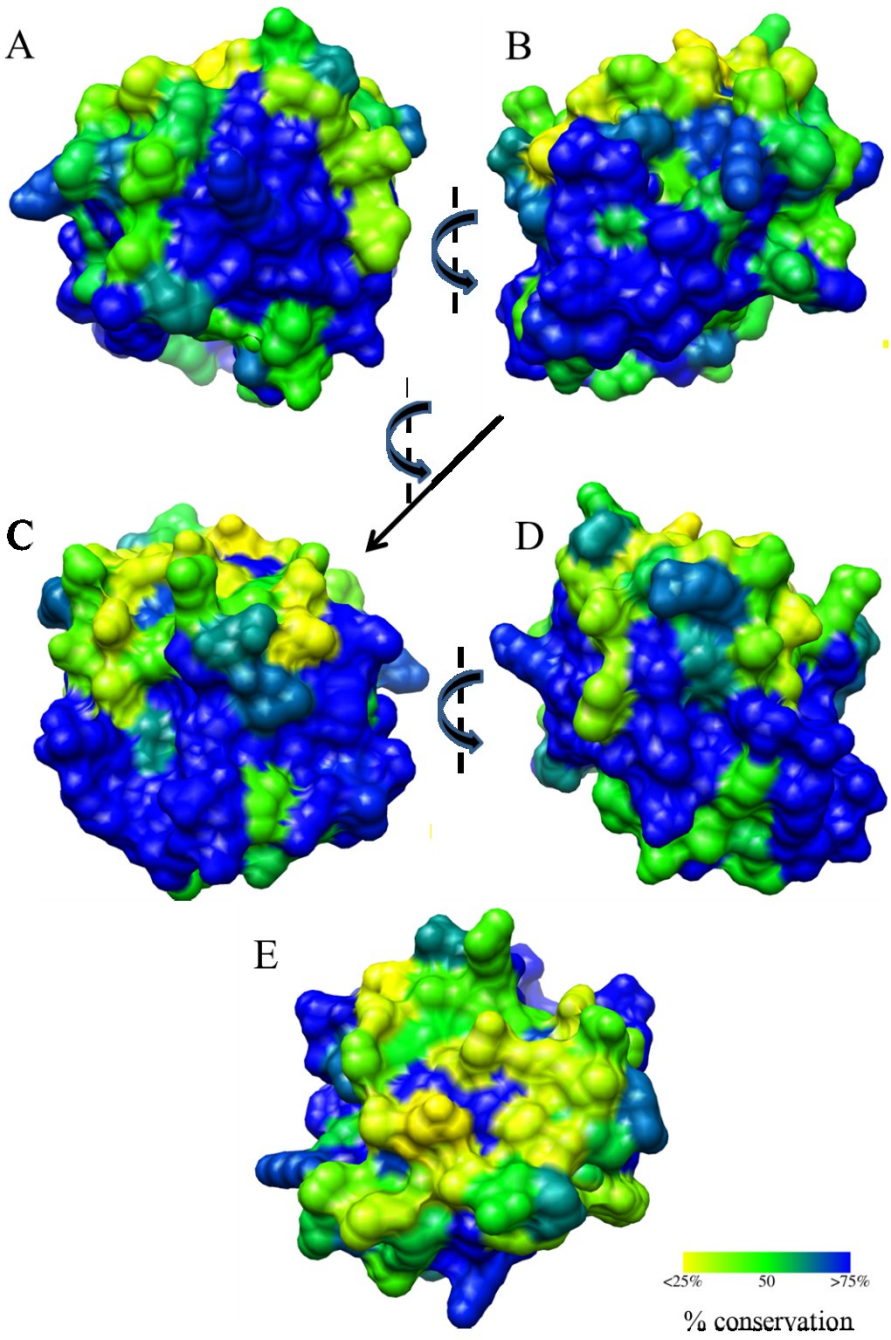

FIG 68 Conservation of residues at the surface of sT. The sT structure is aligned as would be expected if the N-terminal helix is attached to the transmembrane domain in the inner membrane. (A) – (D): Views of the sT structure rotated 90° around the vertical axis in each panel. (E) View of the top of the sT structure. The legend indicates percent conservation for the colors shown. The interface with RI is shown in panel B.

of the holin. By blocking one of these interfaces, RI acts as a chain terminator of holin oligomerization.

Dynamics of RI and the lysis inhibition signal

We have shown that the periplasmic domain of RI is dynamic in nature. The protein is dynamic in the region which changes in conformation between the apo and bound structures (Chapters III and V). However, the dynamics in this region do not necessarily confirm the fact that both structures are relevant in the infection cycle. Analytical ultracentrifugation studies of the RI periplasmic domain in solution showed that the protein is monomeric and globular in solution. So, it is likely that only the bound form of RI is relevant *in vivo* and the unbound/apo extended form is an artifact of the X-ray crystallization conditions. Additionally, residues that are dynamic, including Arg39 and His40, have been implicated in DNA binding in our study of the LIN signal. I propose that the binding of DNA to sRI in the loop region between helices one and two stabilizes the dynamic structure of RI into a conformation that is favorable for binding to the periplasmic domain of T.

The binding of DNA to RI appears to be non-specific in nature, with a randomized sequence of DNA used to show DNA-binding. Likely, the interaction is dictated by electrostatic interactions between the positively charged residues identified as interacting with DNA and the negatively charged phosphate groups of DNA. This conclusion can be tested by mutagenizing the positively charged residues of RI and testing whether DNA binding still occurs. The following positively charged residues have been implicated in DNA binding: His29, Lys32, Arg39, His40, and Lys48. Lysis

inhibition defective alleles of RI have been collected previously at most of these locations (26). These mutants can be exploited to investigate their ability in binding DNA by NMR and *in vivo* experiments (see below). It is predicted that these mutants of RI can still bind to T, in the stable sRI form, as they are not altered in the RI-T interface. Their inhibition of T in T4 infections, however, is overmatched by their dynamic nature and degradation by DegP.

Additional work needs to be done to investigate the role of DNA in lysis inhibition *in vivo*. This can be investigated with the expression of a GFP-tagged allele of T and the addition of the periplasmic domain of RI either incubated or not with DNA. The T protein can then be tracked in the inner membrane and the role of RI with or without DNA in preventing T oligomerization in the inner membrane investigated. N-terminal GFP fusions to T have been shown to be non-functional previously (data not shown). However, the fusion of a GFP variant proficient in proper folding in the periplasmic space has been constructed (T-GFP) and visualized by confocal microscopy (Fig. 69). Several fluorescent foci, indicative of the oligomerization of T-GFP in the

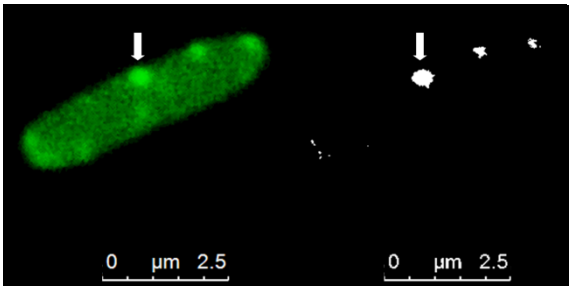

FIG 69 Confocal microscopy of *E. coli* cells expressing *t-gfp*. One patch of T-GFP oligomers is indicated by an arrow. This patch is ~500 nm in diameter. Both images are of the same cell, except background noise has been reduced in the image on the right.

inner membrane are shown. Unlike the wild type allele of T, the T-GFP is delayed in lysis, triggering at nearly 60 min after induction. Whether T-GFP can be inhibited by RI has not been investigated and must be confirmed before further experiments described below.

The addition of purified RI with or without DNA directly to cells induced for T-GFP is, of course, hindered by the presence of the outer membrane and peptidoglycan layer. However, preparation of *E. coli* spheroplasts, in which the outer membrane has been destabilized by the addition of EDTA and the peptidoglycan has been degraded with the addition of lysozyme might prove useful in understanding the role of DNA-binding *in vivo*. Addition of purified sRI and sRI/DNA complexes to spheroplasts induced for T-GFP are expected to show that the sRI/DNA complex is more efficient in imposing inhibition of T-oligomerization and lysis.

Current model for T4 lysis and lysis inhibition

Taking together all the work described in this dissertation, more detailed models for both T4-mediated lysis and lysis inhibition can be constructed. For lysis, the current model is that T accumulates harmlessly in the inner membrane from the beginning of late gene expression, 8 min after infection occurs. As the holin accumulates in the inner membrane, the model is that holin-holin oligomerization occurs using the two soluble domains of T. First, dimerization and oligomerization occurs via the N-terminal domain leucine zipper motif. Also, oligomerization occurs via interactions between the T periplasmic domains. The oligomerization of T in the inner membrane by both of these soluble domains of T leads large 2 dimensional rafts of T. At lysis time, dictated by the

accumulation of a “critical concentration” of T, hole formation occurs. This hole formation might be driven by the exclusion of lipids due to a high local concentration of transmembrane domains driven by oligomerization of the soluble domains. This lipid exclusion leads to a reduction in the proton motive force and hole formation. Hole formation initiates the lysis event, allowing the endolysin to escape the cytoplasmic space to degrade its substrate, the peptidoglycan (Fig. 70).

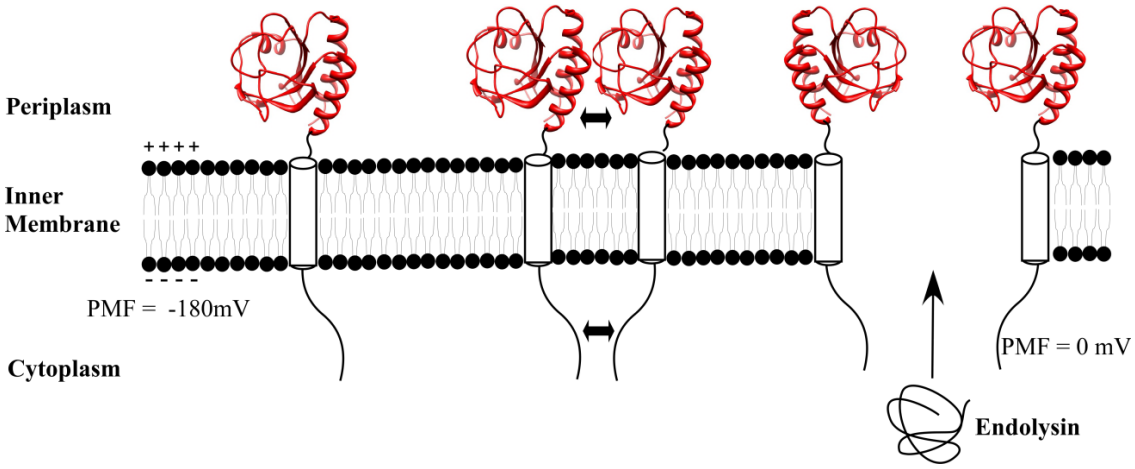

FIG 70 Model for T4 lysis. Oligomerization of the holin proceeds by periplasmic domain interactions and N-terminal domain interactions. This leads to a high local concentration of transmembrane domains (white cylinder), lipid exclusion, and a drop in the proton motive force. Hole formation in the inner membrane leads to the escape of the endolysin.

Based on this model for the pathway to lysis, a detailed model for lysis inhibition can also be constructed (Fig. 71). Within three minutes of a T4 infection, in addition to RI, gene products of the *imm* and *sp* genes are synthesized. The latter gene products are localized to the inner membrane and periplasm, respectively. They are responsible for the inhibition of ejection of DNA into the cytoplasm by subsequent phage infections. RI is localized to the inner membrane in an N-in, C-out orientation by its SAR domain. It is spontaneously released as a soluble protein in the periplasmic space via its SAR domain. If no superinfection happens, RI is inactivated and degraded by DegP (as a result of the presence of the SAR domain) and the lysis pathway proceeds unabated, leading to triggering at ~25 and then lysis of the host (Fig. 70).

However, if a superinfection does occur, the head contents of the superinfecting phage (170 kbp dsDNA genome and ~1000 internal proteins) are shunted into the periplasmic space by the actions of the T4 gene products *imm* and *sp*. This leads to a DNA concentration of 1.7 mM, in terms of bp of DNA, in the periplasmic space, available for RI binding. DNA-binding leads to the stabilization of RI, shifting the equilibrium to the conformation competent for binding T. The stable RI molecules can now bind T, blocking an oligomerization interface (Fig. 71). It appears that RI acts as a chain-terminator for holin-holin oligomerization. Whether binding of RI also inhibits holin-holin interactions by changing the interaction surfaces has not been tested. Purification and structural evaluation of a T oligomerization mutant, such as I88K, would shed light on the structure of T when RI is not bound.

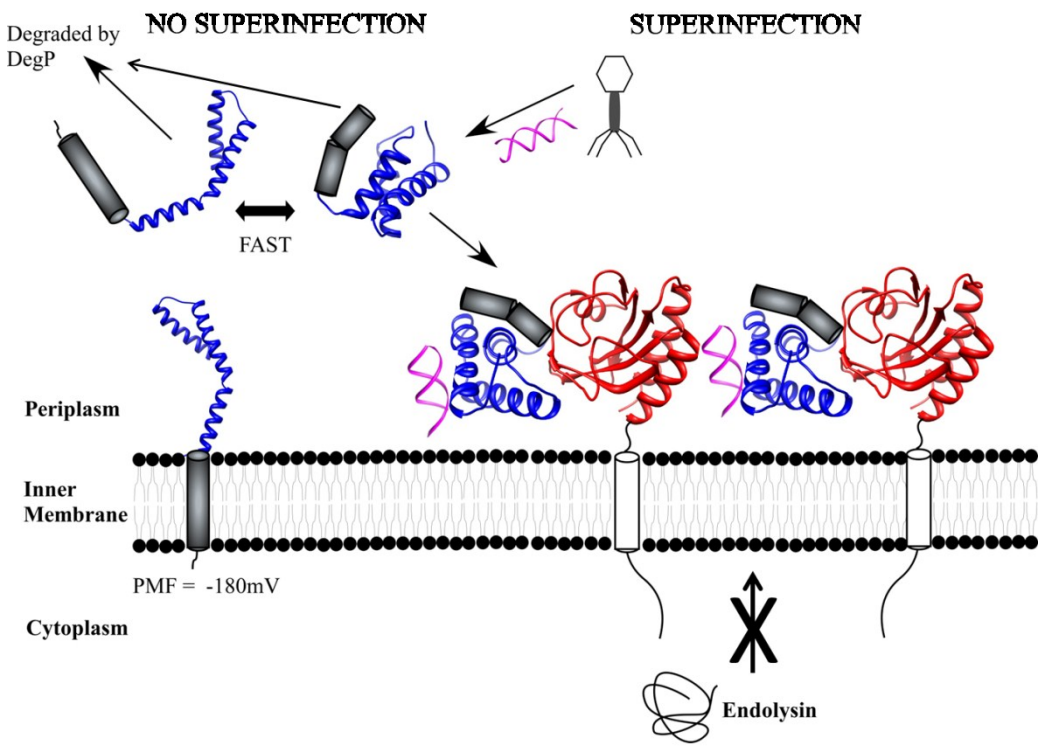

FIG 71 Model for lysis inhibition. If a host is superinfected by a T-even phage, its genome is shunted into the periplasmic space. The DNA binds to RI, stabilizing its structure and leading to an interaction between RI and T. This interaction blocks a holin-holin interface, inhibiting oligomerization and leading to the inhibition of lysis.

Finally, the role of the SAR domain in RI has yet to be investigated during LIN. Continuous superinfection is required (every 10 min) to impose LIN indefinitely. Whether this temporary inhibition of lysis is due to the lability of full length of RI bound to T or due to a continuous increase of T not inhibited by RI in the inner membrane has not been established. Tracking RI during a T4 infection, using GFP fusions, should shed light on its lability during a wild type infection.

REFERENCES

1. **Abedon, S. T.** 2011. Lysis from without. Bacteriophage **1:**46-49.

2. **Agu, C. A., R. Klein, J. Lengler, F. Schilcher, W. Gregor, T. Peterbauer, U. Blasi, B. Salmons, W. H. Gunzburg, and C. Hohenadl.** 2007. Bacteriophage-encoded toxins: the lambda-holin protein causes caspase-independent non-apoptotic cell death of eukaryotic cells. Cell Microbiol **9:**1753-1765.

3. **Altman, E., R. K. Altman, J. M. Garrett, R. J. Grimaila, and R. Young.** 1983. S gene product: identification and membrane localization of a lysis control protein. J Bacteriol **155:**1130-1137.

4. **Annis, M. G., E. L. Soucie, P. J. Dlugosz, J. A. Cruz-Aguado, L. Z. Penn, B. Leber, and D. W. Andrews.** 2005. Bax forms multispanning monomers that oligomerize to permeabilize membranes during apoptosis. EMBO J **24:**2096-2103.

5. **Antignani, A., and R. J. Youle.** 2006. How do Bax and Bak lead to permeabilization of the outer mitochondrial membrane? Curr Opin Cell Biol **18:**685-689.

6. **Antonsson, B., S. Montessuit, B. Sanchez, and J. C. Martinou.** 2001. Bax is present as a high molecular weight oligomer/complex in the mitochondrial membrane of apoptotic cells. J Biol Chem **276:**11615-11623.

7. **Aravind, L., and C. P. Ponting.** 1997. The GAF domain: an evolutionary link between diverse phototransducing proteins. Trends Biochem Sci **22:**458-459.

8. **Arisaka, F., S. Kanamaru, P. Leiman, and M. G. Rossmann.** 2003. The tail lysozyme complex of bacteriophage T4. Int J Biochem Cell Biol **35:**16-21.

9. **Asoh, S., K. Nishimaki, R. Nanbu-Wakao, and S. Ohta.** 1998. A trace amount of the human pro-apoptotic factor Bax induces bacterial death accompanied by damage of DNA. J Biol Chem **273:**11384-11391.

10. **Baase, W. A., L. Liu, D. E. Tronrud, and B. W. Matthews.** 2010. Lessons from the lysozyme of phage T4. Protein Sci **19:**631-641.

11. **Bayles, K. W.** 2007. The biological role of death and lysis in biofilm development. Nat Rev Microbiol **5:**721-726.

12. **Benzer, S.** 1957. The chemical basis of heredity. Johns Hopkins Press, Baltimore.

13. **Benzer, S.** 1955. Fine structure of a genetic region in bacteriophage. Proc Natl Acad Sci U S A **41:**344-354.

14. **Benzer, S.** 1962. The fine structure of the gene. Sci Am **206:**70-84.

15. **Benzer, S.** 1960. Genetic fine structure. Harvey Lect **56:**1-21.

16. **Benzer, S.** 1956. Genetic fine structure and its relation to the DNA molecule. Brookhaven Symp Biol**:**3-5.

17. **Benzer, S.** 1961. On the topography of the genetic fine structure. Proc Natl Acad Sci U S A **47:**403-415.

18. **Benzer, S.** 1959. On the topology of the genetic fine structure. Proc Natl Acad Sci U S A **45:**1607-1620.

19. **Benzer, S., and S. P. Champe.** 1961. Ambivalent rII mutants of phage T4. Proc Natl Acad Sci U S A **47:**1025-1038.

20. **Berry, J., C. Savva, A. Holzenburg, and R. Young.** 2010. The lambda spanin components Rz and Rz1 undergo tertiary and quaternary rearrangements upon complex formation. Protein Sci **19:**1967-1977.

21. **Berry, J., E. J. Summer, D. K. Struck, and R. Young.** 2008. The final step in the phage infection cycle: the Rz and Rz1 lysis proteins link the inner and outer membranes. Mol Microbiol **70:**341-351.

22. **Bessette, P. H., F. Aslund, J. Beckwith, and G. Georgiou.** 1999. Efficient folding of proteins with multiple disulfide bonds in the *Escherichia coli* cytoplasm. Proc Natl Acad Sci U S A **96:**13703-13708.

23. **Bienkowska-Szewczyk, K., B. Lipinska, and A. Taylor.** 1981. The R gene product of bacteriophage lambda is the murein transglycosylase. Mol Gen Genet **184:**111-114.

24. **Blasi, U., K. Nam, D. Hartz, L. Gold, and R. Young.** 1989. Dual translational initiation sites control function of the lambda S gene. EMBO J **8:**3501-3510.

25. **Blasi, U., and R. Young.** 1996. Two beginnings for a single purpose: the dual-start holins in the regulation of phage lysis. Mol Microbiol **21:**675-682.

26. **Burch, L. H., L. Zhang, F. G. Chao, H. Xu, and J. W. Drake.** 2011. The bacteriophage T4 rapid-lysis genes and their mutational proclivities. J Bacteriol **193:**3537-3545.

27. **Cairns, J., G. S. Stent, and J. D. Watson.** 1992. Phage and the origins of molecular biology, expanded ed. Cold Spring Harbor Laboratory Press, Plainview, NY.

28. **Calendar, R.** 2006. The bacteriophages, 2nd ed. Oxford University Press, Oxford.

29. **Chang, C. Y., K. Nam, and R. Young.** 1995. S gene expression and the timing of lysis by bacteriophage lambda. J Bacteriol **177:**3283-3294.

30. **Chen, J., J. L. Song, S. Zhang, Y. Wang, D. F. Cui, and C. C. Wang.** 1999. Chaperone activity of DsbC. J Biol Chem **274:**19601-19605.

31. **Cheng, E. H., B. Levine, L. H. Boise, C. B. Thompson, and J. M. Hardwick.** 1996. Bax-independent inhibition of apoptosis by Bcl-XL. Nature **379:**554-556.

32. **Chipuk, J. E., and D. R. Green.** 2008. How do BCL-2 proteins induce mitochondrial outer membrane permeabilization? Trends Cell Biol **18:**157-164.

33. **Cohen, D.** 1959. A variant of phage P2 originating in *Escherichia coli*, strain B. Virology **7:**112-126.

34. **Cole, C., J. D. Barber, and G. J. Barton.** 2008. The Jpred 3 secondary structure prediction server. Nucleic Acids Res **36:**W197-201.

35. **Collier, N. C., and K. Wang.** 1982. Purification and properties of human platelet P235. A high molecular weight protein substrate of endogenous calcium-activated protease(s). J Biol Chem **257:**6937-6943.

36. **Cornett, J. B.** 1974. Spackle and immunity functions of bacteriophage T4. J Virol **13:**312-321.

37. **Cota-Robles, E. H., and M. D. Coffman.** 1964. Electron microscopy of lysis from without of *Escherichia coli* B by coliphage T2. J Ultrastruct Res **10:**305-316.

38. **Couse, N. L.** 1968. Control of lysis of T4-infected *Escherichia coli*. J Virol **2:**198-207.

39. **Crick, F. H., L. Barnett, S. Brenner, and R. J. Watts-Tobin.** 1961. General nature of the genetic code for proteins. Nature **192:**1227-1232.

40. **Danial, N. N., and S. J. Korsmeyer.** 2004. Cell death: critical control points. Cell **116:**205-219.

41. **de Marco, A.** 2008. Minimal information: an urgent need to assess the functional reliability of recombinant proteins used in biological experiments. Microb Cell Fact **7:**20.

42. **Delaglio, F., S. Grzesiek, G. W. Vuister, G. Zhu, J. Pfeifer, and A. Bax.** 1995. NMRPipe: a multidimensional spectral processing system based on UNIX pipes. J Biomol NMR **6:**277-293.

43. **Delbruck, M.** 1940. The growth of bacteriophage and lysis of the host. J Gen Physiol **23:**643-660.

44. **Demeler, B.** 2005. UltraScan: a comprehensive data analysis software package for analytical ultracentrifugation experiments, p. 210-229. *In* D. Scott, S. Harding, and A. Rowe (ed.), Modern analytical ultracentrifugation: techniques and methods. Royal Society of Chemistry, London, UK.

45. **Demeler, B., and E. Brookes.** 2008. Monte Carlo analysis of sedimentation experiments. Colloid Polym Sci **286:**129-137.

46. **Dewey, J. S., C. G. Savva, R. L. White, S. Vitha, A. Holzenburg, and R. Young.** 2010. Micron-scale holes terminate the phage infection cycle. Proc Natl Acad Sci U S A **107:**2219-2223.

47. **Dewey, J. S., D. K. Struck, and R. Young.** 2009. Thiol protection in membrane protein purifications: a study with phage holins. Anal Biochem **390:**221-223.

48. **Dewson, G., T. Kratina, H. W. Sim, H. Puthalakath, J. M. Adams, P. M. Colman, and R. M. Kluck.** 2008. To trigger apoptosis, Bak exposes its BH3 domain and homodimerizes via BH3:groove interactions. Mol Cell **30:**369-380.

49. **Doermann, A. H.** 1952. The intracellular growth of bacteriophages. I. Liberation of intracellular bacteriophage T4 by premature lysis with another phage or with cyanide. J Gen Physiol **35:**645-656.

50. **Doermann, A. H.** 1948. Lysis and lysis inhibition with *Escherichia coli* bacteriophage. J Bacteriol **55:**257-276.

51. **Doermann, A. H.** 1948. Lysis inhibition with *Escherichia coli* bacteriophages. Genetics **33:**102.

52. **Doermann, A. H., and M. B. Hill.** 1953. Genetic structure of bacteriophage T4 as described by recombination studies of factors influencing plaque morphology. Genetics **38:**79-90.

53. **Dressman, H. K., and J. W. Drake.** 1999. Lysis and lysis inhibition in bacteriophage T4: rV mutations reside in the holin t gene. J Bacteriol **181:**4391-4396.

54. **Duckworth, D. H.** 1970. Biological activity of bacteriophage ghosts and "take-over" of host functions by bacteriophage. Bacteriol Rev **34:**344-363.

55. **Duckworth, D. H.** 1970. The metabolism of T4 phage ghost-infected cells. I. Macromolecular synthesis and ransport of nucleic acid and protein precursors. Virology **40:**673-684.

56. **Dutton, R. J., D. Boyd, M. Berkmen, and J. Beckwith.** 2008. Bacterial species exhibit diversity in their mechanisms and capacity for protein disulfide bond formation. Proc Natl Acad Sci U S A **105:**11933-11938.

57. **Dyall, S. D., M. T. Brown, and P. J. Johnson.** 2004. Ancient invasions: from endosymbionts to organelles. Science **304:**253-257.

58. **Edgar, R. S., R. P. Feynman, S. Klein, I. Lielausis, and C. M. Steinberg.** 1962. Mapping experiments with r mutants of bacteriophage T4D. Genetics **47:**179-186.

59. **Emrich, J.** 1968. Lysis of T4-infected bacteria in the absence of lysozyme. Virology **35:**158-165.

60. **Emrich, J., and G. Streisinger.** 1968. The role of phage lysozyme in the life cycle of phage T4. Virology **36:**387-391.

61. **Ennis, H. L., and K. D. Kievitt.** 1973. Association of the rIIA protein with the bacterial membrane. Proc Natl Acad Sci U S A **70:**1468-1472.

62. **Fabricant, R., and D. Kennell.** 1972. Exclusion of bacteriophages by T2 ghosts. J Virol **10:**872-874.

63. **Farrow, N. A., R. Muhandiram, A. U. Singer, S. M. Pascal, C. M. Kay, G. Gish, S. E. Shoelson, T. Pawson, J. D. Forman-Kay, and L. E. Kay.** 1994. Backbone dynamics of a free and phosphopeptide-complexed Src homology 2 domain studied by 15N NMR relaxation. Biochemistry **33:**5984-6003.

64. **Galonek, H. L., and J. M. Hardwick.** 2006. Upgrading the Bcl-2 network. Nat Cell Biol **8:**1317-1319.

65. **Garcia-Saez, A. J., I. Mingarro, E. Perez-Paya, and J. Salgado.** 2004. Membrane-insertion fragments of Bcl-xL, Bax, and Bid. Biochemistry **43:**10930-10943.

66. **Garen, A.** 1961. Physiological effects of rII mutations in bacteriophage T4. Virology **14:**151-163.

67. **Garrett, J., R. Fusselman, J. Hise, L. Chiou, D. Smith-Grillo, J. Schulz, and R. Young.** 1981. Cell lysis by induction of cloned lambda lysis genes. Mol Gen Genet **182:**326-331.

68. **George, N. M., J. J. Evans, and X. Luo.** 2007. A three-helix homo-oligomerization domain containing BH3 and BH1 is responsible for the apoptotic activity of Bax. Genes Dev **21:**1937-1948.

69. **George, N. M., N. Targy, J. J. Evans, L. Zhang, and X. Luo.** 2010. Bax contains two functional mitochondrial targeting sequences and translocates to mitochondria in a conformational change- and homo-oligomerization-driven process. J Biol Chem **285:**1384-1392.

70. **Georgopoulos, C. P., R. W. Hendrix, A. D. Kaiser, and W. B. Wood.** 1972. Role of the host cell in bacteriophage morphogenesis: effects of a bacterial mutation on T4 head assembly. Nat New Biol **239:**38-41.

71. **Goddard, T. D., and D. G. Kneller.** 2003. SPARKY 3. University of California, San Francisco, CA.

72. **Golec, P., A. Wiczk, A. Majchrzyk, J. M. Los, G. Wegrzyn, and M. Los.** 2010. A role for accessory genes rI.-1 and rI.1 in the regulation of lysis inhibition by bacteriophage T4. Virus Genes **41:**459-468.

73. **Greenfield, N. J.** 2006. Using circular dichroism spectra to estimate protein secondary structure. Nat Protoc **1:**2876-2890.

74. **Grundling, A., U. Blasi, and R. Young.** 2000. Biochemical and genetic evidence for three transmembrane domains in the class I holin, lambda S. J Biol Chem **275:**769-776.

75. **Grundling, A., U. Blasi, and R. Young.** 2000. Genetic and biochemical analysis of dimer and oligomer interactions of the lambda S holin. J Bacteriol **182:**6082-6090.

76. **Grundling, A., M. D. Manson, and R. Young.** 2001. Holins kill without warning. Proc Natl Acad Sci U S A **98:**9348-9352.

77. **Grundling, A., D. L. Smith, U. Blasi, and R. Young.** 2000. Dimerization between the holin and holin inhibitor of phage lambda. J Bacteriol **182:**6075-6081.

78. **Gussin, G. N., and V. Peterson.** 1972. Isolation and properties of rex - mutants of bacteriophage lambda. J Virol **10:**760-765.

79. **Hankin, E. H.** 1896. L'action bactericide des eaux de la Jumna et du Gange sur le vibrion du cholera (in French). Annales de l'Institut Pasteur **10:**511–523.

80. **Heineman, R. H., I. J. Molineux, and J. J. Bull.** 2005. Evolutionary robustness of an optimal phenotype: re-evolution of lysis in a bacteriophage deleted for its lysin gene. J Mol Evol **61:**181-191.

81. **Hershey, A. D.** 1946. Mutation of bacteriophage with respect to type of plaque. Genetics **31:**620-640.

82. **Hershey, A. D., and R. Rotman.** 1949. Genetic recombination between host-range and plaque-type mutants of bacteriophage in single bacterial cells. Genetics **34:**44-71.

83. **Hershey, A. D., and R. Rotman.** 1948. Linkage among genes controlling inhibition of lysis in a bacterial virus. Proc Natl Acad Sci U S A **34:**89-96.

84. **Ho, Y. S., L. M. Burden, and J. H. Hurley.** 2000. Structure of the GAF domain, a ubiquitous signaling motif and a new class of cyclic GMP receptor. EMBO J **19:**5288-5299.

85. **Howard, B. D.** 1967. Phage lambda mutants deficient in r-II exclusion. Science **158:**1588-1589.

86. **Huang, W. M.** 1975. Membrane-associated proteins of T4-infected *Escherichia coli*. Virology **66:**508-521.

87. **Hwang, S., Z. Gou, and I. B. Kuznetsov.** 2007. DP-Bind: a web server for sequence-based prediction of DNA-binding residues in DNA-binding proteins. Bioinformatics **23:**634-636.

88. **Iankovskii, N. K., and V. N. Krylov.** 1975. A genetic and physiologic study of mutations of T4 phage suppressing the lysis defect of gene stII mutants. Genetika **11:**51-60.

89. **Iida, S., and W. Arber.** 1977. Plaque forming specialized transducing phage P1: isolation of P1CmSmSu, a precursor of P1Cm. Mol Gen Genet **153:**259-269.

90. **Jiang, X., and X. Wang.** 2004. Cytochrome C-mediated apoptosis. Annu Rev Biochem **73:**87-106.

91. **Josslin, R.** 1970. The lysis mechanism of phage T4: mutants affecting lysis. Virology **40:**719-726.

92. **Josslin, R.** 1971. Physiological studies on the t gene defect in T4-infected *Escherichia coli*. Virology **44:**101-107.

93. **Kai, T., H. Ueno, Y. Otsuka, W. Morimoto, and T. Yonesaki.** 1999. Gene 61.3 of bacteriophage T4 is the spackle gene. Virology **260:**254-259.

94. **Kaiser, A. D., and F. Jacob.** 1957. Recombination between related temperate bacteriophages and the genetic control of immunity and prophage localization. Virology **4:**509-521.

95. **Kanamaru, S., Y. Ishiwata, T. Suzuki, M. G. Rossmann, and F. Arisaka.** 2005. Control of bacteriophage T4 tail lysozyme activity during the infection process. J Mol Biol **346:**1013-1020.

96. **Kanamaru, S., P. G. Leiman, V. A. Kostyuchenko, P. R. Chipman, V. V. Mesyanzhinov, F. Arisaka, and M. G. Rossmann.** 2002. Structure of the cell-puncturing device of bacteriophage T4. Nature **415:**553-557.

97. **Kao, S. H., and W. H. McClain.** 1980. Baseplate protein of bacteriophage T4 with both structural and lytic functions. J Virol **34:**95-103.

98. **Kao, S. H., and W. H. McClain.** 1980. Roles of bacteriophage T4 gene 5 and gene s products in cell lysis. J Virol **34:**104-107.

99. **Karam, J. D., and J. W. Drake.** 1994. Molecular biology of bacteriophage T4. American Society for Microbiology, Washington, DC.

100. **Kaufmann, T., S. Schlipf, J. Sanz, K. Neubert, R. Stein, and C. Borner.** 2003. Characterization of the signal that directs Bcl-x(L), but not Bcl-2, to the mitochondrial outer membrane. J Cell Biol **160:**53-64.

101. **Kim, H., M. Rafiuddin-Shah, H. C. Tu, J. R. Jeffers, G. P. Zambetti, J. J. Hsieh, and E. H. Cheng.** 2006. Hierarchical regulation of mitochondrion-dependent apoptosis by BCL-2 subfamilies. Nat Cell Biol **8:**1348-1358.

102. **Kim, H., H. C. Tu, D. Ren, O. Takeuchi, J. R. Jeffers, G. P. Zambetti, J. J. Hsieh, and E. H. Cheng.** 2009. Stepwise activation of Bax and Bak by tBid, Bim, and Puma initiates mitochondrial apoptosis. Mol Cell **36:**487-499.

103. **Kluck, R. M., E. Bossy-Wetzel, D. R. Green, and D. D. Newmeyer.** 1997. The release of cytochrome c from mitochondria: a primary site for Bcl-2 regulation of apoptosis. Science **275:**1132-1136.

104. **Krylov, V. N.** 1966. A new r gene of bacteriophage T4B? Genetika **24:**4-5.

105. **Krylov, V. N.** 1970. Possible function of rII genes of bacteriophage T4. Virology **41:**711-717.

106. **Krylov, V. N., and A. Zapadnaya.** 1965. Bacteriophage T4B r mutations sensitive to temperature (rts). Genetika **1:**7-11.

107. **Kuty, G. F., M. Xu, D. K. Struck, E. J. Summer, and R. Young.** 2010. Regulation of a phage endolysin by disulfide caging. J Bacteriol **192:**5682-5687.

108. **Kuwana, T., M. R. Mackey, G. Perkins, M. H. Ellisman, M. Latterich, R. Schneiter, D. R. Green, and D. D. Newmeyer.** 2002. Bid, Bax, and lipids cooperate to form supramolecular openings in the outer mitochondrial membrane. Cell **111:**331-342.

109. **Landsmann, J., M. Kroger, and G. Hobom.** 1982. The rex region of bacteriophage lambda: two genes under three-way control. Gene **20:**11-24.

110. **Levy, R., R. Weiss, G. Chen, B. L. Iverson, and G. Georgiou.** 2001. Production of correctly folded Fab antibody fragment in the cytoplasm of *Escherichia coli* trxB gor mutants via the coexpression of molecular chaperones. Protein Expr Purif **23:**338-347.

111. **Li, B. H., M. Kwasniewski, J. Kirchner, and R. Bockrath.** 1992. RexAB proteins of bacteriophage lambda enhance the effect of photolyase-dimer complexes on lacZ gene expression in *Escherichia coli*. Mol Gen Genet **231:**480-484.

112. **Liu, X., C. N. Kim, J. Yang, R. Jemmerson, and X. Wang.** 1996. Induction of apoptotic program in cell-free extracts: requirement for dATP and cytochrome c. Cell **86:**147-157.

113. **Lovell, J. F., L. P. Billen, S. Bindner, A. Shamas-Din, C. Fradin, B. Leber, and D. W. Andrews.** 2008. Membrane binding by tBid initiates an ordered series of events culminating in membrane permeabilization by Bax. Cell **135:**1074-1084.

114. **Lu, M. J., and U. Henning.** 1989. The immunity (imm) gene of *Escherichia coli* bacteriophage T4. J Virol **63:**3472-3478.

115. **Lu, M. J., and U. Henning.** 1992. Lysis protein T of bacteriophage T4. Mol Gen Genet **235:**253-258.

116. **Lu, M. J., and U. Henning.** 1994. Superinfection exclusion by T-even-type coliphages. Trends Microbiol **2:**137-139.

117. **Lu, M. J., Y. D. Stierhof, and U. Henning.** 1993. Location and unusual membrane topology of the immunity protein of the *Escherichia coli* phage T4. J Virol **67:**4905-4913.

118. **Maaloe, O., and J. D. Watson.** 1951. The transfer of radioactive phosphorus from parental to progeny phage. Proc Natl Acad Sci U S A **37:**507-513.

119. **Marley, J., M. Lu, and C. Bracken.** 2001. A method for efficient isotopic labeling of recombinant proteins. J Biomol NMR **20:**71-75.

120. **Mathews, C. K., and American Society for Microbiology.** 1983. Bacteriophage T4. American Society for Microbiology, Washington, D.C.

121. **Matthews, B. W.** 2005. The structure of *E. coli* beta-galactosidase. C R Biol **328:**549-556.

122. **Matthews, B. W.** 1995. Studies on protein stability with T4 lysozyme. Adv Protein Chem **46:**249-278.

123. **Matz, K., M. Schmandt, and G. N. Gussin.** 1982. The rex gene of bacteriophage lambda is really two genes. Genetics **102:**319-327.

124. **Miller, E. S., E. Kutter, G. Mosig, F. Arisaka, T. Kunisawa, and W. Ruger.** 2003. Bacteriophage T4 genome. Microbiol Mol Biol Rev **67:**86-156.

125. **Moak, M., and I. J. Molineux.** 2004. Peptidoglycan hydrolytic activities associated with bacteriophage virions. Mol Microbiol **51:**1169-1183.

126. **Montelione, G. T., B. A. Lyons, S. D. Emerson, and M. Tashiro.** 1992. An efficient triple resonance experiment using C-13 isotropic mixing for determining sequence-specific resonance assignments of isotopically-enriched proteins. J Am Chem Soc **114:**10974-10975.

127. **Mosig, G.** 1968. A map of distances along the DNA molecule of phage T4. Genetics **59:**137-151.

128. **Moussa, S. H., V. Kuznetsov, T. A. Tran, J. C. Sacchettini, and R. Young.** 2012. Protein determinants of phage T4 lysis inhibition. Protein Sci **21:**571-582.

129. **Muhandiram, D. R., and L. E. Kay.** 1994. Gradient-enhanced triple-resonance three-dimensional NMR experiments with improved sensitivity. J Magn Reson Ser B **103:**203-216.

130. **Nakagawa, H., F. Arisaka, and S. Ishii.** 1985. Isolation and characterization of the bacteriophage T4 tail-associated lysozyme. J Virol **54:**460-466.

131. **Nechushtan, A., C. L. Smith, Y. T. Hsu, and R. J. Youle.** 1999. Conformation of the Bax C-terminus regulates subcellular location and cell death. EMBO J **18:**2330-2341.

132. **Newmeyer, D. D., and S. Ferguson-Miller.** 2003. Mitochondria: releasing power for life and unleashing the machineries of death. Cell **112:**481-490.

133. **Nomura, M., and S. Benzer.** 1961. The nature of the "deletion" mutants in the rII region of phage T4. J Mol Biol **3:**684-692.

134. **Obringer, J. W.** 1988. The functions of the phage T4 immunity and spackle genes in genetic exclusion. Genet Res **52:**81-90.

135. **Pace, C. N., F. Vajdos, L. Fee, G. Grimsley, and T. Gray.** 1995. How to measure and predict the molar absorption coefficient of a protein. Protein Sci **4:**2411-2423.

136. **Paddison, P., S. T. Abedon, H. K. Dressman, K. Gailbreath, J. Tracy, E. Mosser, J. Neitzel, B. Guttman, and E. Kutter.** 1998. The roles of the bacteriophage T4 r genes in lysis inhibition and fine-structure genetics: a new perspective. Genetics **148:**1539-1550.

137. **Pang, T., T. Park, and R. Young.** 2010. Mapping the pinhole formation pathway of S21. Mol Microbiol **78:**710-719.

138. **Pang, T., T. Park, and R. Young.** 2010. Mutational analysis of the S21 pinholin. Mol Microbiol **76:**68-77.

139. **Pang, T., C. G. Savva, K. G. Fleming, D. K. Struck, and R. Young.** 2009. Structure of the lethal phage pinhole. Proc Natl Acad Sci U S A **106:**18966-18971.

140. **Park, T., D. K. Struck, C. A. Dankenbring, and R. Young.** 2007. The pinholin of lambdoid phage 21: control of lysis by membrane depolarization. J Bacteriol **189:**9135-9139.

141. **Park, T., D. K. Struck, J. F. Deaton, and R. Young.** 2006. Topological dynamics of holins in programmed bacterial lysis. Proc Natl Acad Sci U S A **103:**19713-19718.

142. **Parma, D. H., M. Snyder, S. Sobolevski, M. Nawroz, E. Brody, and L. Gold.** 1992. The Rex system of bacteriophage lambda: tolerance and altruistic cell death. Genes Dev **6:**497-510.

143. **Perez-Iratxeta, C., and M. A. Andrade-Navarro.** 2008. K2D2: estimation of protein secondary structure from circular dichroism spectra. BMC Struct Biol **8:**25.

144. **Ramanculov, E., and R. Young.** 2001. An ancient player unmasked: T4 rI encodes a t-specific antiholin. Mol Microbiol **41:**575-583.

145. **Ramanculov, E., and R. Young.** 2001. Functional analysis of the phage T4 holin in a lambda context. Mol Genet Genomics **265:**345-353.

146. **Ramanculov, E., and R. Young.** 2001. Genetic analysis of the T4 holin: timing and topology. Gene **265:**25-36.

147. **Raudonikiene, A., and R. Nivinskas.** 1992. Gene rIII is the nearest downstream neighbour of bacteriophage T4 gene 31. Gene **114:**85-90.

148. **Raudonikiene, A., and R. Nivinskas.** 1993. The sequences of gene rIII of bacteriophage T4 and its mutants. Gene **134:**135-136.

149. **Revel, H. R., and I. Lielausis.** 1978. Revised location of the rIII gene on the genetic map of bacteriophage T4. J Virol **25:**439-441.

150. **Rice, K. C., and K. W. Bayles.** 2008. Molecular control of bacterial death and lysis. Microbiol Mol Biol Rev **72:**85-109.

151. **Rutberg, B., and L. Rutberg.** 1966. Bacteriophage-induced functions in *Escherichia coli* K (lambda) infected with rII mutants of bacteriophage T4. J Bacteriol **91:**76-80.

152. **Rutberg, B., and L. Rutberg.** 1965. Role of superinfecting phage in lysis inhibition with phage T4 in *Escherichia coli*. J Bacteriol **90:**891-894.

153. **Rutberg, L., and B. Rutberg.** 1964. On the Expression of the rII Mutation of T-even bacteriophages in *Escherichia coli* strain B. Virology **22:**280-283.

154. **Saito, M., S. J. Korsmeyer, and P. H. Schlesinger.** 2000. Bax-dependent transport of cytochrome c reconstituted in pure liposomes. Nat Cell Biol **2:**553-555.

155. **Sao-Jose, C., R. Parreira, G. Vieira, and M. A. Santos.** 2000. The N-terminal region of the *Oenococcus oeni* bacteriophage fOg44 lysin behaves as a bona fide signal peptide in *Escherichia coli* and as a cis-inhibitory element, preventing lytic activity on oenococcal cells. J Bacteriol **182:**5823-5831.

156. **Savva, C. G., J. S. Dewey, J. Deaton, R. L. White, D. K. Struck, A. Holzenburg, and R. Young.** 2008. The holin of bacteriophage lambda forms rings with large diameter. Mol Microbiol **69:**784-793.

157. **Schumann, F. H., H. Riepl, T. Maurer, W. Gronwald, K. P. Neidig, and H. R. Kalbitzer.** 2007. Combined chemical shift changes and amino acid specific chemical shift mapping of protein-protein interactions. J Biomol NMR **39:**275-289.

158. **Shinedling, S., D. Parma, and L. Gold.** 1987. Wild-type bacteriophage T4 is restricted by the lambda rex genes. J Virol **61:**3790-3794.

159. **Shub, D. A.** 1994. Bacterial viruses. Bacterial altruism? Curr Biol **4:**555-556.

160. **Slavcev, R. A., and S. Hayes.** 2004. Over-expression of rexA nullifies T4rII exclusion in *Escherichia coli* K(lambda) lysogens. Can J Microbiol **50:**133-136.

161. **Slavcev, R. A., and S. Hayes.** 2002. Rex-centric mutualism. J Bacteriol **184:**857-858.

162. **Slavcev, R. A., and S. Hayes.** 2003. Stationary phase-like properties of the bacteriophage lambda Rex exclusion phenotype. Mol Genet Genomics **269:**40-48.

163. **Slettan, A., K. Gebhardt, E. Kristiansen, N. K. Birkeland, and B. H. Lindqvist.** 1992. *Escherichia coli* K-12 and B contain functional bacteriophage P2 ogr genes. J Bacteriol **174:**4094-4100.

164. **Smith, D. L., D. K. Struck, J. M. Scholtz, and R. Young.** 1998. Purification and biochemical characterization of the lambda holin. J Bacteriol **180:**2531-2540.

165. **Snyder, L.** 1995. Phage-exclusion enzymes: a bonanza of biochemical and cell biology reagents? Mol Microbiol **15:**415-420.

166. **Snyder, L., and K. McWilliams.** 1989. The rex genes of bacteriophage lambda can inhibit cell function without phage superinfection. Gene **81:**17-24.

167. **Stent, G. S.** 1963. Molecular biology of bacterial viruses. W. H. Freeman, San Francisco, CA.

168. **Stewart, M. D., B. Morgan, F. Massi, and T. I. Igumenova.** 2011. Probing the determinants of diacylglycerol binding affinity in the C1B domain of protein kinase Calpha. J Mol Biol **408:**949-970.

169. **Streisinger, G., R. S. Edgar, and G. H. Denhardt.** 1964. Chromosome structure in phage T4. I. Circularity of the linkage map. Proc Natl Acad Sci U S A **51:**775-779.

170. **Streisinger, G., F. Mukai, W. J. Dreyer, B. Miller, and S. Horiuchi.** 1961. Mutations affecting the lysozyme of phage T4. Cold Spring Harb Symp Quant Biol **26:**25-30.

171. **Studier, F. W., and B. A. Moffatt.** 1986. Use of bacteriophage T7 RNA polymerase to direct selective high-level expression of cloned genes. J Mol Biol **189:**113-130.

172. **Summer, E. J., J. Berry, T. A. Tran, L. Niu, D. K. Struck, and R. Young.** 2007. Rz/Rz1 lysis gene equivalents in phages of Gram-negative hosts. J Mol Biol **373:**1098-1112.

173. **Summer, E. J., C. J. Enderle, S. J. Ahern, J. J. Gill, C. P. Torres, D. N. Appel, M. C. Black, R. Young, and C. F. Gonzalez.** 2009. Genomic and biological analysis of phage Xfas53 and related prophages of *Xylella fastidiosa*. J Bacteriol **192:**179-190.

174. **Sun, Q., G. F. Kuty, A. Arockiasamy, M. Xu, R. Young, and J. C. Sacchettini.** 2009. Regulation of a muralytic enzyme by dynamic membrane topology. Nat Struct Mol Biol **16:**1192-1194.

175. **Szewczyk, B., and R. Skorko.** 1981. Lysozyme activity of bacteriophage T4 ghosts. Biochim Biophys Acta **662:**131-137.

176. **Tait, S. W., and D. R. Green.** 2010. Mitochondria and cell death: outer membrane permeabilization and beyond. Nat Rev Mol Cell Biol **11:**621-632.

177. **Takata, T., J. T. Oxford, B. Demeler, and K. J. Lampi.** 2008. Deamidation destabilizes and triggers aggregation of a lens protein, betaA3-crystallin. Protein Sci **17:**1565-1575.

178. **Takeda, S., K. Hoshida, and F. Arisaka.** 1998. Mapping of functional sites on the primary structure of the tail lysozyme of bacteriophage T4 by mutational analysis. Biochim Biophys Acta **1384:**243-252.

179. **Tran, T. A., D. K. Struck, and R. Young.** 2005. Periplasmic domains define holin-antiholin interactions in t4 lysis inhibition. J Bacteriol **187:**6631-6640.

180. **Tran, T. A., D. K. Struck, and R. Young.** 2007. The T4 RI antiholin has an N-terminal signal anchor release domain that targets it for degradation by DegP. J Bacteriol **189:**7618-7625.

181. **Unwin, N.** 1986. Is there a common design for cell membrane channels? Nature **323:**12-13.

182. **Vallee, M., and J. B. Cornett.** 1972. A new gene of bacteriophage T4 determining immunity against superinfecting ghosts and phage in T4-infected *Escherichia coli*. Virology **48:**777-784.

183. **Vallee, M., J. B. Cornett, and H. Bernstein.** 1972. The action of bacteriophage T4 ghosts on *Escherichia coli* and the immunity to this action developed in cells preinfected with T4. Virology **48:**766-776.

184. **Vertommen, D., M. Depuydt, J. Pan, P. Leverrier, L. Knoops, J. P. Szikora, J. Messens, J. C. Bardwell, and J. F. Collet.** 2008. The disulphide isomerase DsbC cooperates with the oxidase DsbA in a DsbD-independent manner. Mol Microbiol **67:**336-349.

185. **Visconti, N.** 1953. Resistance to lysis from without in bacteria infected with T2 bacteriophage. J Bacteriol **66:**247-253.

186. **Wagner, S., L. Baars, A. J. Ytterberg, A. Klussmeier, C. S. Wagner, O. Nord, P. A. Nygren, K. J. van Wijk, and J. W. de Gier.** 2007. Consequences of membrane protein overexpression in *Escherichia coli*. Mol Cell Proteomics **6:**1527-1550.

187. **Wang, I. N., J. Deaton, and R. Young.** 2003. Sizing the holin lesion with an endolysin-beta-galactosidase fusion. J Bacteriol **185:**779-787.

188. **Wang, I. N., D. L. Smith, and R. Young.** 2000. Holins: the protein clocks of bacteriophage infections. Annu Rev Microbiol **54:**799-825.

189. **Watson, J. D.** 1950. The properties of x-ray inactivated bacteriophage. I. Inactivation by direct effect. J Bacteriol **60:**697-718.

190. **Weaver, L. H., and B. W. Matthews.** 1987. Structure of bacteriophage T4 lysozyme refined at 1.7 A resolution. J Mol Biol **193:**189-199.

191. **Wei, M. C., W. X. Zong, E. H. Cheng, T. Lindsten, V. Panoutsakopoulou, A. J. Ross, K. A. Roth, G. R. MacGregor, C. B. Thompson, and S. J. Korsmeyer.** 2001. Proapoptotic Bax and Bak: a requisite gateway to mitochondrial dysfunction and death. Science **292:**727-730.

192. **Weintraub, S. B., and F. R. Frankel.** 1972. Identification of the T4rIIB gene product as a membrane protein. J Mol Biol **70:**589-615.

193. **White, R., S. Chiba, T. Pang, J. S. Dewey, C. G. Savva, A. Holzenburg, K. Pogliano, and R. Young.** 2011. Holin triggering in real time. Proc Natl Acad Sci U S A **108:**798-803.

194. **White, R., T. A. Tran, C. A. Dankenbring, J. Deaton, and R. Young.** 2010. The N-terminal transmembrane domain of lambda S is required for holin but not antiholin function. J Bacteriol **192:**725-733.

195. **Willis, S. N., J. I. Fletcher, T. Kaufmann, M. F. van Delft, L. Chen, P. E. Czabotar, H. Ierino, E. F. Lee, W. D. Fairlie, P. Bouillet, A. Strasser, R. M. Kluck, J. M. Adams, and D. C. Huang.** 2007. Apoptosis initiated when BH3 ligands engage multiple Bcl-2 homologs, not Bax or Bak. Science **315:**856-859.

196. **Xu, M., A. Arulandu, D. K. Struck, S. Swanson, J. C. Sacchettini, and R. Young.** 2005. Disulfide isomerization after membrane release of its SAR domain activates P1 lysozyme. Science **307:**113-117.

197. **Xu, M., D. K. Struck, J. Deaton, I. N. Wang, and R. Young.** 2004. A signal-arrest-release sequence mediates export and control of the phage P1 endolysin. Proc Natl Acad Sci U S A **101:**6415-6420.

198. **Yang, J., X. Liu, K. Bhalla, C. N. Kim, A. M. Ibrado, J. Cai, T. I. Peng, D. P. Jones, and X. Wang.** 1997. Prevention of apoptosis by Bcl-2: release of cytochrome c from mitochondria blocked. Science **275:**1129-1132.

199. **Yang, X., E. A. Stojkovic, J. Kuk, and K. Moffat.** 2007. Crystal structure of the chromophore binding domain of an unusual bacteriophytochrome, RpBphP3, reveals residues that modulate photoconversion. Proc Natl Acad Sci U S A **104:**12571-12576.

200. **Youle, R. J., and A. Strasser.** 2008. The BCL-2 protein family: opposing activities that mediate cell death. Nat Rev Mol Cell Biol **9:**47-59.

201. **Young, I., I. Wang, and W. D. Roof.** 2000. Phages will out: strategies of host cell lysis. Trends Microbiol **8:**120-128.

202. **Young, R.** 2002. Bacteriophage holins: deadly diversity. J Mol Microbiol Biotechnol **4:**21-36.

203. **Young, R.** 1992. Bacteriophage lysis: mechanism and regulation. Microbiol Rev **56:**430-481.

204. **Young, R., and U. Blasi.** 1995. Holins: form and function in bacteriophage lysis. FEMS Microbiol Rev **17:**191-205.

205. **Young, R., and I. N. Wang.** 2006. Phage lysis, p. 104-126. *In* R. Calendar (ed.), The bacteriophages, 2nd ed. Oxford University Press, Oxford.

206. **Zagotta, M. T., and D. B. Wilson.** 1990. Oligomerization of the bacteriophage lambda S protein in the inner membrane of *Escherichia coli*. J Bacteriol **172:**912-921.

207. **Zheng, Y., D. K. Struck, C. A. Dankenbring, and R. Young.** 2008. Evolutionary dominance of holin lysis systems derives from superior genetic malleability. Microbiology **154:**1710-1718.

VITA

Name: Samir H. Moussa

Address: Texas A&M University; Department of Biochemistry & Biophysics
2128 TAMU; College Station, Texas 77843-2128

Email: samir.moussa1@gmail.com

Education:

2003 B.S., Biology. *Minors*: Chemistry and Criminal Justice. Baylor University, Waco, Texas.

2005 M.S., Biology (Environmental Microbiology emphasis). Baylor University, Waco, Texas. *Advisor*: Rene D. Massengale, Ph.D.

2012 Ph.D., Microbiology. Chemistry-Biology Interface Research Training Program (CBI) trainee. Texas A&M University, College Station, Texas. *Advisor*: Ryland F. Young, Ph.D.